EXPERIMENTAL STUDY ON LIQUID IMMISCIBILITY IN SILICATE-CARBONATE SYSTEMS WITH APPLICATIONS TO CARBONATITES

Thesis by

Woh-jer Lee

In Partial Fulfillment of the Requirements

for the Degree of

Doctor of Philosophy

California Institute of Technology

Pasadena, California

1996

(Submitted May 8, 1996)

ACKNOWLEDGMENTS

I have been very lucky to have had the opportunity to do my graduate study at Caltech, and to work with many great scientists here. It has been an exciting and memorable experience for me. I would particularly like to express my thanks to my thesis advisor, Peter Wyllie, who suggested the topic and guided me through the entire study. His consistent encouragement and enthusiasm toward science have greatly inspired me. I would also like to acknowledge the financial support from the National Science Foundation, grant EAR-921886.

I am indebted to George Rossman for introducing me to Infrared Spectroscopy. His door is always open for anyone who needs his help. I would also like to thank the faculty members of the Division: Tom Ahrens, Geoff Blake, Don Anderson, Jason Saleeby, Bob Sharp, Kerry Sieh, Lee Silver, Dave Stevenson, Ed Stolper, Hugh Taylor, Gerry Wasserburg and Yuk Yung. Their great knowledge and scientific instinct have influenced me deeply.

I am grateful to Mike Baker, Dan Sykes and Brad White for teaching me piston cylinder experiments, and Geoff Nichols and Brent McInnes for further technical assistance. Mike Baker has shared with me his invaluable knowledge in both high-pressure experiments and petrological problems. Hans Keppler and Jen Blank instructed me in the use of cold seal pressure vessels. I have benefited from the discussions about glass structures with Jim Kubicki, Sally Newman, Dan Sykes and Youxue Zhang. I am also thankful for the interactions with other members of the Arms Laboratory: Georg Amthauer, Paul Asimow, Neena Bashir, John Beckett, David Bell, Lori Chamberlin, Phil Ihinger, Serge Nadeau and Laura Wasylenki. In addition, thanks are due to John Armstrong, Paul Carpenter and Mary Johnson for teaching me to use electron-beam analytical facilities.

I have enjoyed the first year experience with my classmates Greg Holk, Elizabeth Nagy, Dave Sauer, Dimitri Vlassopoulos and Doug Yule. We worked together and encouraged each other through the tough first year. I am also enriched by long-term friendships from James Chen, Carey Gazis, Weishi Huang, Kuo-Fong Ma, Xiaodong Song and Craig Scrivner. They made my life here more delightful.

Finally, I would like to thank my parents Hsi-Hui and Tsai-Hua, my brother Wo-Lung, and my sister Liang-Hui. Their constant support is the driving force for my success. I wish to thank my uncle and aunt, James and Hsu-Hui, for their faith in me. I am fortunate to have the love from my wife, Mei-Hui, who is always there sharing both my good and bad times. Also, our new-born baby, Kenneth, has further brightened my life at the finishing stage of my Ph.D. study.

ABSTRACT

Phase equilibrium experiments have been conducted in several silicate-carbonate systems to 2.5 GPa in order to understand the magmatic processes involved in the generation of carbonatite complexes. The studied phase fields were intersected by SiO_2-$CaCO_3$, $NaAlSi_3O_8$-$CaCO_3$, $NaAlSiO_4$-$NaAlSi_3O_8$-$CaCO_3$ and primitive nephelinite-(Na,Ca,Mg) carbonate, which along with the analyzed liquid and solid compositions were used to define the positions of the silicate-carbonate miscibility gap and liquidus field boundaries on various compositional projections. These boundaries exert controls on the evolution of silicate-CO_2 and carbonatitic magmas, and vary strongly with temperature, composition and pressure. The size of the miscibility gap decreases with increasing temperature and Mg/Ca of liquids. The extent of the Mg-free miscibility gap decreases with decreasing pressure, whereas the magnesian one shows an opposite trend. The immiscible carbonate-rich liquids could dissolve at most ~80 wt% $CaCO_3$ while still containing significant amounts of silicate and alkalis. The position of the silicate-calcite coprecipitation boundary becomes more carbonate-rich as pressure decreases, and as composition becomes more magnesian and aluminous. Calcite grew remarkably rounded in many experiments. A variety of liquid paths are compared with the field boundaries at different conditions. Partial melting of carbonated peridotite produces dolomitic carbonatites along the coprecipitation boundary, to CO_2-bearing, silica-undersaturated liquids in the primary silicate field. Both types of magmas could potentially ascend to the surface of the earth without much modification. None of them would reach the miscibility gap at mantle conditions. Within the crust, carbonated silicate liquids could either intersect the miscibility gap after substantial crystallization to exsolve alkali-bearing to alkalic carbonatitic liquids, or reach the coprecipitation boundary and evolve towards alkali-enrichment and silicate-depletion without immiscibility. Alkali-bearing, $CaCO_3$-rich immiscible liquids, when separating from their silicate parents, first precipitate silicate minerals during cooling until

calcite is joined, and the residual liquids become more alkalic by further crystallization of calcite. It appears that most calciocarbonatites are cumulates from liquids along the coprecipitation boundary, whereas the natrocarbonatites at Oldoinyo Lengai are produced directly by immiscibility.

TABLE OF CONTENTS

INTRODUCTION

This thesis is largely concerned with experimental boundaries, particularly the limit of liquid immiscibility, for the generation of carbonatite magmas. Each chapter is built on a different phase equilibrium study, progressing from simple to more complex systems, dealing with mutually related issues of the carbonatite problems. Most chapters were prepared as independent papers which have been published or submitted for publication, and for this reason there is overlap between the "Introductions" and "Petrological Applications" of the chapters. This section summarizes from the chapter "Introductions" the main petrological problems, and outlines the experimental system presented in each chapter and the overall experimental design of the study.

The very existence of carbonatite magmas was once debated, but has gradually become accepted due to integrated evidence from field, geochemical and experimental studies (see Gittins and Tuttle, 1966; Bell, 1989). While the early investigations emphasized recognition of the igneous origin of carbonatites, the generation of carbonate-rich magmas has now been linked to several broader petrological problems, such as the formation of carbonatite complexes, CO_2-budget within the mantle, the contribution of carbonate in subduction magmatism, the role of carbonatitic melts in metasomatism, and the enrichment of some economical trace elements associated with carbonatites.

There is a wide variety of occurrence for carbonatites. They are commonly associated with alkaline silicate rocks, indicating a possible genetic link between the two (e.g. Barker, 1989). Most of these carbonatites are intrusive calcite-rich rocks, with the remainder ranging from Mg- to Fe-rich, all containing very minor alkali contents; field relations pointed to their low emplacement temperatures (down to ~600°C). In contrast, effusive carbonatites carrying magmatic calcite and dolomite and low in alkalis appeared to occur at much higher temperature (~1000-1200°C), most of them having no association with silicate rocks (Bailey, 1993). Low-temperature (550-600°C) lavas of an alkalic variety, on the other hand, are erupting at Oldoinyo Lengai, the only active carbonatite

volcano with a composition drastically different from all other carbonatites (Dawson, 1989).

It is evident that CO_2 is present in the mantle, an observation supported by the appearance of carbonate in mantle xenoliths (e.g. Ionov et al., 1993; Pyle and Haggerty, 1994). The involvement of CO_2, either contributed by primordial or recycled carbonate materials, in the melting of mantle assemblages has an important implication to carbonatite genesis. Isotopic data point to an ultimate mantle source for all carbonatite magmas (e.g. Bell and Blenkinsop, 1989), and extensive experimental results further demonstrate that CO_2-bearing silicate to carbonatitic melts, the possible parents for carbonatites, can be generated from carbonated peridotite. Bailey (1993) stated that "carbonate magmatism is a crucial surface expression of deep mantle processes." There is also a prospect that under suitable conditions, subducted oceanic crust would be partially melted, with the associated sediments and carbonate generating CO_2-rich liquids/fluids subsequently interacting with the overlying mantle wedge.

Trace element distribution of carbonatites is significantly different from that of most silicate rocks. Steep REE abundance patterns with very high, light REE enrichments are typical of carbonatites (Woolley and Kempe, 1989). This unusual geochemical signature along with the presence of secondary mineral groups in some mantle xenoliths (i.e. conversion of lherzolite to wehrlite assemblages) suggests the possible occurrence of metasomatic events by carbonate-rich melts (e.g. Green and Wallace, 1988). In addition, economic mineralization associated with such enrichments makes carbonatites a major source of Nb, phosphate and REEs (e.g. Mariano, 1989).

Although it is now generally accepted that carbonatite magmas have their source in the mantle, what remain unclear are the detailed evolution paths of the magmas from mantle to crust. There are presently three favored mechanisms regarding the generation of carbonatitic magmas: by small degree partial melting of carbonated peridotite, by liquid immiscibility of carbonated silicate liquids, and by crystal fractionation of other carbonated

silicate liquids. In particular, liquid immiscibility has been frequently invoked to explain the formation of large-scale carbonatite complexes and small-scale carbonate ocelli and inclusions in mantle xenoliths (see the chapters for references). This interpretation currently appeals to the work of Kjarsgaard and Hamilton (1988, 1989), and Brooker and Hamilton (1990). They described the occurrence of a large miscibility gap in feldspar-carbonate joins, extending essentially to alkali-free compositions, and concluded that the rounded $CaCO_3$ phases in their experiments were immiscible liquids of the same composition. They suggested that a whole range of alkalic to calcic carbonatites can be produced by liquid immiscibility, mainly appealing to the appearance of the large two-liquid field. Since then the discovery has been cited extensively to support the alleged nearly pure $CaCO_3$ liquids interpreted from some petrological observations.

This thesis presents the results of phase equilibrium experiments with emphasis on the limits of immiscibility in the formation of carbonatite magmas. The experiments were designed to determine the compositional range of the miscibility gap in simple to complex systems. In addition, I report another important phase feature in controlling the evolution of carbonated silicate to carbonatitic liquids which has been neglected in most previous immiscibility studies, namely the silicate-carbonate liquidus field boundary where the liquids precipitate both silicate and carbonate minerals. These experimental boundaries provide a basis for examining the three major proposed mechanisms mentioned above, and thus enhance understanding of the origin of carbonatites. The content of each chapter is briefly described as follows.

Debates and relevant advances about the origin and the evolution of carbonatites are summarized in Chapter 1: (1) where carbonatites are from—mantle or crust, (2) what the composition of parental carbonatite magma is—calcic, dolomitic, or sodic, and (3) whether carbonatites are derived from parent silicate magmas by fractional crystallization or by liquid immiscibility. A new experimental result in the system Na_2O-CaO-Al_2O_3-SiO_2-CO_2-H_2O at 0.1 GPa is presented, confirming that crystal fractionation of a hydrous CO_2-

bearing nepheline-normative liquid at moderate temperatures may produce continuous liquid compositions from silicate to carbonate rich. The residual liquid becomes alkali-enriched at temperatures below the high-temperature liquid miscibility gap.

Chapter 2 illustrates the results of the join SiO_2-$CaCO_3$ at 2.5 GPa, showing no sign of immiscibility in the alkali-free compositions. The experimental rounded $CaCO_3$ is interpreted as a calcite crystal, not an immiscible liquid as previously announced (i.e. Kjarsgaard and Hamilton, 1988, 1989). $CaCO_3$-rich liquid in the system quenched to a glass, which is further studied by infrared spectroscopic method to derive information about liquid structure.

The phase fields intersected by the join $NaAlSi_3O_8$-$CaCO_3$ are presented in Chapter 3. The corresponding silicate-carbonate liquid miscibility gap and liquidus field boundaries in the system Na_2O-CaO-Al_2O_3-SiO_2-CO_2 are constructed in the pseudo-ternary diagram, (SiO_2 + Al_2O_3)-CaO-Na_2O, projected from CO_2. Although the geometrical arrangement and temperatures of the field boundaries in the synthetic model system cannot be directly applied to rock assemblages, they illustrate the kinds of processes and controls which may occur in nature. The results define the maximum dissolved $CaCO_3$ content in immiscible carbonatite liquids to be ~80%, and invalidate the claims of immiscible, nearly pure $CaCO_3$ (99%) liquids (Kjarsgaard and Hamilton, 1988, 1989), and thus the associated petrological applications of their followers. Several lines of evidence that the rounded $CaCO_3$ is a crystalline phase are presented in detail. It is concluded that most calciocarbonatites are cumulates along the silicate-calcite liquidus field boundary, and that calcite ocelli in mantle xenoliths grew as crystals, not immiscible carbonate liquids.

The effect of Al/Si in the synthetic system is explored at 1.0 GPa using the join $NaAlSiO_4$-$NaAlSi_3O_8$-$CaCO_3$, reported in Chapter 4. The data are expressed in the compositional triangle and the tetrahedron SiO_2-Al_2O_3-CaO-Na_2O (with excess CO_2) to illustrate the variations of the field boundaries and the corresponding phase assemblages.

The results suggest that alkali-bearing carbonatite liquids are probably quite common in nature, and that Oldoinyo Lengai natrocarbonatites may represent the immiscible carbonatitic liquids near the temperature minimum on the miscibility gap.

Chapter 5 shows the next step of the experimental approach toward natural rock assemblages: determination of the Mg-bearing miscibility gap intersected by nephelinite-dolomite-Na_2CO_3 at 1.0 to 2.5 GPa. The miscibility gap is restricted to more alkali-rich compositions compared to the Mg-free gaps, but expands somewhat with decreasing pressure. The alkali-poor join nephelinite-$CaCO_3$ does not intersect the miscibility gap at 1.0 GPa. The possible reactions for the melting of various carbonated peridotite assemblages are summarized, and the compositions of experimental mantle carbonatitic melts along with several natural rock types are also compared with the miscibility gap. None of the liquid compositions are likely to intersect the liquid immiscibility volume in mantle processes.

Variations and limits of the miscibility gap and liquidus field boundaries as a function of pressure, temperature and composition are further summarized in Chapter 6, and used to construct generalized phase diagrams in the tetrahedron (SiO_2 + SiO_2 + TiO_2)-CaO-(MgO + FeO)-(Na_2O + K_2O) (+ CO_2). The phase diagrams provide a model framework for understanding the formation of a variety of alkaline and carbonatite rocks. The bulk compositions of three categories of silicate-carbonatite assemblages are compared with the framework: (1) effusive calciocarbonatites with mantle debris, (2) mantle carbonate globules and associated glasses in mantle xenoliths, and (3) alkaline complexes with various crystallization trends. It appears that some mantle carbonatite magmas may reach the surface of the earth without much modification, perhaps as diatremes, with their compositions projecting near the silicate-carbonate coprecipitation boundary. Both liquid immiscibility and fractional crystallization are important in the generation of crustal carbonatites. The results also reinforce the conclusion that mantle carbonate ocelli cannot be immiscible carbonatite liquids.

Finally, because of the overlap and repetition in the "Petrological Applications" for each independent chapter, I present an itemized summary of the petrological conclusions following approximately the sequence of applications and conclusions reached in successive chapters.

REFERENCES

Bailey, D. K., 1993. Carbonate magmas. Journal of the Geological Society of London 150, 637-651.

Barker, D. S., 1989. Field relations of carbonatites. In Bell, K. (ed.) Carbonatites: Genesis and Evolution. London: Unwin Hyman, pp. 38-69.

Bell, K. (ed) 1989. Carbonatites: genesis and evolution. London: Unwin Hyman.

Bell, K. & Blenkinsop, J, 1989. Neodymium and strontium isotope geochemistry of carbonatites. In: Bell, K. (ed.) Carbonatites: Genesis and Evolution. London: Unwin Hyman, pp. 278-300.

Dawson, 1989. Sodium carbonatite extrusions from Oldoinyo Lengai, Tanzania: implications for carbonatite complex genesis. In: Bell, K. (ed.) Carbonatites: Genesis and Evolution. London: Unwin Hyman, pp. 255-277.

Green D. H. & Wallace M. E., 1988. Mantle metasomatism by ephemeral carbonatite melts. Nature 336: 459-462.

Ionov, D.A., Dupuy, C., O'Reilly, S.Y., Kopylova, M.G. & Genshaft, Y.S., 1993. Carbonated peridotite xenoliths from Spitsbergen: Implications for trace element signature of mantle carbonate metasomatism. Earth and Planetary Science Letters 119, 283-297.

Kjarsgaard, B. A. & Hamilton, D. L., 1988. Liquid immiscibility and the origin of alkali-poor carbonatites. Mineralogical Magazine 52, 43-55.

Kjarsgaard, B. A.. & Hamilton, D. L., 1989. The genesis of carbonatites by immiscibility. In: Bell, K. (ed.) Carbonatites: Genesis and Evolution. London: Unwin Hyman, pp. 388-404.

Mariano, A. N., 1989. Nature of economic mineralization in carbonatites and related rocks. In: Bell, K. (ed.) Carbonatites: Genesis and Evolution. London: Unwin Hyman, pp. 149-176.

Pyle, J. M. & Haggerty, S. E., 1994. Silicate-carbonate liquid immiscibility in upper-mantle eclogites: Implications for natrosilicic and carbonatitic conjugate melts. Geochimica et Cosmochimica Acta 58, 2997-3011.

Tuttle, O. F. & Gittins, J., 1966. Carbonatites. New York: Interscience.

Watkinson, D. H. & Wyllie, P. J., 1969. Phase equilibrium studies bearing on the limestone-assimilation hypothesis. Bulletin of Geological Society of America 80, 1565-1576.

Watkinson, D. H. & Wyllie, P. J., 1971. Experimental study of the join $NaAlSiO_4$-$CaCO_3$-H_2O and the genesis of alkalic rock-carbonatite complexes. Journal of Petrology 12, 357-378.

Woolley, A. R. & Kempe, D. R. C., 1989. Carbonatites: Nomenclature, average chemical compositions, and element distribution. In: Bell, K. (ed.) Carbonatites: Genesis and Evolution. London: Unwin Hyman, pp. 1-14.

CHAPTER 1

EXPERIMENTAL DATA BEARING ON LIQUID IMMISCIBILITY, CRYSTAL FRACTIONATION, AND THE ORIGIN OF CALCIOCARBONATITES AND NATROCARBONATITES

(Lee W.-J. & Wyllie P. J., 1994. International Geology Review 36: 797-819)

ABSTRACT

Controversies about the role of carbonate-rich melts in processes ranging from mantle metasomatism to carbonatite eruptions involve debates about the following: (1) are carbonatite magmas primary from the mantle, or differentiates from silicate parents in the crust? (2) are parental carbonatite magmas calcic, dolomitic, or sodic? (3) are carbonatite magmas derived in the crust by liquid immiscibility or crystal fractionation? Experimental data provide the following constraints: primary carbonatite magmas formed in mantle lherzolite at depths greater than ~70 km are dolomitic; melts richer in calcite can be formed only in wehrlites at shallower depths; immiscible carbonatite magmas formed in the crust have variable Ca/Na, with no more than 80% dissolved $CaCO_3$, and commonly less; dolomitic melts from fertile peridotite, and more calcic melts from immiscibility, can fractionate to yield sodic melts.

A test experiment confirms previous results in the join $NaAlSiO_4$-$NaAlSi_3O_8$-$CaCO_3$(Ne-Ab-CC)-H_2O (at 0.1 GPa and below 960 °C), illustrating that fractional crystallization of nepheline-normative silicate-CO_2 liquid can yield a residual carbonatitic liquid, precipitating calcite and becoming enriched in Na_2CO_3; the fractionation path passes below the silicate-carbonate liquid miscibility gap which exists at higher temperatures. The experiment with 10% H_2O (near $Ne_{35}CC_{65}$ by weight) at 833 °C identifies the crystallization reaction: 1 liquid + 0.2 melilite(sodic) + 0.2 CO_2 = 0.5 cancrinite + 0.6 calcite + 0.1 H_2O. The liquid quenches to a fine-grained assemblage including laths of nyerereite, equant grains of cancrinite, and calcite mostly precipitated in quench overgrowth rims enclosing cancrinite which border the round, primary calcite crystals. The liquid composition was determined from SEM and EDS analyses over areas up to 2,500 μm^2, modal counts, and mass balance calculations; the maximum H_2O content was assigned using published solubility data, yielding a liquid composition: 26% CaO, 10% Na_2O, 14% Al_2O_3, 15% SiO_2, 23% CO_2 and 11% H_2O, equivalent to 36%

nepheline, 43% calcite and 9% nyerereite with H_2O and about 1% Al_2O_3, slightly enriched in Na_2CO_3 compared with the starting material. Deductions from available experimental studies indicate that fractional crystallization of a hydrous CO_2-bearing nepheline-normative magma at moderate temperatures may produce continuous liquid compositions from silicate to carbonate-rich, precipitating a series of mineral assemblages analogous to rocks at the Oka Complex. Alkali-enriched carbonatite melts capable of precipitating cumulate sovites can be generated in several ways at crustal depths, but there is as yet no experimental evidence for petrological processes capable of forming nearly-pure $CaCO_3$ liquids at feasible temperatures and pressures. Previous claims for such liquids through immiscibility are now revised. The proposed existence of calciocarbonate parental magmas needs substantiation by a viable process.

INTRODUCTION

Three current debates about the origin and evolution of carbonatites are highlighted in the book edited by Bell (1989). Debates are concerned with: (1) where carbonatites come from, mantle or crust, (2) the composition of parental carbonatite magma, calcic, dolomitic, or sodic, and (3) whether carbonatites are derived from parent silicate magmas by fractional crystallization or by liquid immiscibility. This contribution is concerned with specific experimental data bearing on the third debate, but the discussions show that all of these problems overlap in terms of petrological processes.

Gittins (1989) addressed the first question by referring to the dichotomy "between those who saw carbonatites as developing essentially within the crust, or only slightly below it, by modification of a mantle-derived magma and those who emphasized the vexed question of a kimberlite-carbonatite association and took a quantum leap into the bowels of the earth to seek the birthplace of carbonatites." Isotope studies of carbonatites provide an unambiguous mantle signature (e.g. Bell, 1989), but Gittins (1989) pointed out that "what

was not settled, and still remains unclear, is whether carbonatite magmas originate by direct mantle melting or whether they evolve from a silicate, mantle-derived magma during low-pressure fractionation in the crust."

Barker (1989) reviewed the generally accepted field-based conclusion that most carbonatites are subordinate to associated silicate rocks, and therefore likely to be derived from a silicate parent in the crust. He found little evidence from the field relationships of carbonatites for primary carbonatite magma ascending directly from the mantle. Bailey (1993) challenged this view, arguing strongly that effusive calciocarbonatites (Keller, 1989) with mantle debris represent primitive melts from a mantle source. Haggerty (1989) concluded that carbonatites are derived by melting (fractional distillation) of a strongly metasomatized mantle layer about 50-75 km beneath rift zones. Gittins (1989) favored a scheme of primary carbonatite magmas from the mantle, which become "dominantly calcitic" by the time they reach the crust. There is microscopic evidence for primary calcite-rich magmas in mantle xenoliths. Pyle and Haggerty (1994) described the presence of natrosilicic and carbonatitic conjugate melts (calcite ocelli) in metasomatized eclogite xenoliths from Jagersfontein kimberlite. Kogarko and Pacheco (1994) similarly interpreted rounded oval segregations of calcite in silicate glass in a harzburgite nodule from the Canary Islands as quenched primary carbonate melt. These examples, and Bailey's (1993) candidates for mantle-derived calciocarbonatite magmas remain problematic because so far they lack an explanation in terms of feasible phase relationships.

Experimental data reviewed by Eggler (1989), Wyllie (1989), and Wyllie et al. (1990) demonstrate that carbonatite melts can be formed from CO_2-bearing mantle lherzolite at depths greater than about 75 km, but this melt is dominated by calcic dolomite, not calcite. They noted that while the occurrence of primary mantle carbonatite magmas was an interesting possibility, they expected the normal geological expression of such magmas to correspond more closely to that of kimberlites than to the common occurrence of carbonatites as small plutonic intrusions associated with much larger volumes of alkalic

rocks. Eggler (1989) provided an extensive discussion about possible primary mantle-derived carbonatite magmas, with useful displays of primary silicate melts and evolved carbonatites in Figs. 22.2 and 22.3, and cited only two examples among rare candidates for primary carbonatites. Dawson's (1994) description of the lavas and tuffs of the Igwisi Hills in Tanzania appear to match this expectation. He described the lavas as effusive kimberlites, but noted the similarity of the olivine-free matrix to carbonatite, with about 20% CO_2, 44% (CaO + MgO), and 15% SiO_2. Many carbonatites have SiO_2 this high (Woolley and Kempe, 1989), but it is lower in the near-solidus carbonatite melts determined from experiments with lherzolite; SiO_2 content increases with increasing temperature, however, and this lava is a possible example of primary mantle-derived carbonatite magma. Bailey's (1989) account of a mantle-derived carbonate melt (dolomitic) in Zambia is evidence that such melts may sometimes reach the surface. The Polino diatreme containing tuffisite of monticellite calciocarbonatite with mantle xenoliths described by Stoppa and Lupini (1993) is another occurrence with physical characteristics consistent with a mantle source, but again there is the problem of calcite rather than dolomite (see Dalton and Wood, 1993).

The second question, about the composition of parental carbonatite magmas, tends to be clouded by the extent to which carbonatites are viewed as cumulates, or as close representatives of magma composition. The only observed molten carbonatites are the unique natrocarbonatite lavas of Odoinyo Lengai, and Le Bas (1981) proposed that the full diversity of carbonatite rock types could be derived from this type of parental magma. Koster van Groos (1975) interpreted experimental data in terms of primary sodic carbonatite from the mantle being parental for the crustal, calcic carbonatites. Dawson et al. (1987) proposed that some calciocarbonatites are calcified alkali-carbonatites. Twyman and Gittins (1987) and Gittins (1989) rebutted this scheme, explaining the sodic carbonatite melt as a late-stage fractionation product which is consistent with phase relationships (Cooper et al., 1975). Bailey (1993) pointed out that the phase relationships were in fact

more consistent with an origin by remelting of alkali carbonates perhaps deposited in the volcanic edifice as high-temperatre sublimates. There is evidence that natrocarbonatites may be derivative from other carbonatite parents. Kogarko et al. (1991) concluded from the population of Na-rich carbonate inclusions in perovskite and calzirtite from a calciocarbonatite intrusion in Siberia that the parental magma was Ca-rich and developed Na-rich differentiates only during the latest stages. Veksler and Nielsen (1994) reached similar conclusions from carbonate inclusions in melilites from the Gardiner intrusion. Wallace and Green (1988) suggested that natrocarbonatite magmas could form by fractionation of a primary dolomitic magma from a fertile mantle.

The most abundant carbonatites are sovites, and Keller's (1989) recognition of the widespread occurrence of juvenile melt-droplets in carbonatite volcanism points to the eruption of magmas of calcium carbonatitic composition. Cooper and Reid (1991) presented spectacular textural evidence for quenched carbonate-rich liquid which they concluded were compatible with a Ca-rich carbonatite magma carrying liquidus calcite and dolomite and quenching into a subvolcanic environment. Bailey (1993), with additional evidence from calciocarbonatites intrusions occurring without associated silicate rocks, also assigned a major role to parental melts with composition near calcium carbonate. The central problem, therefore, is to determine the parental magma or magmas which precipitate sovites—are $CaCO_3$-rich magmas possible?

With respect to the third question, fractional crystallization or liquid immiscibility, Barker (1989) concluded that the tardiness of carbonatite emplacement into coeval, SiO_2-undersaturated, mafic, silicate plutonic rocks was consistent with their derivation by liquid immiscibility from fractionated silicate magma within the crust, and that silicate-rich carbonatites could be explained by mechanical mixing of nepheline-pyroxene cumulates from ijolitic magma with carbonatite (compare Treiman and Essene, 1985), or by carbonate metasomatism of silicate rocks. For carbonate-rich rocks (carbonatites) associated with kimberlites, however, he concluded that the mineralogical data favored an

origin through crystal-liquid fractionation, not liquid immiscibility. Dawson et al. (1994) presented evidence for coexisting carbonatite and silicate magmas in study of alkali carbonatite lavas from Oldoinyo Lengai. Experiments by Kjarsgaard and Peterson (1991) supported strongly an origin for Shombole carbonatite as immiscible melts from nephelinite, but they added that Mg-carbonatites may have more than one origin. Veksler and Nielsen (1994) concluded that primitive liquids observed as inclusions in Kugda perovskites could produce melilotites and associated carbonatites by fractionation of mica. Wyllie (1966), Watkinson and Wyllie (1971), Fanelli et al. (1986), and Otto and Wyllie (1993) presented experimental evidence that fractional crystallization in some silicate-CO_2 systems could yield residual melts precipitating calcite or dolomite.

Experiments by Kjaarsgaard and Hamilton (1988, 1989) led them to strong advocacy for universal carbonatite origin by liquid immiscibility over the experimentally-based conclusion of Watkinson and Wyllie (1971) that fractional crystallization of some silicate magmas could yield carbonatites. We present here a test and confirmation of the latter conclusion. Both processes may occur and the problem is to define the conditions (mainly magma composition and pressure) leading to one or the other (Lee and Wyllie, 1992a, 1992b, 1992c). We also reaffirm from phase relationships the problems of forming liquid magmas with compositions approaching pure $CaCO_3$ by any process under reasonable geological conditions.

PREVIOUS EXPERIMENTAL STUDIES ON IMMISCIBILITY AND FRACTIONATION

Here, we summarize the two lines of experimental data which need resolution. Watkinson and Wyllie (1971) concluded from experiments in $NaAlSiO_4$-$CaCO_3$-H_2O that fractional crystallization of the high-temperature nepheline-normative silicate liquids could yield low-temperature, calcic, carbonatite-like liquids. Kjarsgaard and Hamilton (1988,

1989) concluded from high-temperature experiments that a silicate-carbonate liquid miscibility gap cut across the compositions $NaAlSi_3O_8$-$NaAlSiO_4$-$CaCO_3$, extending to alkali-free compositions.

Carbonate-silicate liquid immiscibility

Koster van Groos and Wyllie (1966, 1968, 1973) reported immiscibility between silicate and carbonate liquids in plagioclase feldspar-Na_2CO_3 systems at 0.1 GPa, with and without H_2O, and compared the products with silicate magmas, carbonatite magmas and fenitizing solutions. Koster van Groos (1975) extended the range of compositions and pressures, and petrological applications. Verwoerd (1978) studied the miscibility gap in more complex systems at pressures between 0.2 and 1 GPa. Wendlandt and Harrison (1979), Hamilton et al. (1989), and Jones et al. (1995) reported trace element distributions between silicate and carbonate liquids. Hamilton et al. (1979) and Freestone and Hamilton (1980) determined the two-liquid field between natrocarbonatite lavas and phonolitic or nephelinitic magmas from the Oldoinyo Lengai volcano between 0.07 and 0.76 GPa and 900-1250 °C. A simplified version of the projection adopted by Freestone and Hamilton (1980) is used in Fig. 1 to illustrate the more recent results in synthetic systems. Silicate minerals and liquids plot in the lower left region of the triangle, and carbonate minerals and liquids plot near the CaO-Na_2O side.

Kjarsgaard and Hamilton (1988, 1989) confirmed the occurrence of liquid immiscibility between feldspars and calcite at 0.2 GPa and 0.5 GPa, and 1250 °C. The dashed lines A-A define their generalized, CO_2-saturated miscibility gap for several silicate-carbonate joins at 0.5 GPa and 1250 °C. The two notable features of A-A are that the miscibility gap extends all the way to the alkali-free join (contrast Koster van Groos and Wyllie, 1973), and that almost pure $CaCO_3$ liquid coexists with immiscible silicate liquid at 1250 °C. Brooker and Hamilton (1990) reported three immiscible liquids at 1.5 GPa

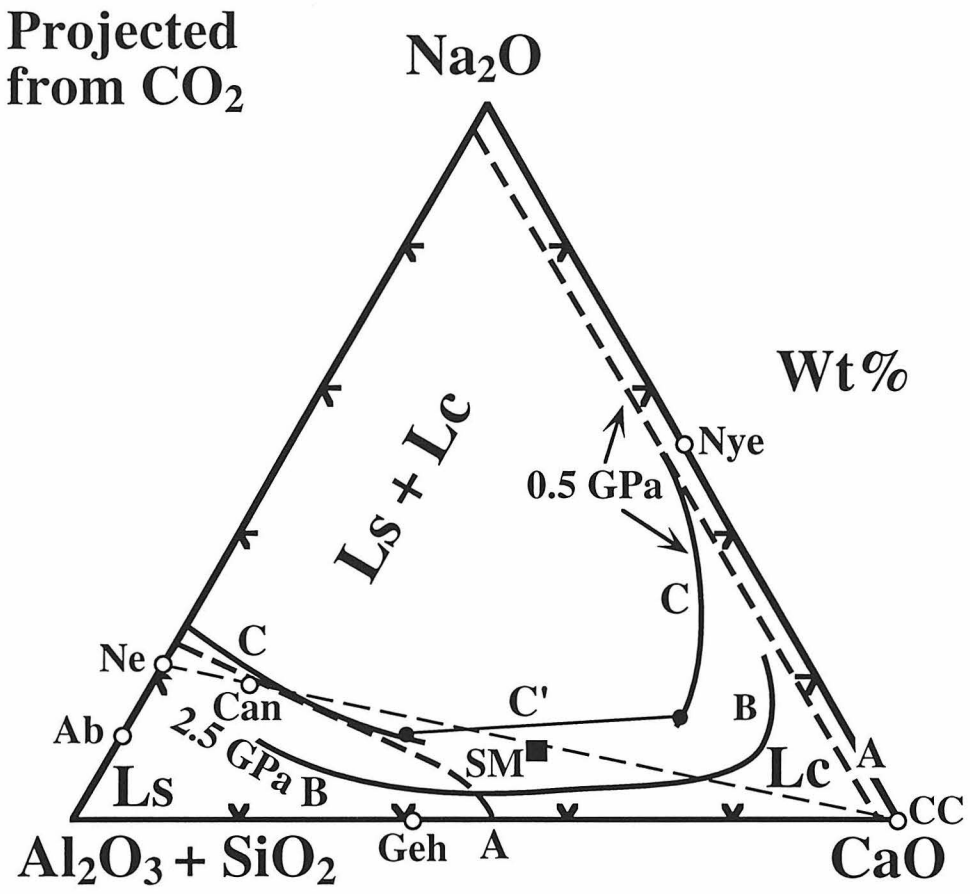

Figure 1. Field boundaries for published liquid miscibility gaps (with excess CO_2) projected into the triangle used by Freestone and Hamilton (1980), after Lee et al. (1994), with selected mineral components (open circles). Curves A-A: boundaries at 1250 °C and 0.5 GPa in the joins feldspars-(Ca+Na)carbonates according to Kjarsgaard and Hamilton (1988, 1989). Curve B-B: the solvus reported by Lee and Wyllie (1992a) in the join $NaAlSi_3O_8$-$CaCO_3$ at 2.5 GPa. Curves C-C: the miscibility gap revised from curves A-A by Kjarsgaard and Hamilton (in preparation; see Macdonald et al., 1993). The composition join Ne-CC intersects the two-liquid field, and the starting mixture SM used in this study is within the projected miscibility gap. Abbreviations: Ls - silicate liquid; Lc - carbonate liquid; CC - calcite, Ne - nepheline, Ab - albite, Nye - nyerereite, Can - cancrinite, Geh - gehlenite.

and 1225 °C, silicate- and carbonate-rich as expected, with the third almost pure $CaCO_3$ in composition.

Lee and Wyllie (1992a, 1992b) confirmed the miscibility gap in $NaAlSi_3O_8$-$CaCO_3$ at 2.5 and 1.5 GPa, and followed it to subliquidus temperatures. Their 2.5 GPa results are represented in Fig. 1 by the miscibility gap B-B. This does not reach the alkali-free compositions, and a conjugate carbonate-rich liquid contains at most 80% dissolved $CaCO_3$ (with about 10% each of Na_2CO_3 and silicate components). Macdonald et al. (1993) presented C-C in Fig. 1 as a revised version of the miscibility gap A-A (Kjarsgaard and Hamilton, in preparation), which is similar in shape to our result B-B at 2.5 GPa, with even less $CaCO_3$ in the carbonate liquid. According to Kjarsgaard (personal communication, 1994), the revision involves textural reinterpretation of the original runs.

In a more complex system, Kjaarsgard and Peterson (1991) found that immiscible liquids between lavas from Shombole volcano and carbonates, at 0.2 GPa and 0.5 GPa between 975 °C and 925 °C, projected into the appropriate, corrected fields in Fig. 1. Additional, similar results were given by Hamilton and Kjarsgaard (1993, Fig. 3). Baker and Wyllie (1990) located the silicate-liquid miscibility gap at 2.5 GPa using mantle-derived, primitive nephelinite, dolomite and alkali carbonate. When projected into Fig. 1 with additional components included (TiO_2 added to SiO_2; MgO and FeO added to CaO; K_2O added to Na_2O), the gap is significantly smaller than those plotted in Fig. 1 for the feldspathic compositions; the immiscible carbonate liquids are restricted to more alkalic compositions. This result added to those in Fig. 1 indicates that the size of the miscibility gap is dependent not only on pressure, but on bulk composition.

Selected phase relations in $NaAlSi_3O_8$-$NaAlSiO_4$-$CaCO_3$-H_2O: fractionation

Watkinson and Wyllie (1969, 1971) determined the phase fields intersected at 0.1 GPa by the joins $NaAlSi_3O_8$-$CaCO_3$-$Ca(OH)_2$ and $NaAlSiO_4$-$CaCO_3$-25%H_2O. The

results for $NaAlSiO_4$-$CaCO_3$-25%H_2O based on runs at 960 °C and below are reproduced in Fig. 2; the position of this composition join (H_2O-free) is plotted in Fig. 1 (dashed line). The interpretation of phase assemblages was based on optical study of crushed fragments in immersion oils, and x-ray powder diffraction. Evidence for liquid immiscibility was sought, but none was found. Patches of dendritic quenched minerals occurred within glass, but without the sharp and rounded interface boundaries that would be expected if the partly crystalline material represented an immiscible liquid.

Figure 3a shows a photomicrograph of crushed fragments of a quenched charge from Watkinson (1965). The open square in Fig. 2 shows the run conditions. The bulk composition corresponds to the square in Fig. 2 plus $Ca(OH)_2$, which causes melting to begin at lower temperature than the solidus in Fig. 2. The primary minerals cancrinite, melilite, and calcite are quite distinctive. The dark material attached to some minerals is fine-grained quenched liquid. Details of its texture and components cannot be discerned, although the birefringence of the aggregates indicates the presence of calcite. Watkinson and Wyllie (1971) concluded that the somewhat rounded grains of $CaCO_3$ represented calcite crystals, and not a liquid immiscible with the fine-grained silicate-carbonate quench aggregates. Wyllie and Tuttle (1960) interpreted subrounded and rounded $CaCO_3$ grains in CaO-CO_2-H_2O (without silicates) to be calcite crystals, and similar interpretations were consistent with observations of Huang and Wyllie (1974), Maaloe and Wyllie (1975), and Lee et al. (1994) in other silicate-carbonate systems.

Kjarsgaard and Hamilton (1988) noted that the join $NaAlSiO_4$-$CaCO_3$ on Fig. 1 cuts across their two-liquid field, A-A. This is also true for the more recent results, curves B-B and C-C. The absence of a miscibility gap in Fig. 2 led Kjarsgaard and Hamilton (1988) to conclude that "the two sets of data are in conflict". Wyllie (1989, p. 522) responded: "Let us avoid 'conflict' where none is established. The two sets of experiments represent very different conditions: those of Kjarsgaard and Hamilton (1988) were at high temperatures, super-liquidus, and mostly H_2O-free, whereas those of

Figure 2. Phase fields intersected by the join $NaAlSiO_4$-$CaCO_3$ with 25% H_2O at 0.1 GPa, after Watkinson and Wyllie (1971), based on runs at 960 °C and below and known data for $CaCO_3$-H_2O (Wyllie and Tuttle, 1960). SM gives the composition of our starting mixture (Fig. 1) projected onto this join, and the temperature of our new experiment. The blank square is a projection of an experiment by Wakinson (1965), with results illustrated in Fig. 3a. Abbreviations: Ne - nepheline, CC - calcite, Can - cancrinite, Mel - melilite, HH - hydroxyhauyne, L - liquid, and V - vapor. The numbered fields are: 1 - HH + Mel + Ne + L + V, 2 - HH + Mel + V, 3 - Can + HH + Mel + V, 4 - Can + Mel + V, 5 - Can + HH + Mel + Ne + V, 6 - Can + HH + Mel + L + V, and 7 - CC + L + V.

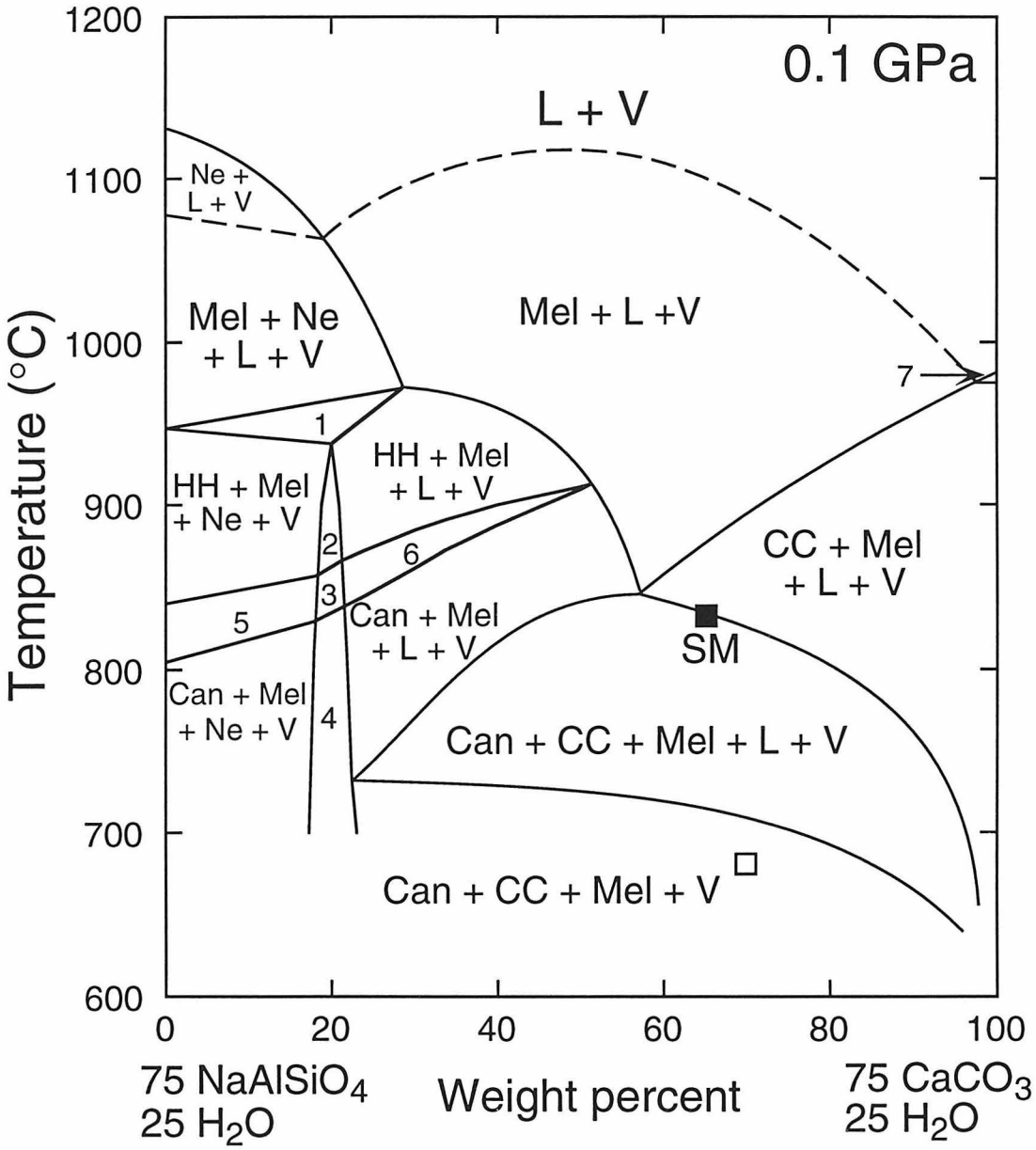
0.1 GPa
L + V
Ne +
L + V
Mel + Ne
+ L + V
Mel + L +V
7
1
HH + Mel
+ L + V
HH + Mel
+ Ne + V
2
6
3
5
Can + Mel
+ L + V
CC + Mel
+ L + V
SM
Can + Mel
+ Ne + V
4
Can + CC + Mel + L + V
Can + CC + Mel + V
Temperature (°C)
1200
1100
1000
900
800
700
600
0
20
40
60
80
100
75 NaAlSiO4
25 H2O
Weight percent
75 CaCO3
25 H2O

Figure 3. Photomicrographs of experimental runs: (b)-(d) are back-scattered electron images from SEM of Run SM.

(a) Crushed fragments in immersion oils from a run at 680 °C and 0.1 GPa in the join $NaAlSiO_4$-$CaCO_3$-$Ca(OH)_2$ (wt.%-30: 63: 7) with 25% H_2O (Fig. 2) illustrating the phases Can + Mel + CC + L; from Watkinson (1965), see Watkinson and Wyllie (1971). The run projects to the open square in the subsolidus region of Fig. 2; the product contains the Fig. 2 phase assemblage plus liquid, because of the additional component $Ca(OH)_2$ (Wyllie and Tuttle, 1960). It shows stubby prism of cancrinite (high relief), subrounded calcite, rectangular melilite plates, and dark masses of very fine-grained quenched L. Scale bar: 100 μm.

(b) Low magnification. There is no sign of immiscible silicate liquid beads. Large euhedral crystals (melilite, light) and small calcite (light spots) are distributed uniformly through the quenched carbonate-rich liquid (dark area, with light spots). The pits include vapor bubbles and cavities produced by plucking during polishing.

(c) Intermediate magnification. The large euhedral melilite crystals (lightest portion within the crystal outline, up to 100 μm) enclose calcite (somewhat darker, rounded), and quenched liquid. Calcite crystals (~10 μm, light) with irregular shapes are distributed through the quenched liquid (dark matrix). The dark equant grains (1-2 μm diameter) in the liquid and marginally enclosed in the calcite are quenched cancrinite. Primary cancrinite is much larger, as shown by the single, dark rounded crystal (~20 μm) in the upper left corner.

(d) High magnification. Calcite and quenched liquid. Calcite crystals have borders enclosing quench cancrinite. The quenched liquid consists of nyerereite (grey laths), quench cancrinite, and rare specks of calcite (1-2 μm).

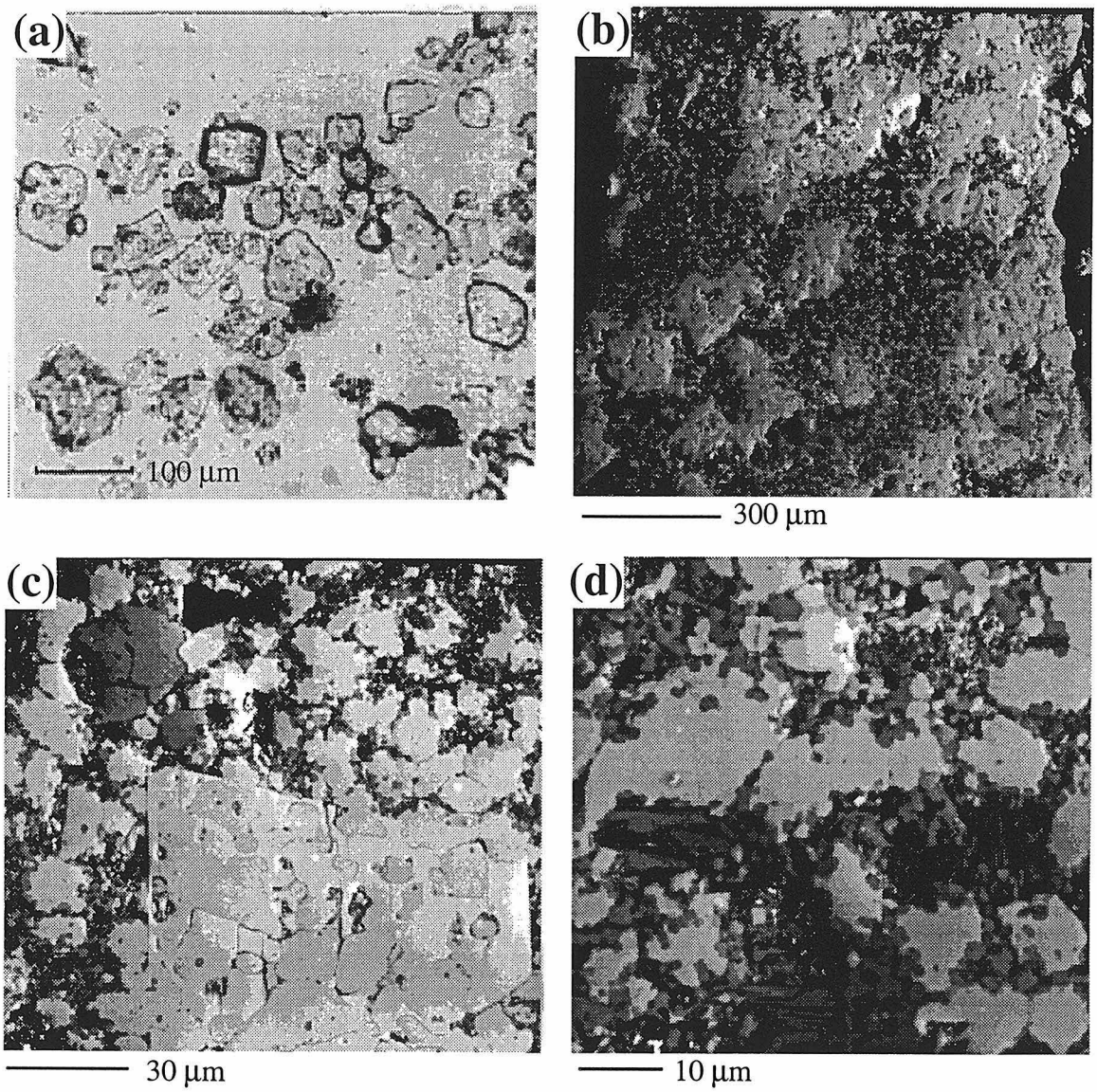
(a)
100 μm
(b)
300 μm
(c)
30 μm
(d)
10 μm

Watkinson and Wyllie (1971) were subliquidus, from 960 °C to 625 °C, and with 25% H_2O." However, the interpretation of these complex systems with non-quenchable phases nearly 30 years ago, using x-ray diffraction and optical examination of crushed fragments in immersion oils, was rudimentary compared with modern methods. Therefore, we considered it necessary to check the earlier results (Fig. 2) with the superior visual aid of a scanning electron microscope.

NEW EXPERIMENTS

The test was to check whether the presence of immiscible silicate and carbonate-rich liquids had been undetected by Watkinson and Wyllie (1971) in the many experimental runs used to construct Fig. 2, as implied by Kjarsgaard and Hamilton (1988, 1989). We chose one composition within the 2-liquid field of Fig. 1 (the solid square SM), very close to the join $NaAlSiO_4$-$CaCO_3$ (Figs. 1 and 2), and ran it at 833 °C and 0.1 GPa. The product was consistent with the previous results, with no evidence for two liquids.

Experimental Methods

The starting material was a mixture of primary standard grade calcite (Alfa Products) and a gel (made by A. F. Koster van Groos) with composition (by weight) 90% $NaAlSiO_4$ and 10% $NaAlSi_3O_8$. These materials were mixed under ethanol for an hour in the proportions 65% calcite and 35% silicate gel. The H_2O content of the mixture was at least 1.6%, determined by weight loss after heating at 300 °C for 2 hours. The mixture was sealed in a gold capsule along with 8.3 wt.% added H_2O, making a total of 10%.

The experiment was done in a rapid-quench cold-seal vessel with external thermocouple, designed and calibrated by Ihinger (1991). Pressure and temperature are accurate to ± 10 °C and ± 10 bars. The capsule was fixed to the top of a metal rod, which

can be moved up and down within the pressure vessel by means of an external magnet. The capsule was placed at the hot-spot of the vessel and held at 833 °C and 0.1 GPa for 24 hours. The run was terminated by removing the magnet and causing the capsule to drop into a water-cooled part of the pressure vessel, where it cooled nearly isobarically to room temperature within 2-3 seconds.

The capsule was peeled open and the sample was separated into two parts. One part was mounted with epoxy in a brass holder and polished without water, and the other part was ground with ethanol. Minerals present were identified by x-ray powder diffraction. The texture was studied on the polished surface using reflected light microscopy and scanning electron microscopy (SEM), providing the basis for distinction among minerals, quenched liquid, and vapor phases. Analyses were made by energy dispersive x-ray spectrometry (EDS).

Experimental Results

X-ray diffraction of the powdered sample after quenching revealed only the minerals melilite, calcite and cancrinite; peaks for portlandite were not detected. The observations described below confirm a phase assemblage of:

sodic melilite + calcite + cancrinite (trace) + liquid + vapor

which is consistent with the result obtained by Watkinson and Wyllie (1971) for the similar composition and temperature on the join $NaAlSiO_4$-$CaCO_3$-25%H_2O (Fig. 2), despite the lower H_2O content and addition of a few % of component $NaAlSi_3O_8$.

The polished surface of the white sample, viewed by the reflected light microscope, shows about 30-40% of large minerals evenly distributed through a sugary matrix. There is no sign of silicate glass beads, large or small. Small rounded cavities probably represent

a former vapor phase, but other cavities are caused by the plucking of minerals during polishing.

Figures 3b-d present back-scattered electron images. Figure 3b shows clusters of euhedral melilite crystals up to 100 μm diameter with smaller calcite grains set in an indeterminate matrix of quenched liquid. Note the cavities left by plucking. A large (70 μm) euhedral crystal of melilite is shown at higher magnification in Fig. 3c. The host melilite (lightest shade) encloses many subrounded calcite crystals (slightly darker grey) with diameters up to 10 μm, and some fine-grained, quenched liquid. About 50% of the sample (excluding the melilite) consists of somewhat irregular calcite grains commonly somewhat larger than the inclusions. Much smaller (1-2 μm), darker grey equant minerals of cancrinite are intergrown marginally with the calcite, and occur also in the regions of quenched liquid. There are also a few larger (~20 μm), subrounded polyhedra of primary cancrinite like the one in Fig. 3c (compare Fig. 3a).

Enlarged details of the calcite and quenched liquid are shown in Fig. 3d. The calcite has marginal overgrowths of calcite enclosing small cancrinites, with a few occurring in the centers. Only cancrinites are readily identified in the spaces between the calcite crystals with overgrowths, and these are set within a uniform matrix of similar color. The matrix includes laths of nyerereite (see below). There is no calcite visible within the interstitial matrix in Fig. 3d, and only rare traces elsewhere in the charge. It appears that during the quench, the calcite component of the liquid nucleated almost exclusively on the prexisting calcite crystals.

Phase compositions

EDS analyses of the mineral and liquid phases are listed in Table 1, and projected into Fig. 4. Melilite compositions plot near A, with about 8 wt.% Na_2O, representing solid solution between gehlenite and soda melilite (63%). This is consistent with Watkinson and

Wyllie's (1971) identification of sodic melilites from refractive indices. Cancrinite analyses plot near B, with the compositions of quench crystals (triangles) somewhat richer in CaO than primary minerals (squares). Quench cancrinites were so small that only spot analyses could be made, and their different composition could be due to sodium migration during analysis, as suggested by analyses of the larger primary cancrinites. Table 1 shows that cancrinite analysis by spot mode has about 3 wt.% less Na_2O than the analyses by rastering mode. The laths occupy a range of compositions near C (filled diamonds), corresponding to nyerereite exhibiting various degrees of Na-migration during analysis, and contaminated by small amounts of cancrinite and possibly calcite. Calcites were analyzed, but not tabulated; some analyses contain trace amounts of Na, Al or Si, but these are interpreted as below the detection limit in the EDS system, or as contamination by the surrounding material.

The original liquid composition could not be obtained by direct measurement of the quench matrix, because calcite was removed during quenching to the overgrowths, and H_2O was lost. In order to determine the liquid composition, we first performed two defocused-beam analyses (open diamonds D, Fig. 4) in the rastering mode of large areas (2,500 μm^2) between the melilites, including the primary calcite grains, and the quenched liquid, quenched cancrinite, nyerereite quench laths, and calcite overgrowths on the primary crystals. The average norm (by mass balance calculations) of the material D is: cancrinite = 44%, calcite = 47%, nyerereite = 9%. Stoichiometric compositions for the three mineral components were used, because of the difficulty in obtaining precise mineral analyses, as outlined above (e.g., Na-migration problem). There was about 2% of Al_2O_3 unaccounted for in the bulk analysis, and this must either be Al_2O_3 in the liquid, or perhaps contamination from the alumina polishing powders.

The amount of calcite quenched from liquid was estimated from modal measurements. Mineral boundaries were traced from SEM photos (Fig. 3d), and for each calcite grain, two sketches were made, estimating the maximum and minimum width of

Table 1. EDS/SEM analyses for Run SM on a volatile-free basis.

	SM	A	B			C			D	
		[Mel]	[Can]		[QC]	[Nye]			[L + CC]	
Wt.%		(4)	(2)	*	(6) *			*		
Na_2O	10.2	7.8	20.7	17.1	16.8	50.7	45.8	45.9	41.2	25.5	14.7	13.4
CaO	51.0	28.8	10.1	10.1	13.8	44.8	40.8	52.6	55.7	71.5	43.8	46.4
Al_2O_3	16.8	26.3	33.6	34.5	32.9	1.5	6.3	0.5	1.3	1.0	20.8	20.6
SiO_2	22.0	37.1	35.7	38.2	36.6	3.0	7.0	1.1	1.8	2.0	20.6	19.6

Abbreviations. SM: starting mixture; A: melilite (Mel); B: primary and quenched cancrinite (Can and QC, respectively); C: quenched nyerereite (Nye); D: quenched liquid + primary calcite (L + CC) over area of 2500 mm^2; *: analyses by spot mode. The parentheses indicate the number of analyses made. The data are all normalized results on a volatile-free basis from original analyses. Notice that all nyerereite analyses (C) are tabulated to show the variations due to contamination by surrounding material and Na-migration during the analyses. The data for calcite are not listed in the table.

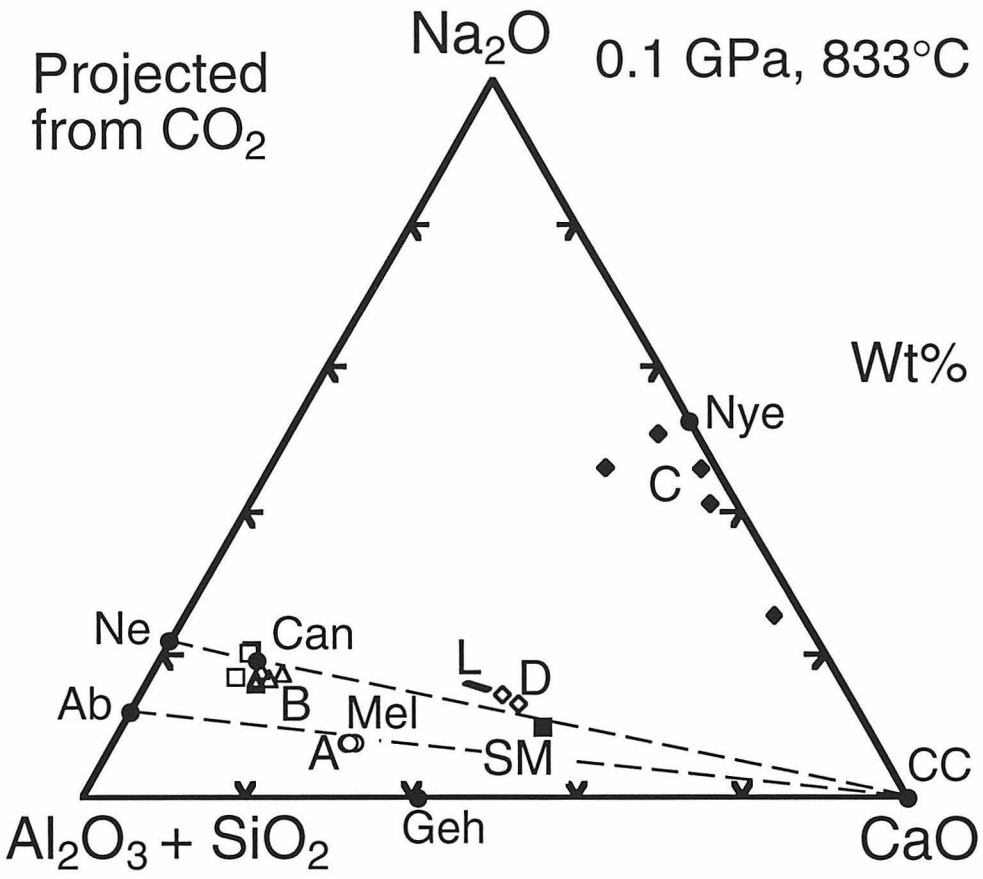

Figure 4. The Hamilton projection (abbreviations, see Fig. 1), giving the compositions of phases analyzed from experiment SM (Table 1). Open circles (A) are sodic melilite (Mel), open squares are cancrinite (Can), open triangles (B) are quenched cancrinite, open diamonds (D) are analyses in raster mode including the dark matrix, quenched cancrinite and calcite grains in Fig. 3d, and closed diamonds (C) are analyses of dark lath-like material (quenched nyerereite, Nye) in Fig. 3d. L is the estimated composition of liquid, calculated from analyses, partial modes, and mass balance.

the quench overgrowth as identified and mapped from the distribution of cancrinite inclusions. The sketches were then point-counted for the areas of the primary calcite and the calcite overgrowths. The minimum estimates for primary calcite included in the two modes averaged 9%, and the maximum amount averaged 15%. Subtraction of primary calcite from the analyses of material D indicates a small range of liquids represented by the area L in Fig. 4.

Table 2 compares the composition of the starting mixture, SM, with the liquid under run conditions. The H_2O-free liquid is the average composition resulting from the two analyses of D (Table 1, Fig. 4) less the two modal estimates for primary calcite. Notice that the appropriate Al_2O_3 has been assigned into the H_2O-free value in Table 2, but it is actually determined later, as indicated in the next paragraph. The 25% CO_2 determined stoichiometrically is a maximum value, because some CO_2 may have been extracted from the vapor during quench. The normalized CO_2-free (volatile-free) liquid composition is also listed; this corresponds to liquid L projected into Fig. 4.

The complete liquid composition listed in Table 2 was derived by distributing the 10% H_2O in the mixture between liquid and vapor. Experimental data on the ratios of H_2O to $H_2O + CO_2$ for a CaO-CO_2-H_2O liquid at 0.1 GPa and 833 °C (Wyllie and Tuttle, 1960) were used to calculate the maximum possible amount of H_2O that would dissolve in the liquid L. A set of mass balance calculations is preformed, using the known compositions of the primary phases, melilite, calcite, and the liquid corresponding to the norm calculation (not listed). These calculations determine the vapor composition, the amount of excess Al_2O_3 in the liquid, and the proportion of each phase, assuming only CO_2 and H_2O in the vapor, and negligible primary cancrinite. The values obtained, $X^L_{H2O} = 0.33$ and $X^V_{H2O} = 0.55$ (weight fraction), are consistent with results in other systems, where H_2O is preferentially partitioned into vapor rather than into carbonate-rich liquid. The phase proportions from the calculations are: liquid 52%, melilite 16%, calcite 26%, vapor 6%, and trace cancrinite. The actual vapor composition contains dissolved solid

components. Watkinson and Wyllie (1971) recorded crystals of $NaHCO_3$ precipitated from vapor during the quench in carbonate-rich compositions in their join, with 25% rather than 10% H_2O, but quantitative data are not available.

INTERPRETATION OF RESULTS

Crystallization reaction

Figure 5a shows the four measured and estimated phase compositions for the starting mixture SM at 833 °C, 0.1 GPa (Figs. 2 and 4; Tables 1 and 2). The reaction tie-figure is projected from (CO_2 + H_2O), and vapor is not shown. The chemography of the tie-figure shows that with decreasing temperature, melilite is resorbed as cancrinite and calcite are precipitated. This figure is opened into a tetrahedron in Fig. 5b, with apex CO_2 + H_2O, neglecting the unknown solubility of other components in the vapor. Cancrinite contains 8.4% CO_2 (stoichiometry), and the liquid contains about 23% CO_2 and 11% H_2O (Table 2). Whether the tie-figure is drawn using analyses normalized for CO_2 alone or for CO_2 + H_2O, the geometry is as shown in Fig. 5c with the line Can + CC piercing the triangle Mel + L + V, consistent with the reaction relationship between melilite and liquid:

liquid + melilite + vapor = cancrinite + calcite

with coefficients determined on the basis of the measured and the estimate phase compositions (Tables 1 and 2):

1 liquid + 0.2 melilite + 0.2 CO_2 = 0.5 cancrinite + 0.6 calcite + 0.1 H_2O.

Figures 5b and c show that in a closed system at equilibrium, CO_2 is extracted from vapor as well as from liquid for the precipitation of cancrinite and calcite.

Table 2. Analyses of liquid and vapor compositions from run SM.

	SM	H_2O-free Liquid	Volatile-free Liquid	Complete Liquid	Vapor
Wt%					
CaO	33.1	30	41	26	--
Na_2O	6.6	12	16	10	--
Al_2O_3	11.6	16	20	14	--
SiO_2	13.6	17	23	15	--
CO_2	26.0	25	--	23	45
H_2O	9.1	--	--	11	55
Total	100.0	100	100	99	100
$H_2O/(H_2O+CO_2)$	0.26	--	--	0.33	0.55

Figure 5. The 5-phase assemblage in Run SM (phase compositions from Fig. 4) corresponds to the reaction CC + Can = Mel + L + V or, with decreasing temperature, a reaction relationship between melilite and L + V, associated with the precipitation of calcite and cancrinite as indicated in Fig. 2. (a) The tie-figure for the vapor-absent assemblage (Fig. 4). (b) The 5-phase tie-figure within a quaternary projection of the 6-component system. (c) The tie-figure from (b) showing relative compositions of the reaction phases. Abbreviations: see Fig. 2.

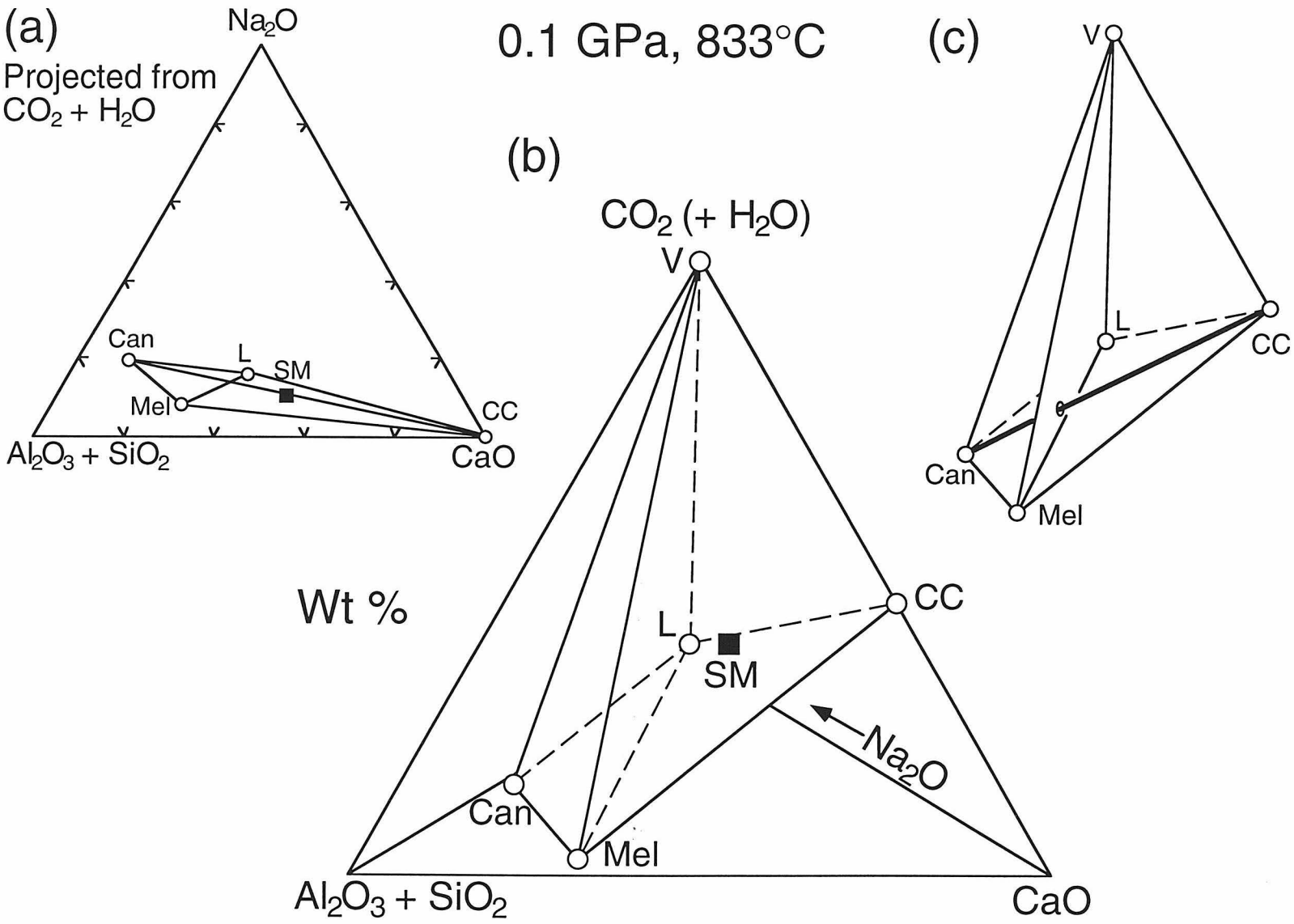
(a)
Projected from
$CO_2 + H_2O$
Na_2O
Can
L
SM
Mel
CC
$Al_2O_3 + SiO_2$
CaO
0.1 GPa, 833°C
(b)
CO_2 (+ H_2O)
V
CC
L
SM
Wt %
Na_2O
Can
Mel
$Al_2O_3 + SiO_2$
CaO
(c)
V
L
CC
Can
Mel

Possible phase diagram for $NaAlSiO_4$-$CaCO_3$-H_2O

The Kjarsgaard and Hamilton (1988, 1989) results in Fig. 1 (curves A-A revised to curves C-C in Macdonald et al., 1993) demonstrate the occurrence of a miscibility gap at high temperatures in the join $NaAlSiO_4$-$CaCO_3$, which is confirmed by our results (curve B-B in Fig. 1). Koster van Groos and Wyllie (1973) found that a miscibility gap persists between plagioclase feldspars and Na_2CO_3 with H_2O added, so we assume that adding 10% H_2O does not destroy the miscibility gap in $NaAlSiO_4$-$CaCO_3$. Therefore, we have represented this high-temperature miscibility gap by the phase field between A and B in Fig. 6 (based on curves C-C in Fig. 1).

Our starting mixture, SM, has composition in the middle of the interval AB (Fig. 1), but there is no evidence for liquid immiscibility. This result is consistent with the results of Watkinson and Wyllie (1971), and we conclude that in the presence of 10% H_2O, immiscible liquids are not encountered at temperatures below 960 °C. Therefore, concluding that both sets of experiments are correct, we present Fig. 6 as an interpretation showing the main features of the phase fields intersected by the join $NaAlSiO_4$-$CaCO_3$ in the presence of H_2O, with the high-temperature miscibility gap terminating downwards at some undetermined temperature, and without attempting to devise detailed connections with the lower temperature phase relationships transferred from Fig. 2. This interpretation is bolstered by new detailed results in $NaAlSi_3O_8$-$CaCO_3$ at higher pressures (Lee and Wyllie, 1992a, 1992b, 1992c), where we have determined that there is indeed an interval for [crystals + liquid + vapor] between the high-temperature miscibility gap and the solidus, even without H_2O to lower the solidus temperature.

Crystallization paths and liquid compositions

Comparing the phase fields and compositions in Figs. 4, 5, and 6, we obtain the

Figure 6. Partly schematic phase diagram showing how two different sets of results can be combined to satisfy both. The phase fields intersected by the join $NaAlSiO_4$-$CaCO_3$ with 25% H_2O at 0.1 GPa, after Watkinson and Wyllie (1971), modified from Fig. 2 to include the high-temperature miscibility gap A-B between silicate-liquid Ls and carbonate-liquid Lc , which is based on C-C in Fig. 1 (Kjarsgaard and Hamilton's revision of their 1988, 1989 curves, A-A). The dotted line is an arbitrary connection, which could be completed in different ways. Note the piercing point P (see text). The liquid composition L from Fig. 4 (run SM) is projected onto the join as the shaded circle [L]. Abbreviations and numbered phase fields: see Fig. 2.

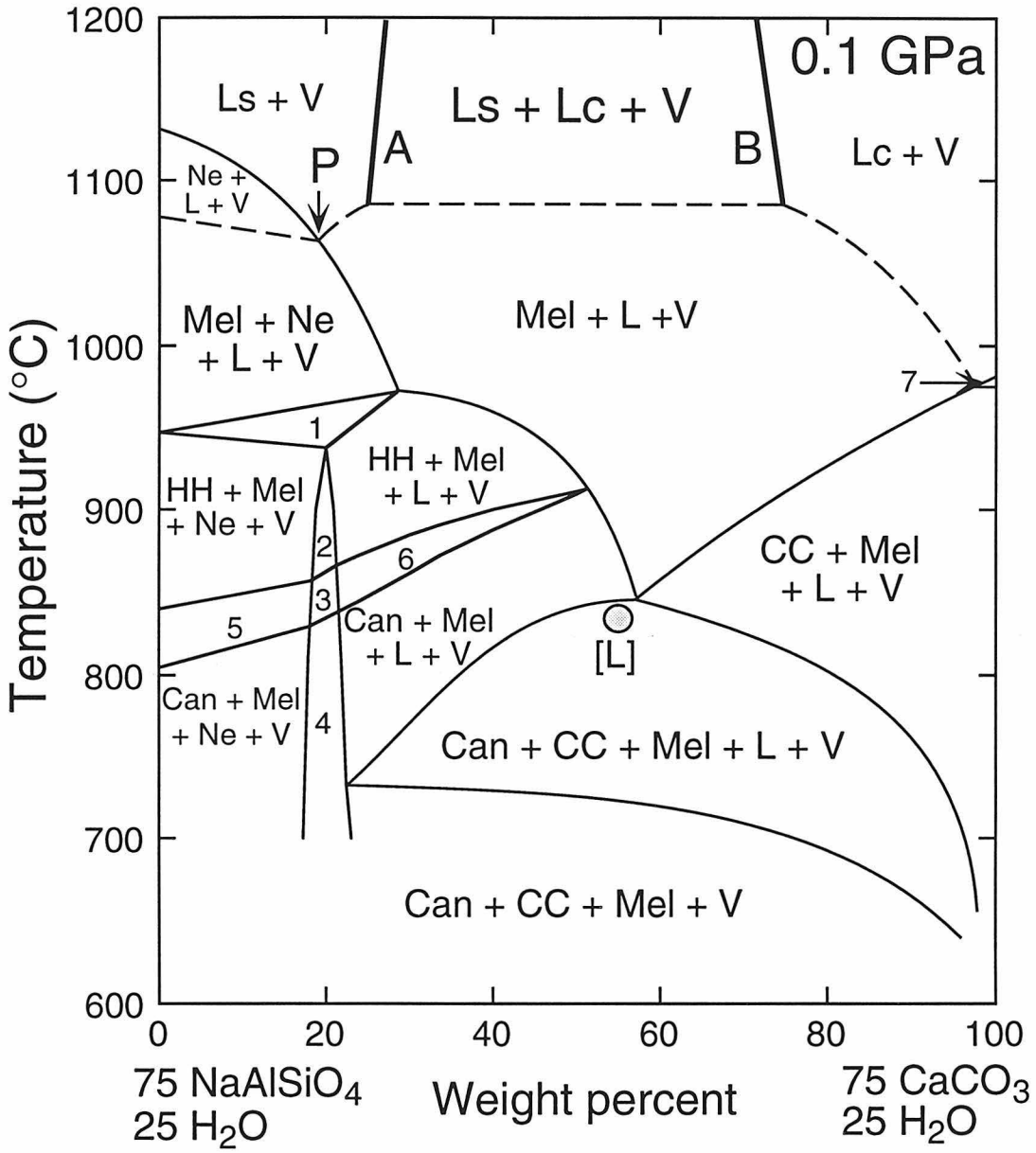
0.1 GPa
Ls + V
Ls + Lc + V
Lc + V
A
B
P
Ne + L + V
Mel + Ne + L + V
Mel + L +V
7
1
HH + Mel + L + V
HH + Mel + Ne + V
2
6
3
5
Can + Mel + L + V
[L]
CC + Mel + L + V
Can + Mel + Ne + V
4
Can + CC + Mel + L + V
Can + CC + Mel + V
Temperature (°C)
1200
1100
1000
900
800
700
600
0
20
40
60
80
100
75 NaAlSiO4
25 H2O
Weight percent
75 CaCO3
25 H2O

following generalizations about closed-system crystallization trends from high temperatures at the silicate end of Fig. 6 to lower temperatures at the carbonate end. Original silicate liquids with dissolved CO_2 and H_2O become enriched in carbonate components, as they precipitate or react with silicate minerals and vapor, and eventually they precipitate cancrinite and calcite. Details of paths of crystallization cannot be read from Fig. 6 because this is a slice through a 6-component system, and mineral and liquid compositions diverge from the join (Fig. 4). Watkinson and Wyllie (1971) approached the problem of interpretation by constructing field boundaries and following paths of crystallization in a schematic pseudoternary system nepheline-melilite-calcite. They described paths of equilibrium and fractional crystallization, and used them to reach the following conclusion derived from the phase fields intersected in Fig. 2. The successive crystalline products of fractional crystallization of an original assemblage of liquid + vapor with composition [90% Ne: 10% CC] + 25% H_2O are the mineral assemblages listed in Table 3, which also shows the approximate temperature intervals within which each assemblage would be precipitated. These assemblages are similar to Oka rock types (less mafic minerals), as shown in Table 3.

It can be seen from Figs. 4 and 6 that the precipitation of nepheline, melilite, hydroxyhuayne, and cancrinite from the initial liquid should drive the residual liquid toward $CaCO_3$, with enrichment in Na_2CO_3. The experimental liquid composition L in Figs. 4 and 5 is slightly enriched in Na_2CO_3 compared with the original mixture SM. The liquid must eventually reach a liquidus boundary between silicates and calcite, shown in Fig. 6 by the upper phase boundary for calcite. Liquid L is a point on this silicate-carbonate field boundary, and projection of L onto Fig. 6 shows its position just below the calcite phase boundary. When this boundary is reached, the coprecipitation of calcite along with silicate(s) will cause the liquid path to change direction, driving it toward enrichment with Na_2CO_3 (Cooper et al., 1975). The coexisting vapor is simultaneously enriched in sodium and H_2O (Watkinson and Wyllie, 1971).

Table 3. Comparison of Oka rocks with corresponding mineral assemblages in phase diagram for $NaAlSiO_4$-$CaCO_3$-H_2O at 0.1 GPa (after Watkinson and Wyllie, 1970).

Mineral assemblages from phase diagram	**Approximate temperatures of crystallization**	**Oka rocks**
nepheline	< ~1100 °C	(1) the jacupirangite-melteigite-ijolite-urtite group
nepheline + melilite	< ~1080 °C	(2) nepheline okaite
hydroxyhaune + melilite	< ~970 °C	(3) okaite
cancrinite + melilite	< ~880 °C	(4) okaite
calcite + cancrinite + melilite	< ~830 °C down to < 700 °C	(5) carbonatites

Details of the connections between the miscibility gap (AB) and the lower-temperature phase fields of Fig. 2 remain unknown. In Fig. 6 we have simply connected them in the simplest way. Note the piercing point P for coprecitation of nepheline and melilite; with this arrangement, a liquid precipitating nepheline would not reach the miscibility gap until after coprecipitation of melilite, and possibly not at all, depending upon the overall phase relationships. Under these conditions, fractional crystallization is the dominant differentiation process. An alternative arrangement could have a piercing point between the liquidus field for nepheline and the miscibility gap at A, which would mean that liquids on this join which precipitate nepheline would reach the miscibility gap at A, and split off a high-temperature carbonate-rich liquid with composition on the consolute surface passing through phase boundary B in Fig. 6. The distribution of 2-liquid tie-lines in Figs. 1 and 7 ensures that the immiscibile carbonate liquid would be considerably enriched in Na_2CO_3.

PETROLOGICAL APPLICATIONS

Three current debates were reviewed in the Introduction: Primary carbonatites from mantle or crust? Parental carbonatite magmas calcic, dolomitic, or sodic? Carbonatite magmas from parent silicate magmas by fractionation or liquid immiscibility? As evident from the discussion, these questions overlap in several ways. An overview is presented in Fig. 7, where we consider the petrological problems associated with these debates in terms of the following processes and topics, based on experimental constraints: (1) the generation of carbonatite melts in mantle peridotite, (2) the generation of immiscible carbonate liquids from a silicate parent magma, (3) the range of compositions of carbonatite magmas which can be derived from silicate rocks or magmas, and (4) the fractionation of silicate parent magmas to residual liquids precipitating carbonates. Fig. 7 corresponds to the projection of Fig. 1, with the additional components required for the

Figure 7. Hamilton projection (see Fig. 1) projected from ($H_2O + CO_2$) showing reported miscibility gaps, natural liquid compositions, and possible paths of crystallization of magmas. KH is a miscibility gap based on C-C (Fig. 1) representing crustal conditions and relatively low Mg contents. BW is a miscibility gap (Baker and Wyllie, 1990) for mantle pressures and more magnesian compositions. Liquid compositions are tabulated in Table 3: WG in area (1) is the projection of the mantle carbonate melt from fertile pyrolite from Wallace and Green (1988); E, the eutectic liquid in the join $CaCO_3$-$Na_2Ca(CO_3)_2$ (Cooper et al., 1975); PH, carbonate-rich liquid in an eclogite xenolith, calculated by Pyle and Haggerty (1994); OL, Oldoinyo Lengai natrocarbonatite (Dawson et al., 1987); F, alkali carbonate fluid inclusion (Le Bas, 1981). Path (2) illustrates the cooling path of a carbonated silicate magma (s) intersecting the two-liquid field KH to form a sodic carbonatite melt (c) at the other end of the tie-line. Path (3) represents the differentiation trend of a high-temperature sovitic magma, remaining in equilibrium with the silicate magma from which it is separating. The trend toward a lower-temperature sodic residuum is required by the precipitation of calcite, but there may be variations depending on the silicate phase relationships along the consolute Ls field boundary. The silicate-carbonate Lc liquidus field boundary at lower temperatures, between path (3) and the carbonate side, probably follows the simple trend shown for path (3). Path (4) represents the cooling path of a hydrous carbonated silicate magma which passes through the liquid composition L of this study (Fig. 4), beneath the miscibility gap (Fig. 6), towards sodium enrichment (Cooper et al., 1975). Abbreviations: Ls - silicate liquid; Lc - carbonate liquid; Nye - nyerereite.

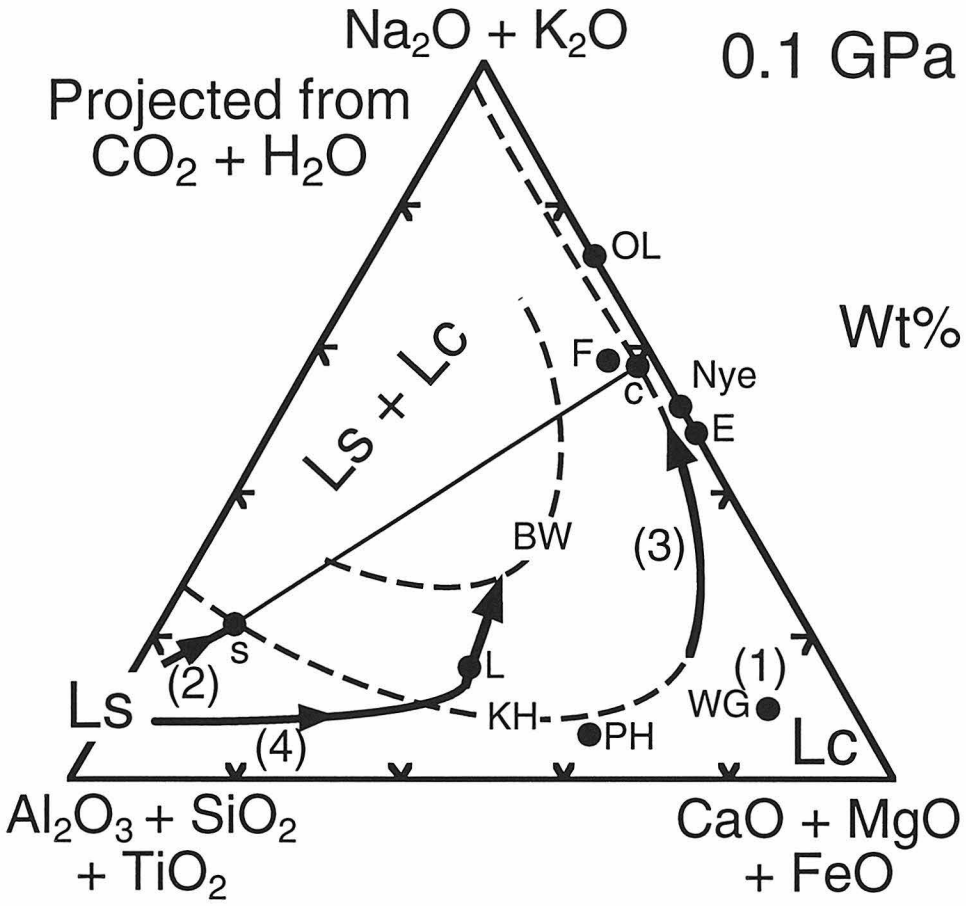
$Na_2O + K_2O$
0.1 GPa
Projected from
$CO_2 + H_2O$
OL
Wt%
F
C
Nye
E
Ls + Lc
BW
(3)
s
(2)
L
(1)
Ls
KH
WG
PH
Lc
(4)
$Al_2O_3 + SiO_2$
$+ TiO_2$
$CaO + MgO$
$+ FeO$

Table 4. Carbonate-rich liquids, experimentally determined, and inferred from rocks.

Wt%	L	WG	E	PH	OL	F
SiO_2	15	2.94	--	15.12	0.10	2.1
TiO_2	--	0.45	--	0.04	0.01	--
Al_2O_3	14	1.95	--	7.58	0.03	1.0
Cr_2O_3	--	0.22	--	--	--	--
Fe_2O_3	--	--	--	--	0.29	--
FeO	--	4.61	--	0.83	--	0.9
MnO	--	--	--	0.03	0.25	--
MgO	--	14.19	--	0.53	0.26	--
CaO	26	21.29	29.7	38.60	13.93	19.8
Na_2O	10	4.99	27.5	3.68	30.30	26.3
K_2O	--	0.35	--	0.24	6.55	6.1
SrO	--	--	--	--	1.41	0.5
BaO	--	--	--	0.06	0.98	4.4
CO_2	23	--	42.8	30.79	33.90	29.2
SO_3	--	--	--	--	3.23	4.4
P_2O_5	--	0.48	--	--	1.13	--
F	--	--	--	--	1.20	1.4
Cl	--	--	--	--	2.45	6.9
H_2O^+	11	--	--	3.08	4.51	--
Less O = Cl, F	--	--	--	--	2.18	2.4
Total	99	51.49	100.0	100.58	100.70	100.0
Na_2O/CaO (molar)	0.4	0.2	0.9	0.09	2.0	1.2
Ca/Mg (molar)	--	1.1	--	0.02	0.03	--

Abbreviation: L - calculated liquid composition from the experiment SM; WG - carbonatite melt in equilibrium with peridotite assemblage determined by Wallace and Green (1988); E - eutectic liquid in the join $Na_2Ca(CO_3)_2$-$CaCO_3$ (Cooper et al, 1975); PH - calculated bulk liquid for immiscible carbonate and natrosilicic liquids by Pyle and Haggerty (1994); OL - fresh natrocarbonatite, BD118, from Oldoinyo Lengai (Dawson et al, 1987); F - fluid/melt inclusion in apatite from ijolite in Le Bas (1981). Note that iron contents are expressed as FeO, except in OL, and CO_2 in WG is not listed.

more complex rocks and magmas listed in Table 4 (Freestone and Hamilton, 1980).

Primary carbonatite melts from the mantle

The reactions controlling the generation of carbonate-rich melts in peridotite, and their compositions, were determined in phase equilibrium experiments and theoretical analyses in model systems including those of Newton and Sharp (1975), Wyllie and Huang (1975, 1976), Eggler (1978), Wendlandt and Eggler (1980a, b), Olafsson and Eggler (1983), Woermann and Rosenhauer (1985), Wyllie (1989), Eggler (1989), and White and Wyllie (1992). The liquid composition is dominated by dolomite, with SiO_2 < 5%, Ca/Mg = ~2 (Wyllie and Huang, 1975; Wyllie et al., 1983), and with alkalis dissolved to the extent that they are available in the source peridotite or fluxing vapor (Wyllie, 1977).

These values were confirmed by the experiments of Wallace and Green (1988) using a fertile pyrolite; specifically, they measured a carbonatite liquid composition with 21% CaO, 14% MgO, 4.6% FeO, and 5% Na_2O (Table 3, WG). WG in area (1) of Fig. 7 is a projection of this composition. Subsequent experiments with a variety of peridotite compositions yielded similar results, with variable alkali contents of the dolomitic (calcic) melts reflecting directly their contents in the source peridotite (Ryabchikov et al., 1982; Thibault et al., 1992; Dalton and Wood, 1993; Sweeney, 1994). In experiments at 5 GPa, Ryabchikov et al. (1989) demonstrated that with increasing pressure, partitioning of Na into carbonate melt becomes less pronounced, due to the stabilization of jadeitic component in clinopyroxene with increasing pressure as also observed for equilibria involving clinopyroxene + aqueous fluid (Ryabchikov et al., 1982).

Wallace and Green (1988), Falloon and Green (1989), and Wyllie and Rutter (1986, see Wyllie, 1987) determined the minimum pressure for the formation of dolomitic carbonatite liquids in natural lherzolite compositions to be between 2 and 2.2 GPa, lower by 0.5-0.8 GPa than in the model systems (Wyllie and Huang, 1975; Eggler, 1978).

Olaffson and Eggler (1983) placed the pressure at 1.75 GPa. Dalton and Wood (1993) confirmed that carbonatitic melts can persist to lower pressures with peridotite, but only if lherzolite is converted to wehrlite (reaction 6y in Figs. 10 and 11D of Wyllie and Huang, 1976) by metasomatic reactions between orthopyroxene and carbonatite melt (e.g. Rudnick et al., 1993), and the melt is then enriched in Ca/Mg.

Figure 7 compares selected liquid compositions from Table 4 with mantle carbonatite (1). PH, the carbonate-rich liquid (which subsequently unmixed yielding calcite ocelli) in an eclogite xenolith reported by Pyle and Haggerty (1994) is significantly more siliceous. The natrocarbonatite lavas of Oldoinyo Lengai (OL) and a fluid inclusion in apatite (F) are far removed from the primary mantle liquid, but Wallace and Green (1988) suggested that extensive fractional crystallization of dolomite from liquid (1) could yield alkalic residual liquids. Sweeney et al. (1995) later indicated that for the process to yield a close match to the OL composition, the parental magma would need to be more silicic, less iron-rich, and with higher K/Na than the liquid (1). Baker and Wyllie (1990) showed that the primary mantle carbonatite liquid (1), and probable liquid paths with progressive melting, are unlikely to intersect the silicate-carbonate liquid miscibility gap at depth. For the relevant magnesian compositions, the miscibility gap BW in Fig. 7 is much reduced compared with the calcic compositions (KH, compare Fig. 1).

The experimental evidence is clear–primary carbonatite magmas from the mantle should be dolomitic. Natrocarbonatites can not be primary magmas from the mantle. The formation of magmas richer in Ca/Mg approaching calciocarbonatite compositions requires conditions that appear to be uncommon in the mantle, namely a wehrlite source. Perhaps primary dolomitic carbonatites can fractionate en route to the surface to yield liquids which precipitate calcite, but there is as yet no experimental evidence for the formation of extremely $CaCO_3$-rich calciocarbonatite liquids from peridotites. The small percentages of mantle-derived primary carbonatite melt expected to be generated in the source rocks are probably similar to those of kimberlite melts, supporting the conclusion that primary

carbonatites should be emplaced as small explosive volcanoes or diatremes, not associated with large volumes of kindred silicate magmas.

Immiscible carbonate liquids

The miscibility gap between silicate and carbonate liquids varies as a function of temperature, pressure, and bulk composition. Figure 7 shows selected polythermal phase boundaries for coexisting silicate (Ls) and carbonate liquids (Lc). The curve KH corresponds to C-C in Fig. 1, for the synthetic MgO-free system Na_2O-CaO-Al_2O_3-SiO_2-CO_2 at crustal pressures (< 0.5 GPa). This field expands with increasing pressure (B-B in Fig. 1). The curve BW represents mantle conditions, determined at 2.5 GPa by Baker and Wyllie (1990) for primitive magnesian nephelinite, dolomite and Na_2CO_3. The miscibility gap is much smaller than C-C; it increases in size with decreasing pressure (Lee and Wyllie, 1994, and manuscript in preparation) in contrast with the MgO-free system. Other variations in bulk composition remain to be explored before the variations in the miscibility gap are completely defined. For example, Kjarsgaard and Peterson (1991) have shown that Na_2O/CaO in the immiscible carbonate liquid depends not only on the same ratio in the silicate liquid, but also rather critically on peralkalinity: $(Na+K)/(Al+Fe^{3+})$.

Nepheline-normative silicate liquids with dissolved carbonate components have compositions in the lower left corner of Fig. 7. With cooling, many such magmas are expected to follow paths which reach the two-liquid field KH. Curve (2) is an example which intersects the miscibility gap at fairly low levels of $CaCO_3$ concentration (s), and exsolves a carbonate melt (c) with composition corresponding to natrocarbonatite, near the alkali carbonate fluid/melt inclusion F (Table 4) reported by Le Bas (1981). If the cooling path involved greater enrichment of the silicate melt in component $CaCO_3$, the exsolved carbonate liquid would also be richer in $CaCO_3$, as indicated for example by the tie-line C'

in Fig. 1. For low-Mg, high-Ca crustal magmas, Fig. 7 indicates that no exsolved carbonatite melt would contain more than 70% $CaCO_3$.

Figure 1 shows that at much higher pressures, liquid immiscibility (B-B) could yield a carbonatite melt with a maximum of 80% $CaCO_3$, but at these high pressures the more appropriate, more magnesian compositions would be involved with a miscibility gap of smaller extent (BW, Fig. 7), involving alkalic, magnesian carbonate melts. These mantle carbonatite melts have compositons far removed from calciocarbonatites, from natrocarbonatites (OL), and from carbonatites derived by partial melting of mantle peridotite (1).

We conclude that enough systems have been determined to support the conclusion that carbonatite magmas generated by liquid immiscibility in the crust can contain a maximum of 70-80% dissolved $CaCO_3$ (Figs. 1 and 7). The appealing conclusion of Kjarsgaard and Hamilton (1988, 1989) that almost pure $CaCO_3$ carbonatite melts can be obtained through liquid immiscibility (dotted lines A-A in Fig. 1) cannot be sustained, according to our results (B-B in Fig. 1, Lee and Wyllie, 1992a, b, manuscript in preparation) and their own revision (to C-C in Fig. 1; revised in Macdonald et al., 1993; Hamilton and Kjarsgaard, 1993). Cooper and Reid (1991) can no longer appeal to these experiments as support for a process of immiscible separation of an extremely Ca-rich carbonatite magma, unless they can generate their differentiated carbonatite magma (alvikite) from an original liquid somewhere on path (3) in Fig. 7. We note further that these relatively high-$CaCO_3$ magmas can be generated by liquid immiscibility only for silicate magmas already greatly enriched in dissolved $CaCO_3$, and we feel that the more common products of liquid immiscibility in the crust should be more sodic carbonatite magmas.

Possible compositions for carbonatite magmas

Carbonate-rich liquids occupy the right-hand side and lower corner of Fig. 7. Experimental studies reviewed above indicate that parental carbonatite magmas should correspond either to the primary dolomitic liquids near (1), or to the carbonate-rich liquids along the Lc side of the 2-liquid field boundary KH. The crystallization of these carbonatite magmas is dominated by the liquidus phase relationships of the carbonates on the right-hand side of Fig. 7, as illustrated by the system $CaCO_3$-Na_2CO_3-K_2CO_3 (Cooper et al., 1975). Precipitation of calcite (higher temperature) enriches the liquid in alkali carbonates. The point E (Table 4) gives the low-temperature sodic residuum at the eutectic just on the calcite side of nyerereite with 47 wt% Na_2CO_3 (molar $Na_2O/CaO = 0.8$). The only observed carbonatite magma is the Oldoinyo Lengai natrocarbonatite lava (OL, Dawson et al., 1987). Eutectic E is separated from the natrocarbonatite by the thermal barrier corresponding to nyerereite composition (Nye). Bailey (1993) suggested for this reason that the OL lava might be formed by partial melting of carbonates preciptated by exhalations within the volcano. Jago and Gittins (1991) and Gittins (1989) suggested that addition of fluorine might break the thermal barrier to allow a calcic carbonatite magma to differentiate to the Oldoinyo Lengai lava composition.

Crystallization of the most $CaCO_3$-rich immiscible magma would therefore follow a path such as (3), if the magma remains in contact with its silicate parent. If the carbonatite magma separates from the silicate magma, it will cool with precipitation of calcite or silicate minerals (depending on the detailed phase relationships) down to another subparallel liquidus field boundary between (3) and the carbonate side. Precipitation of calcite then drives the liquid toward the natrocarbonatite compositions. Kogarko et al. (1991), reported inclusions of nyerereite in perovskite precipitated late in the Guli intrusive sovite, consistent with the presence of a sodic carbonatite residual liquid. Precipitation of dolomite from primary magma (1) would follow a subparallel path (in projection).

F (Le Bas, 1981) and PH (Pyle and Haggerty, 1994) are inclusions in minerals believed to represent magmatic liquids. These are all located near the 2-liquid field

boundary KH. The concentration of natural silicate magmas and coexisting carbonate-rich assemblages near this boundary has been illustrated by Le Bas (1987). Volcanic lapilli and rocks with compositions near to $CaCO_3$ suggested to Keller (1989) and Bailey (1993) that calciocarbonatite magmas with similar compositions exist. We can see no petrological process based on available phase diagrams to explain the formation of nearly pure $CaCO_3$ liquids, now that the miscibility gap A-A (Fig. 1) is invalidated. Figures 1 and 7 show a maximum of 70-80% $CaCO_3$ in liquids formed by petrological processes, and there is no crystallization process that could drive the liquid compositions from these parental magmas toward $CaCO_3$.

We suggest that an explanation may be found in a high-$CaCO_3$ system with H_2O, alkalis (Cooper et al., 1975), or fluorine (Gittins, 1989; Jago and Gittins, 1991) precipitating calcite at moderate temperatures, while residual liquid, fluid, or vapor escapes from the system. Calcite is rapidly separated from the low-viscosity carbonate-rich liquids (Wyllie and Tuttle, 1960). Wyllie and Tuttle (1962) outlined phase equilibrium evidence for the eruption of $CaCO_3$-rich "vesiculating carbonatite flows", with temperatures lowered by H_2O and alkalis. Wyllie (1965) showed from phase relationships in the system CaO-MgO-CO_2-H_2O that at moderate temperatures, a carbonatite magma of simple composition could evolve vapor, dehydrate, and precipitate calcite, or calcite and dolomite, with no remaining magma or hydrous mineral. Could similar processes explain high-$CaCO_3$ cumulate rocks without the need for high-temperature, H_2O-free, nearly pure $CaCO_3$ liquids (Kjarsgaard and Hamilton, 1989; Bailey, 1993)? However, this process retains the problem of the source of the hydrous $CaCO_3$-rich magma.

Fractionation from silicate to carbonatite magmas

Path (2) in Fig. 7 leads a silicate liquid to the miscibility gap, with separation of a sodic carbonatite magma. Watkinson and Wyllie (1971) described a path of fractional

crystallization for silicate liquid in Fig. 7 which produced a series of mineral assemblages reaching carbonatites without liquid immiscibility. The composition of the liquid in one of these phase assemblages, liquid L (molar $Na_2O/CaO = 0.4$), was determined in Fig. 4 for run conditions SM in Fig. 2 (molar $Na_2O/CaO = 0.2$ in starting mixture). Path (4) in Fig. 7 represents the corresponding path of fractional crystallization. The liquid L projects within the miscibility gap (Fig. 7), but Figs. 2 and 6 show that only the single liquid is present, at a temperature well below the region of immiscible liquids. Figure 6 shows that with decreasing temperature, the liquid L has just started to precipitate calcite, and this would cause the illustrated change in direction of the liquid path (4) away from calcite and toward alkalis. With continued fractional crystallization of cancrinite and calcite and resorption of melilite (Fig. 5), the residual liquid should become progressively enriched in alkali carbonates compared with the join $NaAlSiO_4$-$CaCO_3$.

The existence of phase volumes for crystals + liquid +or- vapor at temperatures below the miscibility gap, determined also in the H_2O-free join $NaAlSi_3O_8$-$CaCO_3$ (Lee and Wyllie, 1992a, 1992b), is obscured by the projection (Figs. 1 and 7). Figure 8 reproduces on the lower triangle the synthetic system projections (Ca-Na-Si-Al) from Figs. 7 and 1 and adds a temperature axis, providing a diagrammatic representation of the phase volumes. There is a solidus surface, with temperature strongly dependent on the presence or absence of H_2O, but the prism is drawn only for temperatures above the solidus (neglecting the carbonate-free solidus on the silicate side of Figs. 2 and 6). The top of the prism intersects the miscibility gap, as shown.

The shaded volume is a schematic representation of the 2-liquid volume. It is terminated downwards at a surface below which is part of the volume for crystals + liquid + vapor. This is not a unique surface in the multicomponent projection, and its shape is not precisely known; it will surely vary with H_2O content. However, the known data on silicate-carbonate liquid immiscibility indicates that its temperature is considerably lower for the joins feldspar/nepheline-Na_2CO_3 than for feldspar/nepheline-$CaCO_3$, and this is

Figure 8. Schematic representation of miscibility gap KH and crystallization paths (2) and (4) in Fig. 7, showing temperature variations. The low-temperature surface of the two-liquid field is sketched (see text), exposing the large volume for crystals + L + V below (Fig. 6). KW is based on Koster van Groos and Wyllie (1968). The solidus is at yet lower temperatures (Fig. 6), below the triangle in the lower part of Fig. 8; this isothermal triangle is drawn within the volume for crystals + L + V to show the projections from the higher-temperature phase equilibria. This illustrates how fairly small differences in composition of original silicate melts could be followed by either the separation of immiscible carbonate-rich melts (path 2), or by the fractional crystallization paths passing below the miscibility volume toward enrichment in carbonates and alkalis with the precipitation of calcite (path 4).

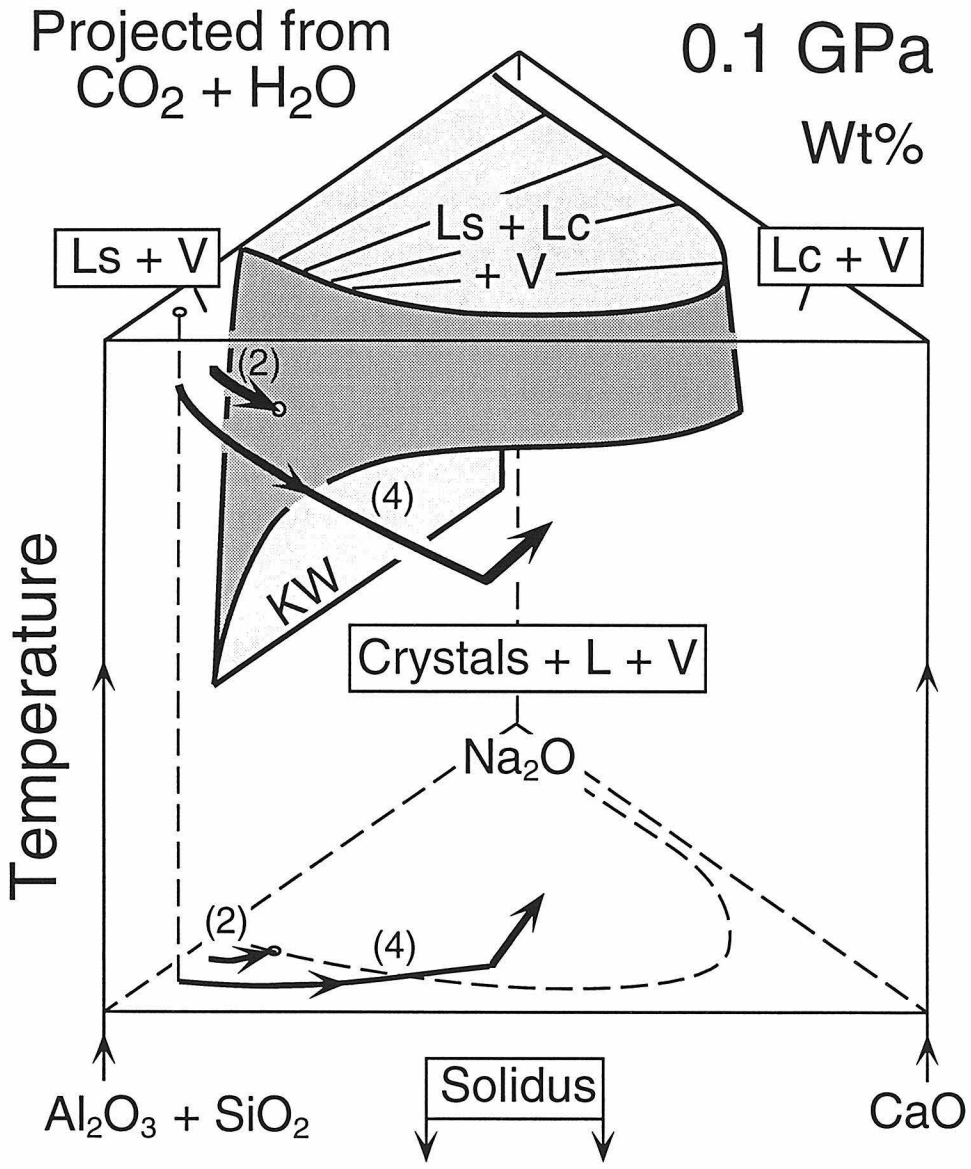
Projected from
$CO_2 + H_2O$
0.1 GPa
Wt%
Ls + V
Ls + Lc
+ V
Lc + V
(2)
(4)
KW
Crystals + L + V
Na_2O
Temperature
(2)
(4)
$Al_2O_3 + SiO_2$
Solidus
CaO

depicted in Fig. 8. KW represents the hydrous, end-member two-liquid field, estimated from results of Koster van Groos and Wyllie (1968). Phase relationships become more complex in the Na_2O corner at pressures above the critical end-point in Na_2CO_3-H_2O at 0.15 GPa and 500 °C (Koster van Groos, 1990). We make no attempt to illustrate the phase volumes on either side of the 2-liquid volume (see Fig. 6), because this only complicates the figure without clarifying the phase relationships of interest. The two paths of crystallization for silicate liquids from Fig. 7 are sketched in three dimensions in Fig. 8. Path (2) reaches the miscibility volume. It is easily seen in Fig. 8 how the route of path (4) from Fig. 7 passes beneath the 2-liquid volume. In fact, with H_2O present, almost the whole range of compositions within the projected miscibility gap KH in Fig. 7 is potentially within reach of liquids following various crystallization paths at temperatures below the shaded volume. Figure 6 shows the large temperature interval for the coexistence of crystals + liquid + vapor when H_2O is present.

The Oka Igneous Complex

The rocks at Oka provide an example of the probelms in resolving different interpretations of field and petrological studies. Petrological accounts include those of Gold (1963, 1967, 1972), Davidson (1963), Wakinson (1970), Treiman and Essene (1985), and Sage and Watkinson (1991). Gold (1967, 1972) concluded that the igneous rocks of the Monteregian Province, including the carbonatites of Oka, could have been formed through differentiation of a mantle-derived silicate magma by fractional crystallization. Sage and Watkinson (1991) presented the results of at least 10 years' mapping of 41 alkalic rock-carbonatite complexes in Ontario. Watkinson (1993, personal communication) is impressed with the evidence for fractionation in these complexes, with the separation and ultimate emplacement of low-viscosity carbonatite magma being at relatively high structural levels. Watkinson (1970) observed crystal settling of apatite from

residual carbonatite melt trapped in a matte of pyroxene and pyrochlore, consistent with precipitation from a highly fluid magma.

Treiman and Essene (1985) studied the rocks from the northern intrusive center of the Oka complex, and concluded that the intrusion consists of intimately intermixed rocks derived from carbonatite magma (some jacupirangites, okaites, melilite-carbonatites) and silicate magma (some jacupirangites, melilitites), while noting that some jacupirangites and okaites are cumulates. Their strongest evidence was from identity of magmatic minerals in rocks that they proposed were derived from contemporaneous immiscible liquid fractions. However, they also pointed out that the magmatic compositions either for the parental melt or for the immiscble liquid pairs are difficult to obtain, and therefore it is not possible to test for liquid immiscibility based on the comparison between compositions of natural rocks and experimental liquids.

Watkinson and Wyllie (1971) discussed the correspondence between the phase assemblages in Fig. 2 and the mineral parageneses containing melilite in alkalic igneous complexes. In particular, the rocks at Oka can be matched in the phase diagram. The parallelism is remarkable, considering the simplicity of the synthetic system compared with the rock system–notably the absence of FeO and MgO, and therefore of ferromagnesian minerals. The synthetic sequence of mineral assemblages is compared in Table 3 with the Oka rock types that they are considered to represent.

The available experimental data may thus be adduced to support the Oka carbonatite origin either by fractional crystallization or by liquid immiscibility. The path of fractional crystallization in Fig. 2 produces the sequence of Oka rock parageneses beneath the liquid miscibility gap AB in Fig. 6, along path (4) in Figs. 7 and 8. However, if the piercing point P in Fig. 6 occurred between the liquidus for nepheline and the miscibility gap, then precipitation of nepheline could drive the liquid directly to the miscibility gap, and an immiscible carbonatite magma would then separate from the carbonated-silicate parent magma as indicated for path (2) in Figs. 7 and 8. What needs to be more precisely

determined is just what are the conditions which control whether a parent silicate magma: (1) reaches a miscibility gap, (2) passes beneath a miscibility gap, or (3) is shielded and diverted from a miscibility gap by a field boundary between liquidus silicate and carbonate minerals (Lee and Wyllie, 1992c).

ACKNOWLEDGEMENTS

This research was supported by the Earth Science section of the U.S. National Science Foundation, grant EAR-921886. Helpful comments from David Eggler and Gary Ernst are appreciated. This is contribution no. 5563 of the Division of Geological and Planetary Sciences, California Institute of Technology.

REFERENCES

Bailey, D. K., 1989, Carbonate melt from the mantle in the volcanoes of south-east Zambia: Nature, v. 338, p. 415-418.

Bailey, D. K., 1993, Carbonate magmas: Jour. Geol. Soc., London, v. 150, p. 637-651.

Baker, M. B. and Wyllie, P. J., 1990, Liquid immiscibility in a nephelinite-carbonate system at 25 kbar and implications for carbonatite origin: Nature, v. 346, p. 168-170.

Barker, D. S., 1989, Field relations of carbonatites, in Bell, K., ed., Carbonatites: Genesis and Evolution: Unwin Hyman, London, p. 38-69.

Bell, K., 1989, editor, Carbonatites: Genesis and Evolution: Unwin Hyman, London, 618 pp.

Brooker, R. A. and Hamilton, D. L., 1990, Three-liquid immiscibility and the origin of carbonatites: Nature, v. 346, p. 459-462.

Cooper, A. F., and Reid, D. L., 1991, Textural evidence for calcite carbonatite magmas, Dicker Willem, southwest Namibia: Geology, v. 19, p. 1193-1196.

Cooper, A. F., Gittins, J., and Tuttle, O. F., 1975, The system Na_2CO_3-K_2CO_3-$CaCO_3$ at 1 kilobar and its significance in carbonatite petrogenesis: Amer. Jour. Sci, v. 275, p. 534-560.

Dalton, J. A., and Wood., B. J.,1993, The compositions of primary carbonate melts and their evolution through wallrock reaction in the mantle: Earth Planet. Sci. Lett., v. 119, p. 511-525.

Davidson, A.,1963, A study of okaite and associated rocks near Oka, Quebec, M.Sc. thesis: University of British Columbia, Vancouver.

Dawson, J. B., 1994, Quaternary kimberlitic volcanism on the Tanzania Craton: Contrib. Mineral. Petrol., v. 116, p. 473-485.

Dawson, J. B., Garson, M. S., and Roberts, B., 1987, Altered former alkalic carbonatite lava from Oldoinyo Lengai, Tanzania: Inferences for calcite carbonatite lavas: Geology, v. 15, p. 765-768.

Dawson, J. B., Pinkerton, H., Pyle, D. M., Nyamweru, C., 1994, June 1993 eruption of Oldoinyo Lengai, Tanzania: Exceptionally viscous and large carbonatite lava flows and evidence for coexisting silicate and carbonate magmas: Geology, v. 22, p. 799-802.

Eggler, D. H., 1978, The effect of CO_2 upon partial melting of peridotite in the system Na_2O-CaO-Al_2O_3-MgO-SiO_2-CO_2 to 35 kb, with an analysis of melting in a peridotite-H_2O-CO_2 system: Amer. Jour. Sci., v. 278, p. 305-343.

Eggler, D. H., 1989, Carbonatites, primary melts, and mantle dynamics, in Bell, K., ed., Carbonatites: Genesis and Evolution: Unwin Hyman, London, p. 561-579.

Falloon, T. J., and Green, D. H., 1989, The solidus of carbonated, fertile peridotite: Earth Planet. Sci. Lett, v. 94, p. 364-370.

Fanelli, M. F., Cava, N., and Wyllie, P. J., 1986, Calcite and dolomite without portlandite at a new eutectic in CaO-MgO-CO_2-H_2O, with applications to carbonatites, in Morphology and Phase Equilibrium of Minerals: Proc. 13th General Meeting, Inter. Mineral. Assoc., Bulg. Acad. Sci., Sofia, p. 313-322.

Freestone I. C. & Hamilton, D. L., 1980, The role of liquid immiscibility in the genesis of carbonatites - an experimental study: Contrib. Mineral. Petrol., v. 73, p. 105-117.

Gittins, J., 1989, The origin and evolution of carbonatite magmas, in Bell, K., ed., Carbonatites: Genesis and Evolution: Unwin Hyman, London, p., 580-600.

Gold, D. P., 1963, The relationship between limestones and alkaline igneous rocks of Oka and St. Hilaire, Quebec, Ph.D. Dissert.: McGill University, Montreal.

Gold, D.P., 1967, Alkaline ultrabasic rocks in the Montreal area, Quebec, in Wyllie, P. J., ed., Ultramafic and Related Rocks: John Wiley, New York, p. 288-302.

Gold, D. P., 1972, The Monteregian Hills: Ultra-alkaline rocks and the Oka carbonatite complex: 24th International Geological Congress, Guidebook B-11.

Haggerty, S. E., 1989, Mantle metasomes and the kinship between carbonatites and kimberlites, in Bell, K., ed., Carbonatites: Genesis and Evolution: Unwin Hyman, London, p. 546-560.

Hamilton, D. L. and Kjarsgaard, B. A., 1993, The immiscibility of silicate and carbonate liquids: S. Afr. J. Geol., 96, 139-142.

Hamilton, D. L., Bedson, P. and Esson, J., 1989, The behaviour of trace elements in the evolution of carbonatites, in Bell, K., ed., Carbonatites: Genesis and Evolution: Unwin Hyman, London, p. 405-427.

Hamilton, D. L., Freestone, I. C., Dawson, J. B., and Donaldson, C. H., 1979, Origin of carbonatites by liquid immiscibility: Nature, v. 279, p. 52-54.

Huang, W. L. and Wyllie, P. J., 1974, Eutectic between wollastonite II and calcite contrasted with thermal barrier in MgO-SiO_2-CO_2 at 30 kilobars, with applications to kimberlite-carbonatite petrogenesis: Earth Planet. Sci. Lett., v. 24, p. 305-310.

Ihinger, P. D., 1991, An experimental study of the interaction of water with granitic melt, Ph.D. Dissert.: California Institue of Technology, Pasadena.

Jago, B. C., and Gittins, J., 1991, The role of fluorine in carbonatite magma evolution: Nature, v. 349, p. 56-58.

Jones, J. H., Walker, D., Pickett, D. A., Murrell, M. T., and Beattie, P., 1995, Experimental investigations of the partitioning of Nb, Mo, Ba, Ce, Pb, Ra, Th, Pa, and U between immiscible carbonate and silicate liquids: Geochim. et Cosmochim. Acta, v. 59, p. 1307-1320.

Keller, J., 1989, Extrusive carbonatites and their significance, in Bell, K., ed., Carbonatites: Genesis and Evolution: Unwin Hyman, London, p. 70-88.

Kjarsgaard, B. A. and Hamilton, D. L, 1988, Liquid immiscibility and the origin of alkali-poor carbonatites: Mineral. Mag., v. 52, p. 43-55.

Kjarsgaard, B. A. and Hamilton, D. L., 1989, The genesis of carbonatites by immiscibility, in Bell, K., ed., Carbonatites: Genesis and Evolution: Unwin Hyman, London, p. 388-404.

Kjarsgaard, B. and Peterson, T., 1991, Nephelinite-carbonatite liquid immiscibility at Shombole Volcano, East Africa: Petrographic and experimental evidence: Mineral. Petrol., v. 43, p. 293-314.

Kogarko, L. N., and Pacheco, A. H., 1994, Mechanism of carbonatized peridotite partial melting, Abstract Volume: 16th General Meeting, Inter. Mineral. Assoc., Societa Italiana di Mineral. e Petrol., Pisa, Italy, p. 208-209.

Kogarko, L. N., Plant, D. A., Henderson, C. M. B., and Kjarsgaard, B. A., 1991, Na-rich carbonate inclusions in perovskite and calzirtite from the Guli intrusive Ca-carbonatite, polar Siberia: Contrib. Mineral. Petrol., v. 109, p. 124-129.

Koster van Groos, A. F., 1975, The effect of high CO_2 pressures on alkalic rocks and its bearing on the formation of alkalic ultrabasic rocks and the associated carbonatites: Amer. Jour. Sci., v. 275, p. 163-185.

Koster van Groos, A. F., 1990, High-pressure DTA study of the upper three-phase region in the system Na_2CO_3-H_2O: Amer. Mineral., v. 75, p. 667-675.

Koster van Groos, A. F., and Wyllie, P. J., 1966, Liquid immiscibility in the system Na_2O-Al_2O_3-SiO_2-CO_2 at pressures to 1 kilobar: Amer. Jour. Sci., v. 264, p. 234-255.

Koster van Groos, A. F., and Wyllie, P.J., 1968, Liquid immiscibility in the join $NaAlSi_3O_8$-Na_2CO_3-H_2O and its bearing on the genesis of carbonatites: Amer. Jour. Sci., v. 266, p. 932-967.

Koster van Groos, A. F., and Wyllie, P. J., 1973, Liquid immiscibility in the join $NaAlSi_3O_8$-$CaAl_2Si_2O_8$-Na_2CO_3-H_2O: Amer. Jour. Sci., v. 273, p. 465-487.

Le Bas, M. J., 1981, Carbonatite magmas: Mineral. Mag., v. 44, p. 133-140.

Le Bas, M. J., 1987, Nephelinites and carbonatites, in Fitton, J. G. and Upton, B. G. J., eds, Alkaline Igneous Rocks: Geological Society Special Publication No. 30, p. 53-83.

Lee, W.-J., and Wyllie, P. J., 1992a, New data on CO_2-rich immiscible liquids in Na_2O-CaO-Al_2O_3-SiO_2-CO_2 from 25 to 1 kb: Carbonatite genesis: EOS, v. 73(14), p. 349-350 (abstract).

Lee, W.-J., and Wyllie, P. J., 1992b, Liquid immiscibility between silicates and carbonates must intersect suitable liquidus field boundaries to have petrogenetic significance, Abstracts: 29th International Geological Congress, Kyoto, p. 571.

Lee, W.-J., and Wyllie, P. J., 1992c, Silicate-carbonate liquid miscibility gaps, and liquidus field boundaries: Carbonatites by immiscibility or fractionation: EOS, v. 73(43), p. 606 (abstract).

Lee, W.-J, and Wyllie, P. J., 1994, Conditions for formation of immiscible carbonate-rich magmas from primitive (magnesian) nephelinite: Geol Soc Am Abstr Prog, v. 26, p. A224 (abstract).

Lee, W.-J., Wyllie, P. J., and Rossman, G. R., 1994, CO_2-rich lass, round calcite crystals and no liquid immiscibility in the system CaO-SiO_2-CO_2 at 2.5 GPa: Amer. Mineral., v. 79, p. 1135-1144.

Maaloe, S., and Wyllie, P. J., 1975, The join grossularite-calcite through the system CaO-Al_2O_3-SiO_2-CO_2 at 30 kilobars: Crystallization range of silicates and carbonates on the liquidus: Earth Planet. Sci. Lett., v. 28, p. 205-208.

Macdonald, R, Kjarsgaard, B. A., Skilling, I. P., Davies, G. R., Hamilton, D. L., and Black, S., 1993, Liquid immiscibility between trachyte and carbonate in ash flow tuffs from Kenya: Contrib. Mineral. Petrol., v. 114, p. 276-287.

Newton, R. C., and Sharp, W. E., 1975, Stability of forsterite+CO_2 and its bearing on CO_2 in the mantle: Earth Planet. Sci. Lett., v. 26, p. 239-244.

Olafsson, M., and Eggler, D. H., 1983, Phase relations of amphibole-carbonate, and phlogopite-carbonate peridotite: petrologic constraints on the asthenopsphere: Earth Planet. Sci. Lett., v. 64, p. 305-315.

Otto, J. W., and Wyllie, P. J., 1993, Relationships between silicate melts and carbonate-precipitating melts in CaO-MgO-SiO_2-CO_2-H_2O at 2 kbar: Mineral. Petrol., v. 48, p. 343-365.

Pyle, J. M., and Haggerty, S. E., 1994, Silicate-carbonate liquid immiscibility in upper-mantle eclogites: Implications for natrosilicic and carbonatitic conjugate melts: Geochim. et Cosmochim. Acta, v. 58, p. 2997-3011.

Rudnick, R. L., Mcdonough, W. F., and Chappell, B. W., 1993, Carbonatite metasomatism in the northern Tanzanian mantle - Petrographic and geochemical characteristics: Earth Planet. Sci. Lett., v. 114, p. 463-475.

Ryabchikov, I. D., Brey, G., Kogarko, L. N. and Bulatov, V. K., 1989, Partial melting of carbonated peridotite at 50 kbar: Geokhimiya, v. 1, p. 3-9.

Ryabchikov, I. D., Schreyer, W., and Abraham, K., 1982, Compositions of aqueous fluids in equilibrium with pyroxenes and olivines at mantle pressures and temperatures: Contrib. Mineral. Petrol., v. 79, p. 80-84.

Sage, R. P., and Watkinson, D. H., 1991, Alkalic rock-carbonatite complexes of the Superior Structural Province, northern Ontario, Canada: Chronique de la Recherche Miniere, v. 504, p. 5-19.

Stoppa, F., and Lupini, L., 1993, Mineralogy and petrology of the Polino monticellite calciocarbonatite (central Italy): Mineral. Petrol., v. 49, p. 213-231.

Sweeney, R. J., 1994, Carbonatite melt compositions in the Earth's mantle: Earth Planet. Sci. Lett., v. 128, p. 259-270.

Sweeney, R. J., Falloon, T. J., and Green, D. H., 1995, Experimental constraints on the possible mantle origin of natrocarbonatite, in Bell, K., and Keller, J., eds., Carbonatite Volcanism: Oldoinyo Lengai and the Petrogenesis of Natrocarbonatites: IAVCEI Proceedings in Vocanology, v. 4, p. 191-207. Springer-Verlag, Berlin.

Thibault, Y., Edgar, A. D., and Lloyd, F. E., 1992, Experimental investigation of melts from a carbonated phlogopite lherzolite: Implications for metasomatism in the continental lithosperic mantle: Amer. Mineral., v. 77, p. 784-794.

Treiman, A. H., and Essene, E. J., 1985, The Oka carbonatite complex, Quebec: geology and evidence for silicate-carbonate liquid immiscibility: Amer. Mineral., v. 70, p. 1101-1113.

Twyman, J. D., and Gittins, J., 1987, Alkalic carbonatite magmas: Parental or derivative? in Fitton, J. G., and Upton, B. G. J., eds., Alkaline Igneous Rocks: Geological Society Special Publication No. 30, p. 85-94.

Veksler, I. V., and Nielsen, T. F. D., 1994, Fractionation of micas and carbonates in ultramafic-alkaline intrusions: new evidence and petrological importance, Abstract Volume: 16th General Meeting, Inter. Mineral. Assoc., Societa Italiana di Mineral. e Petrol., Pisa, Italy, p. 424.

Verwoerd, W. J., 1978, Liquid immiscibility and the carbonatite-ijolite relationship: Preliminary data on the join $NaFe^{3+}Si_2O_6$-$CaCO_3$ and related compositions: Carnegie Inst. Washington Yearb., v. 77, p. 767-774.

Wallace, M. E., and Green, D. H., 1988, An experimental determination of primary carbonatite magma composition: Nature, v. 335, p. 343-346.

Watkinson, D. H., 1965, Melting relationships in parts of the system Na_2O-K_2O-CaO-Al_2O_3-SiO_2-CO_2-H_2O with applications to carbonate and alkali rocks, Ph.D. Dissert.: The Pennsylvania State University, University Park.

Watkinson, D. H., 1970, Experimental studies bearing on the origin of the alkalic rock-carbonatite complex and niobium mineralization at Oka, Quebec: Canadian Mineralogist, v. 10, p. 350-361.

Watkinson, D. H., and Wyllie, P. J., 1969, Phase equilibrium studies bearing on the limestone-assilimilation hypothesis: Bull. Geol. Soc. Amer., v. 80, p. 1565-1576.

Watkinson, D. H., and Wyllie, P. J., 1971, Experimental study of the join $NaAlSiO_4$-$CaCO_3$-H_2O and the genesis of alkalic rock-carbonatite complexes: Jour. Petrol., v. 12, p. 357-378.

Wendlandt, R. F., and Harrison, W. J., 1979, Rare earth partitioning between immiscible carbonate and silicate liquids and CO_2 vapor: Results and implications for the formation of light rare earth-enriched rocks: Contrib. Mineral. Petrol, v. 69, p. 409-419.

Wendlandt, R. F., and Eggler, D. H., 1980, The origins of potassic magmas. 1. Melting relations in the systems $KAlSiO_4$-Mg_2SiO_4-SiO_2 and $KAlSiO_4$-MgO-SiO_2-CO_2 to 30 kilobars. 2. Stability of phlogopite in natural spinel lherzolite and in the system $KAlSiO_4$-MgO-SiO_2-H_2O-CO_2 at high pressures and high temperatrues: Amer. Jour. Sci., v. 280, p. 385-420, p. 421-458.

White, B. S., and Wyllie, P. J, 1992, Solidus reactions in synthetic lherzolite-H_2O-CO_2 from 20-30 kbar, with applications to melting and metasomatism: Jour. of Volcanol. Geotherm. Res., v. 50, p. 117-130.

Woermann, E, and Rosenhauer, M., 1985, Fluid phases and the redox state of the Earth's mantle: Extrapolations based on experimental, phase-theoretical and petrological data: Fortschr. Mineral., v. 63, p. 263-349.

Woolley, A. R., and Kempe, D. R. C., 1989, Carbonatites: Nomenclature, average chemical compositions, and element distribution, in Bell, K., ed., Carbonatites: Genesis and Evolution: Unwin Hyman, London, p. 1-14.

Wyllie, P. J., 1965, Melting relationships in the system CaO-MgO-CO_2-H_2O with petrological applications: Jour. Petrol., v. 6, p. 101-123.

Wyllie, P. J., 1966, Experimental studies of carbonatite problems: the origin and differentiation of carbonatite magmas, in Tuttle, O. F., and Gittins, J., eds., Carbonatites: John Wiley, New York, N. Y, p. 311-352.

Wyllie, P. J., 1977, Mantle fluid compositions buffered by carbonates in peridotite-CO_2-H_2O. Jour. Geol., v. 85, p. 187-207.

Wyllie, P. J., 1987, Discussion of recent papers on carbonated peridotite, bearing on mantle metasomatism and magmatism: Earth Planet. Sci. Lett., v. 82, p. 391-397, p. 401-402.

Wyllie, P. J., 1989, Origin of carbonatites: Evidence from phase equilibrium studies, in Bell, K., ed., Carbonatites: Genesis and Evolution: Unwin Hyman, London, p. 500-545.

Wyllie, P. J., and Huang, W.-L, 1975, Peridotite, kimberlite, and carbonatite explained in the system CaO-MgO-SiO_2-CO_2: Geology, v. 3, p. 621-624.

Wyllie, P. J., and Huang, W.-L., 1976, Carbonation and melting reactions in the system CaO-MgO-SiO_2-CO_2 at mantle pressures with geophysical and petrological applications: Contrib. Mineral. Petrol., v. 54, p. 79-107.

Wyllie, P. J., and Rutter, M., 1986, Experimental data on the solidus of peridotite-CO_2, with applications to alkaline magmatism and mantle metasomatism: EOS, v. 67, p. 390 (abstract).

Wyllie, P. J., and Tuttle, O. F., 1960, The system CaO-CO_2-H_2O and the origin of carbonatites: Jour. Petrol., v. 1, p. 1-46.

Wyllie, P. J., and Tuttle, O. F., 1962, Carbonatitic lavas: Nature, v. 194, p. 1269.

Wyllie, P. J., Baker, M. B., and White, B. S., 1990, Experimental boundaries for the origin and evolution of carbonatites: Lithos, v. 26, p. 3-19.

Wyllie, P. J., Huang, W.-L., Otto, J., and Byrnes, A. P., 1983, Carbonation of peridotites and decarbonation of siliceous dolomites represented in the system CaO-MgO-SiO_2-CO_2 to 30 kbar: Tectonophysics, v. 100, p. 359-388.

CHAPTER 2

CO_2-RICH GLASS, ROUND CALCITE CRYSTALS, AND NO LIQUID IMMISCIBILITY IN THE SYSTEM CaO-SiO_2-CO_2 AT 2.5 GPa

(Lee W.-J., Wyllie P. J. & Rossman G. R., 1994. American Mineralogist 79: 1135-1144)

ABSTRACT

Following reports that the miscibility gap between silicate and carbonate liquids located experimentally on feldspar calcite-joins extended to the alkali-free side of the system CaO-Na_2O-Al_2O_3-SiO_2-CO_2, the melting of a mixture of calcite (70 wt%) and quartz was investigated at 2.5 GPa. The isobaric reaction:

calcite (CC) + quartz (Qz) = liquid (L) + vapor (V)

was reversed at 1350°C. Quartz and rounded calcite crystals were concentrated at the bottom of the capsule and CO_2 was distributed in large vapor bubbles in the glass layer, and at the top of the capsule. The liquid quenched to transparent glass, unusual in carbonate-rich systems. In 2-stage reversal runs, a charge of [L+V] placed subsolidus at 1300°C produced a few rounded calcite grains organized in dendritic patterns; at 1200°C dendritic intergrowths of [CC+Qz] were produced, with some coarser-grained areas. The glass contained about 20 wt% CO_2 based on the geometry of phase boundaries and EDS analysis. There was no evidence for immiscible liquids. The round calcite crystals are equilibrium mineral phases, not quenched $CaCO_3$-liquids, and surface tension effects control their shapes. Infrared spectroscopic studies indicate that $[CO_3]^{2-}$ is the dominant CO_2 species in the glass, and the silicate structure is partially polymerized, probably as a result of interaction between Ca^{2+} and SiO_4 tetrahedra. The phase relationships in the $CaCO_3$-SiO_2 system, the simplest model for subducted oceanic crust with limestone (or for sea-water-altered basalt), show that subducted crust potentially could transport calcite to great depths for long-term storage in the mantle, and could also yield low-SiO_2 carbonate-rich magmas under some thermal conditions. Such carbonate-rich melts may be efficient agents for mantle metasomatism.

INTRODUCTION

Melting relations in silicate-carbonate systems involving carbonate-rich melts are relevant for problems related to mantle metasomatism (Green and Wallace, 1988; Baker and Wyllie, 1992; Yaxley et al., 1991; Hauri et al. 1993), the possible involvement of carbonate-rich melts above subducted oceanic slabs (Sweeney et al., 1992; McInnes and Wyllie, 1992), and the generation of carbonatites and associated volcanism (Bell, 1989). The simplest petrologically relevant system combining silicate and carbonate liquids is CaO-SiO_2-CO_2. Melting relationships in this system (with and without H_2O) have been studied at crustal and mantle pressures (Wyllie and Haas, 1965, 1966; Boettcher and Wyllie, 1969; Huang and Wyllie 1974; Huang et al. 1980).

Liquid immiscibility occurs between silicates and carbonates, extending across a wide range of compositions (Koster van Groos and Wyllie, 1966, 1973; Koster van Groos, 1975; Freestone and Hamilton, 1980), but there are also continuous liquidus paths between some silicate and carbonate-rich melts (Wyllie, 1989; Otto and Wyllie, 1993). There is excellent petrological and experimental evidence that some carbonatites separate from silicate magmas by liquid immiscibility (Le Bas, 1977; Kjarsgaard and Peterson, 1991; Macdonald et al., 1993), but the limits for the intervention of liquid immiscibility have not been completely determined (Lee and Wyllie, 1992a).

Kjarsgaard and Hamilton (1988, 1989) and Brooker and Hamilton (1990) reported miscibility gaps in several feldspar-carbonate systems at 0.2 and 0.5 GPa between 1100°C and 1250°C, and at 1.5 GPa and 1225°C, mostly in the presence of CO_2 vapor. Kjarsgaard and Hamilton (1989) presented a generalized projection of miscibility gaps from all of their systems into the triangle (Al_2O_3+SiO_2)-CaO-Na_2O, as shown in Figure 1. Their miscibility gap at 0.5 GPa and 1250°C extends into alkali-free silicate-carbonate systems, and with nearly-pure $CaCO_3$ as the end-member immiscible carbonate liquid. Brooker and Hamilton (1990) added a second immiscible carbonate-rich liquid to this arrangement. Remarkably rounded, almost pure $CaCO_3$ phases were interpreted as quenched immiscible carbonate liquid. The occurrence of almost pure $CaCO_3$ as an

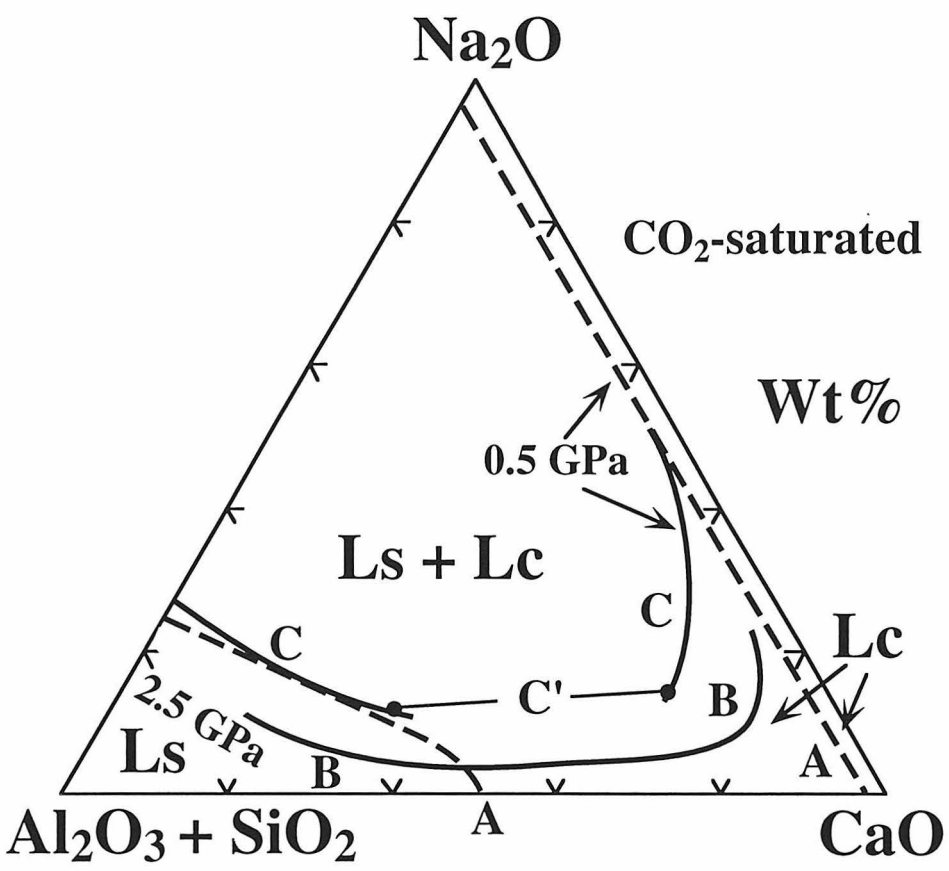

Figure 1. Silicate-carbonate two-liquid fields projected onto the compositional triangle, $(Al_2O_3+SiO_2)$-CaO-Na_2O, CO_2-saturated, showing results (heavy curves) from (A) Kjarsgaard and Hamilton (1988, 1989) at 0.5 GPa and 1250°C, (B) Lee and Wyllie (1992a, manuscript in preparation) at 2.5 GPa, and (C) Kjarsgaard and Hamilton (in preparation) at 0.5 GPa and 1250°C, presented in Macdonald et al. (1993, Fig. 5b). The tie-line C' connects coexisting silicate-rich liquid (Ls) and carbonate-rich liquid (Lc). Note that for A the field Ls + Lc extends all the way to the Na_2O-free side.

immiscible liquid at temperatures several hundred degrees below the fusion temperature of calcite (Irving and Wyllie, 1975) is puzzling. According to these results, a miscibility gap might be expected in the joins $CaCO_3$-SiO_2, $CaCO_3$-$CaSiO_3$ and $CaCO_3$-grossularite previously investigated by Huang et al. (1980), Huang and Wyllie (1974) and Maaloe and Wyllie (1975), at higher pressures (up to 3 GPa). No immiscible liquids were found in these earlier studies, although rounded calcite grains were reported. Lee and Wyllie (1992a, b, manuscript in preparation) studied the phase fields intersected by the join $NaAlSi_3O_8$-$CaCO_3$ at high pressures. The phase relationships required that the rounded $CaCO_3$ phase represented solid calcite under conditions of the experiments, and they defined the miscibility gap at 2.5 GPa as shown in Figure 1. Note that the conjugate Ca-carbonate liquid boundary is quite far removed from pure $CaCO_3$.

Macdonald at al. (1993) compared Kjarsgaard and Hamilton's (1989) original 0.5 GPa miscibility gap with a revised version (Kjarsgaard and Hamilton, in preparation), which is similar to our result at 2.5 GPa (Fig. 1). According to Kjarsgaard (personal communication, 1994) the revision involves textural reinterpretation; he is now satisfied that the rounded, almost pure $CaCO_3$ globules previously interpreted as immiscible liquids are in fact solid calcite under experimental conditions.

In this contribution, we present experiments in the end-member system of Figure 1 to check how the results of Huang et al (1980) compare with the results of Kjarsgaard and Hamilton (1988, 1989) and Brooker and Hamilton (1990). The original studies of Huang and Wyllie (1974) and Huang et al. (1980) in the system CaO-SiO_2-CO_2 at pressures up to 3 GPa relied upon optical examination of crushed fragments in immersion oils and powder X-ray diffraction measurements for the identification of phases. Physical evidence for immiscible liquids was sought, based on criteria established by previous experience (e.g. Koster van Groos and Wyllie, 1966, 1973). Glassy beads were present above the solidus, but evidence overall was interpreted in terms of simple liquidus surfaces, without miscibility gaps in the range of compositions studied. Given the recent results cited above,

however, reexamination of this boundary system is necessary, using the improvements in textural visualization and interpretation offered by the scanning electron microscope (SEM). The liquids previously reported that quenched to glasses with up to 20 weight per cent dissolved CO_2 have now been studied by infrared spectroscopic methods (FTIR). Our new results at 2.5 GPa are consistent with the revised 0.5 GPa results in Figure 1 (Kjarsgaard, personal communication, 1994).

PHASE RELATIONSHIPS IN CaO-SiO_2-CO_2: PREVIOUS STUDIES

Subsolidus reactions in this system have received much attention (Harker and Tuttle, 1956; Tuttle and Harker, 1957; Haselton et al. 1978). Huang et al. (1980) published a detailed PT projection for the system to 3 GPa, combining their new melting results with all relevant published data, including tabulation of the experimental data for Huang and Wyllie's (1974) phase diagram for $CaSiO_3$-$CaCO_3$. Our experiments were conducted on a quartz-calcite mixture. Selected univariant curves emphasizing reactions involving calcite and quartz are reproduced in Figure 2. Calcite and quartz dissociate together in the reaction:

$$\text{calcite} + \text{quartz} = \text{wollastonite} + \text{vapor} \qquad (1)$$

(Harker and Tuttle, 1956, to 0.3 GPa) at pressures up to the invariant point I_2 at 1.85 GPa and 1325°C (Huang et al., 1980), where the assemblage is joined by liquid. Haselton et al. (1978) studied several subsolidus decarbonation reactions and derived CO_2 fugacity data from the results. Their curve for Reaction 1 is somewhat higher than that in Figure 2 at lower pressures, but within error limits it passes through point I_2. Among the array of curves emanating from I_2, the incongruent melting reaction:

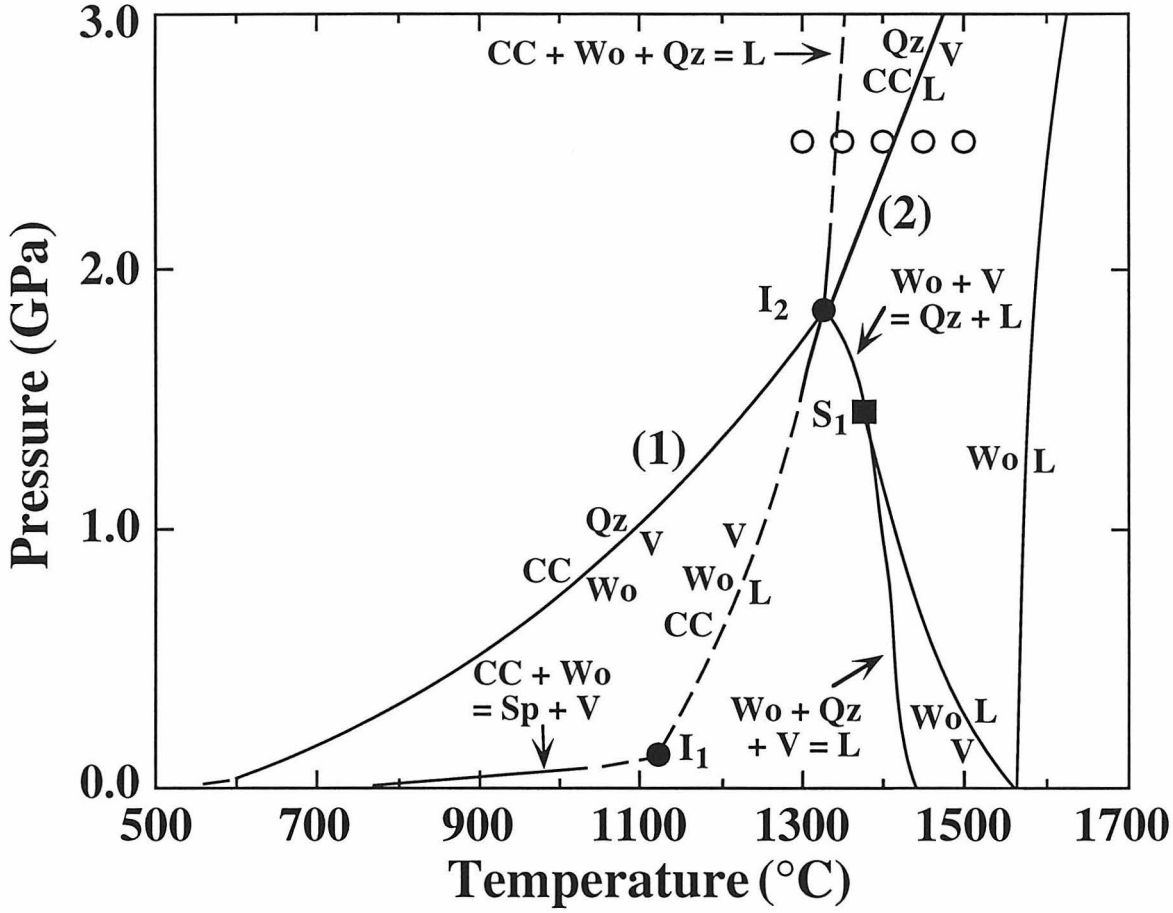

Figure 2. Selected phase relationships in $CaO\text{-}SiO_2\text{-}CO_2$ showing calcite-quartz reactions (Fig. 4 in Huang et al, 1980). Abbreviations: CC = calcite; Wo = wollastonite; Qz = quartz; Sp = spurrite; L = liquid; V = vapor; I = invariant point; S = singular point. The positions of new runs at 2.5 GPa (Table 1) are given by circles. Reactions specified in the text are denoted by numbers (1) and (2).

calcite + quartz = liquid (e) + vapor (v) (2)

rises to higher pressure. The phase relationships and Reaction 2 are illustrated in Figure 3.

Figure 3A shows the phase compositions in the ternary reactions at 2.7 GPa, with liquid field boundary compositions constrained by the several joins studied by Huang et al. (1980). The curve a-b-e-c-d is the vapor-saturated liquidus boundary, giving liquid compositions coexisting with minerals and almost pure CO_2 vapor at v. The field boundaries divide the CO_2-undersaturated liquidus surface into areas for the primary precipitation of calcite, quartz, wollastonite, larnite, and lime. Reaction 2, like 1, is a dissociation reaction, and the liquid compositions formed from mixtures on the join $CaCO_3$-SiO_2 between b and c have lost CO_2. Figure 3B shows the phase fields intersected by the join $CaCO_3$-SiO_2 at 2.7 GPa, according to Huang et al. (1980). The eutectic-like liquid e' in Figure 3B is a projection of the ternary liquid e, as shown in Figure 3A.

Kjarsgaard and Hamilton (1989) did not claim that immiscible liquids existed between quartz or calcium silicates and calcite, but a literal interpretation of their original results in Figure 1, and those of Brooker and Hamilton (1990), implies a miscibility gap between about f' and g' on the line CC-Qz in Figure 3A and B, which corresponds to the interval f and g on the field boundary a-d in Figure 3A (this is no longer required by Kjarsgaard's reinterpretation in preparation, Fig. 1).

EXPERIMENTAL METHOD

Primary standard grade $CaCO_3$ powders (Alfa Products), and reagent grade SiO_2 powders (Puratronic) were dried at 110°C for at least one day. A mixture of 30 wt% quartz and 70 wt% calcite was mixed and ground under ethanol in an agate mortar to

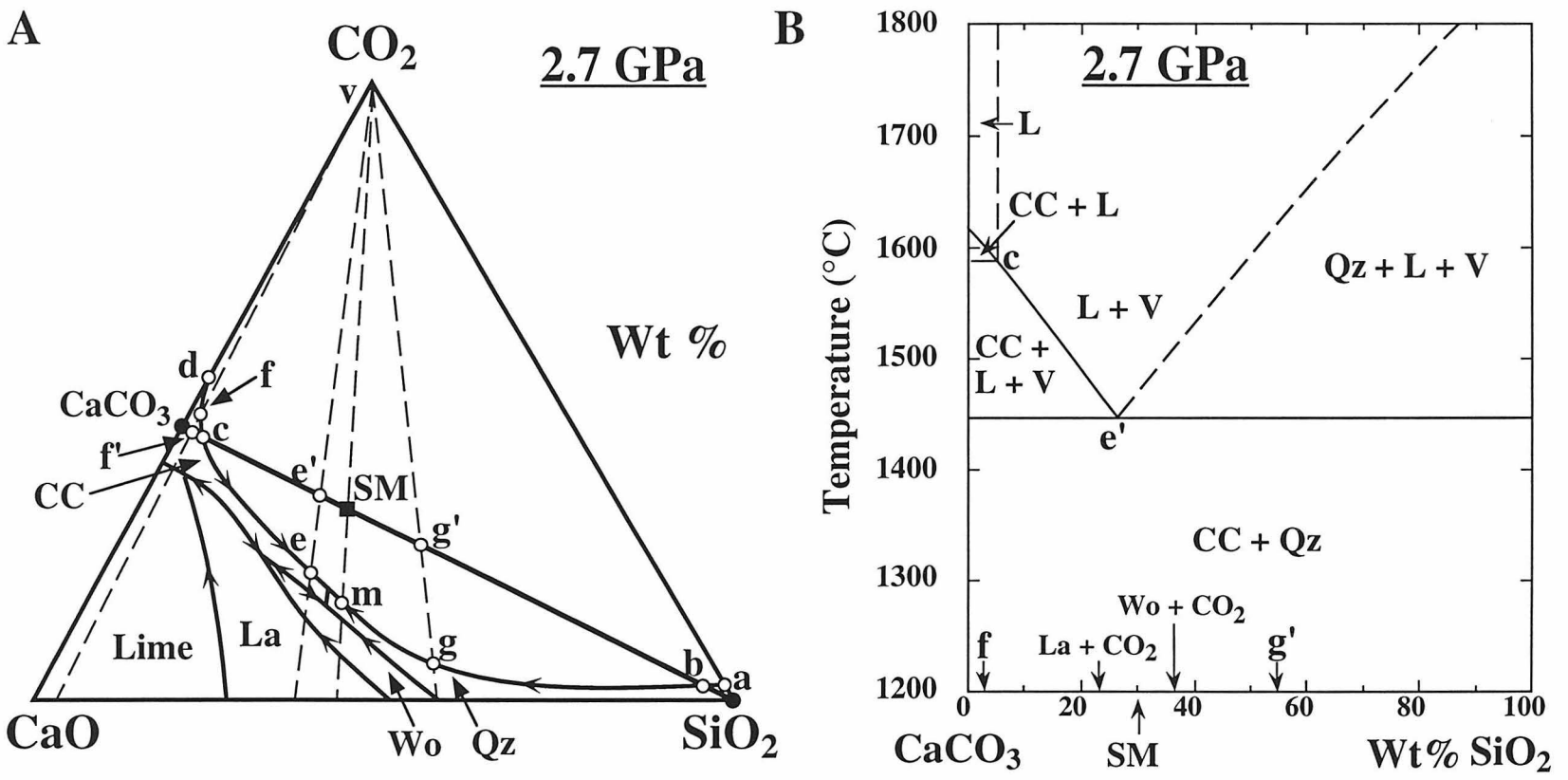

Figure 3. Phase relationships in CaO-SiO_2-CO_2 at 2.7 GPa from Huang et al (1980). Abbreviations as in Figure 2, and La = larnite. Starting mixture used in this study - SM. A. Vapor-absent liquidus surface extending from CaO to the CO_2-saturated liquidus field boundary a-b-g-m-e-c-f-d, giving liquid compositions coexisting with vapor, v. Liquid e is involved in Reaction 2: CC + Qz = L + V. B. Phase fields intersected by the join $CaCO_3$-SiO_2. Compare c, e' and SM in figure A and B.

obtain a fine-grained, uniform mixture. About 5 mg of the mixture for each run was dried for more than an hour in a vacuum drying oven at 110°C before being loaded into about 4 mm long platinum capsules. SM identifies this starting bulk composition in Figure 3.

Experiments were done in 1.27-cm diameter piston-cylinder apparatus, with calcium fluoride as a pressure medium. Temperature was controlled and monitored by $W_{95}Rh_5$-$W_{74}Rh_{26}$ thermocouple with no correction for the effects of pressure on the emf. Run duration varied from half an hour to four hours, depending upon the temperature. Experiments were terminated by turning off the electrical power. The quenching rate was about 100°C/sec for the first 600°C, and it dropped to about 50°C/sec or less at lower temperatures. Pressure was not held constant during quenching. The pressure accuracy is about ± 0.05 GPa and temperature accuracy is estimated to be ± 10°C, according to many previous calibrations with this furnace assembly.

Polished surfaces of run products were analyzed with a Camscan scanning electron microscope fitted with an energy dispersive system (EDS). Quenched liquids and crystals were analyzed using a beam current of 0.1 nA on brass with 15 KV acceleration voltage. The quenched liquids were analyzed in raster modes with covered area of about 100 μm^2. Identification of phases is based on textures and morphology observed with a petrographic microscope (with both reflected and transmitted light) and SEM, and compositions were by EDS. A thin plane-parallel plate of glass from the sample charge of run 151 prepared by polishing both sides was used in a spectroscopic study in order to identify the CO_2 species in glass and to obtain quantitative analyses, utilizing infrared absorption spectra from a Nicolet 60SX FTIR spectrometer. In addition, a polished surface of run 151 was prepared for obtaining the infrared reflectance spectra with a Nicolet Nic-Plan IR microscope.

EXPERIMENTAL RESULTS

The starting mixture SM was selected to be near the projected eutectic e' in Figure 3, just within the field for liquidus quartz. The criteria for identifying Reaction 2 are: (1) appearance of liquid, (2) disappearance of calcite, (3) appearance of a vapor phase, and (4) probably an increase in the size of quartz compared with the subsolidus assemblage. Few melting reactions in silicate-carbonate systems have been satisfactorily reversed, because the liquid commonly crystallizes to a dendritic aggregate during normal rapid quench, and this texture is retained during subsolidus annealing. Therefore, it has been difficult to reach unambiguous conclusions about whether the texture in a reversal experiment was formed during the quench, or during the run at temperature below the solidus. Because the liquid in our experiments quenched to a glass, we were able to study textures of minerals grown from liquid during annealing in two-stage reversal experiments.

Runs are listed in Table 1, and their positions are shown in Figure 2. Experimental products are illustrated in Figures 4, 5 and 7, and the results for runs of various durations (0.5-4 hours) are plotted in Figure 6. For comparison, runs by Huang et al. (1980) on this join at 2.7 GPa varied from 30 to 40 minutes.

Phase Relationships

Fig. 4 illustrates a run with all phases present (no. 24, Fig. 6A). The top part of the charge consists of clear glass enclosing large vapor bubbles, with additional vapor cavities above the glass. The lower part consists of crystals of calcite and quartz, with interstitial glass. The corresponding run of longer duration (no. 28) contains the same assemblages, with the sharp interface between the two parts shown in the SEM microphotographs (Fig. 5A). There are fine dendrites extending about 200 μm into glass from the interface between glass and the crystal layer (Fig. 5B), presumably resulting from nucleation during the quench on calcite crystals. The small percentage of glass

Table 1. Experiment results in the system $CaO\text{-}SiO_2\text{-}CO_2$ at 2.5 GPa for the mixture 70% calcite -30% quartz.

Run	Temperature (°C)	Time (h)	Results Assemblage at *P* and *T*
21	1500	0.5	L + V
151	1500	40 min	L + V
22	1450	0.5	L + V
23	1400	0.5	L + V + CC + Qz
26	1400	2	L + V + CC(tr) + Qz(tr)
24	1350	2	L + V + CC + Qz
28	1350	4	L + V + CC + Qz
27	1300	2	CC + Qz + L(tr)
34R	1500 to 1300	0.5 to 2	L + V + CC + Qz(tr)
35R	1350 to 1300	2 to 2	L + V + CC + Qz
41R	1500 to 1200	0.5 to 2	L + V + CC + Qz

Abbreviation: CC = calcite; Qz = quartz; L = liquid; V = vapor; tr = trace amount. The run numbers marked by R indicate reversal runs. For example, Run 34R was first held at 1500°C for 0.5 hours, and then quenched to 1300°C and held for 2 hours.

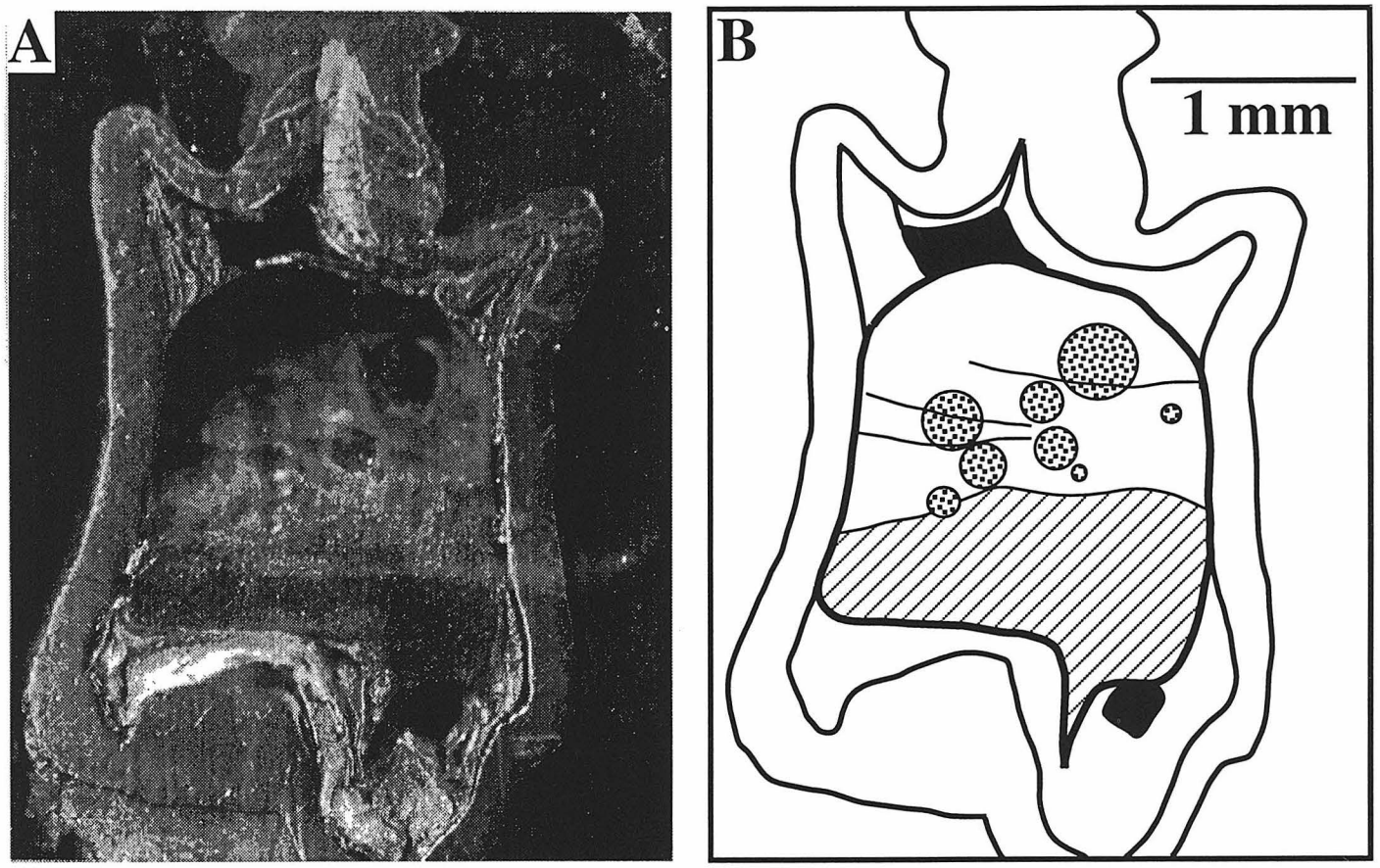

Figure 4. Polished sample from run no. 24: 2.5 GPa, 1350°C, 2 hours (Table 1, Fig. 6A).

A. Photograph of the platinum capsule, sliced open and polished.

B. Sketch identifying the phases. Diagonal shading - calcite and quartz; white area above is clear glass; grey circles and black areas contained vapor during the run.

Figure 5. SEM photomicrograph of run no. 28: 2.5 GPa, 1350°C, 4 hours (Table 1, Fig. 6A) - result similar to that illustrated in Figure 4 - spanning the boundary between crystals and glass.

A. Low magnification. The rounded calcite crystals are medium grey, and the smaller quartz crystals are darker grey. The amount of the interstitial glass (lightest grey) decreases with distance below the boundary.

B. High magnification. Calcite dendrites in glassy area near the boundary between glass and crystals. The medium grey, rounded crystals at the bottom are calcite, and the dark grey, subrounded crystals are quartz.

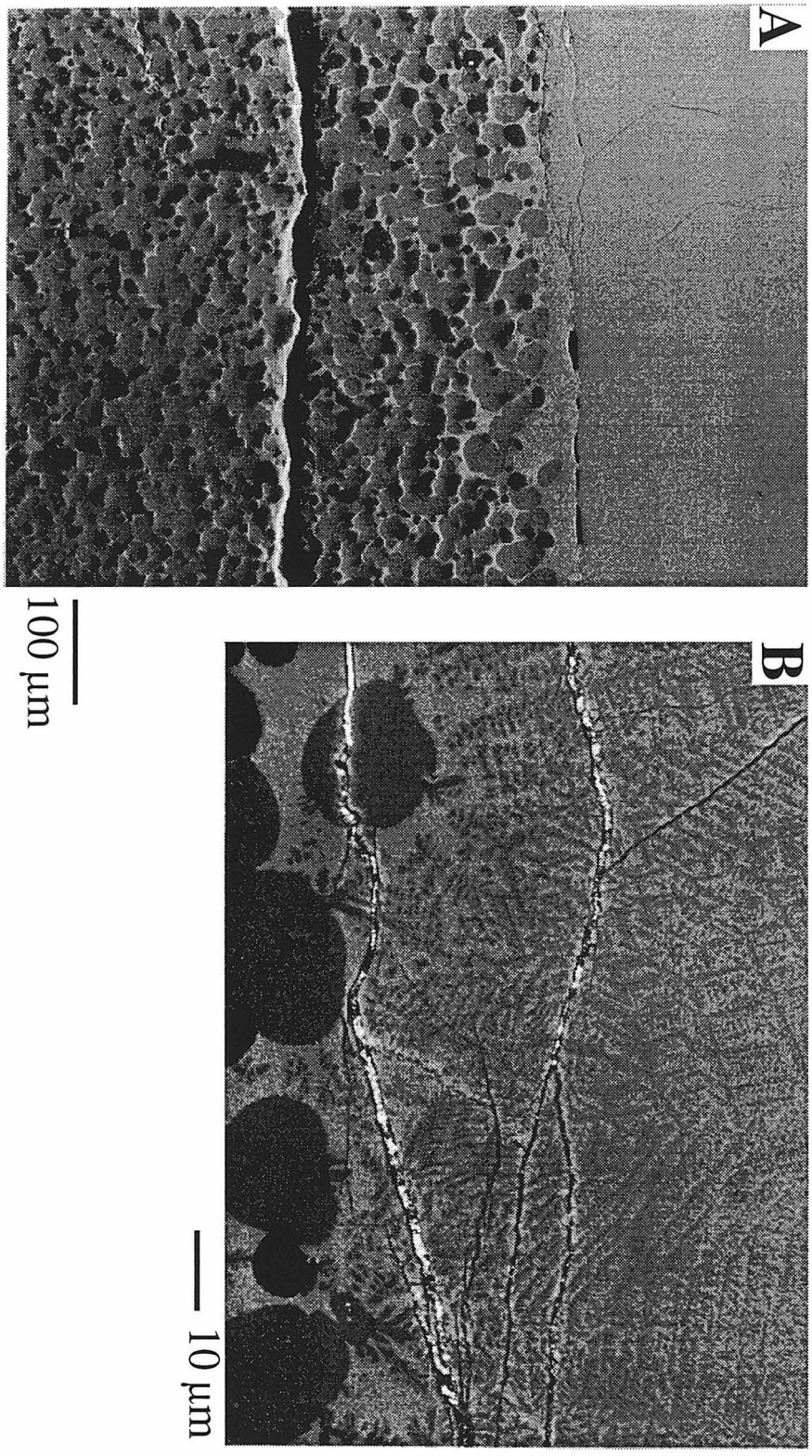
A
100 µm
B
10 µm

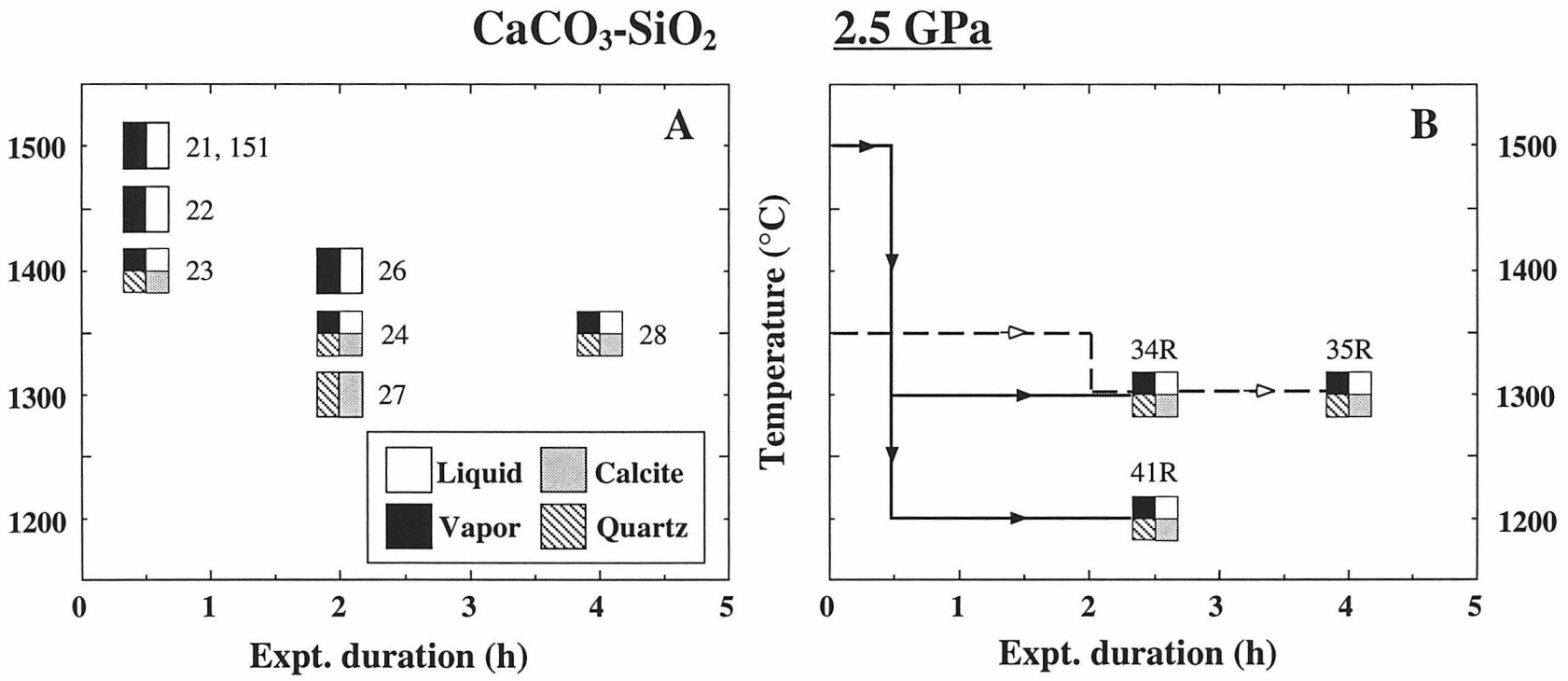

Figure 6. Experimental results and reversal runs, showing the effect of time (for run numbers, see Table 1, and for run positions see Figs. 2 and 3B). A. The 2-hour runs define Reaction 2: CC + Qz = L + V at 1350±50°C. See Table 1 and text for discussion of the phase assemblages for run no. 26 and 27. B. Two-stage reversal runs showing temperature and duration of each stage. Run no. 34R and 41R were first held for 0.5 hours at 1500°C, and run no. 35R was first held at 1350°C for 2 hours.

Figure 7. SEM photomicrographs of runs reversed from the assemblage L+V at 1500°C (Table 1, Fig. 6B). Phases in direction of lighter grey: quartz --> calcite --> liquid.

A. Run no. 34R, held at 1300°C. Glass with calcite dendrites, composed of small rounded units arranged in linear structures.

B. Run no. 41R, held at 1200°C. Calcite dendrites and very small quartz grains with interstitial quenched liquid, with glass increasing in amount locally in regions of coarser grain size.

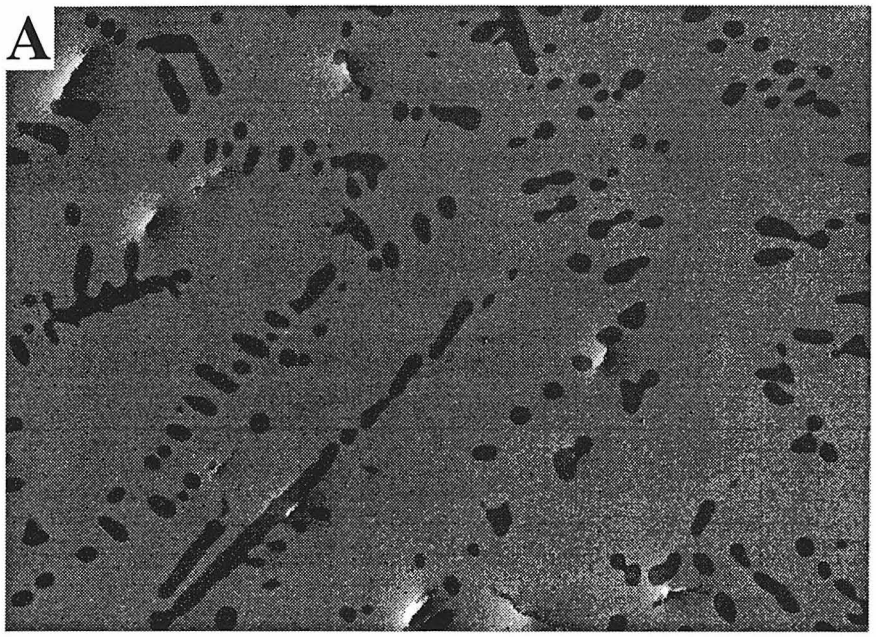
A
100 μm

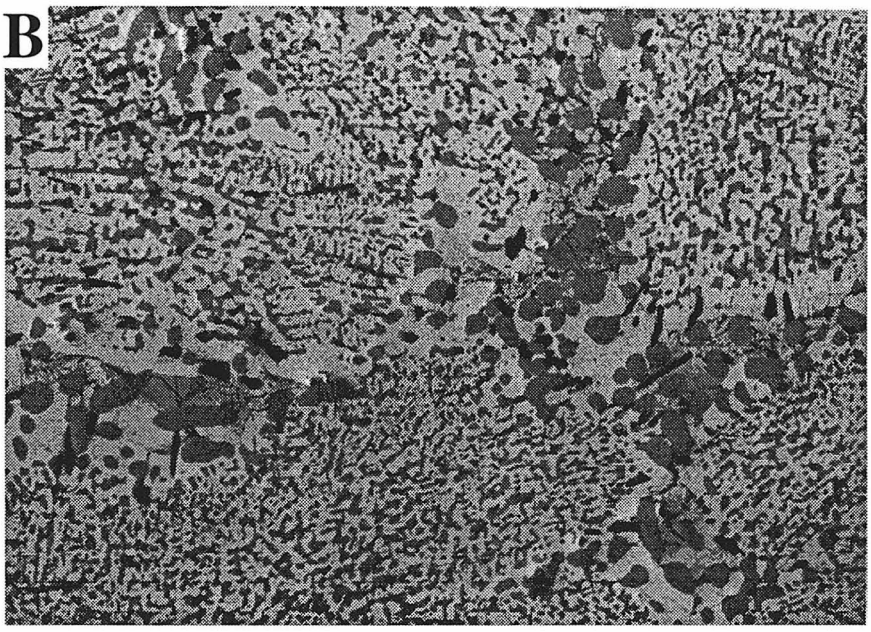
B
100 μm

between the crystals decreases with distance below the interface. The rounded calcite grains in contact with liquid reported by Huang et al. (1980) are clearly displayed. Quartz grains vary from subangular to rounded.

The short-duration run at 1400°C (no. 23) produced the same 4-phase assemblage with similar phase distribution, but the 2-hour run (no. 26, Fig. 6A) was essentially L+V, with traces of calcite and quartz remaining at the bottom of the capsule. The 1300°C run (no. 27) is similar to the lower portion of Figures 4 and 5, but with only a trace of interstitial liquid (estimated 1%) distributed sporadically, and small vapor pits along the boundaries among crystals and liquid. At constant pressure the 4-phase assemblage should be isothermal, so we conclude that Reaction 2 occurs at 1350°C, and attribute the trace of liquid at lower temperature to a trace of absorbed H_2O in the starting material. Calcite formed with polyhedral morphology in contact with other calcite grains, but in the presence of interstitial liquid it became subrounded.

The results of three reversal runs are shown in Figure 6B. Runs 34R and 41R were first held at 1500°C for 0.5 hour to produce liquid and vapor (Fig. 6A), and temperatures were then rapidly lowered into the subsolidus region at 1300°C and 1200°C, respectively, for 2 hours (Fig. 6B). The reversal to 1300°C consisted largely of glass, with vapor bubbles, and some calcite (Fig. 7A), whereas the reversal to 1200°C contained a much higher proportion of crystals (Fig. 7B). Fig. 7A shows sparse, rounded grains to elongated ovoids of calcite with organized structure in dendritic form. A few quartz crystals were found near the edge of the charge. The reversal to 100°C lower consisted for the most part of glass containing fine-grained dendritic calcite-quartz intergrowths, enclosing some irregular areas with much larger, elongated calcite and a few larger prismatic quartz crystals. Reversal run 35R was run initially to generate the 4-phase assemblage of Figure 4, and then lowered through 50°C into the subsolidus region. The upper, originally liquid part produced sparse, rounded calcite in dendritic arrays (compare Fig. 7A), the interface

between the two parts became less well-defined, and a few hexagonal or rounded prismatic crystals of quartz grew in the glass near the interface.

Many more experiments would be necessary to work out the detailed nature of mineral nucleation and growth during subsolidus annealing, but these experiments confirm that Reaction 2 is in reversible equilibrium at temperature near 1350°C, with results consistent with the topology of the phase diagram in Figure 3B. This temperature is about 50°C lower than the curve of Huang et al. (1980). Despite the fact that liquids in many carbonate-rich systems cannot be quenched to glasses, the liquid compositions near e (Fig. 3A) crystallize only slowly even 150°C below the solidus. For the equilibrium assemblage of calcite + quartz to grow, it is necessary for the free CO_2 to diffuse into the subsolidus glass and to combine with Ca^{2+}, which probably has to be extracted from strong bonding in the SiO_4 structural environment.

Rounded calcite without liquid immiscibility

Kjarsgard and Hamilton (1988, 1989) and Brooker and Hamilton (1990) have interpreted rounded and dumbbell-shaped calcites as liquids with compositions equal to or very close to pure $CaCO_3$, immiscible with the silicate-rich liquid in which they were suspended, but Kjarsgaard (personal communication, 1994) is now satisfied with the interpretation of Lee and Wyllie (1992b) that round $CaCO_3$ in the join albite-calcite represents a solid mineral. Although the round calcite in our runs with liquid certainly has the physical appearance of an immiscible liquid (Fig. 5), we are satisfied that its distribution proves it was a mineral under run conditions, and not a $CaCO_3$ liquid.

Evidence that the round calcite represents a mineral phase rather than quenched liquid includes the following: (1) the intermixed distribution of round calcite and quartz beneath a layer of silicate liquid (Fig. 5); (2) the restriction of the assemblage (rounded calcite and other phases) to a few tens of degrees between the solidus and a homogeneous

silicate-CO_2 liquid; (3) the rounded calcites in the run reversed from the liquid field are parts of an organized dendritic feature (Fig. 7A), which represents growth of crystals and not exsolution of liquid (which subsequently solidified to pure $CaCO_3$); (4) the melting temperature of calcite at 2.7 GPa is 1615°C (Fig. 3B), more than 250°C higher than the disappearance of the round phase (labelled calcite) in Fig. 6; (5) the internally consistent phase relations by Huang et al. (1980) for the complete system CaO-SiO_2-CO_2 without intervention of liquid immiscibility, which are now confirmed by our test of the phase fields intersected by the join $CaSiO_3$-$CaCO_3$ at 2.5 GPa (Figs. 2 and 3).

The results in Table 1 and Figure 6, and the samples illustrated in Figures 4, 5 and 7, are consisted with the previous interpretation of a simple eutectic reaction, and we cannot see how these results could be reconciled with a miscibility gap in Figure 3B. The same arguments apply to the round calcites in the join grossularite-$CaCO_3$ at 3.0 GPa (Maaloe and Wyllie, 1975). The rounded shapes of the calcite crystals are most probably the result of surface tension effects between calcite and the carbonate-silicate liquids.

Composition of glass

The composition of the liquid formed from mixture SM in our experiments was estimated from EDS analyses using SEM, complementing the chemographic solubilities represented by the phase diagram, Figure 3A, of Huang et al. (1980). No attempt was made to measure CO_2 solubility by weight loss after ignition or by FTIR.

The ratio of SiO_2 to CaO in the glass from L + V runs measured by EDS/SEM was coincident with that in the starting mixture SM. The presence of vapor confirmed that the glass composition contained less CO_2 than did SM, and therefore lay on the line $\underline{v}$-SM extended in Figure 3A. The determination of CO_2 in the quenched glasses using EDS analysis is based on the deficiency of total detectable elements below 100 %, using calcite as a reference phase, and applying a correction based on quartz analyses. The results

(probable error 1-2 wt%) show decreasing CO_2 solubility with increasing temperature: 1350°C - 17.0 %, 1400°C - 16.9 %, 1450°C - 15.6 %, and 1500°C - 14.2 %. These values straddle m in Figure 3A.

Huang et al. (1980) estimated the position of the CO_2-saturated liquidus field boundary a-b-e-c-d (Fig. 3A) from the geometry of phase fields intersected by several joins through the system. Their field boundary gives a values of about 16 wt% for the CO_2 content of liquid m, which is the liquid composition obtained by projection through v-SM. Complete melting of the mixture SM should yield liquid m and vapor v (compare Fig. 3B).

Structure of glass

The infrared reflectance spectrum of the glass from run 151 is illustrated in Figure 8A. It shows a broad band between 1160 to 1570 cm^{-1}, resulting from the ν_3 vibrational mode of $[CO_3]^{2-}$ unit, which is split into two peaks at 1477 and 1392 cm^{-1}. The peak positioned at 854 cm^{-1} is assigned to the ν_2 vibration of carbonate. Other bands in Figure 8A between 550 and 1160 cm^{-1} are attributed to silicate vibrations. The broad feature between 550-800 cm^{-1} is probably due to the Si-O-Si asymmetric bending and the bridging O asymmetric stretching vibrations. The features between 800-1160 cm^{-1} result from the asymmetric Si-O stretching of SiO_4 tetrahedra. These assignments are summarized in McMillan (1984). The two peaks at 995 and 917 cm^{-1} probably arise from the stretching of silica tetrahedra with two and three non-bridging oxygen, respectively. This gives an indication of partial polymerization in the glass. Figure 8B is an infrared absorption spectrum of the glass quenched from 1500°C (run 151), showing a broad band between 3700 and 2300 cm^{-1} superimposed with two narrower bands centered at 2520 and 2920 cm^{-1}. The broad band is caused by OH^- stretching (equivalent to about 0.5 wt% total water in the glass, using the calibration of Newman et al., 1986),

Figure 8. IR spectra for glass produced from run no. 151, 2.5 GPa, 1500°C, 40 minutes (Table 1, Fig. 6A).

A. Infrared reflectance spectrum from a polished surface of the glass, taken as ratios of reflection intensity of the glass to that of a reference gold surface, illustrating bands from carbonate vibrations around 854 cm^{-1} and between 1160 and 1570 cm^{-1}, and the broad feature for silicate vibrations between 550 and 1160 cm^{-1}.

B. Infrared absorption spectrum from an 80 μm, doubly-polished slab of the glass, illustrating carbonate bands at 1780, 2520 and 2920 cm^{-1}.

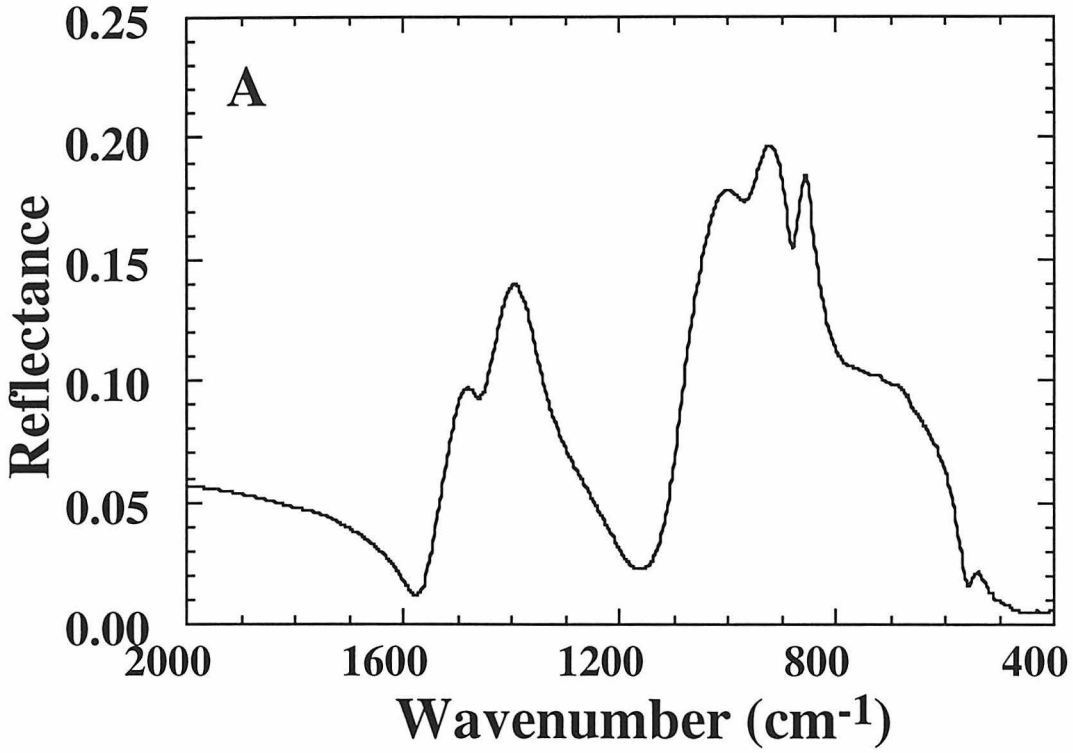
A
Reflectance
0.25
0.20
0.15
0.10
0.05
0.00
2000
1600
1200
800
400
Wavenumber (cm-1)

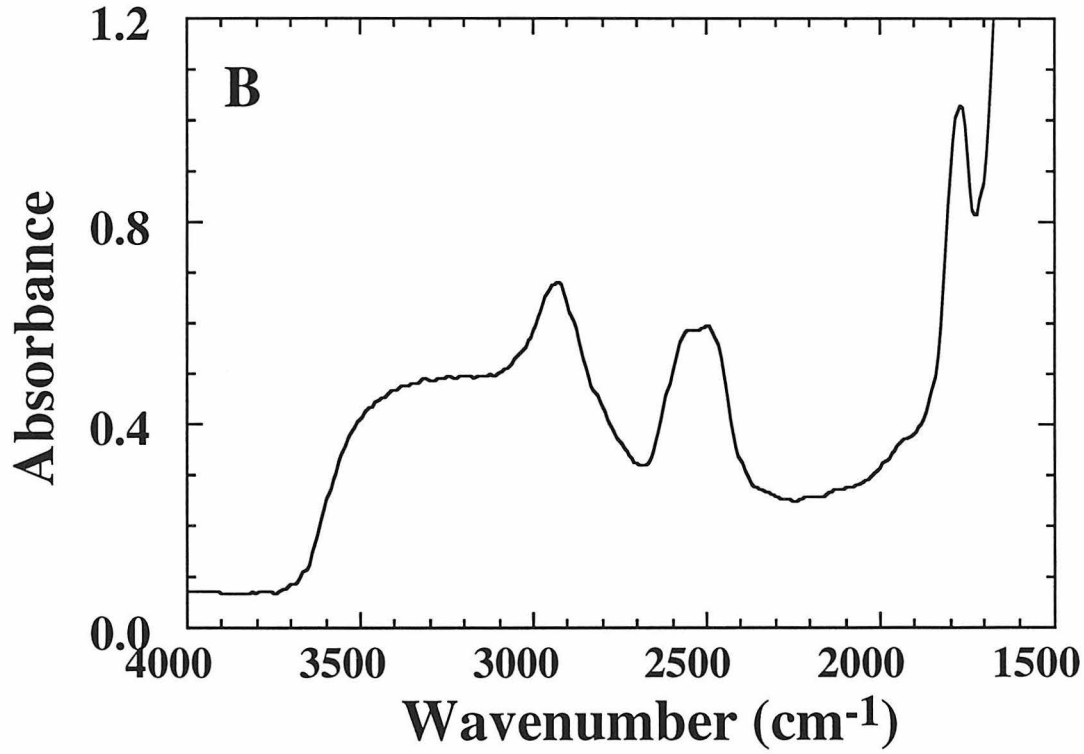
B
Absorbance
1.2
0.8
0.4
0.0
4000
3500
3000
2500
2000
1500
Wavenumber (cm-1)

Table 2. Comparison of integrated molar absorption coefficients between calcite ($CC_{(0001)}$ and CC_{mean}) and the carbonate-rich silicate glass (QzCC glass).

	$CC_{(0001)}$*	CC_{mean}**	QzCC glass (no. 151)
Density [g/cm^3]	2.71		2.79
CO_2 content [wt%]	44.0% (stoichiometry)		13.7% (EDS)
Coefficients at 2500 cm^{-1} [L/(mol·cm^2)]	659	316	660 (±30)
Coefficients at 2900 cm^{-1} [L/(mol·cm^2)]	625	338	570 (±50)

*Coefficients of $CC_{(0001)}$ are calculated values for the (0001) face under unpolarized light, based on the measured intensities of bands using a polarized light with *E* perpandicular to the c-crystallographic axis on a cleavage face.

**Coefficients of CC_{mean} are calculated means over all possible directions of light incident on a calcite crystal, using the expression, $CC_{mean} = -\log[10^{-IA/HW} \times 0.75 + 0.25] \times HW$, where *IA* = integrated absorbance of a band on the (0001) face (calculated) and *HW* = half width of the band.

Note that the uncertainties of the coefficients for the glass were estimated based on the uncertainties on the determination of peak intensity only, whereas the uncertainties of the coefficients for calcite are negligible compared to those for the glass, and therefore are not listed in this table.

and the two bands around 2520 and 2920 cm^{-1} are assigned to the combination of the ν_1+ ν_3 vibrational modes, and the first overtone of ν_3 for $[CO_3]^{2-}$ complex, respectively. The split on the ν_3 mode in Figure 8A is mimicked in the 2520 cm^{-1} band but no longer is resolved in the 2920 cm^{-1} band. The intensity of the characteristic band around 2350 cm^{-1} for the ν_3 antisymmetric stretching mode of molecular CO_2 is insignificant compared to the carbonate bands in the glass spectrum. Therefore, the CO_2 species in the glass is mainly carbonate.

The bands at 2520 and 2920 cm^{-1} discussed above may be used for the quantitative analysis of CO_2 concentrations in glasses, but such an analysis requires a detailed calibration for this purpose. Table 2 compares the CO_2 molar absorption coefficients of a calcite crystal and the glass from run 151, based on chemical data from EDS/SEM, and the IR spectroscopy with the technique described elsewhere (e.g. Fine and Stolper, 1985). The uncertainty is somewhat large if both the uncertainties on the baseline correction for the peaks (Table 2) and CO_2 concentration from EDS are considered. However, it indicates that the absorption coefficients of the carbonate bands in the glass are generally higher than those of calcite (CC_{mean}, a calculated mean over all possible orientation of calcite crystals), and likely due to the greater distortion on the carbonate ions in the glass. The transparent nature of the quenched liquids and the slow growth rate of calcite crystals both during quenching and reversal experiments are likely to be controlled by the liquid structure. However, the detailed effects of liquid structures on the growth mechanism of calcite are not established. Probably the sluggish crystallization is due to the strong interaction of Ca^{2+} with SiO_4 tetrahedra.

DISCUSSION

The main objective of this study was to test for immiscible liquids in the system CaO-SiO_2-CO_2, given the results of Kjarsgaard and Hamilton (1988, 1989) and Brooker

and Hamilton (1990) in related systems summarized in Figure 1. Associated objectives were to examine their interpretation of the rounded and dumbbell shaped $CaCO_3$ phase as a quenched liquid, with the resultant conclusion that the immiscible carbonate liquids could be extremely rich in $CaCO_3$.

No miscibility gap was found between silicate and carbonate liquids at high pressures, consistent with the previous conclusion (Huang et al., 1980) and with Kjarsgaard's revised interpretation in related systems at 0.5 GPa (in Macdonald et al., 1993). The rounded calcite crystals shown in Figure 5 illustrate the tendency of calcite to form in rounded habits in many systems, including those without silicates (e.g. Wyllie and Tuttle, 1960). We presented evidence supporting our conclusion (Lee and Wyllie, 1992a, b) that the round $CaCO_3$ phase in quenched charges in parts of the system Na_2O-CaO-Al_2O_3-SiO_2-CO_2 represented crystalline calcite under experimental conditions, which is now accepted by Kjarsgaard's reinterpretation (personal communication, 1994). This interpretation, along with our results from $NaAlSi_3O_8$-$CaCO_3$ from 1.0 - 2.5 GPa and Kjarsgaard's revised miscibility gap at 0.5 GPa, indicate that although immiscible carbonate liquids may be sovitic, they appear to remain well separated from pure $CaCO_3$ in composition.

The occurrence of metasomatism by carbonate-rich melts in mantle lherzolites is now well established (e.g. Yaxley et al., 1991; Hauri et al., 1993; Ionov et al., 1993). These melts may be derived by the action of CO_2 on lherzolite (e.g. Wyllie and Huang, 1976; Eggler, 1978; Wallace and Green, 1988; Dalton and Wood, 1993), or by CO_2 or melts derived from subducted oceanic crust (Huang et al., 1980; Sweeney et al., 1992). The conditions under which partially carbonated oceanic crust might transport carbonate deep into the earth's interior for long-term storage, might become reduced to generate diamonds (Luth, 1993), or might yield a carbonate-rich melt are of particular interest.

The two reactions in Figure 2 showing the stability limit of dry pelagic limestones, represented by the assemblage calcite+quartz, are situated well above expected

temperatures in subducted oceanic crust, confirming that calcite may survive subduction for storage in the mantle (Huang et al., 1980). In the presence of H_2O, however, reaction and partial melting would yield traces of carbonate-rich melt at much lower temperatures (Wyllie and Haas, 1965; Boettcher and Wyllie, 1969; Huang et al., 1980). The results in Figure 3 focus on the existence of a eutectic, vapor-saturated liquid with composition near CaO - 45%, SiO_2 - 35%, and CO_2 - 20% coexisting with calcite and quartz at 2.5 GPa, and with calcite and wollastonite at pressures below about 1.8 GPa (Fig. 2, Huang et al. 1980). If pockets of pelagic limestones survive subduction, they can generate liquids of this composition at depths of 100 km or more where temperatures reach 1500°C. Such liquids would change composition rapidly by reaction with lherzolite or eclogite, causing significant metasomatic changes in the host rocks as they changed into the carbonate-rich melts in equilibrium with their more mafic hosts.

The significance of the predominance of $[CO_3]^{2-}$ over molecular CO_2 dissolved in the liquids at 2.5 GPa in the system CaO-SiO_2-CO_2 along with the structural information indicates that up to 20 % of carbonates can be incorporated into partially polymerized silicate liquid in presence of a high content of network-modifiers, such as Ca^{2+}. Hence, a CO_2-rich silicate liquid at mantle conditions can evolve to be highly carbonated as silicates are fractionated during magma transportation. The liquid is slow to crystallize, however, compared with most carbonate-rich liquids which cannot be quenched to glasses. The sluggish behavior of liquid carried 50°C below its solidus temperature is shown in Figure 7A, where only a few calcite dendrites have crystallized.

Our partly melted experimental charges demonstrate the ease with which carbonate-rich magma, if formed, could be separated from its source rock (Hunter and McKenzie, 1989; White and Wyllie, 1992). Figure 4 shows a 2-hour run in which all crystals are concentrated into a lower layer with only little interstitial liquid remaining. It appears that the large CO_2 vapor bubbles may take longer to rise through the liquid than minerals take to settle out from the liquid, or than liquid takes to rise from the mineral matrix.

ACKNOWLEDGMENTS

This research was supported by the Earth Science section of the U.S. National Science Foundation grant EAR 92-18806 (P. J. Wyllie) and EAR 91-04059 (G. R. Rossman). This is contribution 5412 of the Division of Geological and Planetary Sciences, California Institute of Technology.

REFERENCES

Baker, M.B., and Wyllie, P.J. (1992) High-pressure apatite solubility in carbonate-rich liquids: Implications for mantle metasomatism. Geochimica et Cosmochimica Acta, 56, 3409-3422.

Bell, K. (1989) (Editor) Carbonatites; genesis and evolution. Unwin Hyman, London, 618p.

Boettcher, A.L., and Wyllie, P.J. (1969) The system CaO-SiO_2-CO_2-H_2O: III. Second critical end-point on the melting curve. Geochimica et Cosmochimica Acta, 33, 611-632.

Brooker, R.A., and Hamilton, D.L. (1990) Three-liquid immiscibility and the origin of carbonatites. Nature, 346, 459-462.

Dalton, J.A., and Wood, B.J. (1993) The compositions of primary carbonate melts and their evolution through wallrock reaction in the mantle. Earth and Planetary Science Letters, 119, 511-525.

Eggler, D.H. (1978) The effect of CO_2 upon partial melting of peridotite in the system Na_2O-CaO-Al_2O_3-MgO-SiO_2-CO_2 to 35 kb, with an analysis of melting in a peridotite-H_2O-CO_2 system. American Journal of Science, 278, 305-343.

Fine, G., and Stolper, E. (1985) The speciation of carbon dioxide in sodium aluminosilicate glasses. Contributions to Mineralogy and Petrology, 91, 105-121.

Freestone, I.C., and Hamilton, D.L. (1980) The role of liquid immiscibility in the genesis of carbonatites - an experimental study. Contributions to Mineralogy and Petrology, 73, 105-117.

Green, D.H., and Wallace, M.E. (1988) Mantle metasomatism by ephemeral carbonatite melts. Nature, 336, 459-462.

Harker, R.I., and Tuttle, O.F. (1956) Experimental data on the P_{CO_2}-T curve for the reaction: calcite + quartz = wollastonite + carbon dioxide. American Journal of Science, 254, 239-256.

Haselton, H.T., Sharp, W.E., and Newton, R.C. (1978) CO_2 fugacity at high temperatures and pressures from experimental decarbonation reactions. Geophysical Research Letters, 5, 753-756.

Hauri, E.H., Shimizu, N., Dieu, J.J., and Hart, S.R. (1993) Evidence for hotspot-related carbonatite metasomatism in the oceanic upper mantle. Nature, 365, 221-227.

Huang, W.-L., and Wyllie, P.J. (1974) Eutectic between wollastonite II and calcite contrasted with thermal barrier in MgO-SiO_2-CO_2 at 30 kilobars, with applications to kimberlite-carbonatite petrogenesis. Earth and Planetary Science Letters, 24, 305-310.

Huang, W.-L., Wyllie, P.J., and Nehru, C.E. (1980) Subsolidus and liquidus phase relationships in the system CaO-SiO_2-CO_2 to 30 kbar with geological applications. American Mineralogist, 65, 285-301.

Hunter, R.H., and McKenzie, D. (1989) The equilibrium geometry of carbonate melts in rocks of mantle composition. Earth and Planetary Science Letters, 92, 347-356.

Ionov, D.A., Dupuy, C., O'Reilly, S.Y., Kopylova, M.G., and Genshaft, Y.S. (1993) Carbonated peridotite xenoliths from Spitsbergen: Implications for trace element signature of mantle carbonate metasomatism. Earth and Planetary Science Letters, 119, 283-297.

Irving, A.J., and Wyllie, P.J. (1975) Subsolidus and melting relationships for calcite, magnesite, and the join $CaCO_3$-$MgCO_3$ to 36 kilobars. Geochimica et Cosmochimica Acta, 39, 35-53.

Kjarsgaard, B.A., and Hamilton, D.L. (1988) Liquid immiscibility and the origin of alkali-poor carbonatites. Mineralogical Magazine, 52, 43-55.

Kjarsgaard, B.A., and Hamilton, D.L. (1989) The genesis of carbonatites by immiscibility. In K. Bell, Ed., Carbonatites; genesis and evolution, 388-404. Unwin Hyman, London.

Kjarsgaard, B.A., and Peterson, T. (1991) Nephelinite-carbonatite liquid immiscibility at Shombole volcano, East Africa: Petrographic and experimental evidence. Mineralogy and Petrology, 43, 293-314.

Koster van Groos, A.F. (1975) The effect of high CO_2 pressures on alkalic rocks and its bearing on the formation of alkalic ultrabasic rocks and the associated carbonatites. American Journal of Science, 275, 163-185.

Koster van Groos, A.F., and Wyllie, P.J. (1966) Liquid immiscibility in the system Na_2O-Al_2O_3-SiO_2-CO_2 at pressures to 1 kilobar. American Journal of Science, 264, 234-255.

Koster van Groos, A.F., and Wyllie, P.J. (1973) Liquid immiscibility in the join $NaAlSi_3O_8$-$CaAl_2Si_2O_8$-Na_2CO_3-H_2O. American Journal of Science, 273, 465-487.

Le Bas, M.J. (1977) Carbonatite-nephelinite volcanism. Wiley, London, 347 p.

Lee, W.-J., and Wyllie, P.J. (1992) New data on CO_2-rich immiscible liquids in Na_2O-CaO-Al_2O_3-SiO_2-CO_2 from 25 to 1 kb: Carbonatite genesis (abstract). EOS Transactions of American Geophysical Union, 73(14), 349-350.

Lee, W.-J., and Wyllie, P.J. (1992) Liquid immiscibility between silicates and carbonates must intersect suitable liquidus field boundaries to have petrogenetic significance. 29th International Geological Congress, Kyoto, Abstracts, 571.

Luth, R.W. (1993) Diamonds, eclogites, and the oxidation state of the Earth's mantle. Science, 261, 66-68.

Maaloe, S., and Wyllie, P.J. (1975) The join grossularite-calcite through the system CaO-Al_2O_3-SiO_2-CO_2 at 30 kilobars: Crystallization range of silicates and carbonates on the liquidus. Earth and Planetary Science Letters, 28, 205-208.

Macdonald, R., Kjarsgaard, B.A., Skilling, I.P., Davies, G.R., Hamilton, D.L., and Black, S (1993). Liquid immiscibility between trachyte and carbonate in ash flow tuffs from Kenya. Contributions to Mineralogy and Petrology, 114, 276-287.

McInnes, B.I.A., and Wyllie, P.J. (1992) Scapolite formation and the production of nephelinitic melts during the subduction of carbonated basalt (abstract). EOS Transactions of the American Geophysical Union, 73(43), 637.

McMillan, P. (1984) A Raman spectroscopic study of glasses in the system CaO-MgO-SiO_2. American Mineralogist, 69, 645-659.

Newman, S., Stolper, E.M., and Epstein, S (1986) Measurement of water in rhyolitic glasses: Calibration of an infrared spectroscopic technique. American Mineralogist, 71, 1527-1541.

Otto, J.W., and Wyllie, P.J. (1993) Relationships between silicate melts and carbonate-precipitating melts in CaO-MgO-SiO_2-CO_2-H_2O at 2 kbar. Mineralogy and Petrology, 48, 343-365.

Sweeney, R.J., Green, D.H., and Sie, S.H. (1992) Trace and minor element partitioning between garnet and amphibole and carbonatitic melt. Earth and Planetary Science Letters, 113, 1-14.

Tuttle, O.F., and Harker, R.I. (1957) Synthesis of spurrite and the reaction wollastonite + calcite = spurrite + carbon dioxide. American Journal of Science, 255, 226-234.

Wallace, M.E., and Green, D.H. (1988) An experimental determination of primaty carbonatite magma composition. Nature, 335, 343-346.

White, B.S., and Wyllie, P.J. (1992) Solidus reactions in synthetic lherzolite-H_2O-CO_2 from 20-30 kbar, with applications to melting and metasomatism. Journal of Volcanology and Geothermal Research, 50, 117-130.

Wyllie, P.J. (1989) Origin of carbonatites: Evidence from phase equilibrium studies. In K. Bell, Ed., Carbonatites; genesis and evolution, 500-545. Unwin Hyman, London.

Wyllie, P.J., and Haas, J.L. (1965) The system $CaO-SiO_2-CO_2-H_2O$: I. Melting relationships with excess vapor at 1 kilobar pressure. Geochimica et Cosmochimica Acta, 29, 871-892.

Wyllie, P.J., and Haas, J.L. (1966) The system $CaO-SiO_2-CO_2-H_2O$: II. The petrogenetic model. Geochimica et Cosmochimica Acta, 30, 525-544.

Wyllie, P.J., and Huang, W.-L. (1976) Carbonation and melting reactions in the system $CaO-MgO-SiO_2-CO_2$ at mantle pressures with geophysical and petrological applications. Contributions to Mineralogy and Petrology, 54, 79-107.

Wyllie, P.J., and Tuttle, O.F. (1960) The system $CaO-CO_2-H_2O$ and the origin of carbonatites. Journal of Petrology, 1, 1-46.

Yaxley, G.M., Crawford, A.J., and Green, D.H. (1991) Evidence for carbonatite metasomatism in spinel peridotite xenoliths from western Victoria, Australia. Earth and Planetary Science Letters, 107, 305-317.

CHAPTER 3

LIQUID IMMISCIBILITY IN THE JOIN $NaAlSi_3O_8$-$CaCO_3$ TO 2.5 GPa AND THE ORIGIN OF CALCIOCARBONATITE MAGMAS

(Lee W.-J. & Wyllie P. J., 1996. Journal of Petrology, in revision;
by permission of Oxford University Press)

ABSTRACT

Field evidence from both intrusive and effusive carbonatites has been interpreted in terms of the occurrence of calcium carbonatite liquids. Experimental evidence adduced to support this conclusion suggested the formation of nearly pure $CaCO_3$ immiscible liquids from a parental silicate-CO_2 melt. Phase relationships in the system Na_2O-CaO-Al_2O_3-SiO_2-CO_2 intersected by the join $NaAlSi_3O_8$-$CaCO_3$ (Ab-CC) at 1.0, 1.5, and 2.5 GPa between 1100 and 1500°C show that the miscibility gap between silicate-rich liquid and carbonate-rich liquid is strongly a function of pressure: 2.5 GPa, between $Ab_{10}CC_{90}$ (by wt%) and $Ab_{65}CC_{35}$ above 1310°C; 1.5 GPa, between $Ab_{23}CC_{77}$ and $Ab_{43}CC_{57}$ above 1285°C; 1.0 GPa, not intersected. The liquidus piercing point between calcite and silicates becomes enriched in $CaCO_3$ with decreasing pressure, from $Ab_{80}CC_{20}$ at 2.5 GPa to $Ab_{47}CC_{53}$ at 1.0 GPa. The analyzed compositions of coexisting liquids permit the construction of liquidus field boundaries and isotherms for the silicate and calcite liquidus surface, and for the miscibility gap between them. On the CO_2-saturated projection Na_2O-CaO-(Al_2O_3+SiO_2) the miscibility gap closes at a critical point towards the sodium-free side of the projection. No immiscible liquid contains more than 80% dissolved $CaCO_3$, and all contain at least 5% Na_2CO_3. A round $CaCO_3$ phase with properties similar to those of immiscible liquid globules is, in fact, crystalline calcite under experimental conditions.

The projected model end-member system Na_2O-CaO-(Al_2O_3+SiO_2)-CO_2 demonstrates the controls exerted on possible magmatic processes by the field boundaries separating liquidus surfaces for silicates, carbonates, and the miscibility gap. These features indicate processes of partial fusion of subducted sediments or sea-water-altered basalt, and controls on the evolution of CO_2-bearing silicate melts. Traces of calcic carbonatite or silicocarbonatite magmas are expected in relatively warm subducted oceanic crust. Original silicate-CO_2 liquids from the mantle may follow paths either to reach (1)

the miscibility gap for exsolution of carbonate-rich liquids, or (2) the silicate-calcite field boundary for coprecipitation of silicate minerals and calcite. Liquid immiscibility plays an important role in the formation of many alkali-bearing carbonatitic magmas. Immiscible carbonate-rich magmas precipitate only silicates until freed from silicate parent, then precipitate only traces of silicate minerals through a wide temperature interval before carbonates are precipitated. We find no support in experiments for the existence of nearly pure $CaCO_3$ calciocarbonatite magmas. Sovites are probably cumulates from immiscible carbonate-rich magmas, and some silicate-carbonatites may be cumulates from silicate magmas enriched in dissolved carbonates by fractional crystallization.

INTRODUCTION

Sovites are the most abundant carbonatites exposed at the Earth's surface (Woolley & Kempe, 1989), but their origins remain uncertain (Bell, 1989; Bailey, 1993). While early field studies provided evidence for their magmatic emplacement (e.g. Brogger, 1921; von Eckermann, 1948), the high melting temperature of calcite and the lack of thermal effects on country rocks argued against the existence of $CaCO_3$-rich sovitic magmas (Bowen, 1924). A resurgence of interest in carbonatites in the 1950s reaffirmed the field evidence for igneous emplacement at moderate temperatures, and the problem of whether sovitic magmas could exist at reasonable geological conditions (Pecora, 1956; Smith, 1956; Heinrich, 1966; Tuttle & Gittins, 1966).

Experimental studies have since confirmed the high melting temperature of calcite, increasing from ~1300°C at 0.1 GPa to ~1500°C at 1.0 GPa (Irving & Wyllie, 1973, 1975), and also shown that dissolved volatile components such as H_2O and F, and alkalis, lower the melting interval of $CaCO_3$ considerably (Wyllie & Tuttle, 1960; Gittins & Tuttle, 1964; Cooper et al., 1975). Wyllie & Tuttle (1960) demonstrated that even a small amount of dissolved H_2O in $CaCO_3$ liquid allowed precipitation of calcite through a wide range of

temperatures, down to ~650°C at 0.1 GPa, which is consistent with the formation of sovite cumulates from a simple carbonatite magma at temperatures consistent with the field observations. Similar demonstrations can be made for the formation of sovite cumulates from dolomitic carbonate liquids (Wyllie, 1965; Fanelli et al., 1986; Otto & Wyllie, 1993; Sweeney et al., 1995), from fluorine-bearing systems (Gittins & Tuttle, 1964; Jago & Gittins, 1991), and from alkali-rich carbonate melts (Cooper et al., 1975).

Field evidence has been adduced for the existence of liquid sovitic magmas from extrusive and intrusive rocks. Keller (1981, 1989) reported tear-drop carbonate lapilli and juvenile carbonatite clasts in several tuff layers in the Kaiserstuhl carbonatites. He considered them to be quenched fragments which preserved the original melt compositions, and noted their similarity to alvikitic dykes and sovitic intrusives in the area. Cooper & Reid (1991) described magmatic textures for Dicker Willem carbonatite dykes which they considered to be compatible with precipitation from Ca-rich carbonatite magma. Rounded grains of calcite discovered in mantle xenoliths have been interpreted as precipitates from immiscible $CaCO_3$-rich liquids (Pyle & Haggerty, 1994; Kogarko & Pcheco, 1994).

The relationship of calciocarbonatite magmas and sovites to primary or parental magmas is still debated. Barker (1989) analyzed the available field evidence, concluding that the carbonatites are generally subordinate to the surrounding silicate rocks, and therefore are likely to be derived from a common silicate-CO_2 parental magma. Bailey (1989, 1993) maintained that this view of volume relationships was incorrect. He reviewed examples of effusive calciocarbonatites, and advocated the concept of primary, relatively high-temperature calciocarbonatite magmas from the mantle.

There is considerable field evidence supporting the role of silicate-carbonate liquid immiscibility in large-scale volcanic to sub-volcanic environments and intrusive complexes (e.g. Dawson, 1966; Le Bas, 1977; Treiman & Essene, 1985; Kjarsgaard & Peterson, 1991; Macdonald et al., 1993; Dawson et al., 1994; Church & Jones, 1995), as well as in

small-scale carbonate globules in mantle xenoliths (e.g. Amundsen, 1987; Pyle & Haggerty, 1994; Kogarko & Pacheco, 1994). Le Bas (1989) strongly advocated that liquid immiscibility can produce a wide spectrum of carbonatite compositions, with (Na_2O + K_2O)/CaO weight ratios ranging from less than 0.6 to 2.3. Advocates of nearly pure $CaCO_3$ magmatic liquids have appealed to the experimental results of Kjaarsgaard & Hamilton (1988, 1989) for the formation of almost pure, high-temperature $CaCO_3$ liquids by immiscibility from feldspathic liquids.

A third process invoked for some carbonatites is fractional crystallization of carbonated silicate melt (e.g. Le Bas, 1977). The feasibility of this process for CO_2-bearing nepheline-normative liquid was confirmed experimentally by Watkinson & Wyllie (1971) and Lee & Wyllie (1994b) from phase fields intersected by the join $NaAlSiO_4$-$CaCO_3$-H_2O at 0.1 GPa, and additional supporting data was given by Otto & Wyllie (1993).

In this contribution, we review experimental data on liquid immiscibility bearing on the origin of sovites, and present new data in a systematic investigation of the ranges of immiscible liquids intersected by the composition join $NaAlSi_3O_8$-$CaCO_3$ at pressures from 1.0 to 2.5 GPa between 1100 and 1500°C (Lee & Wyllie, 1992a, b). Our new results indicate that the maximum $CaCO_3$ that can be dissolved in a carbonate liquid consolute with a silicate liquid is 80 wt%, in contrast with the ~99% $CaCO_3$ reported by Kjarsgaard & Hamilton (1988, 1989); in most likely petrological processes the amount of $CaCO_3$ would be even less.

The synthetic model systems illustrate the effect of silicate-calcite liquidus field boundaries and the liquidus boundaries for the miscibility gap in controlling the paths of crystallization of silicate-CO_2 magmas. The experimental evidence indicates that immiscibility cannot generate nearly pure $CaCO_3$ sovite magmas. The field evidence for the existence of such liquids remains unexplained in terms of the phase equilibrium experiments. $CaCO_3$-rich carbonatite magmas can be generated, and the formation of

plutonic sovites as cumulates from such magmas is favored. The phase boundaries also illustrate the paths of partial fusion for subducted calcite-bearing oceanic crust.

PREVIOUS EXPERIMENTAL STUDIES ON SILICATE-CARBONATE LIQUID IMMISCIBILITY

We review first the previous studies on the system investigated here, and follow with an outline of studies of systems with other components.

Na_2O-CaO-Al_2O_3-SiO_2-CO_2

Figure 1 provides the framework for presenting experimental results in the system Na_2O-CaO-Al_2O_3-SiO_2-CO_2. Figure 1a projects phase compositions from CO_2 onto the tetrahedron Al_2O_3-SiO_2-CaO-Na_2O. Figure 1b shows the tetrahedron collapsed to the triangle (Al_2O_3+SiO_2)-CaO-Na_2O. The compositions of some of the silicate and carbonate minerals encountered in experiments are also plotted. The triangle in Fig. 1b was used by Freestone & Hamilton (1980) to illustrate silicate-carbonate liquid immiscibility, and it was modified to incorporate the components, such as K_2O, MgO, FeO and TiO_2, in order to describe liquid compositions in more complex systems. We refer to it as the Hamilton projection.

Koster van Groos & Wyllie (1966, 1968) used results from the joins Ne-NC and Ab-NC (Fig. 1a) and reported immiscibility between $NaAlSi_3O_8$-rich and Na_2CO_3-rich melts up to 0.1 GPa, initially dry and then with H_2O added. Koster van Groos & Wyllie (1973) found that the miscibility gap persisted with 50% An added to Ab and with 10% H_2O at 0.1 GPa, at temperatures above 750°C. Extrapolation of the miscibility gap boundaries in the composition triangle $NaAlSi_3O_8$-$CaAlSi_2O_8$-Na_2CO_3 (Ab-An-NC in Figs. 1a and 1b) suggested that the gap would close off at a critical point before the silicate

Figure 1. (a) Compositional tetrahedron Al_2O_3-SiO_2-CaO-Na_2O, showing silicate and carbonate phases relavant to the system Na_2O-CaO-Al_2O_3-SiO_2-CO_2, normalized to a CO_2-free basis. The solid circles denote the compositions of these phases, with abbreviations: Ab - albite, Ne - nepheline, An - anorthite, Gr - grossular, Wo - wollastonite, Scap - scapolite, Lar - larnite, Geh - gehlenite, Can - cancranite, CC - calcite, Nye - nyererite, and NC - natrocarbonate. The open circles are projections of the phases on the basal triangle SiO_2-CaO-Na_2O from Al_2O_3. The studied join Ab-CC is indicated by the heavy straight line. (b) Compositional triangle (Al_2O_3 + SiO_2)-CaO-Na_2O, projected from CO_2 (Hamilton projection), showing the same silicate and carbonate phases (solid circles).

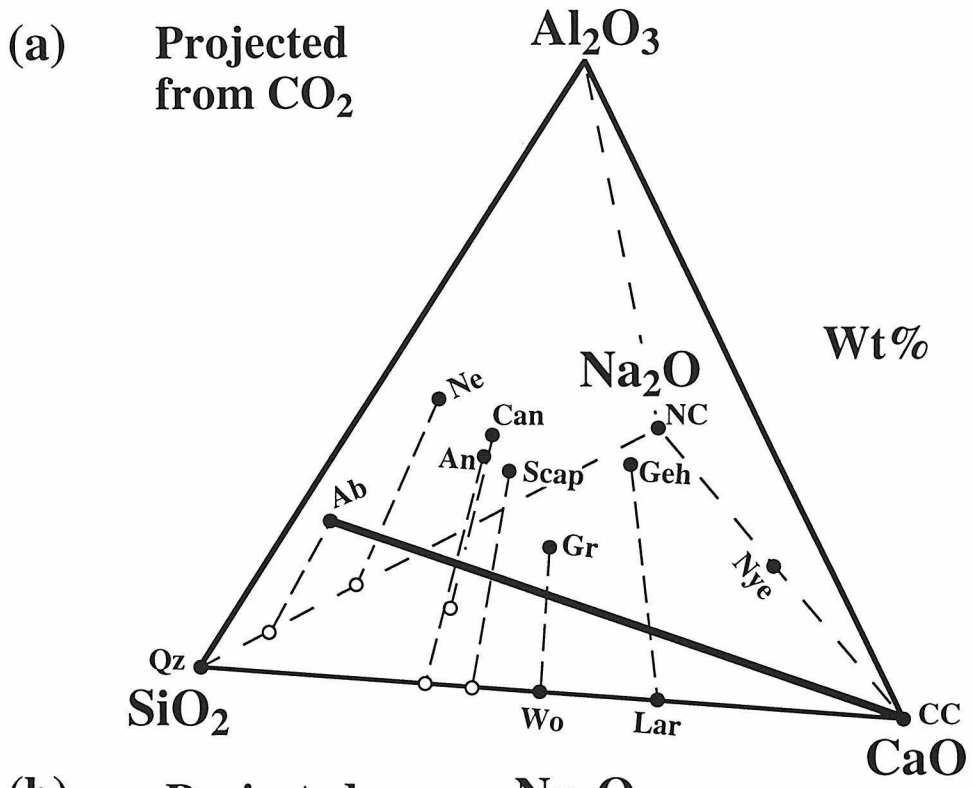
(a)
Projected
from CO_2
Al_2O_3
Wt%
Na_2O
Ne
Can
NC
An
Scap
Geh
Ab
Gr
Nye
Qz
SiO_2
Wo
Lar
CC
CaO

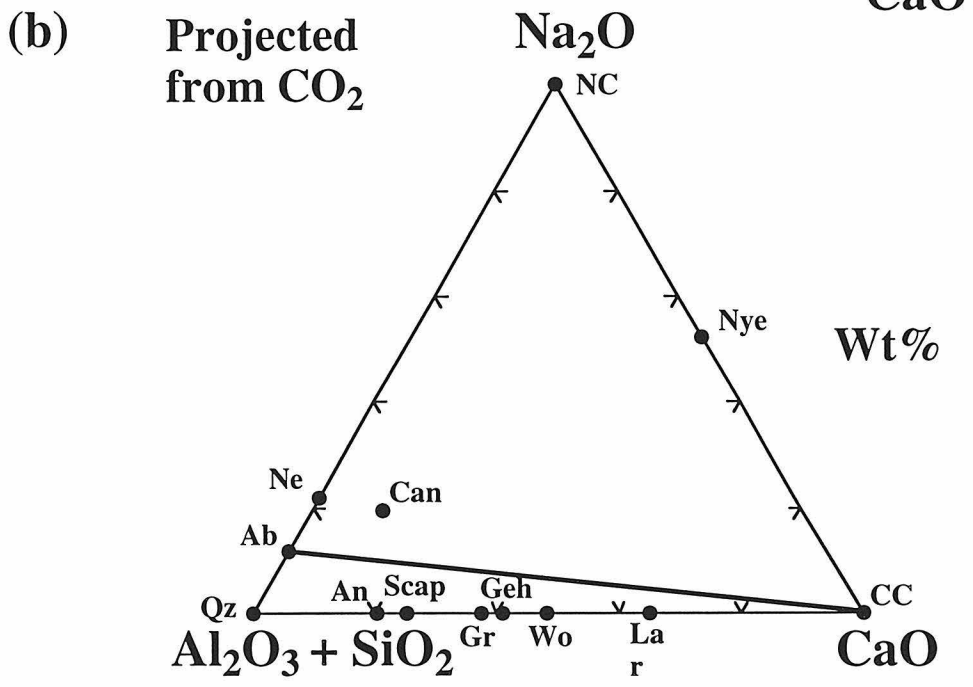
(b)
Projected
from CO_2
Na_2O
NC
Nye
Wt%
Ne
Can
Ab
An
Scap
Geh
Qz
CC
Gr
Wo
La
r
$Al_2O_3 + SiO_2$
CaO

component reached anorthite composition; i.e. the miscibility gap would not reach the alkali-free side (Al_2O_3+SiO_2)-CaO of the triangle in Fig. 1b. Analyses of the quenched liquids showed that the silicate liquid was peralkaline, and the coexisting carbonate liquid was strongly enriched in calcium.

Kjarsgaard & Hamilton (1988, 1989) reported liquid immiscibility in the joins feldspar-(Na,Ca) carbonate between 0.2-0.5 GPa at 1250°C, with reconnaissance runs at 1.5 GPa (Ab-An-NC-CC in Fig 1). Their results at 1250°C and 0.5 GPa are shown by the dashed lines "A-A" in Fig. 2 (corresponding to Fig. 1b); their two-liquid field Ls + Lc extends all the way to the alkali-free side of the projection, and the immiscible carbonate liquid composition extends to almost pure $CaCO_3$. Brooker & Hamilton (1990) studied the same system at 1225°C and 1.5 GPa, and reported the occurrence of three immiscible liquids, Ls + Lc coexisting with nearly pure $CaCO_3$ liquid.

Lee & Wyllie (1992a, b) studied the join albite-calcite (Ab-CC in Fig. 1), and defined the polythermal two-liquid miscibility gap at 2.5 GPa as illustrated by curve B in Fig. 2 (see Lee et al., 1994). Experimental details will be provided below. Kjarsgaard & Hamilton (in preparation; presented in Fig. 5, Macdonald et al., 1993) subsequently revised the textural interpretation of Kjarsgaard & Hamilton's (1988, 1989) results, with the result given as curves "C-C" in Fig. 2, with a represenative tie-line C', for 0.5 GPa and 1250°C. This interpretation is now consistent with our results.

Silicate-carbonate liquid immisciblity in other systems

Koster van Groos (1975) used a variety of silicate rock components to extend the range of two-liquid compositions at pressures up to 1 GPa. Verwoerd (1978) determined a miscibility gap at 0.2 and 1 GPa in a join between synthetic ijolite and calcite-bearing natrocarbonatite. Freestone & Hamilton (1980) used natural rocks from Oldoinyo Lengai, ranging from felsic nephelinite to phonolite, mixed with synthetic carbonatite with variable

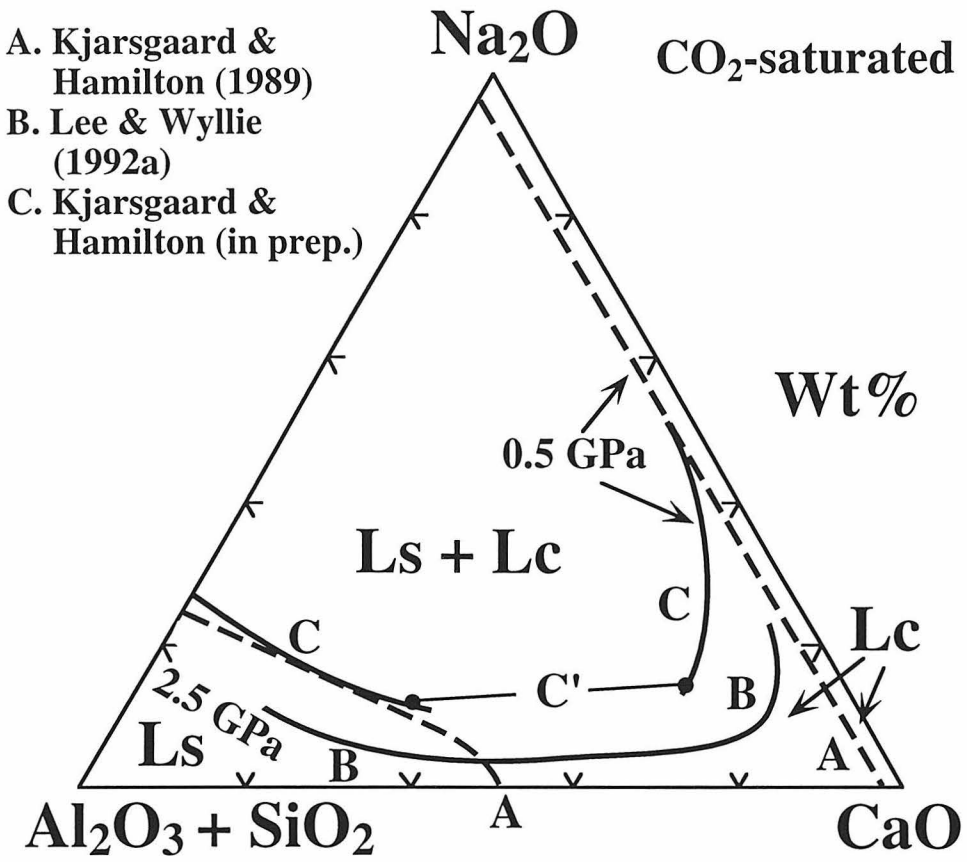

Figure 2. Silicate-carbonate two-liquid fields projected onto the CO_2-saturated, Hamitlon projection (Al_2O_3 + SiO_2)-CaO-Na2O, showing results (heavy curves) from (A) Kjarsgaard & Hamilton (1988, 1989) at 0.5 GPa and 1250°C, (B) Lee & Wyllie (1992a, b, this study) at 2.5 GPa, and (C) Kjarsgaard & Hamilton (in prep.) at 0.5 GPa and 1250°C, presented in Macdonald et al. (1993, Fig. 5b). The tie-line C' connects coexisting silicate-rich liquid (Ls) and carbonate-rich liquid (Lc). Note that for A the field Ls + Lc extends all the way to the Na2O-free side.

Na/Ca in experiments at crustal pressures and temperatures between 900 and 1250°C. The miscibility gap expands with increase in P_{CO_2} and decrease in temperature, and closes away from Na_2O-rich compositions (compare curves B-B and C-C, Fig. 2, in contrast with dashed curves A-A). Their results show that melts of phonolite to nephelinite composition are immiscible with alkali-rich carbonate melts. Kjarsgaard et al. (1995) further generated immiscible alkali-rich carbonatite liquids along with solid phases at 50-375 MPa and 700-850°C, utilizing starting compositions of carbonated peralkaline nephelinite. They compared the phase compositions in experiments and natural lavas from Oldoinyo Lengai, and suggested that the P-T conditions operating to produce the natrocarbonatite lavas are quite low, i.e. $\leq$ 100 MPa and $\leq$ 750°C. A similar study on the evolved silicate rocks by Kjarsgaard & Peterson (1991) provided evidence of liquid immiscibility in the formation of alkali-poor carbonatites. They used two nephelinite lavas from Shombole volcano which contained carbonate-rich globules representing quenched liquid, and performed experiments with and without additional calcite at 0.2-0.5 GPa and 975-925°C. They concluded that the full range of Ca-Mg-(Na + K) carbonatites could be generated by liquid immiscibility from nephelinitic magmas of different compositions.

Baker & Wyllie (1990) determined the extent of silicate-carbonate liquid immiscibility at 2.5 GPa and 1050-1300°C using mixtures of magnesian (primitive) nephelinite, dolomite and sodium carbonate. The magnesian two-liquid field at 2.5 GPa projected into the Hamilton diagram is much smaller than the fields for Mg-free systems in Fig. 2. Lee & Wyllie (1994a) reported that the two-liquid field for magnesian liquids expanded with decreasing pressure to 1.0 GPa, but remained smaller than the miscibility gaps of Mg-free liquids plotted in Fig. 2.

There have been few determinations of trace element partitioning between immiscible silicate-carbonate liquids. Wendlandt & Harrison (1979) measured the partition coefficients of rare earth elements between carbonate and silicate liquids and vapor in the system K_2O-Al_2O_3-SiO_2-CO_2 at 0.5 and 2 GPa between 1100 and 1300°C.

Hamilton et al. (1989) determined the distribution coefficients of trace elements between phonolite/sodium-rich carbonate and nephelinite/calcium-rich carbonate liquid pairs at 0.1-0.6 GPa and 1050-1250°C, delineating the partitioning behaviors of those elements as a function of pressure, temperature and structure of the silicate conjugate melt. Jones et al. (1995) reported silicate liquid/carbonate liquid partition coefficients for a suite of incompatible elements at 0.7 to 2 GPa between 1100 and 1400°C, using a synthetic mid-ocean-ridge basalt composition with (Na,Ca)-carbonate.

EXPERIMENTAL METHODS

The starting materials stored in dessicators were: (1) primary standard grade $CaCO_3$ powders (Alfa Product), dried at 110°C for at least one day; (2) Amelia albite crystals, dried at 110°C for at least one day; (3) synthetic albite glass, dehydrated at 800°C for 2 hours; (4) starting mixtures ground with ethanol in an agate mortar to obtain fine-grained, uniform samples. Most starting mixtures used albite crystals, but $Ab_{40}CC_{60}$ and $Ab_{90}CC_{10}$ were also made with albite glass. All starting mixtures (about 5 mg for each run) were held for more than an hour in a vacuum drying oven at 110°C before being loaded into about 4 mm long platinum capsules. Starting mixtures dried in this way contain about 0.6 wt% H_2O, as estimated from an IR study of carbonated silicate glass from the join quartz-calcite (Lee et al., 1994).

Experiments were done in 1.27-cm diameter piston-cylinder apparatus, with calcium fluoride as a pressure medium. Temperature was controlled and monitored by $W_{95}Rh_5$-$W_{74}Rh_{26}$ thermocouple with no correction for the effects of pressure on the EMF. Run duration varied from run to run, typically less than 4 hours for liquidus conditions and up to 24 hours at subsolidus conditions. Experiments were terminated by turning off the electrical power, and the quenching rate was about 100°C per second for the first 600°C and dropped to slower than 50°C/sec at lower temperature. For most

experiments, pressure was not held constant during quenching. Pressure accuracy is about ±0.05 GPa, and temperature accuracy is estimated to be ±10°C. No pressure correction was made for the effects of friction.

Run products were mounted in a brass-holder with petropoxy, polished by Al_2O_3 powers and cleaned by compressed air, without using water, and then carbon-coated. Phases were identified by textures and morphology observed under the petrographic microscope (reflected and transmitted light) and a Camscan scanning electron microscope (SEM) fitted with an energy dispersive x-ray system (EDS). Phases were analyzed by EDS using a beam current of 0.1 nA on brass. The quenched liquids were analyzed up to ten times in raster modes with covered area of several tens square micrometers. Phases encountered (Figs. 1-4) are silicate-rich liquid (Ls), carbonate-rich liquid (Lc), calcite (CC), albite (Ab), wollastonite (Wo), and vapor (V).

Several approaches were used to test for the attainment of equilibrium: (1) increasing the run duration, (2) comparing results from mixtures using albite glass or crystals, (3) using two-stage reversal runs from liquid into two-liquid field. An example of the effect of increasing run duration at constant pressure and temperature is shown by runs #5 and #51 for $Ab_{40}CC_{60}$ at 1300°C and 2.5 GPa (Table 1). Run #5 for 1 hour shows calcite crystals in the process of melting, obviously out of textural equilibrium (Fig. 4a); crystal-liquid boundaries showed both concave and convex curvatures. A second (carbonate-rich) liquid was present in narrow seams between crystals. After 4 hours, run #51 contained only silicate-rich liquid and rounded calcite with vapor; the carbonate-rich melt had disappeared. Results from the two starting mixtures $Ab_{40}CC_{60}$ with albite crystals or glass were compared at 1400°C and 2.5 GPa for 1 hour (Runs #6 and #8, Table 1), after which both had formed two immiscible liquids and vapor, with the liquids in both runs having similar compositions. Albite glass normally reacts faster than albite crystals. This experiment indicates that 1 hour is sufficient for attainment of equilibrium with crystalline starting materials at the liquidus.

Table 1. Experimental results for the join $NaAlSi_3O_8$-$CaCO_3$ (Ab-CC).

Run	Starting Composition wt.% $NaAlSi_3O_8$	$CaCO_3$	Press. GPa	Temp. °C	Time hr	Interpretted phase assemblage	Additional phase and description
47	20	80	2.5	1450	1	Lc + V	
46	20	80	2.5	1400	1	CC + Lc + Ls + V	
53	20	80	2.5	1400	4	CC + Lc + Ls + V	
45	20	80	2.5	1350	1	CC + Ls + V	
52	20	80	2.5	1350	4	CC + Lc + Ls + V	
59R	20	80	2.5	1450	1		
				1350	6	CC + Lc + Ls + V	
40	40	60	2.5	1500	1	Lc + Ls + V	
54	40	60	2.5	1450	1	Lc + Ls + V	
56	40	60	2.5	1450	2	Lc + Ls + V	
6	40	60	2.5	1400	1	Lc + Ls + V	
8*	40	60	2.5	1400	1	Lc + Ls + V	
50	40	60	2.5	1350	1	Lc + Ls + V	
5	40	60	2.5	1300	1	CC + Lc + Ls + V	
51	40	60	2.5	1300	4	CC + Ls + V	
3	40	60	2.5	1250	1	CC + Ab	
14	40	60	2.5	1250	24	CC + Ls + V	
2	40	60	2.5	1200	1	CC + Ab	
7	40	60	2.5	1200	24	CC + Ab	L(tr), V(tr)
9*	40	60	2.5	1200	24	CC + Ab (glass?)	L(tr), V(tr)
4	40	60	2.5	1150	4	CC + Ab	
39	40	60	2.5	1100	4	CC + Ab	
42	50	50	2.5	1450	1	Ls + V	
43	50	50	2.5	1400	1	Lc + Ls + V	
49	50	50	2.5	1350	2	Lc + Ls + V	
58R	50	50	2.5	1450	1		
				1350	2	Lc + Ls + V	
60R	50	50	2.5	1450	1		

				1350	6	Lc + Ls + V	
48	50	50	2.5	1300	2	CC + Ls + V	
37	65	35	2.5	1400	1	Ls + V	
44	65	35	2.5	1300	2	CC + Ls + V	
38	65	35	2.5	1250	2	Ab + CC	
36	65	35	2.5	1200	4	Ab + CC	
61	80	20	2.5	1300	2	Ls + V	CC(tr),
Ab(qn)							
63	80	20	2.5	1250	24	Ab + CC + Ls + V	
62	80	20	2.5	1100	24	Ab + CC	L(tr), V(tr)
57	90	10	2.5	1400	2	Ls + V	
55	90	10	2.5	1350	2	Ab + Ls + V	
11	90	10	2.5	1300	1	Ab + Ls + V	
17*	90	10	2.5	1300	1	Ab (glass?) + Ls + V	
10	90	10	2.5	1200	24	Ab + CC	L(tr), V(tr)
85*	40	60	2.0	1300	2	CC + Lc + Ls + V	
91	20	80	1.5	1300	2	CC + Lc + V	
92	30	70	1.5	1300	2	CC + Lc + Ls + V	
86*	40	60	1.5	1300	4	Lc + Ls + V	
90	40	60	1.5	1250	4	CC + Ls + V	
94	50	50	1.5	1300	2	Ls + V	
102	50	50	1.5	1250	4	CC + Ls + V	
105	50	50	1.5	1200	4	CC + Ab + Ls + V	
101	65	35	1.5	1275	2	Ls + V	
103	65	35	1.5	1250	4	Ls + V	
104	65	35	1.5	1225	4	Ls + V	
111	65	35	1.5	1200	4	CC + Ab + Ls + V	
113	75	25	1.5	1225	4	Ab + Ls + V	
109	10	90	1.0	1400	1	L + V	Wo(qn)
95	10	90	1.0	1350	3	CC + L + V	
84	20	80	1.0	1350	2	L + V	
107	20	80	1.0	1300	2	L + V	
110	20	80	1.0	1250	2	CC + L + V	

82	20	80	1.0	1200	2	CC + L + V	
93	30	70	1.0	1250	2	L + V	
108	30	70	1.0	1200	2	CC + L + V	
88	40	60	1.0	1300	2	L + V	
87	40	60	1.0	1250	2	L + V	
81*	40	60	1.0	1200	2	L + V	
106	40	60	1.0	1175	4	CC + L + V	Wo(tr)
83*	40	60	1.0	1150	4	CC + Wo + L +V	Olig(tr)
97	50	50	1.0	1175	4	L + V + Wo(tr)	
96	50	50	1.0	1150	4	CC + Wo + L + V	
80	65	35	1.0	1150	2	Wo + L + V	
79	80	20	1.0	1150	2	Ab + Wo + L + V	

*: albite glass starting material. R: reversals. tr: trace phase. qn: quenched phase. Phase abbreviation: CC - calcite, Ab - albite, Ls - silicate-rich liquid, Lc - carbonate-rich liquid, Wo - wollastonite, Olig - oligoclase, V - vapor, and L - liquid.

Several reversal runs were carried out. For example, the runs with mixture $Ab_{50}CC_{50}$ (#58 and #60, Table 1) were first held at 1450°C and 2.5 GPa for an hour where they formed L + V (see run #42), and then lowered to 1350°C isobarically for 2 and 6 hours, respectively, into the field defined by other runs as Ls + Lc + V. Both runs produced the 2-liquid phase assemblage. On the basis of these and other tests, we estimated that at 2.5 GPa, 1 to 2 hours were sufficient for runs above 1350°C and with more than 50% albite along the join. With increasing calcite and lower temperatures at the liquidus, up to 4 hours were required. We applied the same criteria to the experiments at 1.5 and 1.0 GPa. At subsolidus condition, runs were generally held for 24 hours.

EXPERIMENTAL RESULTS FOR $NaAlSi_3O_8$-$CaCO_3$

We studied the join $NaAlSi_3O_8$-$CaCO_3$ (Ab-CC) at pressures of 2.5 GPa, 1.5 GPa, and 1.0 GPa, at temperatures from 1500 to 1100°C, with emphasis on mapping the liquid miscibility gap, the liquidi for albite and for calcite, and the piercing point between these liquidus fields for the coprecipitation of albite and calcite; the liquidus for wollastonite is also intersected at 1.0 GPa. Melting temperatures for albite and calcite are taken from Boyd & England (1963), and from Irving & Wyllie (1975). We illustrate the key features for phase identification (Figs. 3 and 4), the phase fields intersected (Table 1, Figs. 5-7), and the analyses of the liquids which provides the first step for the construction of phase diagrams (Table 2, Figs. 8-12).

Identification of phases

Identification of the phases involved interpretation of features from macro- to micro-scale. The silicate-rich liquid (Ls) and the carbonate-rich liquid (Lc) commonly separated completely into discrete, large volumes (Figs. 3a and 3b), and Ls tended to form

Figure 3. (a) Sketch of cross section for the sample charge run #6 (2.5 GPa, 1400°C, $Ab_{40}CC_{60}$, Table 1), showing a large silicate bead (Ls) surrounded by quenched carbonate-rich liquid (Lc), and the separation of vapor phase (V, black pore space) from the immiscible liquids. The outline is the Pt capsule. (b) Back scattered electron (BSE) microphotograph for the polished surface of the same charge, from the lower left corner in (a), showing silicate-rich glass (light gray portion) and quenched carbonate-rich liquid with intergrowth of calcite crystals (light gray rounded material with size up to 10 mm) and interstitial silicate rich material (dark grey). (c) Sketch of cross section for run #52 (2.5 GPa, 1350°C, $Ab_{20}CC_{80}$), showing an assemblage of Ls + Lc + CC + V (Table 1). The shaded area in the lower portion of the capsule represents cumulative of calcite crystals with only trace interstitial liquid.

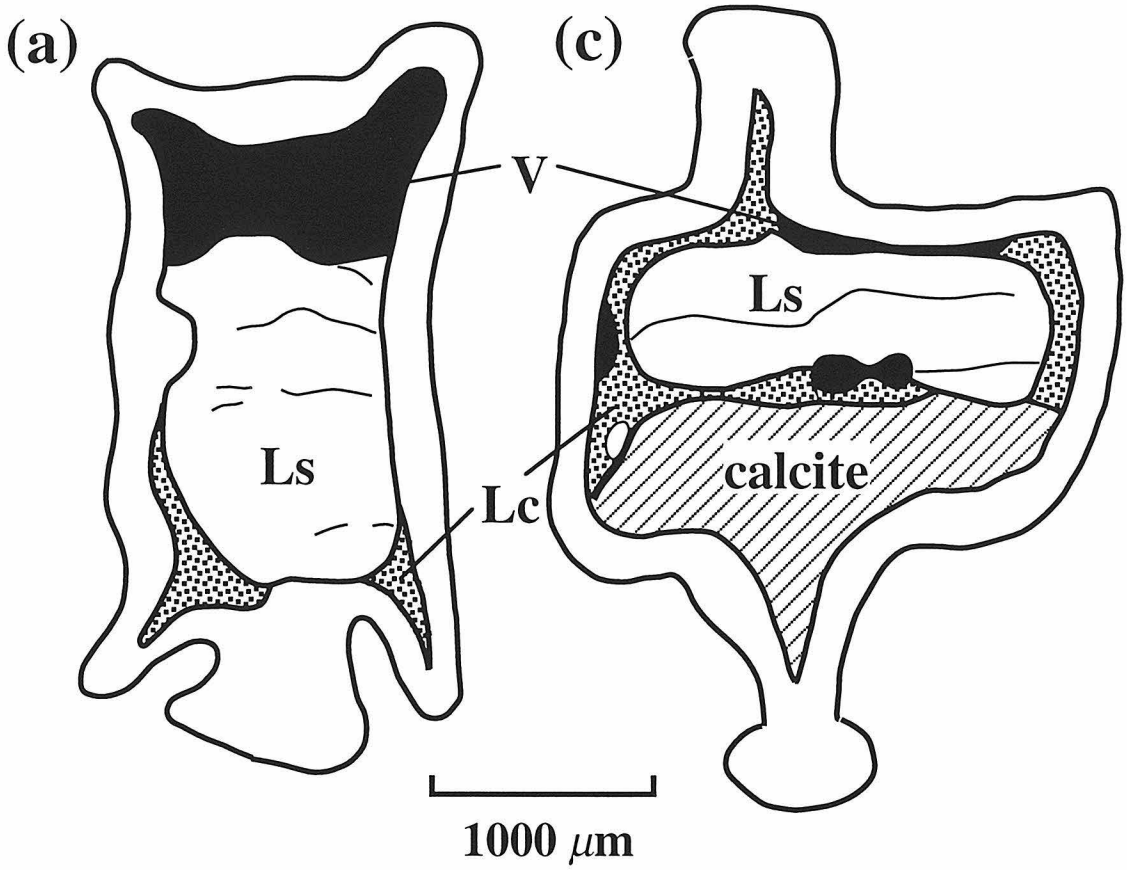
(a)
(c)
V
Ls
Lc
Ls
calcite
1000 μm

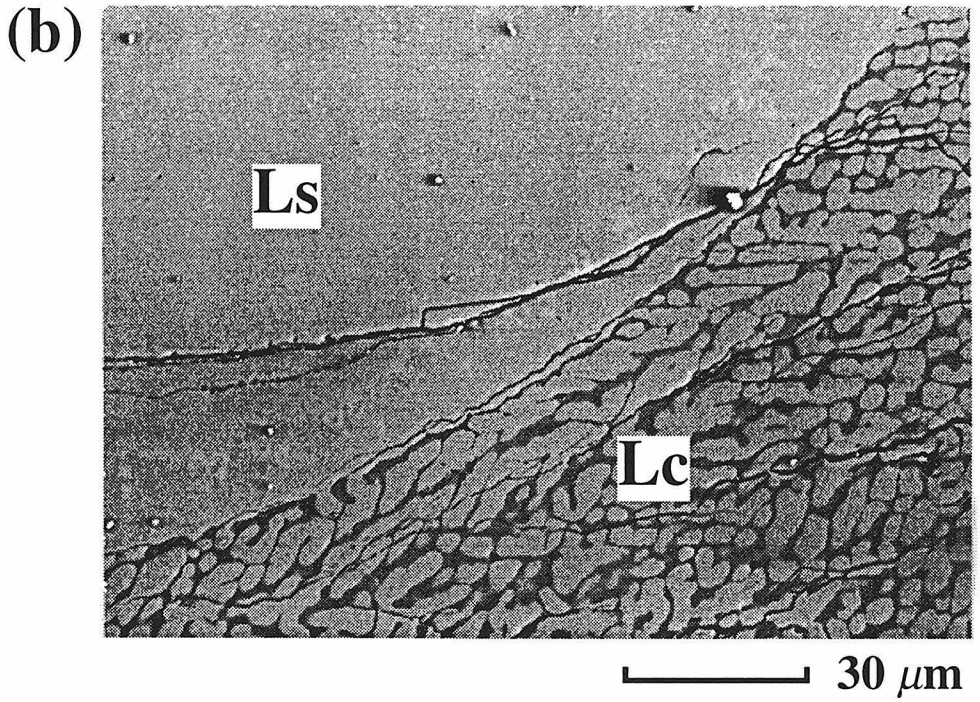
(b)
Ls
Lc
30 μm

a single bead with concave-outward surfaces. At near-liquidus temperatures the vapor phase also separated completely. The microscopic characteristics of the liquids, which changed with composition, pressure and temperature, could thus be determined with certainty from the discrete volumes, and identified in phase assemblages containing interstitial liquid. Figure 3b is a microscopic view of the boundary between Ls and Lc in Fig. 3a. Calcite crystals, as coexisted with immiscible liquids, accumulated below the liquids, with almost complete separation as in Fig. 3c.

Vapor is present in all runs above the solidus, easily identified as spherical cavities in quenched liquids and within or at the margins of calcite (Figs. 4b and d). In near-solidus runs, the size of vapor vesicles is several order of magnitude smaller than in runs near the liquidus. In high-temperature runs, the vapor forms large bubbles which tend to rise to the top of the capsule leaving empty space after the capsule is opened (Fig. 3a).

Silicate-rich liquids (Ls) quench to transparent to translucent glass, and calcite-rich liquids (Lc) quench to dendritic calcite (in various forms) with interstitial silicate-rich material. Figure 3b shows detail of the two-phase quenched Lc against the uniform glass, Ls. The light dendritic calcite (pure $CaCO_3$ according to SEM analyses) is set in darker, silicate-rich material. The outlines of individual calcite grains are rounded or ameboid, but the geometrical arrangement of the grains into obvious dendrites confirms the crystallographic control on the quenched material; these small, rounded calcite grains (1-10 μm) are crystals, unrelated to liquid immiscibility during quenching. When two liquids are present, Ls tends to rise above Lc, but surface tension effects dominate and a large glass bead forms in the center of the capsule, forcing Lc into corners below and above Ls (Figs. 3a and c). At 1.0 GPa where no immiscible liquids were found, there is continuous change in texture of quenched liquids between these two end-members; transparent glass persists with increasing $CaCO_3$ component up to mixture $Ab_{40}CC_{60}$, and the dendritic calcite increases in size to 10 μm in liquid quenched from mixture $Ab_{10}CC_{90}$.

Figure 4 illustrates liquids coexisting with crystals. Within the fields of Ab + Ls + V and Ab + CC + Ls + V, the liquids quenched to an intimate intergrowth of albite and carbonate, probably with some glass. Figure 4a shows near-solidus conditions, with light-colored Ls interstitial between albite crystals in typical partially melted texture. Figure 4d shows in the field CC + L + V, the charge containing suspended calcite crystals in liquid also contains a lower layer of calcite concentrated at the bottom of a capsule (cf. Fig. 3c). Figure 4b shows the non-equilibrium texture for a short-duration run #5 discussed above. The liquid Ls (dark) forms irregular globules, with no organized relationship to the calcite crystals. The outlines of hexagonal calcite crystals are marked by thin seams of a liquid which are richer in carbonate (Lc). In runs of longer duration, Ls may rise into a separate layer above the calcite or maintain calcite grains in suspension (Fig. 4d).

Calcite occurs in a variety of forms, depending on the bulk composition of starting mixtures and phase assemblage. Figure 4c for the assemblage Ab + CC shows the rounded to subrounded equant grains (light-colored, 5-10 μm) which are characteristic of subsolidus calcite under many conditions. Figure 4b shows the growth of calcite into much larger hexagonal forms approaching 100 μm in size, during non-equilibrium progressive melting. With longer runs, as more liquid is formed, the calcite becomes rounded, as shown in Fig. 4d. Small rounded calcite grains formed in Lc during quench are organized in dendritic forms, as described above (Fig. 3b). The remarkably rounded shapes of calcite suspended in Lc in Fig. 4d are strongly reminiscent of immiscible liquids (Kjarsgaard & Hamilton, 1988, 1989; Brooker & Hamilton, 1990). However, we summarize below compelling evidence that these are crystalline calcite during run conditions.

Albite, in some runs containing a few percent CaO, crystallizes at each pressure studied. Figs. 4c and 4a shows albite coexisting with rounded crystalline calcite (subsolidus) and with interstitial liquid, respectively. Albite crystals are usually euhedral near the liquidus, with size up to 20 μm. Albite grows as a quench mineral in some runs.

Figure 4. (a) BSE microphotograph of polished surface for run #11 (2.5 GPa, 1300°C, $Ab_{90}CC_{10}$), showing a phase assemblage of Ab + Ls + V (Table 1). The dark grains are albite crystals, with light interstitial liquid and vapor bubbles. (b) BSE image for run #5 (2.5 GPa, 1300°C, $Ab_{40}CC_{60}$), revealing the features of progressively melting (Table 1, cf. longer-duration run #51). Large pieces of calcite (lightest grey) grew with slightly wet hexagonal shape in conjunction with other grains, but formed both convex and concave geometries adjacent to quenched liquid (grey), indicating the run did not reach equilibrium. (c) BSE microphotograph for run #10 (2.5 GPa, 1200°C, $Ab_{90}CC_{10}$), illustrating a subsolidus run product (cf. Fig. 4a; Table 1). Light grains are rounded to subrounded calcite crystals, distributed sporadically between albite crystals. (d) BSE image for run 82 (1.0 GPa, 1200°C, $Ab_{20}CC_{80}$), showing a charge in the field L + CC + V (Table 1). Notice that the calcite crystals (grey) are remarkably rounded, suspended in quenched carbonate-rich liquid (light grey). Vapor bubbles are filled in material during sample preparation for SEM.

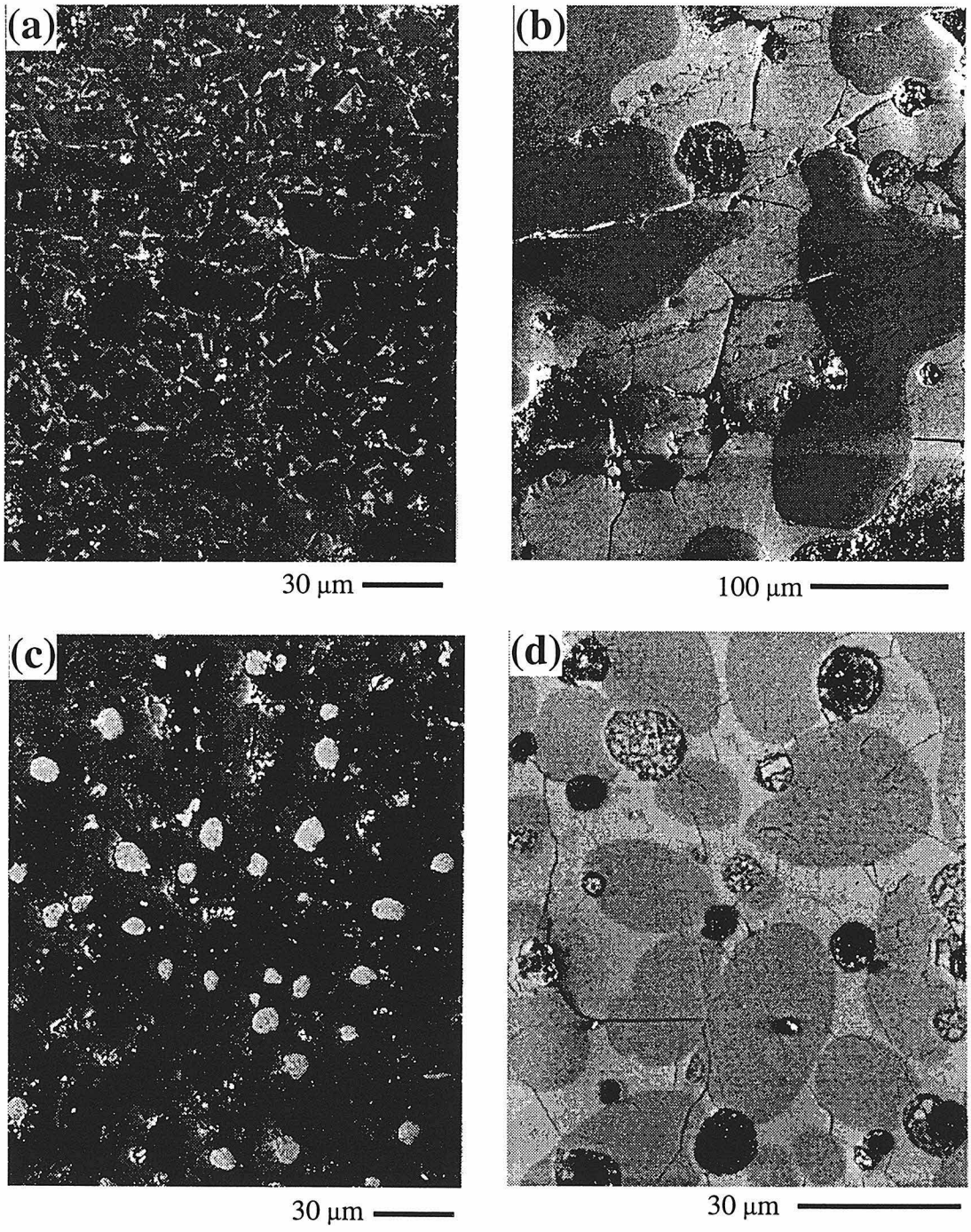
(a)
30 μm
(b)
100 μm
(c)
30 μm
(d)
30 μm

Wollastonite grows with liquid as rectangular crystals in the central part of the join at 1.0 GPa. Acicular wollastonite is interpreted to be a mineral precipitated during the quench. Run #79 shows two populations of crystals, one with rectangular shape, and the other greatly elongated.

Phase fields intersected at 2.5 GPa, 1.5 GPa, and 1.0 GPa

Results for 2.5 GPa are listed in Table 1 and plotted in Fig. 5. The determination of the field boundaries relies not only on the phase assemblages in the runs but also on the information extracted from the liquid compositions at different temperatures, and phase proportions based on the mass-balance consideration. Note the wide miscibility gap between about $Ab_{10}CC_{90}$ and $Ab_{65}CC_{35}$ at 1310°, which extrapolates toward a critical point (a point on the critical curve extending across the liquidus dome above the miscibility gap) apparently not far above 1500°C. The two-liquid field divides the liquidus for calcite into two parts separated by the piercing points R and Q, the high-temperature part where calcite coexists with Lc, and the lower-temperature part where it coexists with Ls. The liquidus piercing point between calcite and albite, P, is located near 1290°C and $Ab_{80}CC_{20}$.

The textures of runs at 1200°C and 1150°C were quite different from those at higher temperatures, and the solidus was interpreted to be at 1225°C. The 1200°C and 1300°C runs for mixture $Ab_{90}CC_{10}$ are shown in Figs. 4c and 4a, respectively, with the low-temperature calcite replaced by interstitial liquid at the higher temperature. There is also a trace of interstitial liquid in some runs in the field labelled Ab + CC, but we attribute this to the trace of water present in the starting mixtures.

The phase fields intersected at 1.5 GPa plotted in Fig. 6 from experimental results listed in Table 1 show the same phase fields intersected at 2.5 GPa (Fig. 5), but with significant differences. The miscibility gap is very much smaller, between about $Ab_{23}CC_{77}$ to $Ab_{43}CC_{57}$ above 1285°C. Liquidus temperatures are shifted downwards by

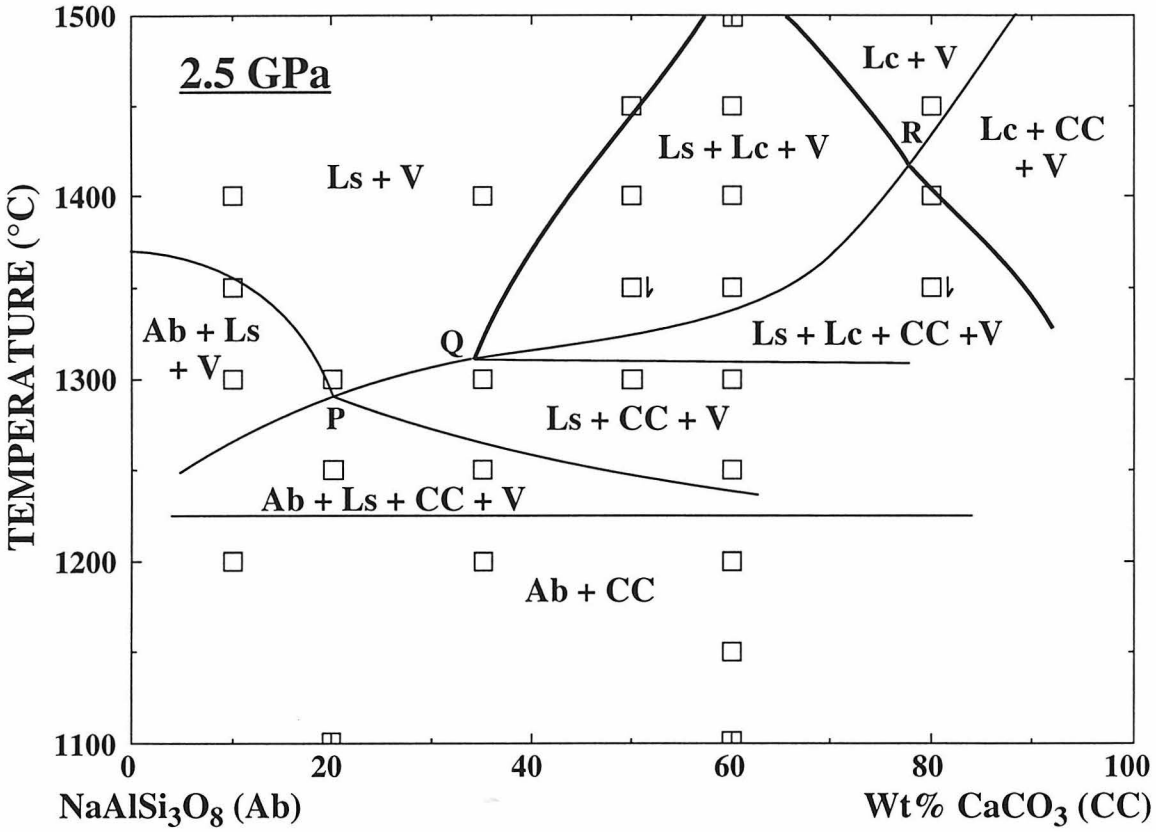

Figure 5. Isobaric phase fields intersected by the join albite-calcite at 2.5 GPa, based on phase assemblages in experiments marked by open squares (Table 1), and liquid compositions from some critical runs. Squares with an arrow indicate additional reversal experiments (Table 1). The melting temperatures of calcite and albite were determined from literature. The most significant feature is the presence of a miscibility gap between $Ab_{10}CC_{90}$ and $Ab_{65}CC_{35}$ above 1310°C (bounded by heavy curves). The consolute is probably slightly above 1500°C, although is not determined here. The composition of the piercing point for coprecipitation of albite and calcite occurs at $Ab_{80}CC_{20}$ (point P). Points Q and R denote the intersections of the two-liquid field and the calcite liquidus field on the join. The solidus is estimated to be 1225°C. Vapor is present at all experiments above solidus. Abbreviations: Ls - silicate-rich liquid, Lc - carbonate-rich liquid, Ab - albite, CC - calcite, V - vapor.

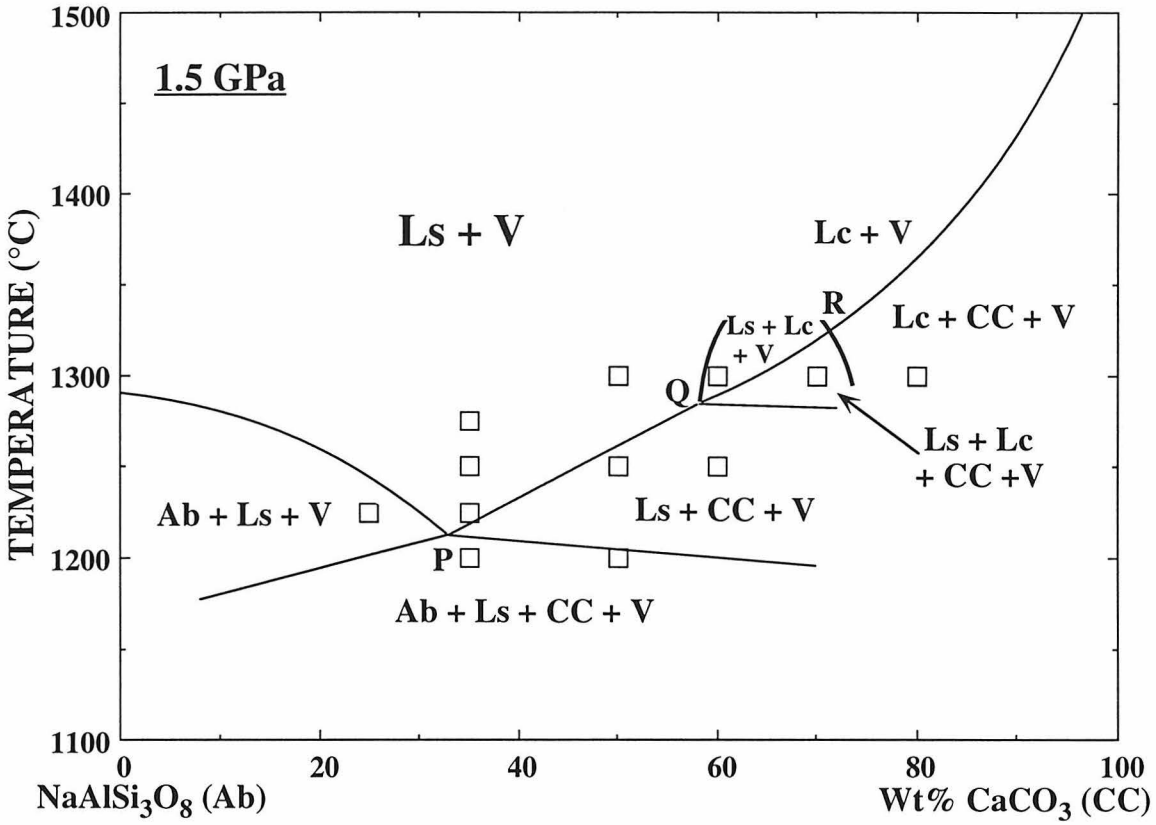

Figure 6. Isobaric phase fields intersected by the join Ab-CC at 1.5 GPa. The phase fields present are considered to be analogous to 2.5 GPa results, except that the temperature range and the extent and position of each field varies. The miscibility gap is narrower to between $Ab_{25}CC_{75}$ and $Ab_{43}CC_{57}$. Solidus is not determined. The piercing point P is located at $Ab_{67}CC_{33}$ on the join, which contains more dissolved calcite than high pressure results. Vapor is present in all runs.

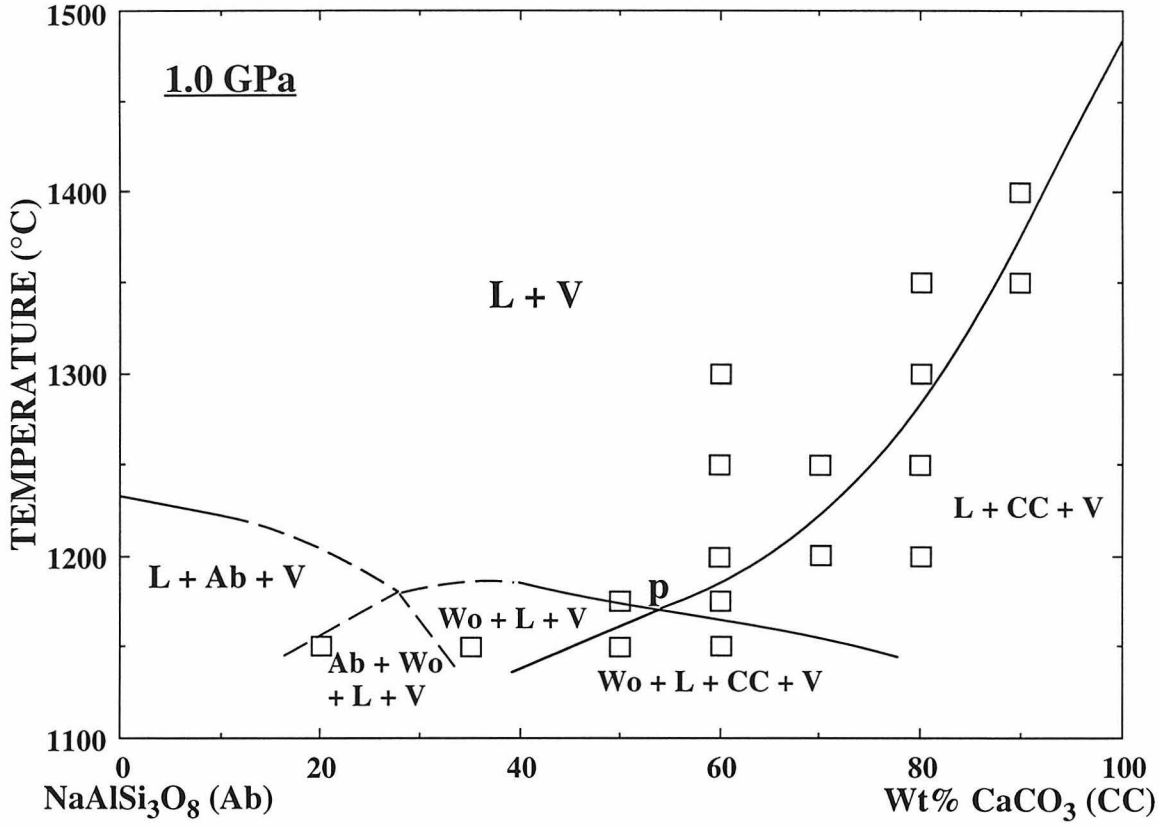

Figure 7. Intersected isobaric phase fields at 1.0 GPa, showing no miscibility gap at this pressure. Other than albite, wollastonite (Wo) liquidus field is also intersected. The piercing point p is now located at $Ab_{47}CC_{53}$ on the join. Vapor is present in all runs.

about 100°C, and the liquidus piercing point between albite and calcite at about 1210°C has shifted toward $CaCO_3$, with composition $Ab_{67}CC_{33}$. The solidus was not sought.

Although the miscibility gap is so small, its presence is confirmed by two critical runs at 1300°C. Run #86 consists of a silicate-rich bead surrounded by quenched carbonate-rich liquid, as commonly seen in the charges quenched from the two-liquid field at 2.5 GPa (Fig. 3a). In run #92 two liquids were distinguished texturally, but their compositions determined by SEM/EDS analyses were not very different from each other, which explains why physical separation of a glassy bead did not occur.

Figure 7 shows the phase fields intersected at 1.0 GPa, based on results in Table 1, with no miscibility gap. The liquidus for calcite is well bracketed down to the piercing point between calcite and wollastonite at $Ab_{47}CC_{53}$ and about 1170°C. The composition and temperature of the piercing point limiting the liquidus for calcite is thus greatly enriched in $CaCO_3$ compared with the results at higher pressures. The experiments at 1150°C indicate the intersection of liquidus surfaces for calcite, wollastonite and albite, with the configuration sketched in Fig. 7, but we did not define the details beyond the calcite-wollastonite piercing point.

Liquid compositions and the miscibility gap at 2.5 GPa

The compositions of coexisting Ls and Lc were analyzed (SEM/EDS), and a selection of results at 2.5 GPa is listed in Table 2 (normalized CO_2-free). Each analysis listed is the average of 10 measurements. Values for 1350°C are plotted on the Hamilton projection (Fig. 1b) in Fig. 8. The open circles represent data from raster-mode analyses (area several ten μm^2), and the solid circles are the average values listed in Table 2. The triangles are spot analyses (several μm^2) of different components of the quenched carbonate-rich liquids, calcite dendrites and interstitial silicate component (Fig. 3b).

The results are shown for the three starting mixtures (solid squares), $Ab_{50}CC_{50}$, $Ab_{40}CC_{60}$, and $Ab_{20}CC_{80}$. The phase assemblages for each run can be seen in Fig. 5. Ls projects close to the composition join Ab-CC, but Lc is enriched in Na_2CO_3 compared with the join. The analyses of Lc are more scattered than those of Ls, because of the heterogeneous nature of these quenched liquids. For the starting mixture $Ab_{50}CC_{50}$, the open triangles in Fig. 8a show that Lc quenches to calcite and a silicate-carbonate matrix that is significantly enriched in Na_2CO_3. For $Ab_{40}CC_{60}$, Fig. 8b shows that the components of the quenched liquid Lc are simply calcite and a silicate glass somewhat enriched in Na_2CO_3 compared with the join Ab-CC. In Figs. 8a and 8b, Ls and Lc are colinear with the starting mixture, but in Fig. 8c the starting mixture lies within the triangle Ls + Lc + CC.

The average liquid compositions and tie-lines determined for 2.5 GPa and 1350°C in Fig. 8 are combined in the isobaric isothermal section, Fig. 9a. The curved lines represent the 1350°C isotherm on the surface enclosing the liquid miscibility gap. The isotherm for Ls is smoothly defined, but the points defining an isotherm for Lc are more scattered, because the analyses are less consistent for reasons discussed above (Fig. 8). These liquidus isotherms terminate at the corners of the 3-phase triangle Ls + Lc + CC. A similar set of analyses for the same three mixtures at 1400°C (see Fig. 5; average analyses listed in Table 2) provide a set of diagrams comparable with Fig. 8. The corresponding isobaric isotherm is given in Fig. 9b. Note that the triangle for Ls + Lc + CC for this temperature is much narrower than at 1350°C (Fig. 9a).

The effect of increased temperature in decreasing the compositional difference between the immiscible liquids is displayed in Fig. 5, which shows the intersection of the 2-liquid volume by the join Ab-CC at 2.5 GPa. The same effect is shown more precisely in Fig. 10, where the average liquid compositions for each starting mixture (from Fig. 8) are projected orthogonally onto the join. Each starting mixture defines a different part of the liquidus surface for miscibility gap (Fig. 8). Therefore, for each mixture, there is a

Table 2. Immiscible liquid compositions on a CO_2-free basis (weight percent) from the experiments at 2.5 GPa.

Run(SM)	Temp (°C)	Phase	SiO_2	Al_2O_3	Na_2O	CaO
56(Ab_{40})	1450	Ls	35.9(0.6)	11.9(0.6)	6.8(1.0)	46.3(0.9)
		Lc	15.4(2.8)	2.6(1.0)	7.9(1.6)	74.1(4.2)
53(Ab_{20})	1400	Ls	34.7(2.1)	11.6(0.8)	3.7(0.8)	50.0(2.7)
		Lc	25.1(1.4)	7.2(0.8)	5.3(1.1)	62.4(2.0)
6(Ab_{40})	1400	Ls	42.0(1.4)	13.0(0.6)	6.2(1.1)	48.7(2.0)
		Lc	15.3(1.5)	2.9(0.5)	8.8(1.4)	73.0(2.9)
43(Ab_{50})	1400	Ls	45.1(0.8)	13.3(0.5)	7.8(1.1)	33.6(0.5)
		Lc	14.0(1.5)	2.9(0.4)	8.1(1.1)	75.0(2.6)
52(Ab_{20})	1350	Ls	41.6(0.7)	13.2(0.3)	5.4(0.7)	39.8(0.4)
		Lc	17.6(1.8)	3.8(0.4)	8.5(1.2)	70.2(2.7)
50(Ab_{40})	1350	Ls	45.2(0.7)	13.8(0.4)	7.0(0.9)	34.0(0.6)
		Lc	12.9(2.6)	2.4(0.8)	8.4(1.9)	76.3(4.8)
49(Ab_{50})	1350	Ls	50.0(0.7)	15.0(0.7)	7.6(0.6)	27.3(0.6)
		Lc	12.1(2.8)	2.1(0.6)	11.8(2.0)	74.0(3.1)

Ab_{20}: 20 wt% Ab + 80 wt% CC. Values in parentheses are standard deviations of the mean. SM - starting mixture.

Figure 8. Experimenal liquid compositions plotted on the Hamilton projection, showing individual analyses and average compositions of quenched silicate-rich and carbonate-rich liquids from 1350°C and 2.5 GPa for the starting mixtures (a) $Ab_{50}CC_{50}$, (b) $Ab_{40}CC_{60}$, and (c) $Ab_{20}CC_{80}$. Open circles represent data from raster-mode analyses (covered area of several tens μm^2) with avreage composition of each liquid (solid circles). Also shown in (a) and (b) are the analyses (open triangles) of spot mode (several μm^2) for quenched-grown calcite and interstitial silicate-rich material (i.e. light and dark parts in Fig. 3b) within the quenched carbonate-rich liquids.

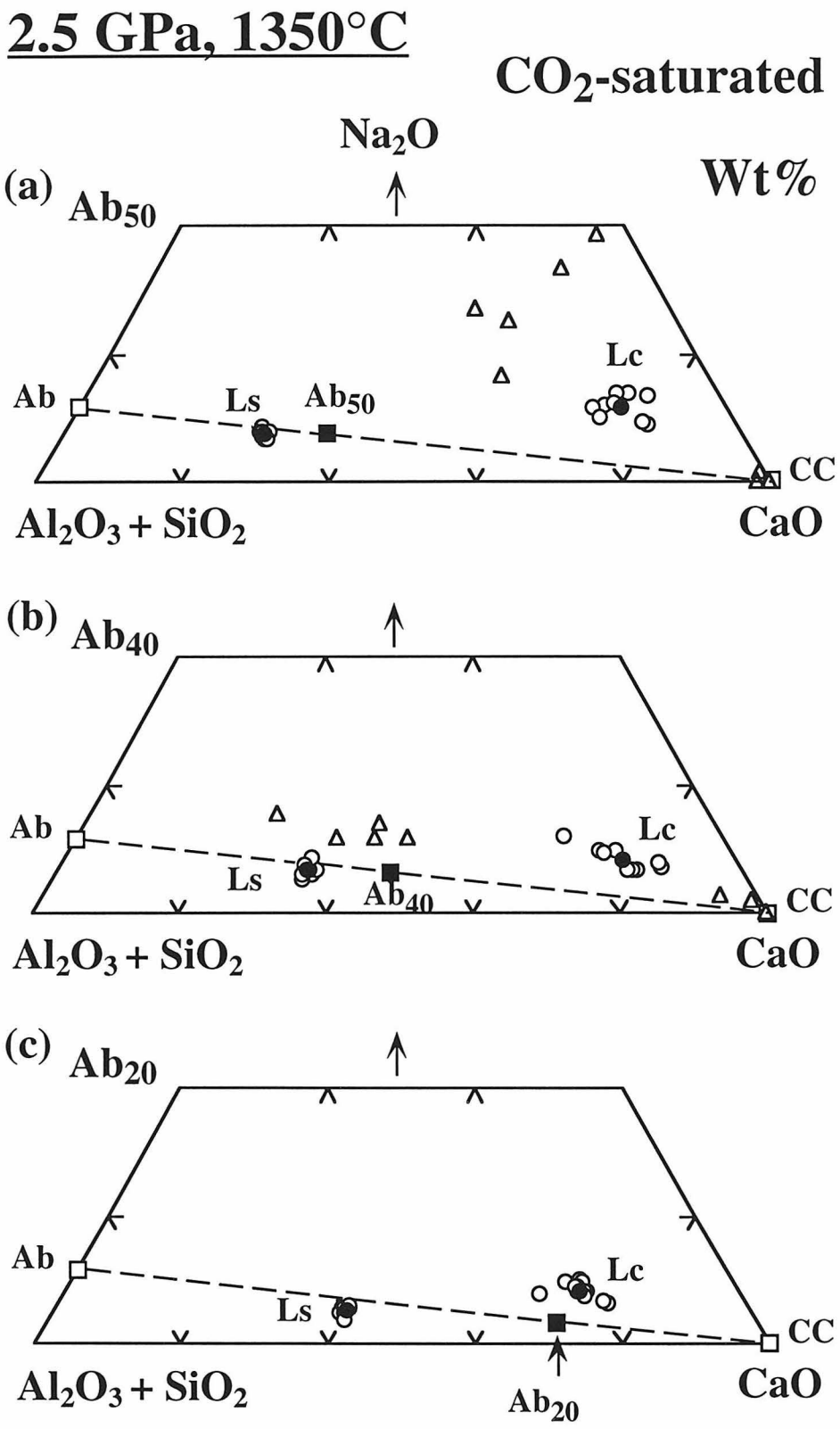
2.5 GPa, 1350°C
CO2-saturated
Na2O
Wt%
(a)
Ab50
Ab
Ls
Ab50
Lc
CC
Al2O3 + SiO2
CaO
(b)
Ab40
Ab
Ls
Ab40
Lc
CC
Al2O3 + SiO2
CaO
(c)
Ab20
Ab
Ls
Lc
CC
Al2O3 + SiO2
Ab20
CaO

Figure 9. Two-liquid isotherms at 2.5 GPa at (a) 1350°C and (b) 1400°C, plotted on the Hamilton projection. Solid circles denote the average liquid compositions (Table 2). The tie-lines connect Ls and Lc, showing the compositions of coexisting two-liquid pairs. The three-phase triangles for bulk composition $Ab_{20}CC_{80}$ indicate the assemblages of silicate-rich and carbonate-rich liquids along with calcite. (c) combines isotherms from (a) and (b) with that at 1450°C (based on two-liquid compositions from run #56, Table 2) to construct part of the two-liquid surface and liquidus field boundaries on the Hamilton projection. Arrows indicate the cooling directions. Point P is the piercing point for coprecipitation of albite and calcite on the join Ab-CC, which constrains the liquidus field boundary between silicates and calcite, and points Q and R are intersections of the two-liquid field by the calcite liquidus surface on the join Ab-CC (Fig. 5). Point K indicates the critical point (Ls = Lc) on the boundary between two-liquid field and calcite liquidus field, where heavy dashed line K-CC is the temperature maximum on the calcite liquidus surface.

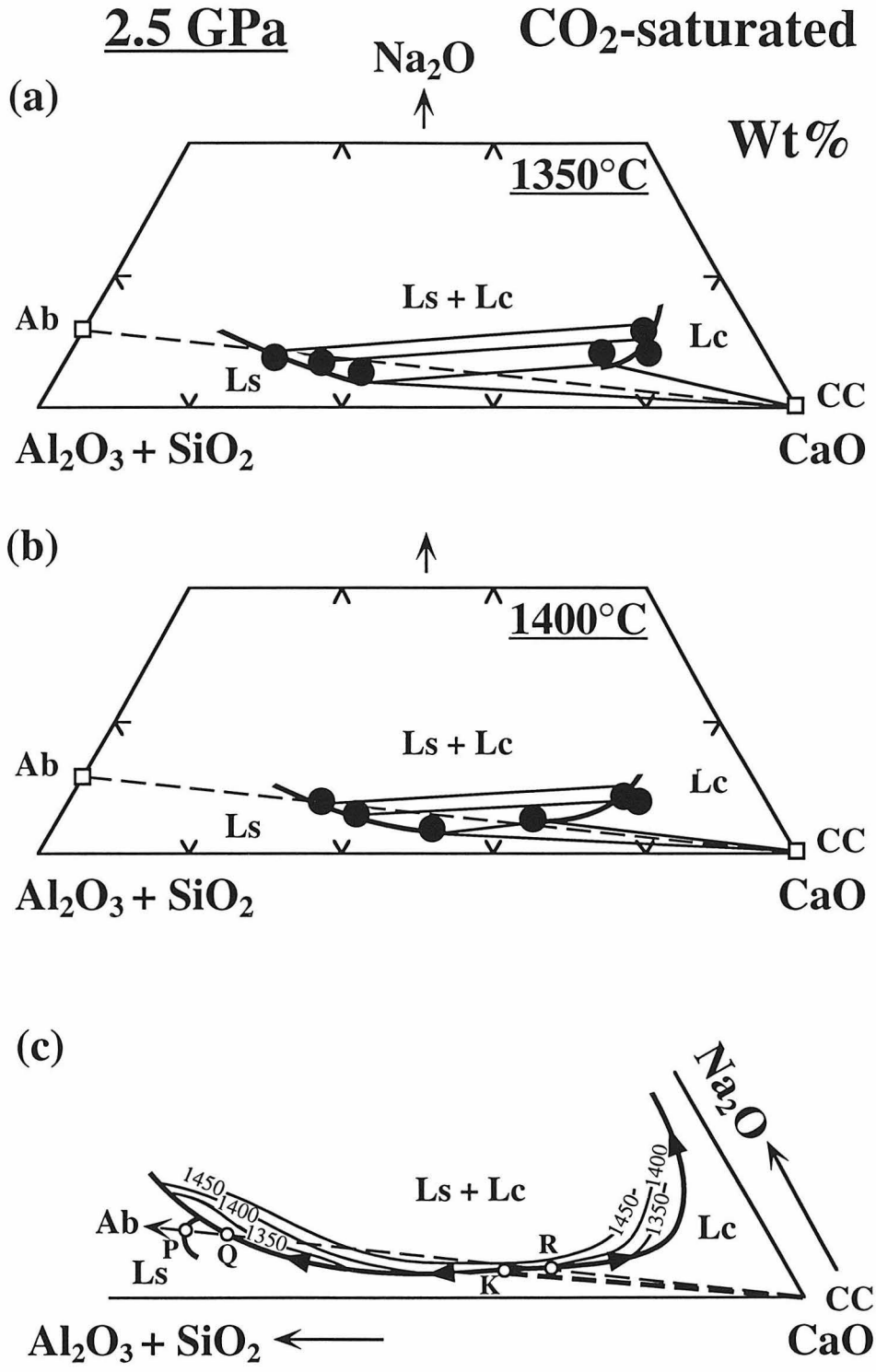
2.5 GPa
CO2-saturated
(a)
Na2O
Wt%
1350°C
Ab
Ls + Lc
Lc
Ls
CC
Al2O3 + SiO2
CaO
(b)
1400°C
Ab
Ls + Lc
Lc
Ls
CC
Al2O3 + SiO2
CaO
(c)
Na2O
1450
1400
1350
Ab
P
Q
Ls
Ls + Lc
R
K
1450
1400
1350
Lc
CC
Al2O3 + SiO2
CaO

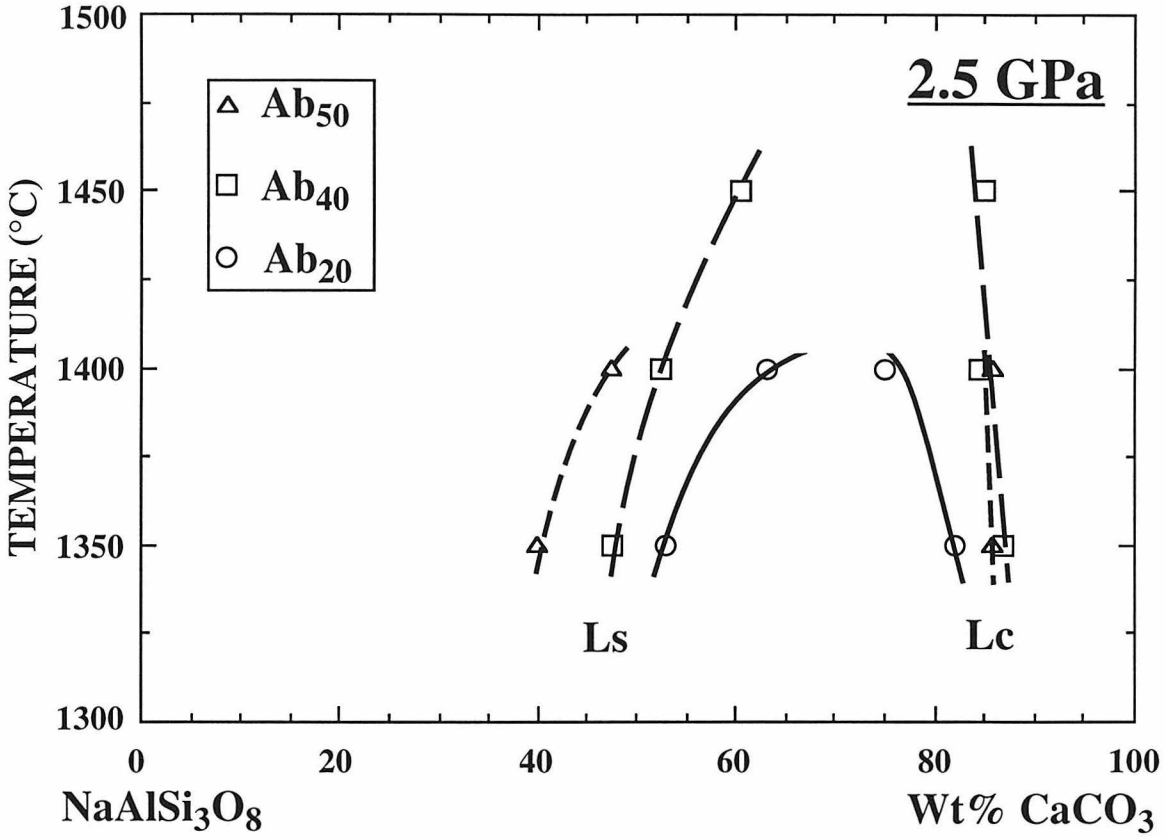

Figure 10. Two-liquid compositions at 2.5 GPa (Table 2, Fig. 9c) projected onto the join Ab-CC. Triangles, squares and circles represent the three sets of liquid compositions from the starting mixtures $Ab_{50}CC_{50}$, $Ab_{40}CC_{60}$ and $Ab_{20}CC_{80}$, respectively. The three pairs of curves passing through each set of data locate on the surface of the two-liquid dome (Fig. 9c). The solid curves from $Ab_{20}CC_{80}$ further delineate the field boundary between the two-liquid dome and the calcite liquidus surface. The figure shows that the size of the miscibility gap decreases with temperature.

different pair of liquid composition curves for the solvus intersection (Fig. 10). Runs with mixture $Ab_{20}CC_{80}$ (open circles) contain calcite in addition to the two liquids, and these liquid compositions (the corners of the 3-phase triangles in Figs. 9a and 9b) lie on two field boundaries on the surface of the miscibility gap, defining the compositions of liquids which coexist with calcite and a second liquid: Ls(Lc,CC) and Lc(Ls,CC). These phase boundaries terminate in Fig. 10 at temperature somewhat above 1400°C where the mixture Ab_{20} passes from the two-liquid volume into the single-liquid volume.

These phase relationships provide the basis for begining to map the liquidus surface, along with its field boundaries. The 1350°C and 1400°C liquidus isotherms from Figs. 9a and 9b are superimposed in Fig. 9c, and a sketched 1450°C isotherm is added, based on the one pair of immiscible liquid compositions available at this temperature (Fig. 5, Table 2 and Fig. 10). For visual clarity, the isotherms in Fig. 9c have been shifted slightly in such a way that all three curves have similar geometry without crossing over each other. These isotherms in 5-component space may actually cross when projected into Fig. 9, but the uncertainty in analyses of Lc (Fig. 8) does not permit this determination.

The isotherms map the liquidus surface of the miscibility gap volume which rises from the liquidus field boundary, the heavy line with arrows passing through points Q-K-R. This field boundary, (Ls + Lc),CC, passes through the corners of the 3-phase triangles in Figs. 9a and 9b, and over a temperature maximum at the critical point K where the 3-phase triangle terminates at the dashed line in Fig. 9c, at temperature somewhat above 1400°C (cf. Fig. 10). The points R and Q are defined in composition and temperature by the piercing points on the join Ab-CC in Fig. 5, separating the miscibility gap liquidus from the liquidus surface for calcite. The liquidus field boundary for the coprecipitation of calcite and albite passes through the piercing point P in Fig. 5, and down to meet the miscibility gap field boundary as shown in Fig. 9c. The compositions of points R, Q and P in Fig. 9c have been calculated CO_2-free for consistency with the analyses plotted in Figs. 8 and 9, and they are all slightly shifted toward Ab on the line Ab-CaO, compared

with their positions in Fig. 5. Note that the liquidi intersected in Fig. 5 provide points on the line Ab-CC in Fig. 9c for isotherms on the liquidus surfaces for albite and calcite, which will be useful in later phase diagram constructions.

Effect of pressure on the miscibility gap

Figure 11 compares the liquidus relationships intersected by the Ab-CC join at the pressures 1.0, 1.5 and 2.5 GPa (from Figs. 5-7). Liquidus temperatures increase with increasing pressure. The miscibility gap is not intersected at 1.0 GPa, very small at 1.5 GPa, and significant at 2.5 GPa. The size of the miscibility gap thus increases with pressure.

Note that where the miscibility gap is present, the calcite liquidus is divided into two sections, for Lc and Ls. The limit of the calcite liquidus, which is the low-temperature piercing point P between calcite and a silicate mineral, shifts strongly toward the albite component with increasing pressure. At 1.0 GPa it contains about 53 wt% $CaCO_3$, and this decreases to about 35% and 20% at 1.5 and 2.5 GPa, respectively. At 1.0 GPa, a liquidus field for wollastonite appears between those for albite and calcite (compare Huang & Wyllie, 1974, and Huang et al., 1980, for coprecipitation of calcite and wollastonite in CaO-SiO_2-CO_2).

The decrease in size of the miscibility gap with decreasing pressure is also shown by isobaric isotherms in the Hamilton projection, Fig. 12. Although we do not have three isotherms at the same temperature, the effect of temperature on the miscibility gap discussed above allows us to attribute the trend in Fig. 12 to the pressure differences. The dashed-line isotherm 1-1 for 1350°C at 2.5 GPa is from Fig. 9a. The solid-line isotherm 2-2 for 1300°C at 1.5 GPa passes through four points based on the four average analyses of quenched liquids from the two runs in Fig. 6, which were obtained in the same way as those plotted in Fig. 8, but were not tabulated. A corresponding isotherm for 1.0 GPa

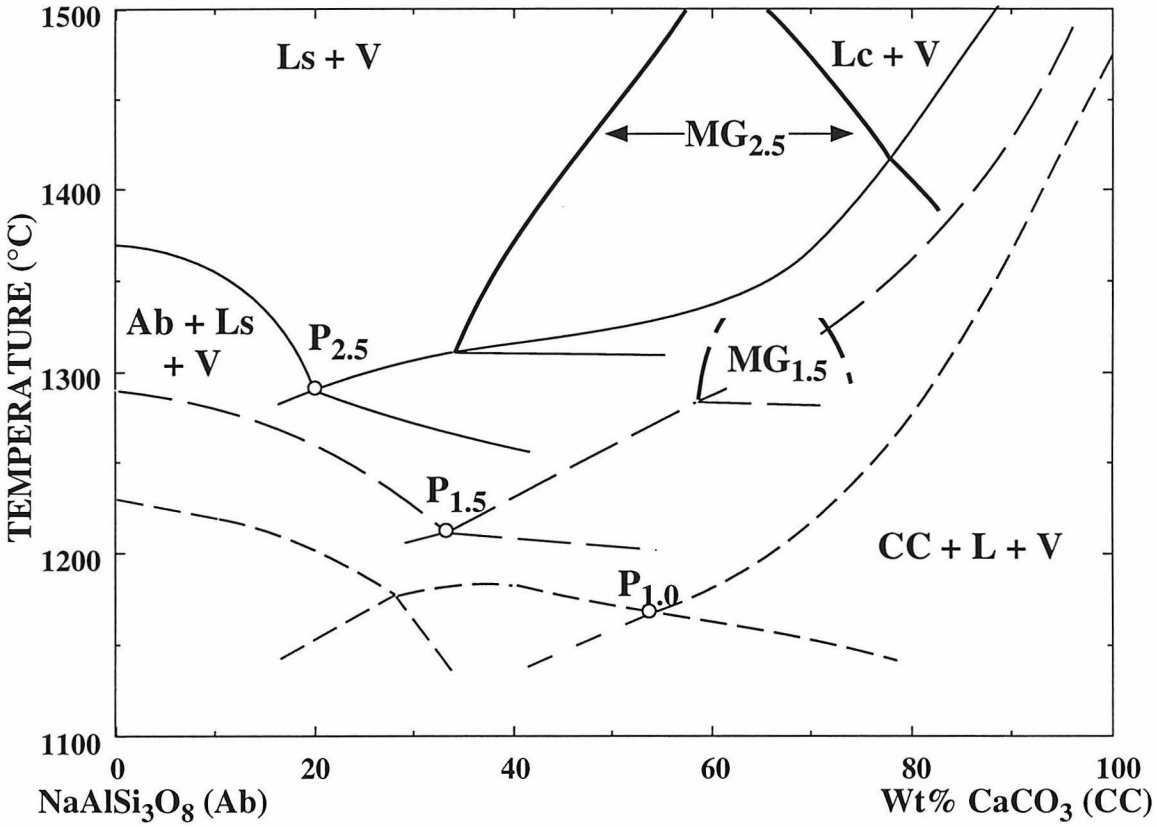

Figure 11. Superimposed phase field diagram at 2.5, 1.5, and 1.0 GPa, showing the effect of pressure on the size of the intersected two-liquid field and the position of the piercing point. The symbols $MG_{2.5}$ and $MG_{1.5}$ represent miscibility gaps at 2.5 and 1.5 GPa, and the positions of the piercing points $P_{2.5}$, $P_{1.5}$, and $P_{1.0}$ are indicated by open circles for 2.5, 1.5, and 1.0 GPa. Solid, long-dashed, and short-dashed curves are phase field boundaries at 2.5, 1.5 and 1.0 GPa, respectively.

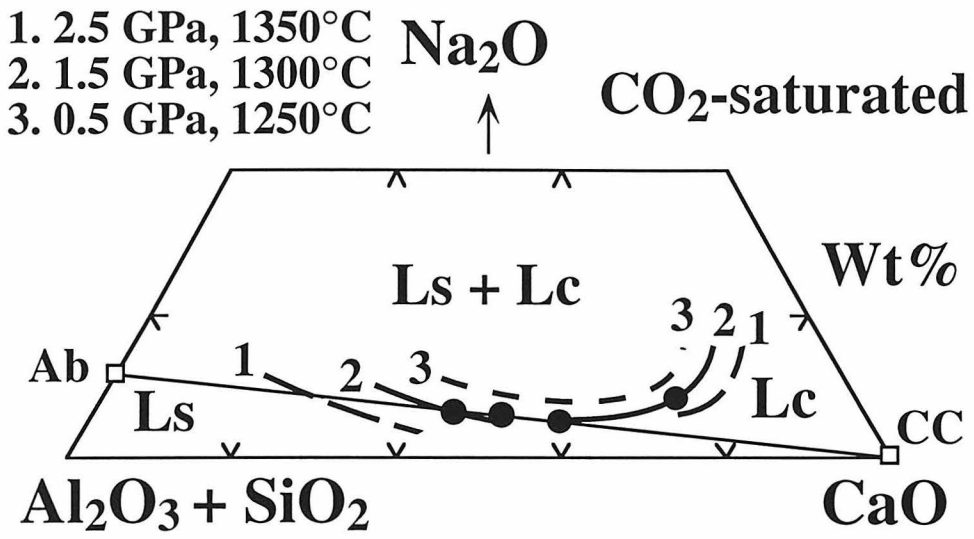

Figure 12. Two-liquid isotherms on the Hamilton projection at 2.5 GPa and 1350°C (Fig. 9a; curves 1-1), and at 1.5 GPa and 1300°C (curves 2-2), showing the decrease in size of the two liquid field with decreasing pressure. Solid circles represent two-liquid compositions for runs #86 and #92 (Table 1) at 1.5 GPa and 1300°C. The inferred two-liquid isotherm at 1250°C and 0.5 GPa is expressed by curve 3, extrapolated from curves 1-1 and 2-2.

does not intersect the join Ab-CC (Fig. 11), and it is therefore displaced further toward Na_2O. Given these results, it is to be expected that the miscibility gap at 0.5 GPa would not intersect the join Ab-CC, and our estimate of an isotherm for 0.5 GPa at 1250°C is given by the dashed-line 3.

LIQUIDUS SURFACE IN CaO-Na_2O-Al_2O_3-SiO_2-CO_2 at 2.5 GPa

The liquidus diagram with field boundaries and isotherms sketched in Figs. 13, 14 and 15a is based on the new results for phase fields intersected by the join Ab-CC (Fig. 5), measured liquid compositions and constructed isotherms (Figs. 8 and 9), extrapolated and connected with published data from several related systems to provide an overview of the whole system. The compositions taken from Fig. 5 were recalculated CO_2-free, causing slight shift toward Ab.

Figure 13a shows the new experimental results in the Hamilton projection, with 2x vertical exaggeration to provide a clearer view of the crowded relationships below the join Ab-CC. The figure connects the miscibility gap liquidus surface of Fig. 9c to the edges of the system. The field boundary for the coexistence of liquids Ls + Lc (with minerals) passes through points Q and R (piercing points in Fig. 5). The field boundary passes over the critical point K where Ls = Lc, associated with the closure of the three-phase triangle Ls + Lc + CC (heavy dashed line, Fig. 13a) at temperature somewhat higher than 1400°C, as indicated by extrapolation from Figs. 9a and 9b, and Fig. 10 (mixture Ab_{20}).

The liquidus data for the side $CaCO_3$-Na_2CO_3 are based on the calcite melting point at 1575°C (Irving & Wyllie, 1975) and the experimental data of Cooper et al. (1975) for $CaCO_3$-Na_2CO_3 at 0.1 GPa. The latter temperatures were increased for Fig. 13a by the known differential for calcite melting between the pressures 0.1 and 2.5 GPa (about 265°C).

Figure 13. (a) Lower portion of the Hamilton projection with vertical exaggeration of 2, showing the field boundaries separating the surfaces for the two-liquid field, silicate liquidus field, and calcite liquidus field, with isotherms on each surface, and arrows on the field boundaries for indications of the liquid paths. See Fig. 9c for notations K, P, Q and R. Liquidus field boundary bewteen calcite and silicates extends somewhat arbitrarily from point E (35% SiO_2, 1400°C) on the (Al_2O_3 + SiO_2)-CaO side between wollastonite and calcite, passes through P on the join Ab-CC, and is terminated by the two-liquid field at F. The arrow-headed line from F points towards the composition of the carbonate-rich liquid G immiscible to F. The isotherms on the calcite liquidus surface and near point P are based on the results on the join Ab-CC, extrapolations from the join NC-CC at 0.1 GPa in Cooper et al. (1975), and the position of the fixed point E. (b) Complete Hamilton projection to proper scale, showing the same features as in (a). The miscibility gap field boundary is extended to the (Al_2O_3 + SiO_2)-Na_2O side at M and N, and M-N defines a two-liquid tie-line on the CaO-free axis. The curve G-O indicates the silicate-carbonate liquidus field boundary in the Na_2O-rich Lc region, and the surface N-G-O represents the silicate liquidus field for precipitation of silicates from liquids Lc. The tie-line connecting immiscible two-liquid compositions F and G is chosen to be approximately parallel to tie-lines reported by Kjarsgaard & Hamilton (1989) at 0.5 GPa (Fig. 2).

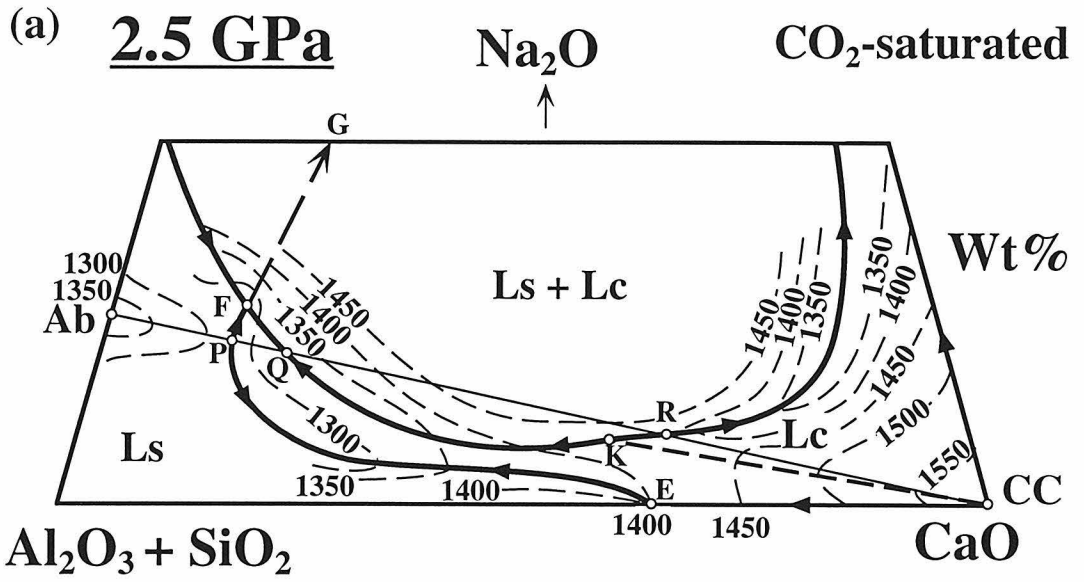
(a)
2.5 GPa
Na2O
CO2-saturated
G
Wt%
1300
1350
Ab
F
P
Q
1450
1400
1350
Ls + Lc
1450
1400
1350
1350
1400
1450
1500
1550
R
Lc
K
Ls
1300
1350
1400
E
CC
1400
1450
Al2O3 + SiO2
CaO

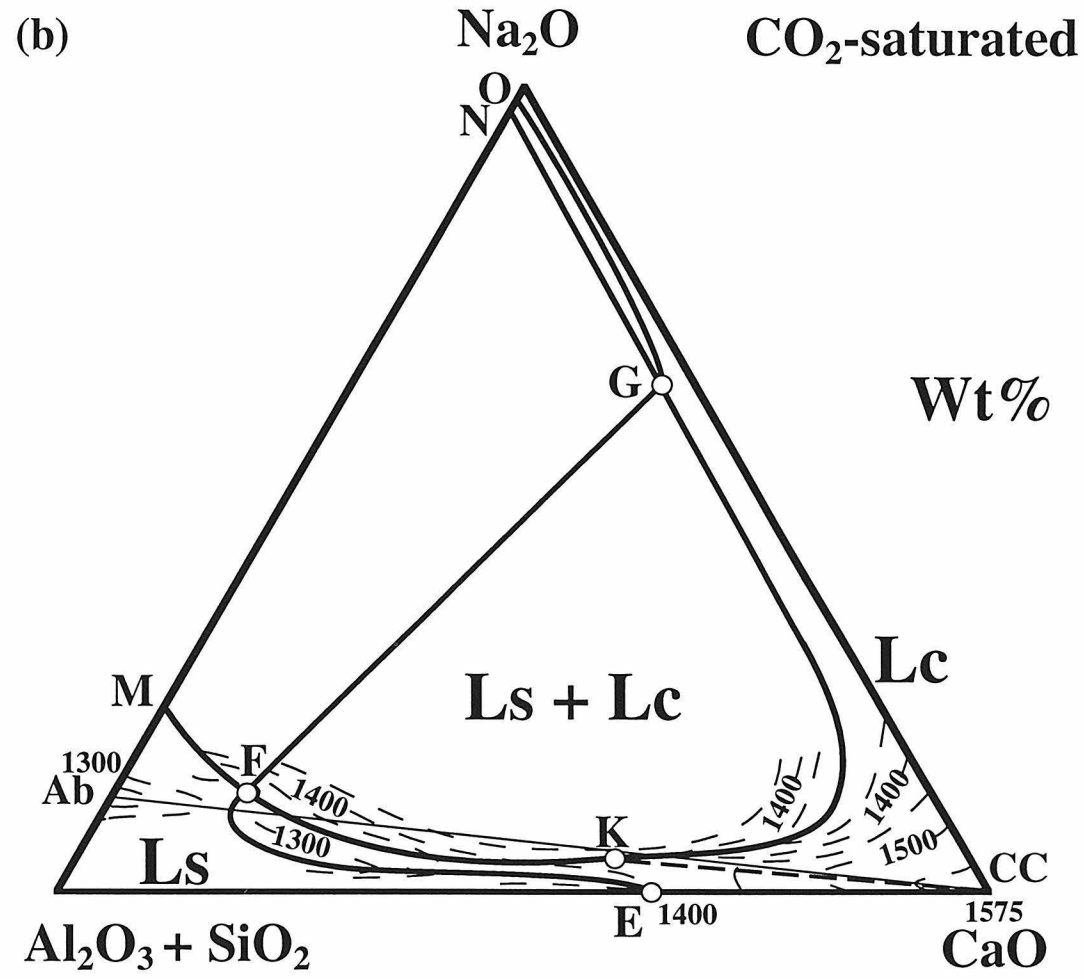
(b)
Na2O
CO2-saturated
O
N
G
Wt%
Lc
M
Ls + Lc
1300
Ab
F
1400
1300
K
1400
1400
1500
Ls
CC
E
1400
1575
Al2O3 + SiO2
CaO

The phase relationships on the bottom side, CaO-(Al_2O_3 + SiO_2), assume a simple eutectic relationship between calcite and a silicate mineral. In fact, the phases and boundaries will vary significantly depending on Al_2O_3/SiO_2 in the system, and the minerals present between E and the corner (Al_2O_3+SiO_2). The point E was chosen based on results of three experimental studies: $CaCO_3$-grossularite (Maaloe & Wyllie, 1975), $CaCO_3$-wollastonite (Huang & Wyllie, 1974; Huang et al., 1980), and $CaCO_3$-SiO_2 (Huang et al., 1980; Lee et al., 1994). Eutectics between calcite and grossularite or wollastonite are situated between 50-55% silicate, and that between calcite and quartz is at about 28% SiO_2. The eutectic temperatures (between 2.5 and 3.0 GPa) are between 1350°C and 1450°C. In all three systems, the calcite liquidus field is limited by a eutectic liquid with at least 35% SiO_2 (recalculated to CO_2-free basis), and this is the value adopted in Fig. 13a, at temperature 1400°C.

A field boundary extends from E, separating the liquidus surface for calcite from that for silicates. Its position is not defined and it will vary according to Al_2O_3/SiO_2 in the system, but there is not much variation possible. It is constrained to cross the join Ab-CC at piercing point P (cf. Figs. 5 and 9c), passing over a temperature maximum on the liquidus. Presumably it continues down-temperature to meet the miscibility gap field boundary at some point F (although it could become involved with the nepheline or jadeite liquidus). The field boundary from E surely extends to lower temperatures, but we have not attempted to invent phase relationships on this silicate-carbonate boundary between E and P.

The framework of field boundaries and liquidus temperatures in the bounding systems permits construction of the liquidus surface isotherms in Fig. 13a, and the distribution of arrows as given on the field boundaries. The isotherms on the liquidus dome of the miscibility volume were constructed in Fig. 9c. The isotherms on the calcite liquidus surface are connected from those at the miscibility gap field boundary to the appropriate temperatures on the sides of the Hamilton triangle, passing over a thermal

maximum associated with the line CC-K. The arrangement between E and P depends on unknown phase realtionships, but temperatures are known between Q and P (Fig. 5). We have made no attempt to sketch field boundaries or isotherms on the silicate liquidus surface, except near the join Ab-CC, where temperatures are provided by Fig. 5. The phases and boundaries will vary significantly depending on Al_2O_3/SiO_2 in the system, and the minerals present between E and the corner ($Al_2O_3 + SiO_2$).

Figure 13b shows the liquidus surfaces of Fig. 13a in the context of the complete Hamilton projection, to proper scale; many of the details depicted in Fig. 13a cannot be resolved. There is a single tie-line drawn from F to G, approximately parallel to tie-lines reported by Kjarsgaard and Hamilton at 0.5 GPa (Fig. 2). This line is significant because it divides the two-liquid field boundary into sections where the coexisting liquids precipitate calcite or silicate. Liquids Ls-Lc on the continuous section F-K-G precipitate first calcite; liquids on the two sections M-F (Ls) and N-G (Lc) precipitate silicates first. The silicate liquidus surface from N-G is bounded by another silicate-carbonate liquidus field boundary, G-O, separating the Na_2O-rich Lc into narrow silicate and carbonate liquidus surfaces, as shown in Fig. 13b. We have not attempted to squeeze into the narrow carbonate liquidus field estimated isotherms and field boundaries based on the results of Cooper et al (1975) at 0.1 GPa.

Figure 14 opens the Hamilton projection of Fig. 13 into a tetrahedron, with the CO_2 component added as an apex, and includes the relevant mineral phase positions (Fig. 1). This illustrates the relationships between the silicate liquids with low CO_2 solubilities and the carbonate-rich liquids. Figures 14 and 15a illustrate the distinction between immiscible liquid pairs, identified as Ls (silicate-rich) and Lc (carbonate-rich), and liquidus surfaces for silicate minerals and carbonate minerals. Ls and Lc are defined compositionally in relative terms around the miscibility gap field boundary, with the distinction made at the critical composition K. Silicate-rich liquids Ls from K-F precipitate calcite, whereas carbonate-rich liquids Lc from N-G precipitate silicates. For clarification in the following

Figure 14. (a) Silicate and carbonate liquidus surfaces intersected by the two-liquid field, projected into the compositional tetrahedron (Al_2O_3 + SiO_2)-Na_2O-CaO-CO_2. The vapor saturated field boundary on the face (Al_2O_3 + SiO_2)-CaO-CO_2 is based on Huang et al. (1980). Low CO_2 solubility is assumed for silicate liquidus surface. Also projected on the tetrahedron are the phases (Fig. 1) related to the studied system. (b) Two-liquid compositions (solid circles, runs #49, #50 and #52) at 2.5 GPa and 1350°C projected into the compositional tetrahedron (Al_2O_3 + SiO_2)-Na_2O-CaO-CO_2. CO_2 contents were estimated from shortfalls to 100% of EDS analyses (not tabulated). Compare Fig. 9a for the liquid compositions. The heavy curves are two-liquid isotherms, and the tie-lines connect the coexisting silicate-rich and carbonate-rich liquids. Notice that vapor is present with liquids, as indicated in (b). (c) Tie-figures showing the phase assemblages for runs #50 and #52.

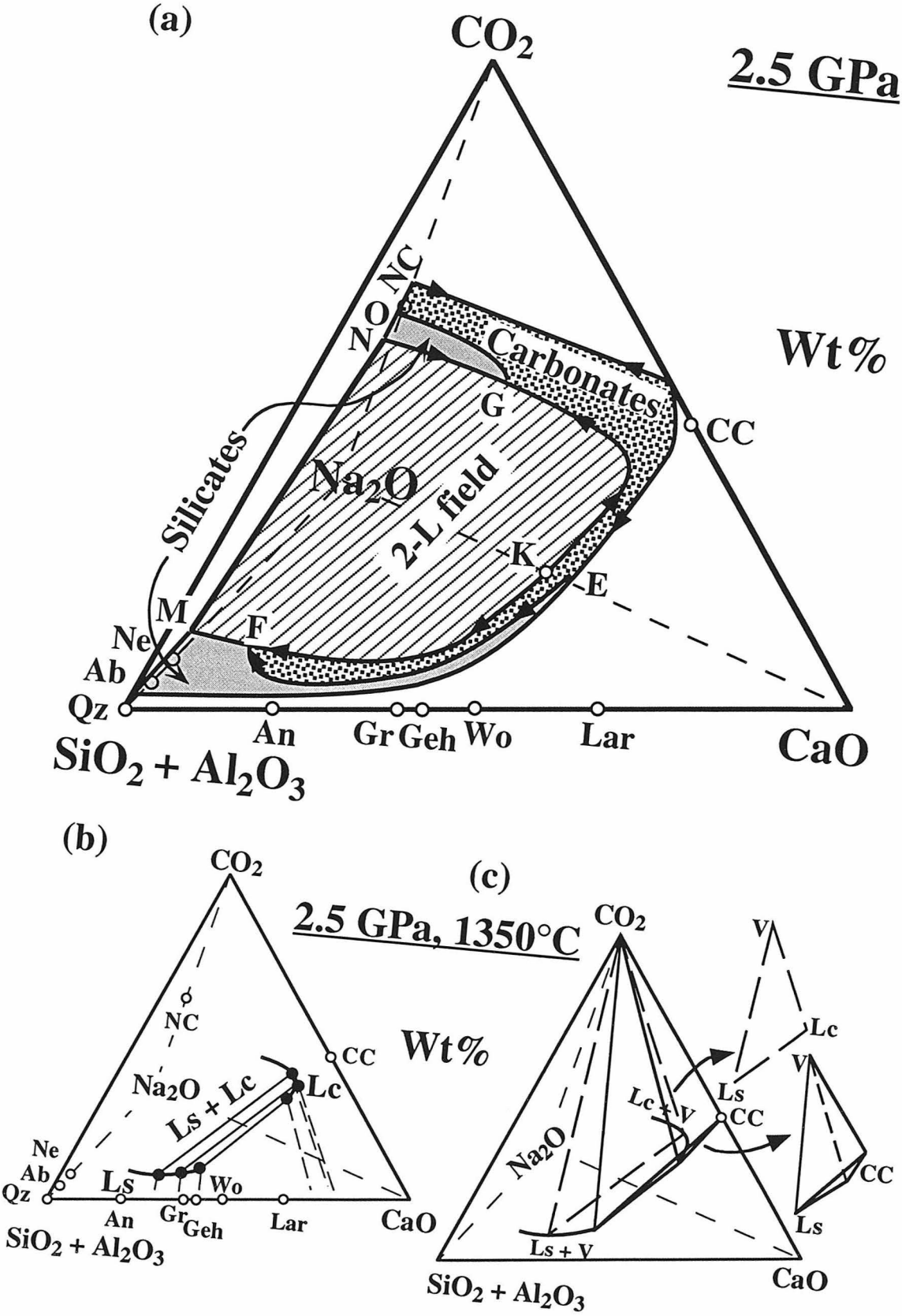
(a)
CO_2
2.5 GPa
Wt%
NC
O
N
Carbonates
G
CC
Silicates
Na_2O
2-L field
K
E
M
F
Ne
Ab
Qz
An
Gr
Geh
Wo
Lar
CaO
$SiO_2 + Al_2O_3$
(b)
CO_2
NC
CC
Wt%
Na_2O
Ls + Lc
Lc
Ne
Ab
Qz
Ls
An
Gr
Geh
Wo
Lar
CaO
$SiO_2 + Al_2O_3$
(c)
2.5 GPa, 1350°C
CO_2
V
Lc
V
Ls
Lc + V
CC
Na_2O
CC
Ls
Ls + V
CaO
$SiO_2 + Al_2O_3$

Figure 15. (a) Same surfaces and field boundaries as in Fig. 13, also representing the projection of the features on the basal triangle (Hamilton projection) from CO_2 in Fig. 14a. Curves E-F and G-O are the silicate-carbonate liquidus field boundaries, and curve M-F-K-G-N indicates the miscibility gap field boundary (B-B, Fig. 2). (b) Schematical phase diagram at 1 GPa, showing the same field boundaries as in (a), identified by the same letters in lower case. The field boundary m-f-k-g-n is constructed with geometry similar to that of the 2.5 GPa boundary M-F-K-G-N, and is placed between curves B-B and C-C (at 0.5 GPa) of Fig. 2, without intersecting the join Ab-CC. Curve e-f is the wollastonite-calcite liquidus field boundary. There is an additional field boundary in the silicate liquidus surface, which is between wollastonite and albite near the studied join, and between wollastonite and quartz near the (Al_2O_3 + SiO_2)-CaO side. The positions of the two field boundaries are constrained by the piercing points on the joins albite-calcite (this study) and quartz-calcite (Huang & Wyllie, 1974). Notice the tie-line f-g, corresponding to F-G at 2.5 GPa (Fig. 13b), is now moved to more $CaCO_3$-rich compositions.

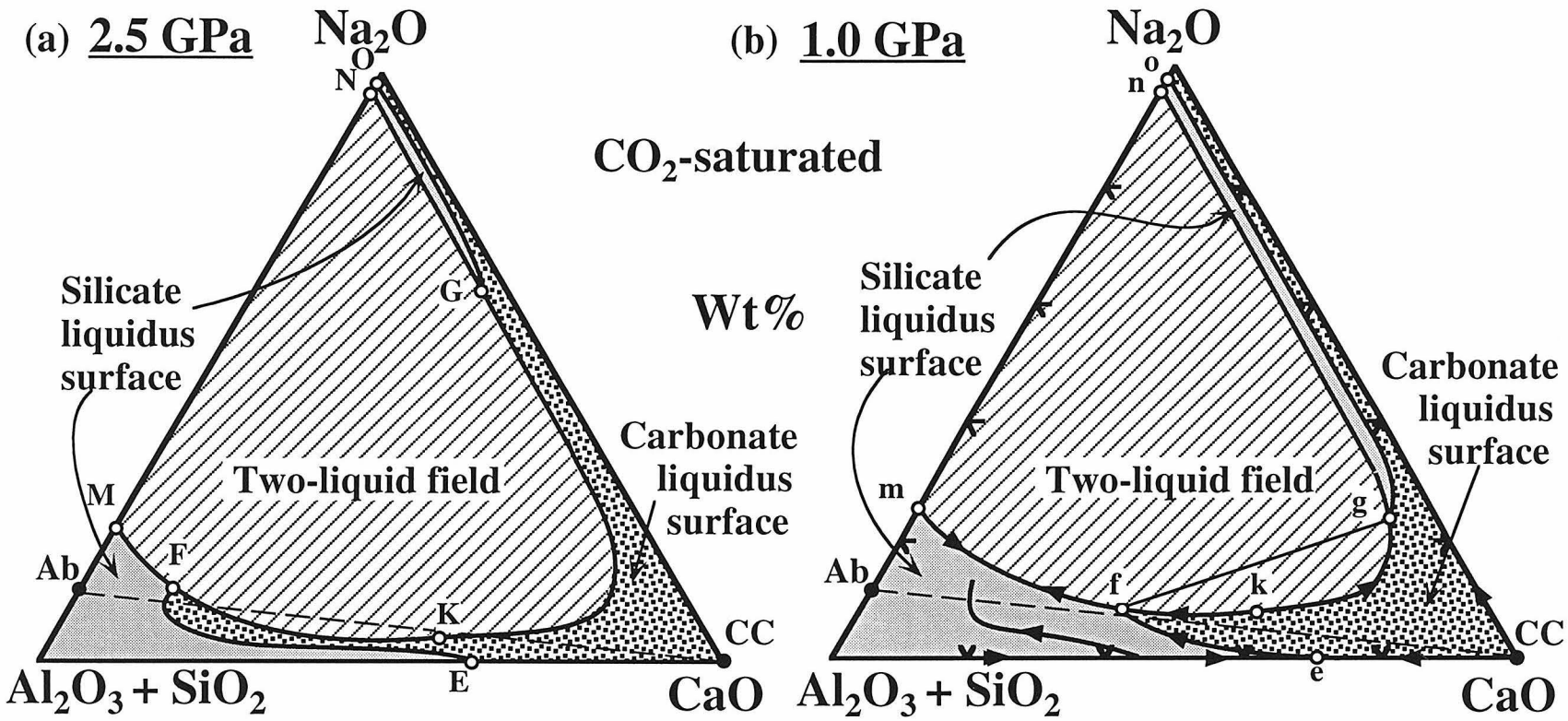
(a) 2.5 GPa
Na_2O
N
O
Silicate liquidus surface
G
Two-liquid field
Carbonate liquidus surface
M
F
Ab
K
CC
E
$Al_2O_3 + SiO_2$
CaO
CO_2-saturated
Wt%
(b) 1.0 GPa
Na_2O
n
o
Silicate liquidus surface
Carbonate liquidus surface
Two-liquid field
m
g
Ab
f
k
CC
e
$Al_2O_3 + SiO_2$
CaO

discussions, CO_2-bearing liquids Ls on the silicate liquidus surface (Figs. 14a, 15) are referred to as carbonated silicate liquids.

All of our melting experiments contained vapor, so the liquidus phase relationships in Figs. 13-15 are those on the CO_2-saturated liquidus surface. The CO_2-contents of the projected liquids of Figs. 13 and 15a outside of the miscibility gap are shown in Fig. 14a by the shaded surface. The high-temperature liquidus dome above the miscibility gap is not shown, and the "2-L field" is the ruled surface for coexisting liquids Ls + Lc which are just saturated with CO_2 and minerals, situated below the miscibility gap.

The field boundary on the front face of Fig. 14a corresponds to the CO_2-saturated boundary in the system CaO-SiO_2-CO_2 (Huang et al., 1980). The silicate liquidus boundary with very low CO_2 content rises toward CO_2 as CaO/SiO_2 increases, reaching about 20 wt% for compositions near E (Lee et al., 1994). It reaches the high levels shown for CaO because at 2.5 GPa molten calcite dissolves a few per cent CO_2 (Huang & Wyllie, 1976). The liquidus surface near Ls, associated with quartz, feldspars and nepheline, remains near the base of the tetrahedron. There are no data on CO_2 solubility in Na_2CO_3 liquids, but we assume that the liquid Lc remains at least as high within the tetrahedron as the $CaCO_3$-rich liquidus surface. The bounding phase relationships on the left-hand triangle are defined by the two short segments of silicate and carbonate liquids shown, connected by the tie-line Ls + Lc (M-N). These limits constrain the three-dimensional representation of Figs. 13 and 15a in Fig. 14a.

The spatial position of the miscibility gap field boundary M-F-K-G-N is based on the limiting framework outlined in Fig. 14a and the liquid analyses from Fig. 8, summarized in Fig. 9a. The values of CO_2 for the liquids plotted in Figs. 8 and 9a were assumed to be the shortfalls from 100% of EDS analyses. Figure 14b shows the spatial positions of the liquid compositions, their projected positions on the base of the tetrahedron, and the 1350°C isotherm on the miscibility gap liquidus dome. Figure 14c shows the same isotherm, as well as the positions of a 3-phase triangle generating the

volume for Ls + Lc + V, and the 4-phase tetrahedron Ls + Lc + CC + V rising above the 3-phase triangle in Fig. 9a. As evident in Fig. 9c, the positions of these isotherms are very close to the two-liquid field boundary sketched in Fig. 14a.

Effect of pressure on phase field geometry

Figures 14a and 15a illustrate the distribution of the main liquidus field boundaries and surfaces at 2.5 GPa. A key feature is the field boundary between silicates and calcite, E-P-F, with tie-line F-G to the immiscible carbonate liquid. Figure 15b is a sketch for 1.0 GPa, with the same field boundaries as in Fig. 15a (shifted in location) identified by the same letters in lower case. The piercing points on the join Ab-CC are taken from Fig. 7 (with adjustment for CO_2 as discussed above). The main differences for 1.0 GPa are (1) the miscibility gap is smaller, no longer crossing the join Ab-CC, and (2) the invariant liquid f is much richer in $CaCO_3$ than its counterpart F at 2.5 GPa; (3) The liquidus surface for calcite is accordingly much smaller, and (4) the silicate liquidus surface extends much further around the miscibility gap (m-f and n-g) than at 2.5 GPa (M-F and N-G). An additional complication in Fig. 15b is the appearance of a liquidus surface for wollastonite between quartz or albite and calcite (Figs. 5 and 7; Huang et al., 1980).

The position of the tie-line F-G or f-g (controlled by the position of the silicate-calcite liquidus field boundary) limits the range of silicate liquids Ls which exsolve immiscible carbonate-rich liquids Lc. The pressure effect in this system is very large. At 2.5 GPa, carbonated silicate liquids can only reach the section M-F of the miscibility gap, yielding only highly alkalic carbonate-rich liquids (N-G). At 1.0 GPa, carbonated silicate liquids may reach the section m-f of the miscibility gap, yielding carbonate-rich liquids with compositions n-g reaching high $CaCO_3$ contents.

RECONCILIATION OF CONTRASTING RESULTS IN THE SYSTEM Na_2O-CaO-Al_2O_3-SiO_2-CO_2

Hamilton & Kjarsgaard (1993) recently reviewed some of the divergent results published for the system Na_2O-CaO-Al_2O_3-SiO_2-CO_2, including their own results (Kjarsgaard & Hamilton, 1988, 1989) summarized in Fig. 2 which show two very significant features: (1) a wide miscibility gap between silicate and carbonate liquids in the absence of alkalis (A-A), and (2) the occurrence of essentially pure $CaCO_3$ liquids. They also plotted the three-immiscible liquids (one reportedly near pure $CaCO_3$) found by Brooker & Hamilton (1990) at 1.5 GPa. They cited the discovery of liquid immiscibility between albite-rich liquid and sodium carbonate liquids by Koster van Groos & Wyllie (1966, 1968), but concluded that because there was no Ca-component the results were "not too applicable to rock systems". This had been remedied by Koster van Groos & Wyllie (1973) with the addition of anorthite, and extension of the two-liquid field with liquid compositions: nepheline-normative silicate, and carbonate enriched in Ca/Na. Extrapolation of the results suggested that the miscibility gap would close at a critical liquid composition still containing sodium.

Several additional sets of experiments have bearing on whether or not the miscibility gap extends to alkali-free, calcium-rich compositions. Huang & Wyllie (1974) and Maaloe & Wyllie (1975) found no liquid immiscibility in the Na-free joins wollastonite-$CaCO_3$ and grossularite-$CaCO_3$ at 3.0 GPa, and Huang et al. (1980) found none in the system CaO-SiO_2-CO_2 through a range of pressures (Lee et al., 1994).

Experiments by Watkinson & Wyllie (1969, 1971) on nepheline-calcite and albite-calcite were reported by Hamilton & Kjarsgaard (1993) as Ca-rich systems showing no miscibility gap, and Kjarsgaard & Hamilton (1988) concluded that the absence of liquid immiscibility in the join nepheline-calcite conflicted with their results. Wyllie (1989) pointed out that "conflict" was not established, because the two sets of experiments were at

very different conditions. Those of Kjarsgaard & Hamilton (1988) were at high temperatures, super-liquidus and mostly H_2O-free, whereas those of Watkinson & Wyllie (1971) were subliquidus, below 980°C, and with 25% H_2O. Lee & Wyllie (1994b) have subsequently demonstrated that the low-temperature fractionation path in the hydrous system can pass below a high-temperature two-liquid volume. These two sets of experimental results are thus reconciled.

The results in the Na-free systems are consistent with our new results defining closure of the miscibility gap at K in Fig. 9c and in Fig. 13, where the field boundary F-Q-K-R-G corresponds to the curve B-B in Fig. 2. The curve B-B was described by Lee & Wyllie (1992a, 1992b), and Lee et al. (1994). Kjarsgaard & Hamilton (in preparation, in Macdonald et al., 1993) revised the interpretation of their experiments and presented the miscibility gap C-C in Fig. 2 to replace the dashed curves A-A. The two-liquid isotherm pairs A-A and C-C for 0.5 GPa and 1250°C from Fig. 2 are reproduced in Fig. 16 as 4-4 and 5-5, respectively. Our experimentally determined field boundaries in Figs. 9c and 13 are for 2.5 GPa, but the two-liquid isotherm is also estimated for 0.5 GPa and 1250°C, as shown by dashed curve 3 in Fig. 12, and this is reproduced in Fig. 16 as curve 3. The curve fits remarkably well with the revised isotherm 5-5 of Kjarsgaard & Hamilton, and these two sets of experimental results now appear to be reconciled. The reconciliation invalidates the claim for the existence of immiscible liquids with compositions of nearly pure $CaCO_3$.

What about the report from Brooker & Hamilton (1990) for the coexistence of three immiscible liquids at 1.5 GPa and 1225°C: silicate, Na-bearing carbonate, and almost pure $CaCO_3$? Their three-phase triangle showing the compositions of the three liquids corresponds topologically to the triangle which we interpret as (Ls + Lc + calcite) in Fig. 9, which indicates the probable reason for the different published results. The phase which has been interpreted as immiscible $CaCO_3$-liquid we interpret as rounded calcite, crystalline under run conditions, for reasons discussed below.

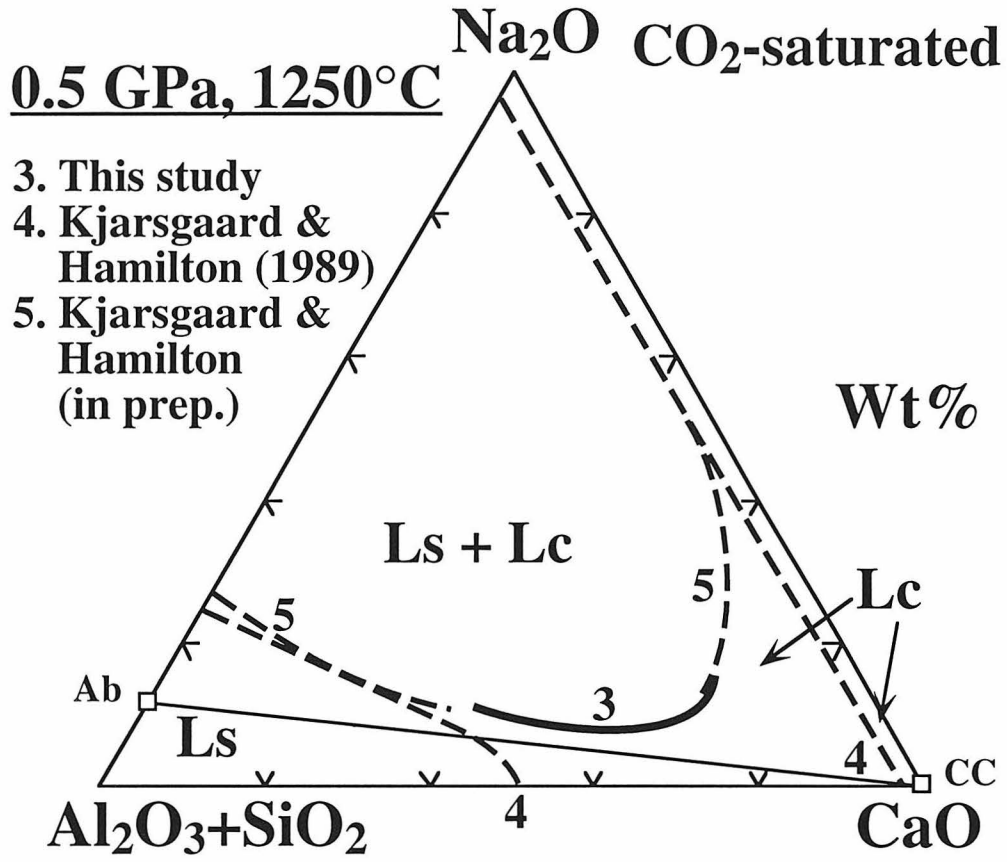

Figure 16. Comparison of the two-liquid isotherms at 0.5 GPa and 1250°C from different studies: curve 3 - our estimated isotherm (Fig. 12), curves 4-4 - the isotherms from Kjarsgaard & Hamilton (1989; A-A, Fig. 2), and curves 5-5 - the isotherms from Kjarsgaard & Hamilton (in prep.; C-C, Fig. 2). It shows a good agreement between curves 3 and 5-5, and curves 4-4 are now invalidated.

Rounded, crystalline calcite

Rounded calcite has been described as an equilibrium mineral phase in many systems (e.g. Maaloe & Wyllie, 1975; Huang et al., 1980), including silicate-free systems (Wyllie & Tuttle, 1960; Cooper et al., 1975, Plate 1A and B; Fanelli et al., 1986), but its remarkably fluid morphology was not apparent until viewed with the scanning electron microscope (Brooker & Hamilton, 1990; Lee et al., 1994). The rounded calcite grains in Fig. 4d certainly appear to have many physical characteristics of quenched liquids, including the criteria of rounded and ameboid shapes, coalescence, and inclusions of vapor. Evidence of this type cited by Kjarsgaard & Hamilton (1988, 1989) and Brooker & Hamilton (1991) is certainly persuasive–the calcite bodies look like quenched immiscible liquids, but we have convinced ourselves from several lines of evidence that the rounded $CaCO_3$ phases in Fig. 4d were crystalline calcite during the run, and not almost pure $CaCO_3$-melt. Furthermore, Kjarsgaard (1994, personal communication) is now satisfied that the rounded $CaCO_3$ phase in his experiments was a solid at experimental conditions.

The existence of pure, or almost pure $CaCO_3$-melt at 1250°C, about 150°C below the fusion curve at 0.5 GPa, is improbable. An appeal to contamination by traces of H_2O would lower the solidus temperature, but would have only a small effect on the liquidus temperature (Wyllie & Tuttle, 1960). The coexistence of pure $CaCO_3$-melt with silicate melt is thermodynamically unlikely. The EDS analyses of Kjarsgaard & Hamilton (1988) show that the rounded phase is not quite pure, having up to 1% of (Na_2O + Al_2O_3 + SiO_2). We attributed our similar results to analytical limitation on EDS technique and to contamination problems, partly due to the fact that in sample preparation all charges were polished and cleaned without using water.

The distribution of the round $CaCO_3$ phase in the phase diagram is consistent with its occurrence as a mineral, but not as an immiscible liquid. In Fig. 7, a smooth curve extending down in temperature from the melting point of calcite is closely bracketed by

runs with (a) quenched liquid, and (b) quenched liquid + round $CaCO_3$ phase. The composition of the $CaCO_3$ phase remains constant in all runs. We are unable to design a phase diagram involving immiscible liquids from this collection of runs, but the curve is precisely what one would expect for the liquidus of calcite.

Figure 4b shows a short-duration experiment (#5) in the process of melting, with disequilibrium texture. Seams of liquid trace hexagonal outlines for some calcite crystals, but some rounded edges are also visible. When repeated for a longer time (#51), the originally hexagonal calcite has become the round $CaCO_3$ phase suspended in silicate-rich liquid. Interpretation of the round $CaCO_3$ phase as a solid mineral has provided internally consistent phase diagrams in Figs. 5-7; it would be difficult to construct complete phase diagrams if the round $CaCO_3$ phase was a quenched, immiscible liquid.

Figures 4c and 4a show the change in texture of starting mixture $Ab_{90}C_{10}$ at 2.5 GPa (Fig. 5) when the temperature is raised from 1200°C to 1300°C. The low temperature assemblage of (albite + rounded calcite) is replaced by the assemblage (albite + liquid). The round calcite (Fig. 4c), which is generally smaller than the round calcite formed with liquid present (e.g. Fig. 4d), also occurs in the other two runs listed as subsolidus in Fig. 5. The replacement of round $CaCO_3$ by interstitial Ls with increased temperature is readily explained by the fusion of crystalline calcite with albite, but it would be difficult to explain these small rounded grains packed in albite as a liquid immiscible with a trace of H_2O-derived liquid.

Quenched carbonate-rich liquids are characterized by dendritic textures (Fig. 3b; Wyllie & Tuttle, 1960; Kjarsgaard & Peterson, 1991; Hamilton & Kjarsgaard, 1993). We made thin sections of some samples, and some larger grains developed incipient rhombohedral fractures during polishing. Each round $CaCO_3$ grain extinguished uniformly, and we could detect no sign of dendritic texture.

PATHS OF CRYSTALLIZATION

Phase equilibrium studies of silicate-carbonate liquid immiscibility are of three types: location of the miscibility gap in (1) synthetic model systems such as the subject of this paper, and (2) more complex systems between natural rock compositions and carbonates (Freestone & Hamilton, 1980; Baker & Wyllie, 1990); and (3) determination of the crystallization sequence for a mixture of a rock with carbonate (Hamilton & Kjarsgaard, 1993). The approaches in (1) and (2) commonly consider an isotherm on the immiscibility liquidus dome as the controlling feature for the generation of carbonatite magmas. Lee & Wyllie (1992c) pointed out that another important control on petrological processes is the liquidus field boundary between silicates and carbonates, such as E-P-F and e-f in Figs. 13 and 15. This field boundary may serve as a barrier between some carbonated silicate magmas and the miscibility gap. Liquids reaching these boundaries precipitate calcite along with silicate minerals. The location of features such as this in the synthetic model systems (1) provides explanations for observed sequences of crystallization in experiments with complex rock systems (2 and 3).

Figures 13 and 15 compare the main liquidus features in our system at two pressures, 2.5 GPa and 1.0 GPa. The lower parts of these figures have been expanded in Fig. 17 by vertical exaggeration, following Fig. 13a, but in addition the positions of the field boundaries have been somewhat distorted in order to show relationships more clearly. There are significant differences in the geometry of phase fields at the two pressures, as outlined above.

Consider starting liquids of carbonated silicate melts. Note the different paths possible for liquids ranging from nepheline-normative to quartz-normative compositions, at 2.5 GPa and 1.0 GPa. At both pressures, both nepheline-normative and quartz-normative liquids may follow paths reaching the silicate-calcite liquidus field boundary E-P-F or e-p-f, with precipitation of calcite. At 2.5 GPa, only nepheline-normative liquids can reach the miscibility gap, between M and F, producing a limited range of alkali-rich

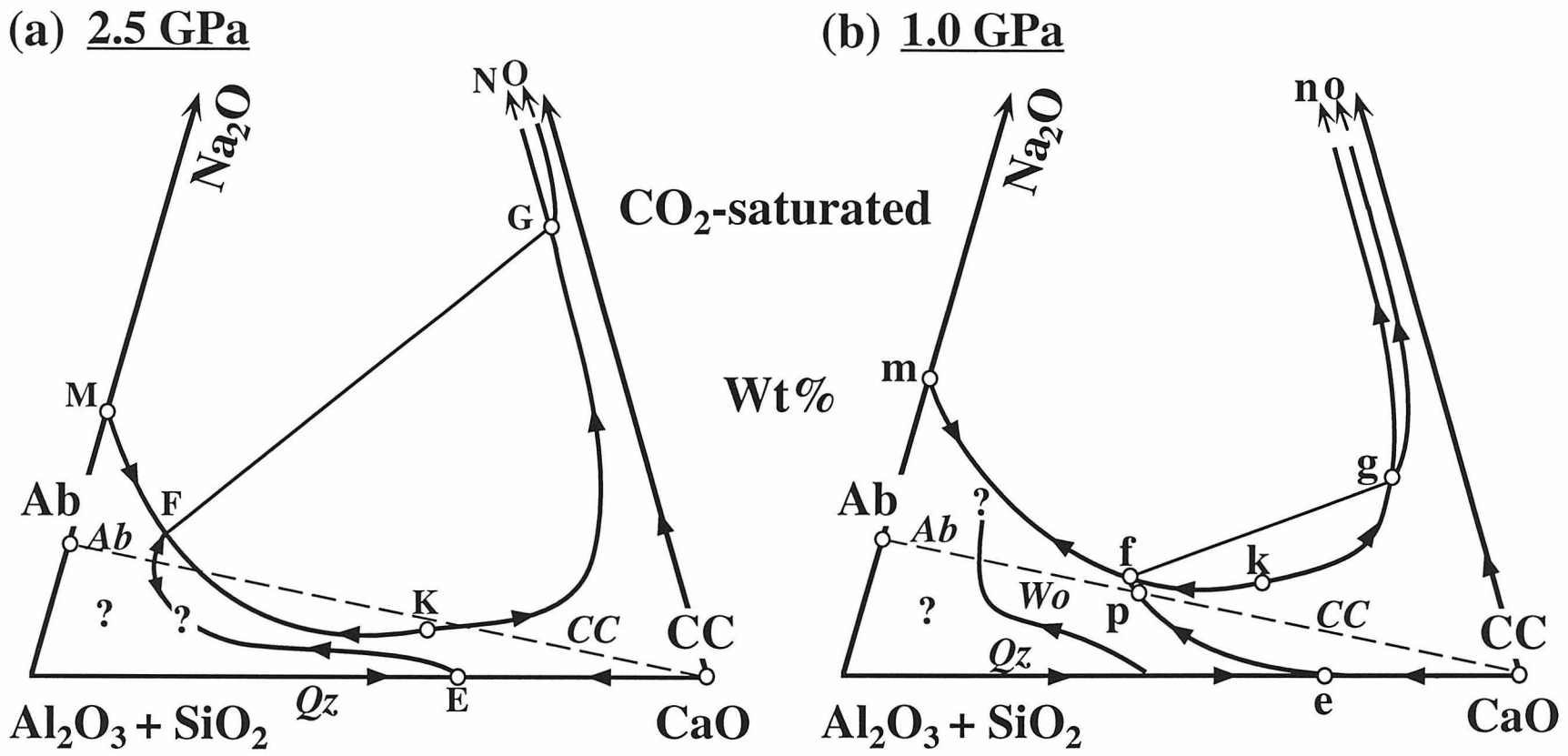

Figure 17. The liquidus field boundaries illustrated in Figs. 13, 14a and 15 at (a) 2.5 GPa, and (b) 1.0 GPa, with vertical exaggeration of 2, and some distortion for better illustration of the pressure effect on these boundaries. The italic characters Ab, Qz, Wo and CC indicate the liquidus fields for albite, quartz, wollastonite and calcite. As indicated by the question marks, the detailed phase relationships in the silicate liquidus surface are not well-known.

carbonate liquids, G-N (Fig. 13). The silicate-calcite field boundary E-P prevents quartz-normative liquids from reaching the miscibility gap at 2.5 GPa. At 1.0 GPa, both nepheline-normative and albite-normative liquids may reach the miscibility gap between m and f. Quartz-normative liquids may reach the silicate-calcite field boundary e-p-f and follow it to the miscibility gap at f, where $CaCO_3$-rich liquid g is exsolved; with equilibrium cooling, the silicate liquid Ls moves from f toward m, and the carbonate liquid Lc moves along g-n. Alternatively, quartz-wollastonite field boundary may prevent Ab-rich quartz-normative liquids from reaching the silicate-calcite field boundary, but we have insufficient data to discuss details.

At both pressures, the immiscible carbonate liquids Lc do not precipitate carbonate minerals while they remain on boundaries G-N and g-n in contact with the silicate liquids Ls (except for liquids G and g). If the liquids Lc are removed from the immiscible silicate hosts, then they may cool across the silicate liquidus (N-G-O or n-g-o) precipitating only silicate minerals until they reach the field boundaries O-G or o-g where carbonates are precipitated in abundance, probably some hundreds of degrees lower than the field boundaries N-G and n-g.

EFFECT OF Mg ON PHASE RELATIONSHIPS

Many carbonatites contain significant amounts of MgO in carbonates or silicates, and parental silicate magmas contain variable amounts of MgO, and there are some published experimental results using rocks (Table 3) which illustrate the effect of increasing Mg/Ca in the system. The Hamilton projection in Fig. 18 includes the components (MgO + FeO*).

Our Mg-free miscibility gap field boundary at 2.5 GPa (Figs. 9, 13) is replotted in Fig. 18a. Baker & Wyllie (1990) used a magnesian nephelinite (NEPH, Table 3) believed

Table 3. Compositions (wt%) of starting silicate rocks in the studies of Freestone & Hamilton (1980; N, PN and P), Kjarsgaard & Peterson (1991; SH40 and SH49), and Baker & Wyllie (1990; NEPH). N, PN, and P are nephelinite, phonolitic nephelinite and phonolite, respectively, from Oldoinyo Lengai. SH40 and SH49 are two nephelinite lava samples from Shombole volcano. NEPH is a primitive nephelinite from Hawaii.

	N	PN	P	SH40	SH49	NEPH
SiO_2	41.93	46.34	52.88	45.30	39.60	38.06
TiO_2	0.92	1.05	0.93	1.53	2.03	2.59
Al_2O_3	15.55	18.10	19.89	17.00	12.60	10.84
Fe_2O_3	6.41	6.31	4.07	6.00	8.00	4.74
FeO	2.28	1.31	1.58	1.80	2.00	9.09
MnO	0.24	0.19	0.03	0.23	0.28	0.22
MgO	1.28	1.30	0.45	1.20	1.89	14.96
CaO	10.89	5.97	2.67	8.16	12.60	10.96
Na_2O	10.26	12.00	10.63	9.40	8.40	2.57
K_2O	4.95	4.80	4.91	3.77	3.23	0.93
P_2O_5	0.54	0.12	0.11	0.23	0.33	0.87
H_2O^-	0.85	1.28	0.02	1.90	1.70	1.59
CO_2	2.39	1.14	0.15	2.90	5.80	0.33

Figure 18. (a) Comparison of our miscibility gap field boundary at 2.5 GPa (curve 1; B-B, Fig. 2) and the magnesian two-liquid isotherm at 2.5 GPa and 1250°C from Baker & Wyllie (curve 2), showing that the size of the miscibility gap decreases with increasing Mg/Ca of liquids in the revised Hamilton projection, (SiO_2 + Al_2O_3 + TiO_2)-(CaO + MgO + FeO*)-(Na_2O + K_2O), projected from CO_2. FeO* indicates the total iron content expressed as FeO. (b) Comparison of the miscibility gaps from Baker & Wyllie (1990; curve 2), Freestone & Hamilton (1980; curve 3 at 0.3 GPa and 1100°C), and Kjarsgaard & Peterson (1991; curves 4-4 at 0.5 GPa and 900-1025°C). Also plotted are the corresponding starting silicate rock compositions from eah study (Table 3): NEPH - primitive nephelinite from Hawaii (curve 2), N - nephelinite, PN - phonolitic nephelinite, and P - phonolite from Oldoinyo Lengai (curve 3), and SH40 and SH49 - nephelinites from Shombole (curves 4-4). The latter two sets of rocks are highly differentiated compared to NEPH.

(a)

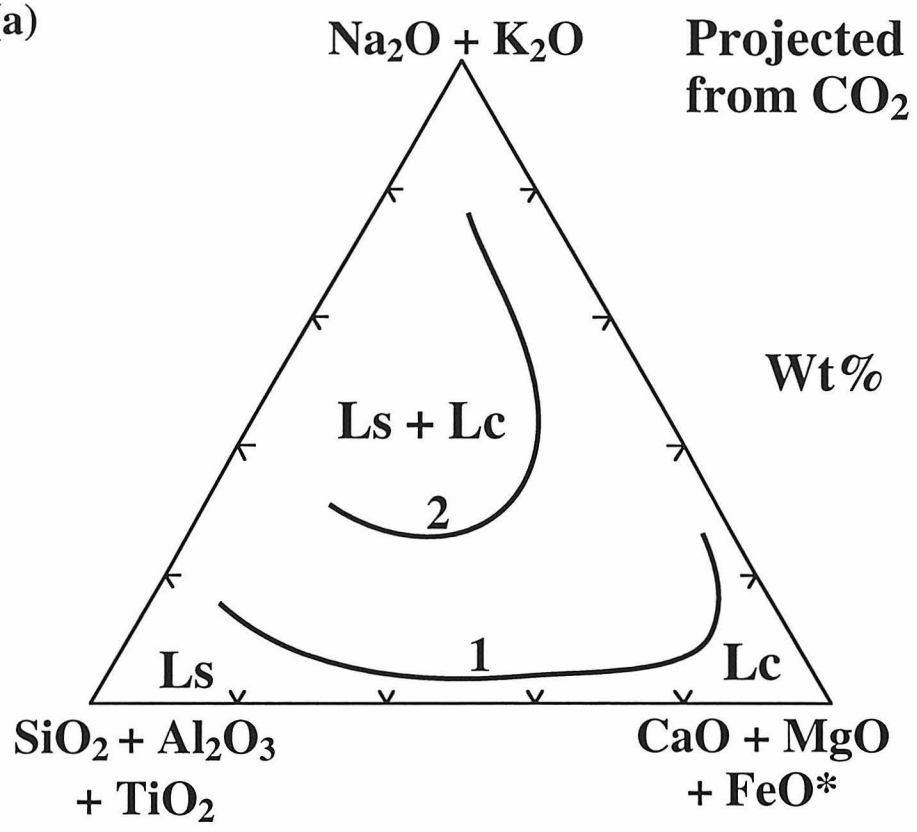
Na2O + K2O
Projected from CO2
Wt%
Ls + Lc
2
1
Ls
Lc
SiO2 + Al2O3 + TiO2
CaO + MgO + FeO*

(b)

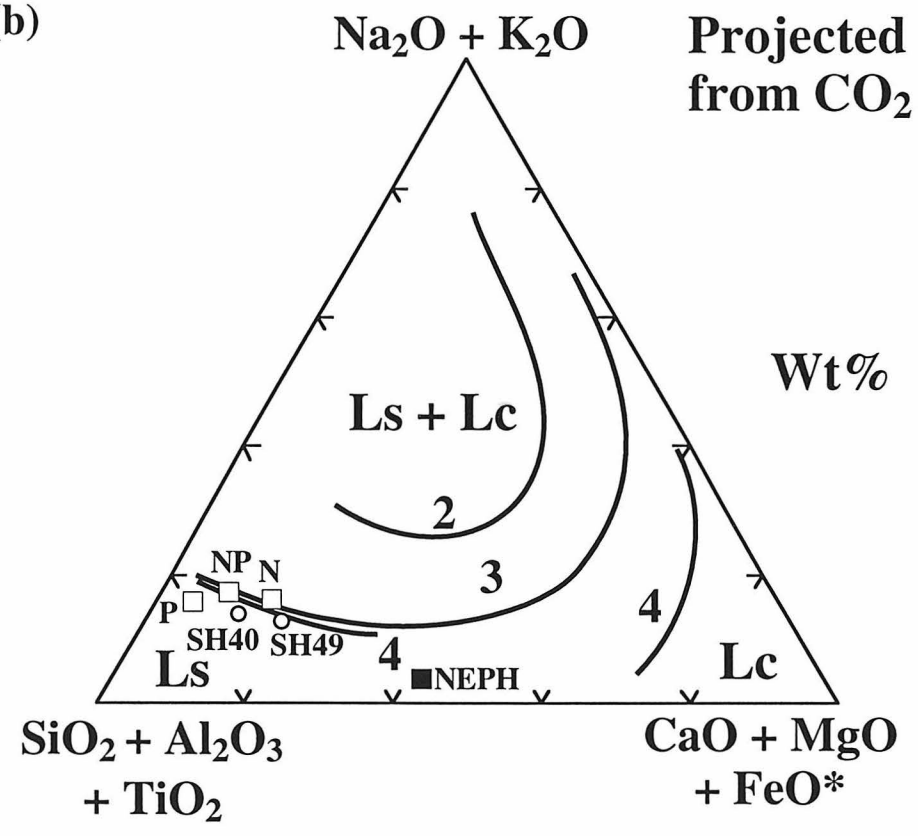
Na2O + K2O
Projected from CO2
Wt%
Ls + Lc
2
3
4
NP
N
P
SH40
SH49
Ls
4
NEPH
Lc
SiO2 + Al2O3 + TiO2
CaO + MgO + FeO*

to represent a primitive melt from the mantle to determine curve 2, a 1250°C isotherm near the miscibility gap field boundary at 2.5 GPa. These curves show that with increasing Mg/Ca at 2.5 GPa, the size of miscibility gap decreases significantly. The temperature of isotherm 2 is slightly lower than that for curve 1 (>1300°C, Fig. 9c), but curve 2 shrinks at higher temperatures (Baker & Wyllie, 1990) so the conclusion about Mg/Ca holds.

Figure 18b compares the miscibility gap (2) from Fig. 18a with those determined for two other Mg-bearing rock systems (Table 3). Two sets of low-magnesian silicate rocks (3) N, PN, P from Freestone & Hamilton (1980), and (4) SH40, SH49 from Kjarsgaard & Peterson (1991) are both highly evolved, containing 3-5% K_2O and 8-12% Na_2O, with low Mg contents and Mg-numbers, but high Fe^{3+}/Fe^{2+}. Figure 18b shows that the miscibility gap increases in size from the more magnesian curve (2) to the curves (3) and (4) with lower Mg. Similarly, the curves (3) and (4) indicate a somewhat smaller miscibility gap than curve (1) (Fig. 18a) with no Mg, but direct information of the effect of Mg/Ca is not attainable, due to the different experimental conditions (pressure and temperature) among the studies.

Lee & Wyllie (1994a) showed that with decreasing pressure, the magnesian miscibility gap (2, Fig. 18) expands, whereas the size of the miscibility gap in the system Na_2O-CaO-Al_2O_3-SiO_2-CO_2 decreases with decreasing pressure (Fig. 12). The latter trend is consistent with the finding of Freestone & Hamilton (1980) that the two-liquid field in their Mg-poor system (curve 3, Fig. 18b) at 1100°C is narrower at lower pressure.

PETROLOGICAL APPLICATIONS

Magmatic processes in the mantle are not well represented in our end-member Mg-free system Na_2O-CaO-Al_2O_3-SiO_2-CO_2 (Figs. 1, 13-15). The effect of increasing Mg in reducing the extent of the miscibility gap is shown in Fig. 18a (2). Baker & Wyllie (1990) compared the gap (2) with the probable paths of partial melt compositions from carbonated

mantle, and concluded that intersection was unlikely; the primary mantle carbonatite melts would be deficient in alkalis compared with the miscibility gap field boundaries. However, the field boundaries outlined in Figs. 13-15 do represent quite closely calciocarbonate magmas, recently proposed as primary from the mantle (e.g. Bailey, 1993), and do indicate the controls exerted on possible processes by the field boundaries separating liquidus surfaces for silicates, carbonates and the miscibility gap. The end-member system also facilitates interpretation of melting relationships in siliceous limestones and sea-water-altered basalt in subducted oceanic crust.

Carbonatitic melts and metasomatism within the mantle

Proposals that calciocarbonatite magmas (e.g. Keller, 1989) may be primary melts from the mantle (e.g. Bailey, 1993) or derived during ascent from a more primitive carbonatite magma (e.g. Gittins, 1989) have been reviewed in detail by Lee & Wyllie (1994b). Bailey (1993) presented the most comprehensive arguments for the existence of primary calciocarbonatites.

Menzies & Hawkesworth (1987), Meen et al. (1989) and Menzies & Chazot (1994) have published detailed reviews on mantle metasomatism. The geochemistry of mantle xenoliths is currently interpreted in terms of metasomatic agents including H_2O-rich vapors, silicate melts, carbonatite liquids, and carbonated silicate liquids. There is increasing metasomatic evidence for the occurrence of carbonate-rich melts in the mantle. The phase relationships determined for peridotite-carbonate assemblages which outline the range of carbonatitic liquids formed in mantle rocks at various depths were reviewed by Lee & Wyllie (1994b). They concluded that primary carbonatite magmas from the mantle should be dolomitic; natrocarbonatite magmas cannot be primary; the formation of magmas richer in Ca/Mg requires a wehrlite source; there is no experimental evidence for

the formation of almost pure $CaCO_3$ calciocarbonatite liquids from mantle peridotites (except possibly involving wehrlite in petrological processes not yet well defined).

Carbonate ocelli in mantle xenoliths

Experimental data show that carbon dioxide in the upper mantle should form dolomite or magnesite in lherzolite and harzburgite (Wyllie & Huang, 1975, 1976; Eggler, 1978). The rarity of carbonates in peridotite xenoliths is attributed to explosive decomposition of carbonates coexisting with peridotite minerals during transport to the surface (Eggler, 1975; Wyllie, 1978; Wyllie et al., 1983; Canil, 1990). Reports of carbonate ocelli or globules within mantle xenoliths and xenocrysts, however, confirm the presence of carbonate minerals in the mantle (Amundsen, 1987; Ionov et al., 1993; Pyle & Haggerty, 1994; Kogarko & Pacheco, 1994; McInnes & Cameron, 1994). The currently prevalent view is that the carbonate-rich ocelli represent quenched immiscible carbonatitic liquids, and the processes which produced the ocelli have been related to the generation of large-scale carbonatite magmas within the crust (Pyle & Haggerty, 1994; Kogarko & Pacheco, 1994).

Amundsen (1987) interpreted three components of Spitsbergen lherzolite xenoliths as immiscible liquids, based on the textural relationship among the basaltic, ultramafic, and carbonatitic phases. The globular carbonate is near magnesite composition, containing several percent of FeO, and trace amounts of other components. Ionov et al. (1993) amplified this interpretation, proposing liquid immiscibility between Na-Al silicate liquid (basaltic) and carbonate-rich, magnesian silicate liquid, with the latter further separating into Mg-rich silicate liquid (ultramafic) and carbonate globules either by liquid immiscibility or rapid crystal fractionation.

Pyle & Haggerty (1994) described calcite ocelli and natrosilicic quenched melts in metasomatized upper-mantle eclogite samples from the Jagersfontein kimberlite, South

Africa. They proposed that carbonated mantle with suitable bulk composition undergoing melting produced a carbonated silicate melt, which subsequently separates an immiscible liquid with composition similar to the calcite ocelli (containing up to 1% silicate) enclosed in natrosilicic glass.

Kogarko & Pacheco (1994) described rounded oval segregations of Ca-enriched carbonate and sulfide globules in silicate glass in harzburgite nodule from the Canary Islands. They proposed that the suboceanic harzburgite had previously been metasomatized by primary carbonatitite melt, that the carbonatized mantle was partially melted during adiabatic decompression of mantle, and that the three associated phases (silicate, sulfide and calcite) were the products of liquid immiscibility. They suggested that the assemblage represented "a micro model of the generation of the carbonatitic magmas during the process of the partial melting of carbonatized metasomatized oceanic mantle."

Analyses of the carbonate globules commonly reveal minor silica, alkalis and other components. Given the small size of the phases analyzed, possible inclusions of silicate minerals or liquid, possible contamination due to sample preparation, and the limitations of the analytical techniques, it remains uncertain whether the compositions of the calcite ocelli are effectively pure $CaCO_3$ or whether they contain other components as required by liquid immiscibility relationships.

The results of Kjarsgaard & Hamilton (1988, 1989; curve A-A, Fig. 2) were cited by Pyle & Haggerty (1994) and Kogarko (1994, personal communication) to support their conclusion that the calcite ocelli represented immiscible liquids. These experimental results have now been revised (curves B-B and C-C, Fig. 2) and there is no experimental evidence for the formation of almost pure $CaCO_3$, immiscible liquids.

We have presented evidence that crystalline calcite can grow in silicate-carbonate liquids with remarkably rounded morphology (Fig. 4d) simulating the characteristics of liquids. Given the determined phase relationships, we prefer the interpretation that the calcite ocelli in mantle samples represent crystals such as those in the phase field CC + Ls

(+ V) shown in Fig. 5 (see Fig. 13a); at 1300°C the liquid is siliceous. On the basis of available experimental evidence, we do not expect ocelli of calcite to occur in apparent equilibrium with peridotites, but only with the more alkalic, siliceous glassy phases. The compositions of the Na-rich aluminosilicate glass inclusions reported by Pyle & Haggerty (1994) and McInnes & Cameron (1994) contain only a few per cent of, or nearly no CaO, MgO, and FeO, which makes them unlikely candidates for liquids in equilibrium with peridotite, or for silicate liquids immiscible with Ca-carbonate-rich liquids (Fig. 18).

The high-pressure miscibility gap in the magnesian system (Fig. 18a, curve 2) involves alkaline carbonatite liquids containing less than 40% (Ca + Mg + Fe)-carbonates, and significant proportions of silicate components. These immiscible liquids cannot quench to globules of nearly pure magnesite or dolomite. There is thus no experimental evidence supporting the interpretation of immiscible "magnesite liquids" in Spitsbergen lherzolite (Amundsen, 1987; Ionov et al., 1993).

Liquidus paths to calciocarbonatite magmas

There are two perennial questions still debated: (1) do calciocarbonatite liquid magmas extremely rich in $CaCO_3$ exist, and if so (2) how are they derived from parent rocks or parent magmas? Despite the field evidence adduced for the existence of $CaCO_3$-rich magmas (Keller, 1989; Bailey, 1993), and the conclusions from experiments by Kjarsgaard & Hamilton (1988, 1989) that calciocarbonatite magmas could consist of nearly pure $CaCO_3$, Lee & Wyllie (1994a) concluded that carbonatite liquids which have some connection with silicate parents contain a maximum of 80% $CaCO_3$, and probably less at crustal pressures. This conclusion is here reinforced in Figs. 12-15, with agreement by Kjarsgaard & Hamilton (curves 4-4 in Fig. 16), by Kjarsgaard & Peterson (1991; curves 4-4 in Fig. 18b for carbonate liquids exsolved from evolved nephelinites of

Shombole volcano), and by Hamilton & Kjarsgaard (1993, Fig. 3) for experiments with Shombole lavas and calcite.

Liquids in nature with such high concentrations of $CaCO_3$ would certainly merit the title "calciocarbonatite magma", but they would not solidify to carbonatites composed essentially of calcite. The early experimental observation of rapid crystal settling in synthetic carbonatite magmas is consistent with the formation of carbonatite rocks by crystallization differentiation, i.e. most plutonic carbonatites are cumulates (Wyllie & Tuttle, 1960; Wyllie, 1966), a view shared by Hamilton & Kjarsgaard (1993).

The fact that liquids with 70-80% dissolved $CaCO_3$ exist in a phase diagram does not mean that they can necessarily be produced during magmatic processes. The key factors controlling the paths of crystallization of carbonated silicate magmas are illustrated in the end-member synthetic system of Figs. 13-15, expanded in Fig. 17: (1) the liquid miscibility gap within the field boundaries M-F-K-G-N (or m-f-k-g-n), (2) the position of K (or k) separating the consolute liquids Ls (M-F-K, m-f-k) and Lc (K-G-N, k-g-n), (3) the silicate-carbonate liquidus field boundary E-F (or e-f) separating the silicate liqudus surface from the carbonate liquidus surface, (4) its continuation (G-O or g-o) for carbonate-rich liquids, and (5) the tie-line F-G (or f-g) connecting the two field boundaries. The positions of these features change with pressure.

A cooling carbonated silicate liquid in Fig. 15a (17a) may follow one of three paths, with variations as a function of pressure:

(1) the liquid may reach the miscibility gap field boundary between M and F, and exsolve immiscible Lc with composition between N and G. At this pressure, only alkalic carbonate liquid is generated. At lower pressures, 1.0 GPa in Fig. 15b (17b), the limiting tie-line f-g has migrated toward $CaCO_3$, so that the carbonate-rich liquid g contains close to the maximum possible dissolved $CaCO_3$ for Lc. The phase relationships involving the precipitation of wollastonite require that the 1.0 GPa field boundary f-m must decrease in temperature from f, and the consolute carbonate liquid must similarly decrease in

temperature from g. Available evidence indicates that K is a temperature maximum on the field boundary between F-G or f-g, so the immiscible liquids cannot pass closer together than F-G or f-g.

(2) the liquid may reach the silicate-carbonate field boundary E-F where calcite is coprecipitated. Depending on the original liquid composition and the phase relationships, the liquid then may (a) crystallize completely to silicates and calcite, or it may (b) reach the miscibility gap at point F and exsolve carbonate liquid G. At lower pressures, 1.0 GPa in Fig. 15b (17b), the shift of E-F to e-f shows that much more $CaCO_3$ can be concentrated in the silicate liquid before precipitation of calcite occurs.

(3) the liquid may terminate at an eutectic point involving only silicate minerals, evolving CO_2 vapor, without reaching either M-F or E-F. At lower pressures, 1.0 GPa in Fig. 15b (17b), the shift of E-F to e-f opens up a larger silicate liquidus with more field boundaries, and probably more opportunites for the silicate liquid to precipitate only silicate minerals.

Whether a carbonated silicate liquid is nepheline- or quartz-normative may be a decisive factor in whether it follows path (1) or (2b) to exsolution of a carbonate liquid, or path (2a) to coprecipitation of calcite. Alternatives for path (3) cannot be evaluated without details of the field boundaries for the silicate-CO_2 liquidus, which varies with Al_2O_3/SiO_2 as well as with pressure.

A carbonate-rich liquid exsolved from a silicate liquid (e.g. G-N or g-n in Figs. 15 and 17) does not immediately precipitate carbonates. As long as the carbonate liquid remains in equilibrium with the liquid on the silicate liquidus surface, only silicate minerals are precipitated. If the carbonate-rich liquid is separated from its silicate parent, then it may cool down the silicate surface N-G-O or n-g-o precipitating a small amount of silicate minerals before reaching the field boundaries G-O or g-o for the coprecipitation of silicates with carbonates. The temperature interval before carbonates are precipitated may reach hundreds of degrees.

Applications to magmas must take into account the variations in positions of the miscibility gap and the silicate-carbonate field boundary as a function of composition. Figure 18a shows significant reduction in the size of the miscibility gap with increasing Mg/Ca in the bulk system. The silicate-carbonate liquidus field boundary at 2.5 GPa intersected by Fig. 18a has not been measured, but it starts near the (CaO + MgO + FeO*) corner (Wyllie & Huang, 1976), and it passes through the composition of the near-solidus liquid from dolomite-lherzolite (Wyllie & Huang, 1976; Wyllie et al., 1983; Wallace & Green, 1988). This point projects quite near the corner (CaO + MgO + FeO*) in Fig. 18a (Baker & Wyllie, 1990), and the boundary therefore may extend from this region to a point on the miscibility gap field boundary close to the two-liquid isotherm 2. Baker & Wyllie (1990) sketched a melting path for dolomite-peridotite roughly parallel to the bottom side of the triangle, clearly separated from the liquid miscibility gap.

Figure 18b shows the combined effect of pressure and Mg/Ca on the distribution of the phase fields. The two-liquid fields for crustal pressures (curves 3 and 4-4), determined from evolved nephelinites with carbonates are much larger than the field 2 for magnesian primitive nephelinite at mantle pressures. The lava compositions N, PN, P, SH40 and SH49 (see figure legend) used in various experiments project near to the silicate limbs of the miscibility gaps. Those liquids through crystallization could thus easily reach a two-liquid field for exsolution of carbonate-rich liquids.

Carbonates and carbonated melts in subducted oceanic crust

Calcite is a common mineral associated with oceanic crust, either in limestone or as veins produced by low-temperature alteration of seawater. The petrological aspects of subducted oceanic crust with carbonate include: (1) the generation of volatile influx (CO_2 + H_2O) from oceanic crust in triggering the melting of the overlying mantle wedge, (2) the melting of subducted sediments, and (3) the production of melts within the altered basalts,

which may be converted into carbonated eclogites, perhaps corresponding to the mantle xenoliths in kimberlite described by Pyle & Haggerty (1994).

Sweeney et al. (1992) presented experimental data on trace and minor element partitioning between garnet and amphibole and carbonatitic melt at mantle conditions, and attempted to quantify how the interaction of the carbonatite melts with a lhezolitic mantle affects trace element budgets. They evaluated the influence of (CO_2 + H_2O) vapors on the melting of mantle wedge above the subducted oceanic crust, and defined the region where incipient melting of the mantle would generate some carbonate-rich melts before changing composition toward the more basic melts erupted in arc environments.

Whether temperatures in subducted oceanic crust become high enough to permit melting of sediments remains uncertain (e.g. Davies & Stevenson, 1992; Peacock et al., 1994), but the prospect is real under some conditions (Nichols et al., 1994). Treiman & Essene (1983) proposed that eclogite with carbonate would melt during subduction. McInnes & Cameron (1994) proposed that magmas were generated during subduction of altered basaltic crust with carbonate material.

Huang & Wyllie (1974) and Huang et al. (1980) reported a high-temperature eutectic liquid in CaO-SiO_2-CO_2 with composition near 50% $CaCO_3$ and 50% $CaSiO_3$ (see E in Figs. 13-15). Although some subducted pelagic limestone could escape dissociation or melting and be carried to considerable depths for long-term storage of carbon in the mantle, they concluded that with the aid of H_2O to lower melting temperatures, subducted siliceous limestone could generate carbonatitic liquids. Boettcher & Wyllie (1969) studied the effects of H_2O in near-solidus reactions in CaO-SiO_2-CO_2-H_2O. The formation of hydrous calc-silicates in siliceous limestones lowers the solidus temperature with vapor to temperatures below 525°C at depths greater than 75 km, with hydrous liquid compositions dominated by $CaCO_3$ containing less than 20% dissolved silicates. This is the lowest known melting temperature for any subducted material.

Figures 13-15 provide a very simple end-member model system for interpretation of the melting relationships of carbonated basalt, amphibolite or eclogite. Consider a starting mixture of plagioclase with a few per cent of calcite in the joins Ab-CC or Ab-An-CC (Fig. 1), with plagioclase representing the basalt. There is a wide melting interval with coexistence of feldspar and calcite (Figs. 5-7), and the liquid compositions must follow the feldspar-calcite field boundary (E-F, Figs. 13-15) which is so far undetermined (except at the few fixed points shown in Figs. 13a and 5-7). Additional experiments on the carbonated silicate liquidus surface (Ls) are required to define melting paths.

Approximate CO_2 concentrations of the near-solidus liquids estimated by deficiency to 100% in EDS analyses are about 5 % throughout the pressure range (1.0-2.5 GPa), gradually increasing with increasing temperature near the piercing points P, up to 10% at 1.0 GPa, but remaining about 5 % at 2.5 GPa. The liquids produced by small degrees of partial melting in these joins are carbonated silicate melts, rather than carbonatitic liquids.

The piercing points P in Figs. 5-7 and 11 give a further indication of liquid compositions above the solidus, and their changes with depth. At 2.5 GPa (80 km depth) Fig. 5 shows a liquid P with about 80% feldspar and 20% $CaCO_3$ (less the CO_2 displaced into the vapor). At 1.5 GPa (50 km depth) Fig. 6 shows an increase to 30% $CaCO_3$ component (which is consistent with the EDS results outlined above). At 1.0 GPa (40 km depth) this trend toward increasingly carbonated liquids with decreasing pressure continues, with the silicate-calcite piercing point reaching about 55% $CaCO_3$ component (Figs. 7 and 11). However, the situation is complicated by the intersection of the wollastonite liquidus (Fig. 15).

The positions of the piercing points P are outside the two-liquid field (Fig. 11), and the silicate-calcite field boundaries (E-F in Figs. 13-15) separate the silicate liquidus fields from the miscibility gap for all compositions with sodium contents lower than those on the join Ab-CC. Therefore, liquids produced during progressive melting of model basalt-

calcite are unlikely to generate immiscible liquids within a wide temperature range between 1.0 and 2.5 GPa. Nepheline-normative compositions, however, may produce liquids reaching the miscibility gap.

Melting temperatures in the dry system are too high for partial melting to be a factor beneath volcanic arcs. Experimental studies in many other simple systems indicate that with addition of H_2O, the melting temperatures are greatly reduced, and the ratio carbonate/silicate is not greatly changed compared with the dry system (e.g. Wyllie, 1966; Boettcher & Wyllie, 1969). According to this simple model system, therefore, we would expect that in relatively warm subduction zones (Peacock et al., 1994; Nichols et al., 1994) carbonated basalt should yield carbonated silicate liquids, the amount of liquid depending on the amount of calcite available, and the amount of carbonate component in the liquid decreasing as a function of depth.

McInnes & Cameron (1994) addressed the possibility that a feldspathic mineral (possibly scapolite) contributes significantly to the first liquid produced in subducted, seawater-altered basalt. McInnes & Wyllie (1992, in preparation) determined the phase fields intersected by the composition join MORB-$CaCO_3$ at 1.0 GPa, using an anhydrous mid-ocean ridge basalt. They reported a silicate-carbonate liquidus piercing point near 35% $CaCO_3$ (cf. Fig. 11). An analyzed near-solidus liquid at 900°C is nepheline-normative, containing about 12% alkalis and 9% CO_2. Parallel experiments conducted with natural, hydrous seawater-altered basalt have not yet yielded satisfactory analyses of the quenched liquids.

Yaxley & Green (1994) synthesized an altered (hydrated) oceanic basalt (garnet-amphibolite) with 10% calcite, and studied its melting relationships between 1.5-3.5 GPa and 700-1000°C. They reported that broad beam analyses of severely quench-modified liquids, coexisting with dolomite or calcite, provided approximate compositions of two hydrous liquids at 750°C and 850°C and 2.5 GPa, described as broadly dacitic, becoming andesitic with increasing melting. CO_2 contents were "minor". The analogous phase

fields in our simple (anhydrous) model system are for (Ab + Ls + CC + V) or (Wo + Ls + CC + V) above the solidus in Figs. 5-7.

Treiman & Essene (1983) considered the thermodynamics of melting eclogite + CO_2, concluding that the assemblage would melt at reasonable temperatures, 700-1000°C at 2.5 GPa. They assumed that the melts could be carbonatitic, analogous to those from peridotite-CO_2, but the actual Na_2O and CO_2 contents remained unconstrained. They proposed that eclogite with carbonate could be sources for sodic carbonatites and associated alkalic magmas. In terms of Figs. 13-15, this interpretation requires that carbonated silicate liquids would be generated which reached a miscibility gap corresponding to M-F (or m-f), and evolved alkalic carbonate liquids along a field boundary corresponding to N-G (or n-g).

ACKNOWLEDGEMENTS

This research was supported by the Earth Science section of the U.S. National Science Foundation, grant EAR-921886.

REFERENCES

Amundsen, H. E. F., 1987. Evidence for liquid immiscibility in the upper mantle. *Nature* **327**, 692-695.

Bailey, D. K., 1989. Carbonate melt from the mantle in the volcanoes of south-east Zambia. *Nature* **338**, 415-418.

Bailey, D. K., 1993. Carbonate magmas. *Journal of the Geological Society of London* **150**, 637-651.

Baker, M. B., & Wyllie, P. J., 1990. Liquid immiscibility in a nephelinite-carbonate system at 25 kbars and implications for carbonatite origin. *Nature* **346**, 168-170.

Barker, D. S., 1989. Field relations of carbonatites. In Bell, K. (ed.) *Carbonatites: Genesis and Evolution*. London: Unwin Hyman, pp. 38-69.

Bell, K. (ed) 1989. *Carbonatites: genesis and evolution*. London: Unwin Hyman.

Boettcher, A. L & Wyllie, P. J., 1969. The system CaO-SiO_2-CO_2-H_2O: III. Second critical end-point on the melting curve. *Geochimica et Cosmochimica Acta* **33**, 611-632.

Bowen, N. L., 1924. The Fen area in Telemark Norway. *American Journal of Science* **8**, 1-11.

Boyd, F. R & England, J. L., 1963. Effect of pressure on the melting of diopside, $CaMgSi_2O_6$, and albite, $NaAlSi_3O_8$, in the range up to 50 kilobars. *Journal of Geophysical Research* **68**, 311-323.

Brogger, W. C., 1921. Die Eruptivgesteine des Kristianiagebietes. IV. Das Fengebiet in Telemark, Norwegen. Norsk Videnskapsselskapets, Skrifter I. *Math Naturw Klasse* **9**.

Brooker, R. A. & Hamilton, D. L., 1990. Three-liquid immiscibility and the origin of carbonatites. *Nature* **346**, 459-462

Canil, D., 1990. Experimental study bearing on the absence of carbonate in mantle-derived xenoliths. *Geology* **18**, 1011-1013.

Church, A. A. & Jones, A. P., 1995. Silicate-carbonate immiscibility at Oldoinyo Lengai. *Journal of Petrology* **36**, 869-889.

Cooper, A. F. & Reid, D. L., 1991. Textural evidence for calcite carbonatite magmas, Dicker Willem, southwest Namibia. *Geology* **19**, 1193-1196.

Cooper, A. F., Gittins, J. & Tuttle, O. F., 1975. The system Na_2CO_3-K_2CO_3-$CaCO_3$ at 1 kilobar and its significance in carbonatite petrogenesis. *American Journal of Science* **275**, 534-560.

Davies, J. H. & Stevenson, D. J., 1992. Physical model of source region of subduction zone volcanics. *Journal of Geophysical Research* **97**, 2037-2070.

Dawson, J. B., 1966. Oldoinyo Lengai - an active volcano with sodium carbonatite lava flows. In: Tuttle, O. F. & Gittins, J. (eds.) *Carbonatites*. New York: John Wiley, pp. 155-168.

Dawson, J. B., Pinkerton, H., Pyle, D. M. & Nyamweru, C., 1994. June 1993 eruption of Oldoinyo Lengai, Tanzania: Exceptionally viscous and large carbonatite lava flows and evidence for coexisting silicate and carbonate magmas. *Geology* **22**, 799-802.

Eggler, D. H., 1975. Peridotite-carbonate relations in the system CaO-MgO-SiO_2-CO_2: *Carnegie Institution of Washington Yearbook* **74**, 468-474.

Eggler, D. H., 1978. The effect of CO_2 upon partial melting of peridotite in the system Na_2O-CaO-Al_2O_3-MgO-SiO_2-CO_2 to 35 kb, with an analysis of melting in a peridotite-H_2O-CO_2 system. *American Journal of Science* **278**, 305-343.

Fanelli, M. F., Cava, N. & Wyllie, P. J., 1986. Calcite and dolomite without portlandite at a new eutectic in CaO-MgO-CO_2-H_2O, with applications to carbonatites. In: *Morphology and Phase Equilibrium of Minerals*. Proceedings 13th General Meeting, International Mineralogical Association, Bulgarian Academy of Science, Sofia, pp. 313-322.

Freestone I. C. & Hamilton, D. L., 1980. The role of liquid immiscibility in the genesis of carbonatites - an experimental study. *Contributions to Mineralogy and Petrolology* **73**, 105-117.

Gittins, J. & Tuttle, O. F., 1964. The system CaF_2-$Ca(OH)_2$-$CaCO_3$. *American Journal of Science* **262**, 66-75.

Hamilton, D. L. & Kjarsgaard, B. A., 1993. The immiscibility of silicate and carbonate liquids. *South African Journal of Geology* **96**, 139-142.

Hamilton, D. L., Bedson, P. & Esson, J., 1989. The behaviour of trace elements in the evolution of carbonatites. In: Bell, K. (ed.) *Carbonatites: Genesis and Evolution*. London: Unwin Hyman, pp. 405-427.

Heinrich, E. W., 1966. *The geology of carbonatites*. Chicago: Rand McNally.

Huang, W.-L. & Wyllie, P. J., 1974. Eutectic between wollastonite II and calcite contrasted with thermal barrier in MgO-SiO_2-CO_2 at 30 kilobars, with applications to kimberlite-carbonatite petrogenesis. *Earth and Planetary Science Letters* **24**, 305-310.

Huang, W.-L. & Wyllie, P. J., 1976. Melting relationships in the systems CaO-CO_2 and MgO-CO_2 to 36 kilobars. *Geochimica et Cosmochimica Acta* **40**, 129-132.

Huang, W. L., Wyllie, P. J. & Nehru, C. E., 1980. Subsolidus and liquidus phase relationships in the system CaO-SiO_2-CO_2 to 30 Kbar with geological applications. *American Mineralogist* **65**, 285-301.

Ionov, D.A., Dupuy, C., O'Reilly, S.Y., Kopylova, M.G. & Genshaft, Y.S., 1993. Carbonated peridotite xenoliths from Spitsbergen: Implications for trace element signature of mantle carbonate metasomatism. *Earth and Planetary Science Letters* **119**, 283-297.

Irving, A. J. & Wyllie, P. J., 1973. Melting relationships in systems CaO-CO_2 and MgO-CO_2 to 36 kilobars, with comments on CO_2 in the mantle. *Earth and Planetary Science Letters* **20**, 220-225.

Irving, A. J. & Wyllie, P. J., 1975. Subsolidus and melting relationships for calcite, magnesite, and the join $CaCO_3$-$MgCO_3$ to 36 kilobars. *Geochimica et Cosmochimica Acta* **39**, 35-53.

Jago, B. C. & Gittins, J., 1991. The role of fluorine in carbonatite magma evolution. *Nature* **349**, 56-58.

Jones, J. H., Walker, D., Pickett, D. A., Murrell, M. T. & Beattie, P., 1995. Experimental investigations of the partitioning of Nb, Mo, Ba, Ce, Pb, Ra, Th, Pa, and U between immiscible carbonate and silicate liquids. *Geochimica et Cosmochimica Acta* **59**, 1307-1320.

Keller, J., 1981. Carbonatite volcanism in the Kaiserstuhl alkaline complex: Evidence for highly fluid carbonatitic melts at the earth's surface. *Journal of Volcanology and Geothermal Research* **9**, 423-431.

Keller, J., 1989. Extrusive carbonatites and their significance. In: Bell, K. (ed.) *Carbonatites: Genesis and Evolution*. London: Unwin Hyman, pp. 70-88.

Kjarsgaard, B. A. & Hamilton, D. L., 1988. Liquid immiscibility and the origin of alkali-poor carbonatites. *Mineralogical Magazine* **52**, 43-55.

Kjarsgaard, B. A. & Hamilton, D. L., 1989. The genesis of carbonatites by immiscibility. In: Bell, K. (ed.) *Carbonatites: Genesis and Evolution*. London: Unwin Hyman, pp. 388-404.

Kjarsgaard, B. & Peterson, T., 1991. Nephelinite-carbonatite liquid immiscibility at Shombole Volcano, East Africa: petrographic and experimental evidence. *Mineralogy and Petrology* **43**, 293-314.

Kjarsgaard, B. A., Hamilton, D. L. & Peterson, T. D., 1995. Peralkaline nephelinite/carbonatite liquid immiscibility: Comparison of phase compositions in experiments and natural lavas from Oldoinyo Lengai. In Bell, K. & Keller, J. (eds.) *Carbonatite Volcanism: Oldoinyo Lengai and the Petrogenesis of Natrocarbonatites. IAVCEI Proceedings in Volcanology* **4**, Berlin: Springer-Verlag, pp. 163-190.

Kogarko, L. N. & Pacheco, A. H., 1994. Mechanism of carbonatized peridotite partial melting. Abstract Volume, 16th General Meeting, International Mineralogical Association, Societa Italiana di Mineralogy e Petrology, Pisa, Italy, pp. 208-209.

Koster van Groos, A. F., 1975. The effect of high CO_2 pressures on alkalic rocks and its bearing on the formation of alkalic ultrabasic rocks and the associated carbonatites. *American Journal of Science* **275**, 163-185.

Koster van Groos, A. F. & Wyllie, P. J., 1966. Liquid immiscibility in the system Na_2O-Al_2O_3-SiO_2-CO_2 at pressures to 1 kilobar. *American Journal of Science* **264**, 234-255.

Koster van Groos, A. F. & Wyllie, P. J., 1968. Liquid immiscibility in the join $NaAlSi_3O_8$-Na_2CO_3-H_2O and its bearing on the genesis of carbonatites. *American Journal of Science* **266**, 932-967.

Koster van Groos, A. F. & Wyllie, P. J., 1973. Liquid immiscibility in the join $NaAlSi_3O_8$-$CaAl_2Si_2O_8$-Na_2CO_3-H_2O. *American Journal of Science* **273**, 465-487.

Le Bas, M. J., 1977. *Carbonatite-nephelinite volcanism*. London: John Wiley.

Le Bas, M. J., 1989. Diversification of carbonatite. In: Bell, K. (ed.) *Carbonatites: Genesis and Evolution*. London: Unwin Hyman, pp. 428-447.

Lee, W.-J. & Wyllie, P. J., 1992a. New data on CO_2-rich immiscible liquids in Na_2O-CaO-Al_2O_3-SiO_2-CO_2 from 25 to 1 kb: Carbonatite genesis. *EOS* **73**, 349-350.

Lee, W.-J. & Wyllie, P. J., 1992b. Liquid immiscibility between silicates and carbonates must intersect suitable liquidus field boundaries to have petrogenetic significance, Abstracts. *29th International Geological Congress, Kyoto*, 571.

Lee, W.-J. & Wyllie, P. J. 1992c. Silicate-carbonate liquid miscibility gaps, and liquidus field boundaries: Carbonatites by immiscibility or fractionation. *EOS* **73**, 606.

Lee, W.-J & Wyllie, P. J., 1994a. Conditions for formation of immiscible carbonate-rich magmas from primitive (magnesian) nephelinite. *Geological Society of America, Abstracts with Programs* **26**, A224.

Lee, W.-J. & Wyllie, P. J., 1994b. Experimental data bearing on liquid immiscibility, crystal fractionation, and the origin of calciocarbonatites and natrocarbonatites. *International Geology Review* **36**, 797-819.

Lee, W.-J., Wyllie, P. J. & Rossman, G. R., 1994. CO_2-rich glass, round calcite crystals and no liquid immiscibility in the system CaO-SiO_2-CO_2 at 2.5 GPa. *American Mineralogist* **79**, 1135-1144.

Maaloe, S. & Wyllie, P. J., 1975. The join grossularite-calcite through the system CaO-Al_2O_3-SiO_2-CO_2 at 30 kilobars: Crystallization range of silicates and carbonates on the liquidus. *Earth and Planetary Science Letters* **28**, 205-208.

Macdonald, R, Kjarsgaard, B. A., Skilling, I. P., Davies, G. R., Hamilton, D. L. & Black, S., 1993. Liquid immiscibility between trachyte and carbonate in ash flow tuffs from Kenya. *Contributions to Mineralogy and Petrology* **114**, 276-287.

McInnes, W. I. A. & Cameron, E. M., 1994. Carbonated, alkaline hybridizing melts from a sub-arc environment: Mantle wedge samples from the Tabar-Lihir-Tanga-Feni arc, Papua New Guinea. *Earth and Planetary Science Letters* **122**, 125-141.

McInnes, B. I. A. & Wyllie, P. J., 1992. Scapolite formation and the production of nephelinitic melts during the subduction of carbonated basalt (abstract). *EOS* **73**, 637.

Meen, J. K., Ayers, J. C. & Fregeau, E. J., 1989. A model of mantle metasomatism by carbonated alkaline melts: Trace element and isotopic compositions of mantle source regions of carbonatite and other continental igneous rocks. In: Bell, K. (ed.) *Carbonatites: Genesis and Evolution*. London: Unwin Hyman, pp. 464-499.

Menzies, M. A. & Chazot, G., 1994. Mantle metasomatism-the transfer of silicate and non-silicate melts in the earth's mantle. *International symposium on the physics and chemistry of the upper mantle, Sao Paulo, Brazil*, pp. 117-136.

Menzies, M. A. & Hawkesworth, C. J. (eds) 1987. *Mantle metasomatism*. London: Academic Press.

Nichols, G. T., Wyllie, P. J. & Stern, C. R., 1994. Subduction zone melting of pelagic sediments constrained by melting experiments. *Nature* **371**, 785-788.

Otto, J. W. & Wyllie, P. J., 1993. Relationships between silicate melts and carbonate-precipitating melts in CaO-MgO-SiO_2-CO_2-H_2O at 2 kbar. *Mineralogy and Petrology* **48**, 343-365.

Peacock, S. M, Rushmer, T. & Thompson, A. B., 1994. Partial melting of subducting oceanic crust. *Earth and Planetary Science Letters* **121**, 227-244.

Pecora, W. T., 1956. Carbonatites: a review. *Bulletin of Geological Society of America* **67**, 1537-1556.

Pyle, J. M. & Haggerty, S. E., 1994. Silicate-carbonate liquid immiscibility in upper-mantle eclogites: Implications for natrosilicic and carbonatitic conjugate melts. *Geochimica et Cosmochimica Acta* **58**, 2997-3011.

Sweeney, R. J., Green, D. H. & Sie, S. H., 1992. Trace and minor element partitioning between garnet and amphibole and carbonatitic melt. *Earth and Planetary Science Letters* **113**, 1-14.

Sweeney, R. J., Falloon, T. J. & Green, D. H., 1995. Experimental constraints on the possible mantle origin of natrocarbonatite. In Bell, K. & Keller, J. (eds.) *Carbonatite Volcanism: Oldoinyo Lengai and the Petrogenesis of Natrocarbonatites. IAVCEI Proceedings in Volcanology* **4**, Berlin: Springer-Verlag, pp. 191-207.

Smith, W. C., 1956. A review of some problems of African carbonatites. *Quarterly Journal of the Geological Society of London* **112**, 189-220.

Treiman, A. H. & Essene, E. J, 1983. Mantle eclogite and carbonate as sources of sodic carbonatites and alkalic magmas. *Nature* **302**, 700-703

Treiman, A. H. & Essene, E. J., 1985. The Oka carbonatite complex, Quebec: Geology and evidence for silicate-carbonate liquid immiscibility. *American Mineralogist* **70**, 1101-1113.

Tuttle, O. F. & Gittins, J., 1966. *Carbonatites*. New York: Interscience.

Verwoerd, W. J., 1978. Liquid immiscibility and the carbonatite-ijolite relationship: Preliminary data on the join $NaFe^{3+}Si_2O_6$-$CaCO_3$ and related compositions. *Carnegie Institution of Washington Yearbook* **77**, 767-774.

Von Eckermann, H., 1948. The alkaline district of Alno Island. *Sveriges Geologiska Undersokning, Serie Ca,* **36**, 176.

Watkinson, D. H. & Wyllie, P. J., 1969. Phase equilibrium studies bearing on the limestone-assimilation hypothesis. *Bulletin of Geological Society of America* **80**, 1565-1576.

Watkinson, D. H. & Wyllie, P. J., 1971. Experimental study of the join $NaAlSiO_4$-$CaCO_3$-H_2O and the genesis of alkalic rock-carbonatite complexes. *Journal of Petrology* **12**, 357-378.

Wendlandt, R. F. & Harrison, W. J., 1979. Rare earth partitioning between immiscible carbonate and silicate liquids and CO_2 vapor: Results and implications for the formation of light rare earth-enriched rocks. *Contributions to Mineralogy and Petrology* **69**, 409-419.

Woolley, A. R. & Kempe, D. R. C., 1989. Carbonatites: Nomenclature, average chemical compositions, and element distribution. In: Bell, K. (ed.) *Carbonatites: Genesis and Evolution*. London: Unwin Hyman, pp. 1-14.

Wyllie, P. J., 1965. Melting relationships in the system CaO-MgO-CO_2-H_2O with petrological applications. *Journal of Petrology* **6**, 101-123.

Wyllie, P. J., 1966. Experimental studies of carbonatite problems: the origin and differentiation of carbonatite magmas. In: Tuttle, O. F. & Gittins, J. (eds.) *Carbonatites*. New York: John Wiley, pp. 311-352.

Wyllie, P. J., 1978. Mantle fluid compositions buffered in peridotite-CO_2-H_2O by carbonates, amphibole, and phlogopite. *Journal of Geology* **86**, 687-713.

Wyllie, P. J., 1989. Origin of carbonatites: Evidence from phase equilibrium studies. In: Bell, K. (ed.) *Carbonatites: Genesis and Evolution*. London: Unwin Hyman, pp. 500-545.

Wyllie, P. J. & Huang, W.-L, 1975. Peridotite, kimberlite, and carbonatite explained in the system CaO-MgO-SiO_2-CO_2. *Geology* **3**, 621-624.

Wyllie, P. J. & Huang, W.-L., 1976. Carbonation and melting reactions in the system CaO-MgO-SiO_2-CO_2 at mantle pressures with geophysical and petrological applications. *Contributions to Mineralogy and Petrology* **54**, 79-107.

Wyllie, P. J. & Tuttle, O. F., 1960. The system CaO-CO_2-H_2O and the origin of carbonatites. *Journal of Petrology* **1**, 1-46.

Wyllie, P. J., Huang, W.-L., Otto, J. & Byrnes, A. P., 1983. Carbonation of peridotites and decarbonation of siliceous dolomites represented in the system CaO-MgO-SiO_2-CO_2 to 30 kbar. *Tectonophysics* **100**, 359-388.

Yaxley, G. M. & Green, D. H., 1994. Experimental demonstration of refractory carbonate-bearing eclogite and siliceous melt in the subduction regime. *Earth and Planetary Science Letters* **128**, 313-325.

CHAPTER 4

LIQUID IMMISCIBILITY IN THE JOIN $NaAlSiO_4$-$NaAlSi_3O_8$-$CaCO_3$ AT 1 GPa WITH APPLICATIONS TO THE FORMATION OF CRUSTAL CARBONATITES

ABSTRACT

Recent field and experimental studies on the Oldoinyo Lengai volcanism have provided evidence supporting the origin of natrocarbonatites by silicate-carbonate liquid immiscibility. This magma unmixing process has also been strongly advocated to explain the formation of calciocarbonatites. The melting relationships in the join $NaAlSiO_4$-$NaAlSi_3O_8$-$CaCO_3$ (Ne-Ab-CC) at 1.0 GPa demonstrate the existence of a large miscibility gap between 10 and 70 wt% $CaCO_3$ of the join. The silicate-rich and carbonate-rich boundaries of the miscibility gap intersect the nepheline and melilite liquidi, respectively, with the latter separating the miscibility gap from the calcite liqiudus field. The liquidus field boundaries defining the miscibility gap, and the silicate and carbonate liquidus surfaces, along with the possible cooling directions on the boundaries are constructed in the CO_2-saturated, pseudo-ternary system (SiO_2 + Al_2O_3)-CaO-Na_2O, based on the measured two-liquid compositions and the phase fields intersected by the join Ne-Ab-CC. These features are compared with the phase diagram on the same projection near the join Ab-CC at 1 GPa to deduce the compositional effect on the positions of the field boundaries, the minerals involved, and possible crystallization paths for carbonated silicate liquids. In this model system, silicate-CO_2 liquids with high Al/Si (near Ne-CC) would follow paths to the miscibility gap to exsolve calcite-rich to alkalic carbonatite liquids, while precipitating silicate minerals (melilite, anorthite, nepheline). With decreasing Al/Si of the system toward Ab-CC, albite and wollastonite start to crystallize, calcite liquidus field is intersected by the miscibility gap, and the range of immiscible carbonate-rich liquids derived from silicate liquids becomes somewhat limited to more alkalic compositions. A cooling silicate-CO_2 liquid thus may either reach the miscibility gap, or the silicate-calcite liquidus field boundary, depending on the initial liquid composition and its cooling path. Carbonate-rich liquids, as separated from their silicate parents, would first precipitate only silicates through a temperature interval, then reach the

liquidus field boundary to crystallize both silicate and carbonate minerals at lower temperatures. Natrocarbonatite magmas may be produced directly by liquid immiscibility, whereas a majority of sovites may represent crystal cumulates from immiscible, $CaCO_3$-rich carbonatite liquids.

INTRODUCTION

The world's only active carbonatite volcano at Oldoinyo Lengai has been one of the central interests in carbonatite petrology since the extrusions of high-alkali carbonate lavas in 1960 (see a review in Dawson, 1989). Some of the recent advances on field, geochemical and experimental studies of the natrocarbonatite volcanism are compiled in Bell and Keller (1995), with the most recent activities to 1993 also reported by Dawson et al. (1994, 1996) and Church and Jones (1995). These studies revealed the complexities of magmatic evolution even within a single carbonatite-nephelinite eruptive center (Bell and Keller, 1995).

The uniqueness of natrocarbonatites from Oldoinyo Lengai in contrast to the majority of calciocarbonatites has raised debates concerning the origin and evolution of carbonatites, particularly the relationships between the two types of magmas. Isotopic signatures of the natrocarbonatite lavas fall in the ranges for calciocarbonatites, and confirm that both share a common source in the mantle (see Bell and Keller, 1995), but it remains controversial whether one type of magmas or rocks could be derived from the other, and if so, by what processes. Some calciocarbonatite lavas revealed texture interpreted by several studies as the results of calcite pseudomorphs after nyerereite, i.e. secondary calcification from originally alkali carbonatites (Deans and Roberts, 1984; Dawson et al., 1987). However, Keller (1981, 1989) reported the occurrence of juvenile melt-droplets in the Kaiserstuhl carbonatites, and interpreted it to be consistent with primary nature of the calcitic carbonatite lavas. Bailey (1993) further summarized the available field evidence,

concluding that some effusive calciocarbonatite do preserve primary magmatic texture. While these studies focused on the recognition of primary calciocarbonatite lavas, it is worth noting that most calciocarbonatites are intrusive rocks (Woolley and Kempe, 1989).

Despite their unusual occurrence, natrocarbonatite magmas were proposed to be parental to all calciocarbonatites (which could subsequently evolve to magnesio- and ferrocarbonatites), with alkali loss through fluids as the possible mechanism linking the two compositional extremes (Le Bas, 1981). This view was challenged by Twyman and Gittins (1987) who indicated that progressive loss of water and alkalis would induce crystallization thus preventing the formation of a calcite-dolomite magma. They proposed that alkali-rich carbonatitic liquids could be derived from low alkalic, olivine sovitic liquids, a crystal fractionation scheme consistent with the phase relationships in K_2CO_3-Na_2CO_3-$CaCO_3$ (Cooper et al., 1975). Indeed the trace element data by Keller and Spettel (1995) indicate that the natrocarbonatite lavas are highly differentiated. This reflects that they were derived from other magmas, either a silicate parent or a carbonate-rich liquid, and either by liquid immiscibility or by crystal fractionation. Kogarko et al. (1991) analyzed the mineral inclusions in both early and late crystallized phases from a calciocarbonatite at polar Siberia, concluding that the magma became enriched in alkalis during cooling. Lee and Wyllie (1994) confirmed the generation of alkali-rich carbonatitic liquids from nepheline-normative liquids through crystal fractionation, under H_2O-saturated conditions. The integrated evidence in Bell and Keller (1995) led them to conclude that the Oldoinyo Lengai volcanism is exotic, having little bearing on the general origin of carbonatites. They also indicated that the available evidence favors the interpretation for the occurrence of natrocarbonatite lavas by liquid immiscibility (also see Church and Jones, 1995; Dawson et al., 1996).

Silicate-carbonate liquid immiscibility has been demonstrated experimentally in both synthetic systems (Koster van Groos and Wyllie, 1966, 1968, 1973; Voewoerd, 1978; Kjarsgaard and Hamilton, 1988, 1989; Brooker and Hamilton, 1990; Lee and

Wyllie, 1992a, b, 1996a) and natural systems (Koster van Groos, 1975; Freestone and Hamilton, 1980; Baker and Wyllie, 1990; Kjarsgaard and Peterson, 1991; Hamilton and Kjarsgaard, 1993; Kjarsgaard et al., 1995; Lee and Wyllie, 1996b). Element partitioning between silicate and carbonate-rich liquids was studied by Wendlandt and Harrison (1979), Hamilton et al. (1989) and Jones et al. (1994). Many of the previous studies were summarized elsewhere (e.g. Lee and Wyllie, 1996a), and are not repeated here. Several examples of the experimentally determined liquid miscibility gaps are illustrated in Fig. 1, projected on the CO_2-saturated, compositional triangle (SiO_2 + Al_2O_3 + TiO_2)-(CaO + MgO + FeO)-(Na_2O + K_2O) (the triangle revised from Freestone and Hamilton, 1980). Curve A-A is a polythermal two-liquid miscibility gap in the synthetic system Na_2O-CaO-Al_2O_3-SiO_2-CO_2 at 2.5 GPa (Lee and Wyllie, 1996a), while B-B is a pair of two-liquid isotherms in the same system at 0.5 GPa and 1250°C, based on Kjarsgaard and Hamilton (in preparation). Curves C-C are based on the results from natural assemblages of Shombole Volcano, determined by Kjarsgaard and Peterson (1991). These curves illustrate the similarity in geometry of the miscibility gaps (notice they become narrower as they approach the alkali-free baseline), with the variations as a function of pressure, temperature and composition.

In this study, we present the phase relationships including liquid immiscibility at 1 GPa in the system Na_2O-CaO-Al_2O_3-SiO_2-CO_2 intersected by the join $NaAlSiO_4$-$NaAlSi_3O_8$-$CaCO_3$ (Ne-Ab-CC). The framework for showing the mineral and liquid compositions in the system is provided in Fig. 2. Figure 2a is a compositional tetrahedron SiO_2-Al_2O_3-CaO-Na_2O (+ CO_2), showing the relevant mineral phases and the studied join (triangle Ne-Ab-CC). In Fig. 2b, the Al_2O_3 and SiO_2 components are combined, and the tetrahedron in Fig. 2a is reduced to a triangle. More components can be added into the projections to show the results in complex systems, as in Fig. 1. We construct the pseudo-ternary and quaternary phase diagrams in these projections, and discuss the possible liquid paths leading to a variety of carbonatite compositions at crustal conditions.

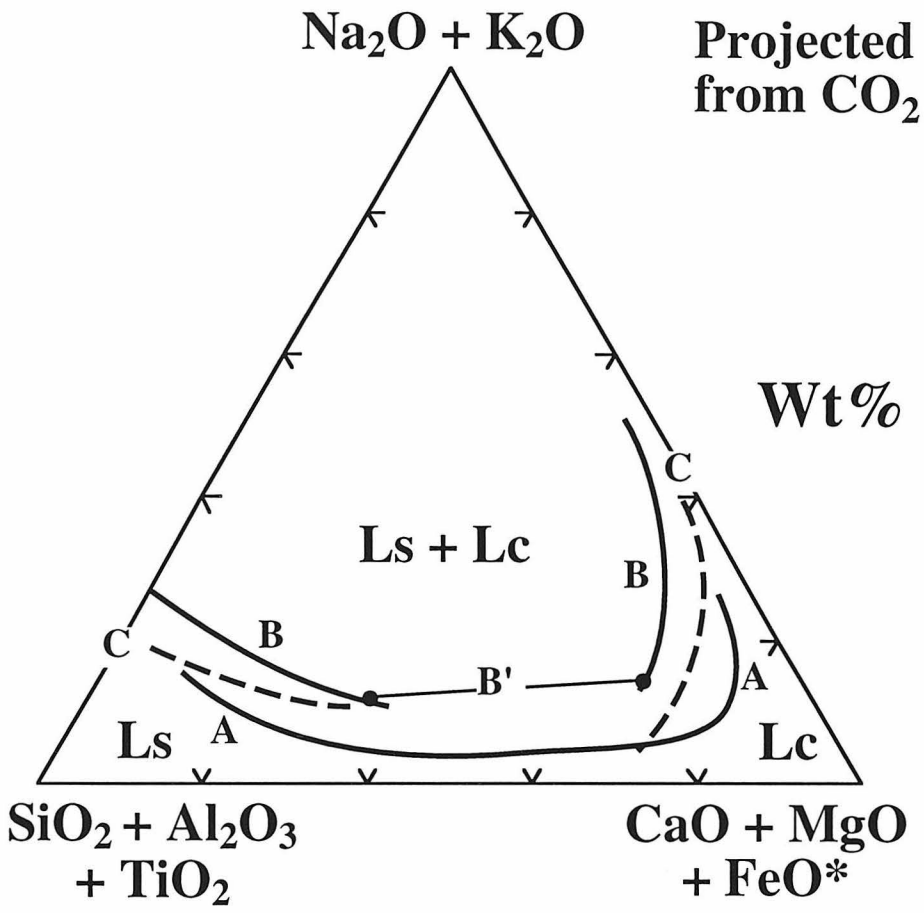

Figure 1. Examples of miscibility gaps in previous experimental studies. Curve A-A is an Mg-free miscibility gap field boundary at 2.5 GPa by Lee and Wyllie (1996a), and curves B-B show the two-liquid solvus revised from Kjarsgaard and Hamilton (1989) at 1250°C and 0.5 GPa in the same system (Kjarsgaard and Hamilton, in preparation), with a tie-line B' connecting the immiscible liquids. Curves C-C were determined using a nephelinite lava of Shombole by Kjarsgaard and Peterson (1991; 0.5 GPa and 975-925°C).

Figure 2. (a) Compositional tetrahedron Al_2O_3-SiO_2-CaO-Na_2O, projected from CO_2, showing silicate and carbonate phases relevant to the system Na_2O-CaO-Al_2O_3-SiO_2-CO_2. The solid circles denote the compositions of these phases, with abbreviations: Ab - albite, Ne - nepheline, An - anorthite, Gr - grossular, Wo - wollastonite, Scap - scapolite, Lar - larnite, Geh - gehlenite, Can - cancranite, CC - calcite, Nye - nyerereite, and NC - sodium carbonate. The open circles are the projections of the phases through Al_2O_3 to the basal triangle. The heavy triangle indicates the studied join Ne-Ab-CC. (b) Compositional triangle (Al_2O_3 + SiO_2)-CaO-Na_2O (+ CO_2), showing the same silicate and carbonate phases (solid circles). Our starting mixtures lie slightly below line Ne-CC, with 10 % Ab in the bulk silicate material.

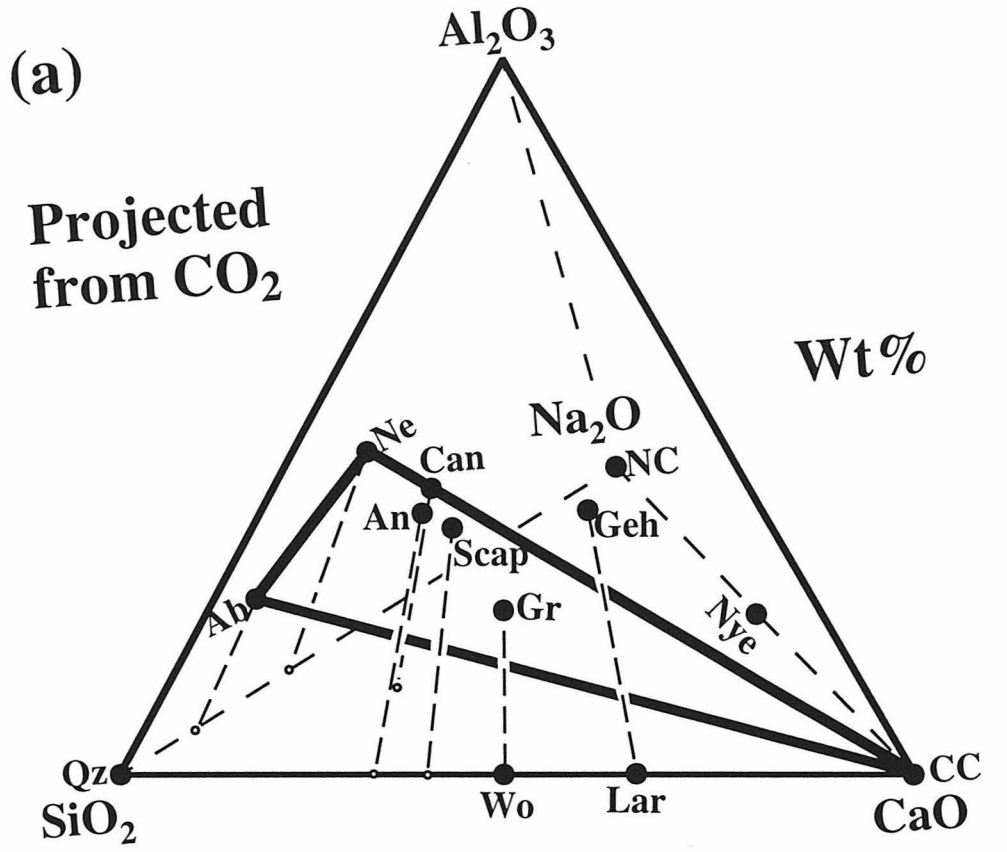
(a)
Projected from CO_2
Al_2O_3
Wt%
Na_2O
Ne
Can
NC
An
Geh
Scap
Ab
Gr
Nye
Qz
SiO_2
Wo
Lar
CC
CaO

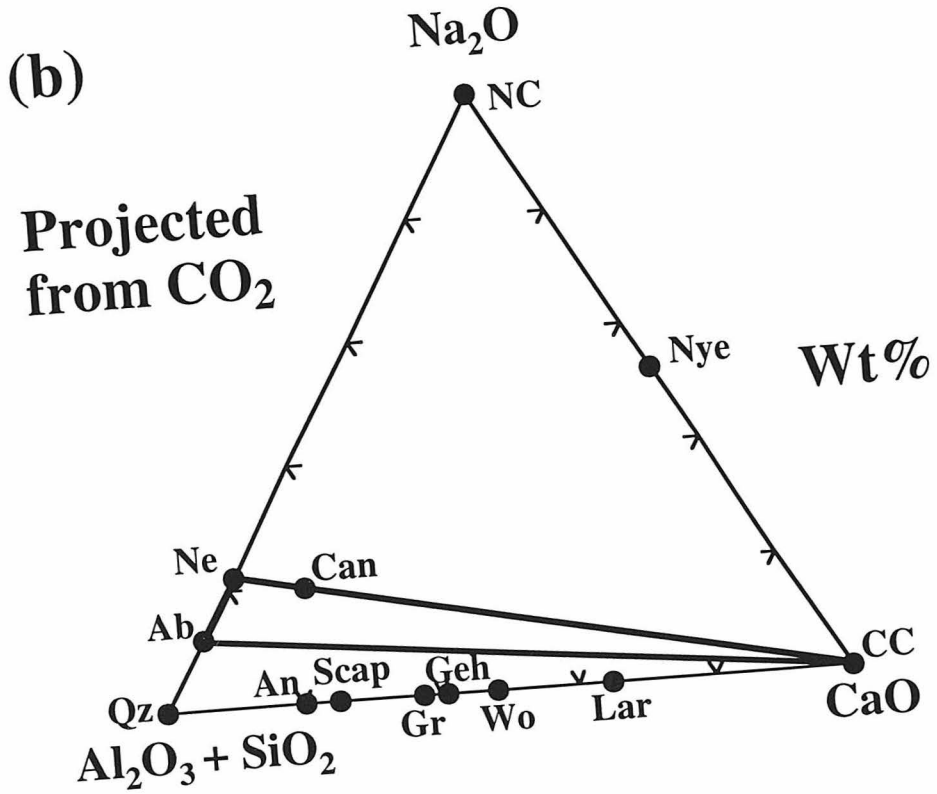
(b)
Projected from CO_2
Na_2O
NC
Nye
Wt%
Ne
Can
Ab
CC
An
Scap
Geh
Qz
Gr
Wo
Lar
CaO
$Al_2O_3 + SiO_2$

EXPERIMENTAL METHODS

The starting materials were: (1) primary standard grade $CaCO_3$ powders (Alfa Product), dried at 110°C for at least one day; (2) synthetic glass of 90 wt% $NaAlSiO_4$ and 10 wt% $NaAlSi_3O_8$ (prepared by Koster van Groos), dehydrated at 800°C for 4 hours; (3) starting mixtures ground with ethanol in an agate mortar for 1 hour. All starting mixtures (~5 mg for each run) were held for more than an hour in a vacuum drying oven at 110°C before being loaded into about 4 mm long platinum capsules.

Experiments were done in 1.27-cm diameter piston-cylinder apparatus, with calcium fluoride as a pressure medium. Temperature was controlled and monitored by $W_{95}Rh_5$-$W_{74}Rh_{26}$ thermocouple with no correction for the effects of pressure on the EMF. Run duration varied from 1 to 12 hours. Experiments were terminated by turning off the electrical power while the system remained near isobaric, and the quenching rate was about 100°C per second for the first 600°C. Pressure accuracy is about ±0.05 GPa, and temperature accuracy is estimated to be ±10°C. No pressure correction was made for the effects of friction.

Run products were mounted in a brass-holder with petropoxy, polished by Al_2O_3 powers and cleaned by compressed air, without using water, and then carbon-coated. Phases were identified by textures and morphology observed under the petrographic microscope and a Camscan scanning electron microscope (SEM) fitted with an energy dispersive x-ray system (EDS). Phases were analyzed by EDS using a beam current of 0.1 nA on brass.

EXPERIMENTAL RESULTS

The phases encountered include nepheline (Ne), calcite (CC), melilite (Mel), anorthite (An), scapolite (Scap), silicate-rich liquid (Ls), carbonate-rich liquid (Lc), and

vapor (V), with examples illustrated in Fig. 3. The experimental conditions and the interpreted phase assemblages are summarized in Table 1 and Fig. 4. Table 2 and Fig. 5 provide the selected chemical analyses for some immiscible silicate-carbonate liquid pairs in the experiments.

Identification of phases

Nepheline is present in a wide compositional range along the join (Table 1, Fig. 4). Both equilibrium and quenched nepheline appeared in our experiments. It is sometimes difficult to distinguish one occurrence from the other in a sample charge, but our interpretation of the nepheline-precipitating field in Fig. 4 is consistent with the overall phase relationships. Figure 3a illustrates an example of unambiguous primary nepheline from run 132, which formed large crystal prisms up to 50 x 20 μm^2 (the outlined crystals). There are some minute crystals (several μm across) near the large nepheline, although they are not discernible in the picture. Such small-sized, angular crystal form is used as the major criterion for identifying quench nepheline. Figure 3b shows another example of quench nepheline from run 123, where dark, irregular nepheline grains (~5 μm) are enclosed in silicate-rich glass (light color) surrounded by quenched carbonate-rich liquid (dendritic texture). The equilibrium nepheline crystals produced below 1200°C are generally small (~10 μm). Chemically, nepheline contains less than 1 wt% to about 6 wt% CaO, increasing towards calcite-rich side of the join. The nepheline compositions generally project onto the line between Ne and An in Fig. 2, suggesting that their CaO contents might have resulted from the solid solutions dominantly with anorthite. Bowen (1912) reported that at 1 atmosphere nepheline could dissolve as much as 35 wt% anorthite, with CaO equivalent to 7 %.

Melilite, scapolite and anorthite grew from some experiments in the calcite-rich portion of the join (Fig. 4, Table 1). The compositions of these phases are close to Geh,

Figure 3. Back-scattered electron photomicrographs showing the experimental phases (Table 1). (a) Equilibrium nepheline (the outlined crystals) set in glassy matrix, with interstitial quench nepheline not discernible in the image (run 132). (b) Quenched immiscible silicate-rich liquid with dark quench nepheline crystals, surrounded by quenched carbonate-rich liquid of dendritic texture (run 123). (c) Elongated anorthite (intermediate gray) set in quenched carbonate-rich liquid (run 149). Nepheline also occurred, but is not distinguishable in the picture with the dark quench nyerereite. (d) Scapolite (~30 μm, near rectangular crystals) enclosed in quenched carbonate-rich liquid (dendritic texture) and in the lower calcite layer (massive material; scapolite not discernible). Melilite appeared as the lightest-colored crystals (run 121). (e) Melilite laths (light color) with quenched carbonate-rich liquid (run 120). (f) Enlarged feature for quenched carbonate-rich liquid, including calcite dendrites (light, rounded material), interstitial nyerereite (dark) with silicate-rich lamellae (lightest; run 119).

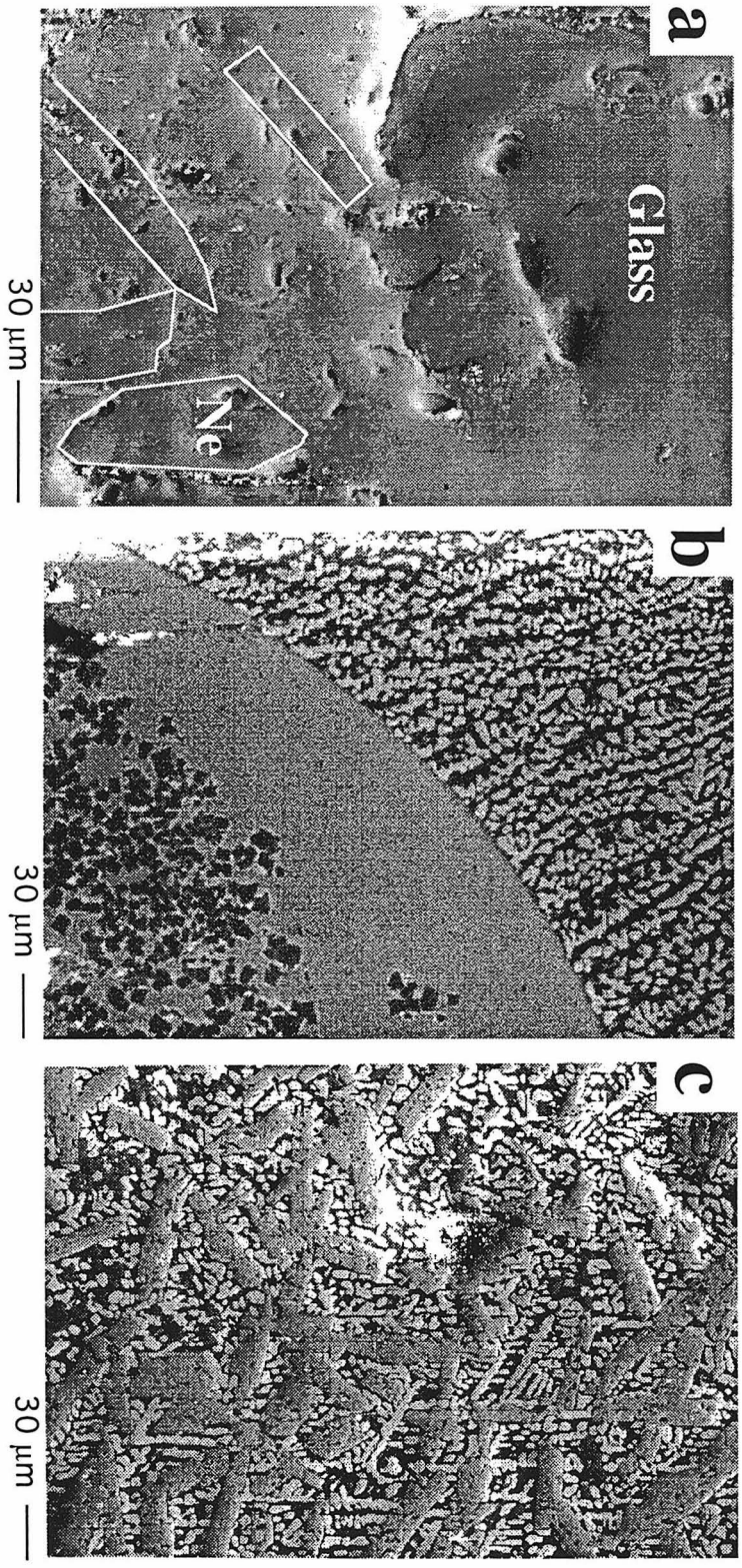
a
Glass
Ne
30 μm
b
30 μm
c
30 μm

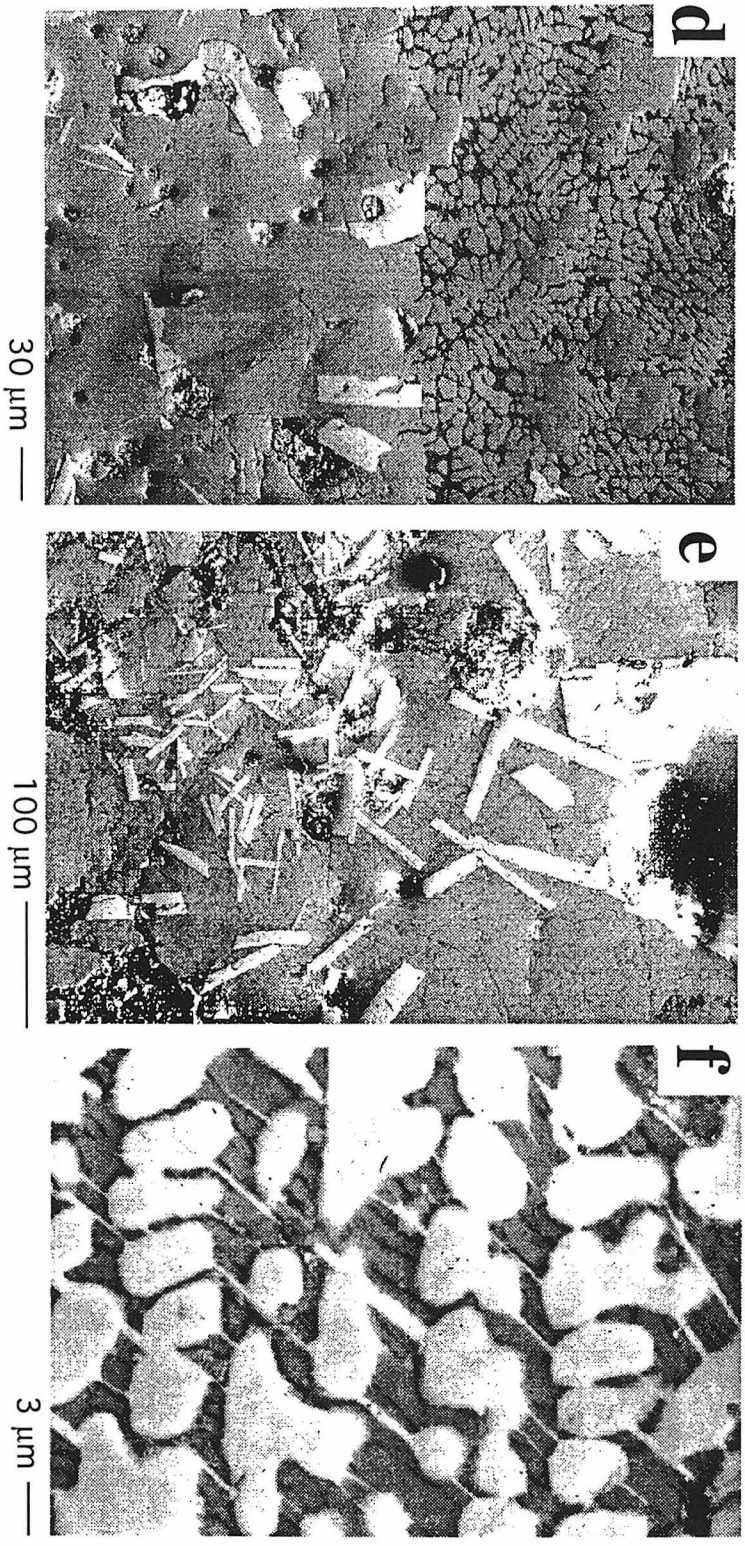
d
30 μm
e
100 μm
f
3 μm

Table 1. Experimental results for the join $NaAlSiO_4$-$NaAlSi_3O_8$-$CaCO_3$.

Run	Starting Mixture (wt%) Silicate	$CaCO_3$	Press. GPa	Temp. °C	Time hr	Interpreted phase assemblage
120	20	80	1.0	1300	2	Mel + Lc + V
121	20	80	1.0	1250	4	Scap + Mel + CC + Lc + V
122	20	80	1.0	1200	4	Ne + An + Mel + CC + Lc + V
117	40	60	1.0	1300	1.5	Ls + Lc + V
119	40	60	1.0	1250	2	An + Mel + Ls + Lc + V
149	40	60	1.0	1200	4	Ne + An + Lc + V
118	40	60	1.0	1150	4	Ne + An + CC + Lc + V
123	60	40	1.0	1250	2	Ls + Lc + V
148	60	40	1.0	1150	4	Ne + An + CC + Lc + V
130	70	30	1.0	1350	2.5	Ls + Lc + V
127	70	30	1.0	1300	2	Ls + Lc + V
128	80	20	1.0	1400	1	Ls + V
129	80	20	1.0	1350	2	Ls + Lc + V
145	80	20	1.0	1300	2	Ls + Lc + V
150	80	20	1.0	1250	4	Ne + Ls + Lc + V
131	90	10	1.0	1400	1	Ls + V
132	90	10	1.0	1350	2	Ne + Ls + V
144	90	10	1.0	1300	12	Ne + Ls + Lc + V
147	90	10	1.0	1300	6	Ne + Ls + Lc + V
146	90	10	1.0	1250	6	Ne + Ls + Lc + V

Starting silicate glass: 90 wt% $NaAlSiO_4$ + 10 wt% $NaAlSi_3O_8$. Phase abbreviations: Ne - nepheline, An - anorthite, Mel - melilite, Scap - scapolite, CC - calcite, Ls - silicate-rich liquid, Lc - carbonate-rich liquid, V - vapor.

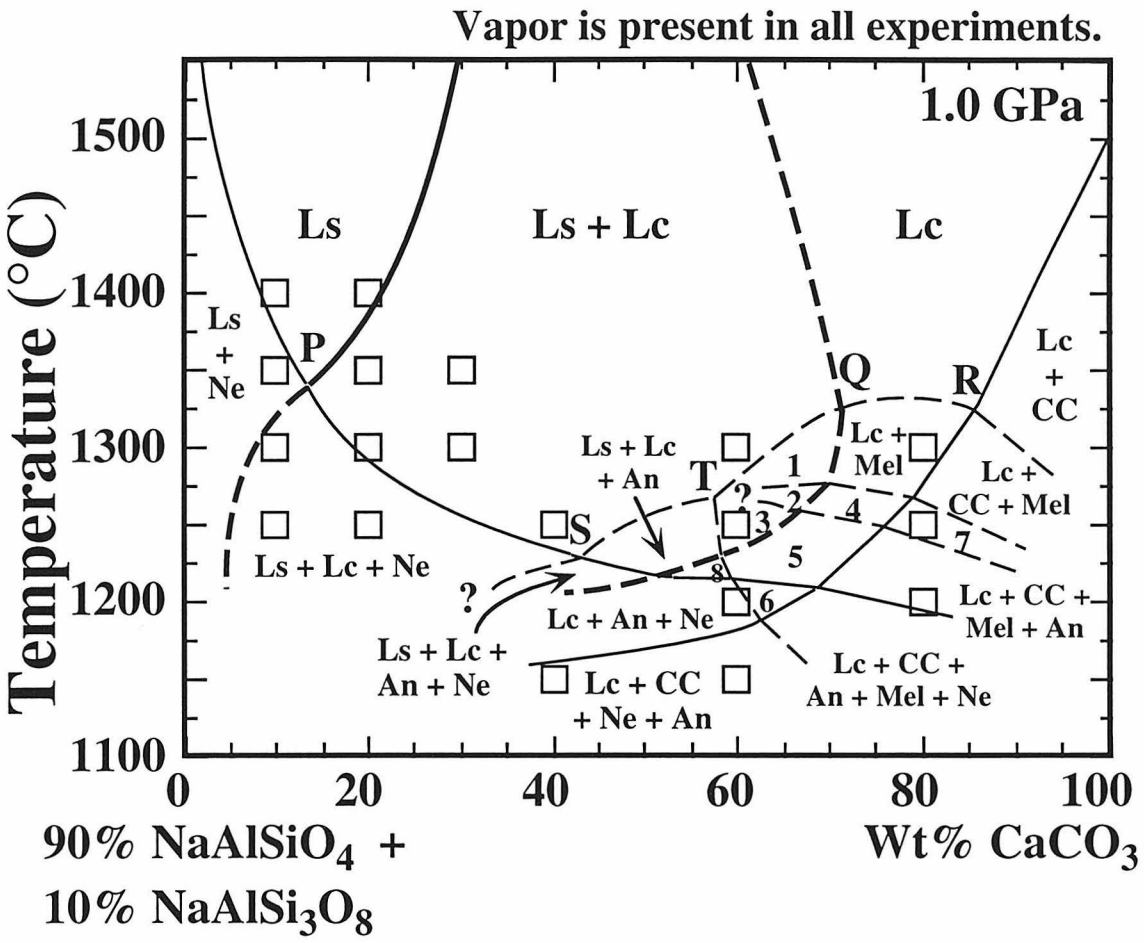

Figure 4. Phase fields intersected by the join Ne90Ab10-CC at 1.0 GPa. Abbreviation: Ls - silicate-rich liquid, Lc - carbonate-rich liquid, Ne - nepheline, CC - calcite, Mel - melilite, An - anorthite, Scap - scapolite. See text for the description of piercing points P, Q, R, T and S.

Scap, and An, respectively, in Fig. 2. Melilite commonly formed large prismatic crystals (lightest crystals, Figs. 3d and e) with size up to 100 x 30 μm^2, and contained a few percent of Na_2O, possibly representing a solid solution between soda melilite and gehlenite. Scapolite was produced only in run 121, often with inclusions of carbonate-rich melt (rectangular crystals to 30 μm in the layer of quenched carbonate-rich liquid, Fig. 3d). Anorthite formed elongated crystals (to 30 μm in length) within carbonate-rich liquids, or intergrown with nepheline, calcite or melilite (Figs. 3c and d).

Calcite present in the join Ne-Ab-CC always formed a distinct layer at the lower portion of a charge, as shown in Fig. 3d, and commonly intergrew with nepheline, melilite or anorthite. In the layers, some hexagonal forms of calcite crystals can be readily seen. In contrast, calcite crystals in many silicate-carbonate systems are rounded, and sometimes suspended in liquids (cf. Huang et al., 1980; Lee et al., 1994). Quenched calcite (~several μm) was produced in carbonate-rich liquids, and usually associated with quenched nyerereite (Figs. 3b-f).

Liquid was produced in all experiments (Fig. 4, Table 1), and was quenched to a variety of textures, depending on the composition of a liquid and temperature before quenching. Silicate-rich liquids at high temperatures usually quenched to a glass, but at lower temperatures to produce a glass with quenched nepheline (Fig. 3b). Quenching of carbonate-rich liquids always formed crystal aggregates, producing calcite dendrites with nyerereite and some thin lamellae of residual silicate-rich material (Fig. 3f).

The presence of vapor is evident by the appearance of pore space on the top portion of a capsule, and bubbles trapped in quenched liquids. It is difficult, however, to determine whether or not it occurred in some lower temperature experiments (e.g., runs 148 and 118 at 1150°C), due to the complex quenching textures. We believe that vapor is present at these run conditions as well.

Intersected phase fields

Figure 4 illustrates the phase fields intersected by the join Ne-Ab-CC at 1 GPa, with the experimental conditions indicated by the open squares, and listed in Table 1. The solid-lined phase field boundaries are well-constrained by our data, and it is more uncertain for the boundaries expressed by the dashed curves. As shown in the diagram, the phase relationships are rather complex at lower temperatures (< 1300°C) near calcite-rich portion of the join, involving the crystallization of melilite, anorthite, scapolite, calcite and nepheline, and the field boundaries are thus partly schematic on this part of the figure. Notice that vapor is present in all experiments, and the solidus is not determined.

There exists a large miscibility gap between silicate-rich and carbonate-rich liquids, as shown in Fig. 4 (heavy solid and dashed curves). The silicate-rich liquid limb (solid curve) is well-bracketed near the piercing point P (the intersection of the miscibility gap and the nepheline liquidus), with a somewhat arbitrary slope above 1400°C showing increasing calcite solubility in the immiscible silicate-rich liquids at higher temperatures. The carbonate-rich liquid boundary is largely schematic (dashed), bounded at 70 ± 10 % CC in the join, based on the experiments with the mixtures of 60 and 80 % CC (Fig. 4, Table 1), and on internal consistency with the phase diagrams to be presented later. Above the piercing point Q (the intersection of the miscibility gap and the melilite liquidus), the curve extends to high temperatures with a negative slope implying increase of dissolved silicate components in carbonate-rich liquids. Below Q, immiscible liquids are joined by the precipitation of solid phases, and interpretation of the quenched products becomes more difficult. We conclude that immiscible silicate-rich liquid no longer appears at 1200°C from the mixture of 60 % CC (run 149, Table 1, Fig. 4). The carbonate-rich liquid boundary is thus drawn to swing towards the Ne-rich direction at lower temperatures, and between runs 119 and 149 (Table 1). Accurate determination of this boundary requires more detailed experimental work.

Neither the fusion temperature of nepheline nor the melting relationships of the join $NaAlSiO_4$-$NaAlSi_3O_8$ have been determined experimentally at 1 GPa. The hypothetical congruent melting temperature of 90 % $NaAlSiO_4$ + 10 % $NaAlSi_3O_8$ in Fig. 4 is estimated to about 1620°C, the 1 atmosphere temperature (Greig and Barth, 1938) plus 110°C for the pressure increase (assumed the same as for $NaAlSi_3O_8$ determined by Boyd and England, 1963). The curve extending from the melting temperature at the silicate end in Fig. 4 is the nepheline liquidus which drops precipitously as calcite is added to the system. The liquidus is intersected by the miscibility gap at 1330°C and 14 % CC (point P). At temperatures lower than P, the accurate position for the field boundary below which nepheline precipitates from immiscible liquids (i.e. between the fields Ls + Lc and Ls + Lc + Ne) is uncertain, due to the difficulty in determining whether or not the nepheline was an equilibrium phase, particularly in runs 123, 127 and 145 (Table 1, Fig. 4). These three experiments produced small angular nepheline enclosed by silicate glass (i.e. Fig. 3b)—we interpret the crystals as a quenched product based on the morphological consideration discussed previously, and locate the field boundary between runs 145 and 150, and below 123 (Table 1), as shown in Fig. 4.

The melilite liquidus is intersected by the miscibility gap and the calcite liquidus at the piercing points Q and R. The fields marked 2, 4, and 7 in Fig. 4 indicate a small temperature interval where scapolite may be stable. There are also phase fields for the precipitation of anorthite covering a wide compositional range of the join, below the scapolite stability fields. The scapolite-anorthite temperature relationship is consistent with the results of Goldsmith and Newton (1978), and we assume the field boundary between the two stability fields to be a simple carbonation/decarbonation relation. Notice that between the Lc limb of the miscibility gap (dashed heavy curve below Q) and the field boundaries for the precipitation of calcite (solid curve below R) are the fields where assemblages of silicate minerals can be crystallized from carbonate-rich liquids.

The melting temperature of calcite at 1 GPa is 1500°C (Irving and Wyllie, 1975), which provides an additional constraint on the calcite liquidus. The calcite-precipitating fields are first intersected by the melilite liquidus at 1325°C (point R), then joined by scapolite, anorthite, and finally nepheline at 1200°C and below. Contrary to the results in the join Ab-CC (Lee and Wyllie, 1992a, b, 1996a), the calcite liquidus here does not intersect the two-liquid field.

Two-liquid compositions

The compositions for selected seven pairs of immiscible liquids are presented in Figs. 5 and 6, and Table 2. Among the experiments, four produced a silicate glass without quenched nepheline, associated with a quenched carbonate-rich liquid (runs 117, 119, 129, and 130; Table 1, Fig. 4). Three individual measurements for each liquid are provided in Fig. 5a, and the various symbols represent the results from the different runs. The analyses for the silicate glasses are rather uniform, as indicated in Fig. 5a near Ls. Silicate-rich liquids in the other two-liquid experiments (runs 123, 127, and 145; Table 1, Fig. 4) quenched to a silicate glass + quenched nepheline, and the results are plotted in Fig. 5b. The bottom projection illustrates the data for run 123. The open diamonds near Ne are the representative composition for quenched nepheline crystals. The open triangles are for the glassy portion of the sample charge. The actual liquid composition should therefore lie between the open diamonds and the squares. We analyzed two larger areas (> 1,000 μm^2) including both glass and nepheline for the silicate liquid, indicated by the solid diamonds in the projection. The data are now restricted to a relatively small range between glass and nepheline compositions. The silicate liquid compositions from runs 127 and 145 were similarly obtained, and are plotted in Fig. 5b.

Carbonate-rich liquids commonly quenched to calcite dendrites with nyerereite and minor amounts of residual silicate-rich material (Fig. 3f). The quench products show large

Table 2. Average compositions of immiscible liquids on a CO_2-free basis (weight percent)

Run	129		130		117		119	
Phase	Ls	Lc	Ls	Lc	Ls	Lc	Ls	Lc
SiO_2	39.3	1.3	38.1	1.9	34.7	4.0	36.5	2.3
Al_2O_3	31.8	0.5	31.2	0.8	29.5	1.5	30.3	1.3
CaO	11.2	57.9	16.0	63.6	28.3	73.8	24.6	80.4
Na_2O	17.6	40.2	14.7	33.6	7.5	20.7	8.7	16.0

Run	145		127		123	
Phase	Ls	Lc	Ls	Lc	Ls	Lc
SiO_2	39.5	1.5	39.0	1.2	39.9	2.2
Al_2O_3	33.3	1.8	33.1	1.0	31.9	0.7
CaO	9.7	65.5	12.4	60.2	14.7	77.0
Na_2O	17.4	31.2	15.5	37.6	13.6	20.1

Figure 5. (a) Individual analyses for the immiscible liquids from runs 117, 119, 130 and 129. The open circles indicate the relevant starting mixtures (60 wt% CC for 117 and 119, 30 % for 130, and 20 % for 129). Silicate-rich liquids (near Ls) quenched to a uniform glass, whereas carbonate-rich liquids (Lc) quenched to calcite dendrites with nyerereite, showing large heterogeneity in composition (analyzed areas ~100 μm^2). Notice that small amounts of melilite and anorthite were also precipitated in run 119. (b) Measurements of the two-liquid compositions in runs 123, 127 and 145. Only one Lc analysis for run 145 is shown, covering ~1000 μm^2 analyzed area. Silicate-rich liquids quenched to glass (open triangles) with nepheline (open diamonds). Analyses on large areas (~1000 μm^2) of quenched silicate liquids integrating both glassy portions and nepheline crystals are considered to represent the actual liquid compositions (solid diamonds).

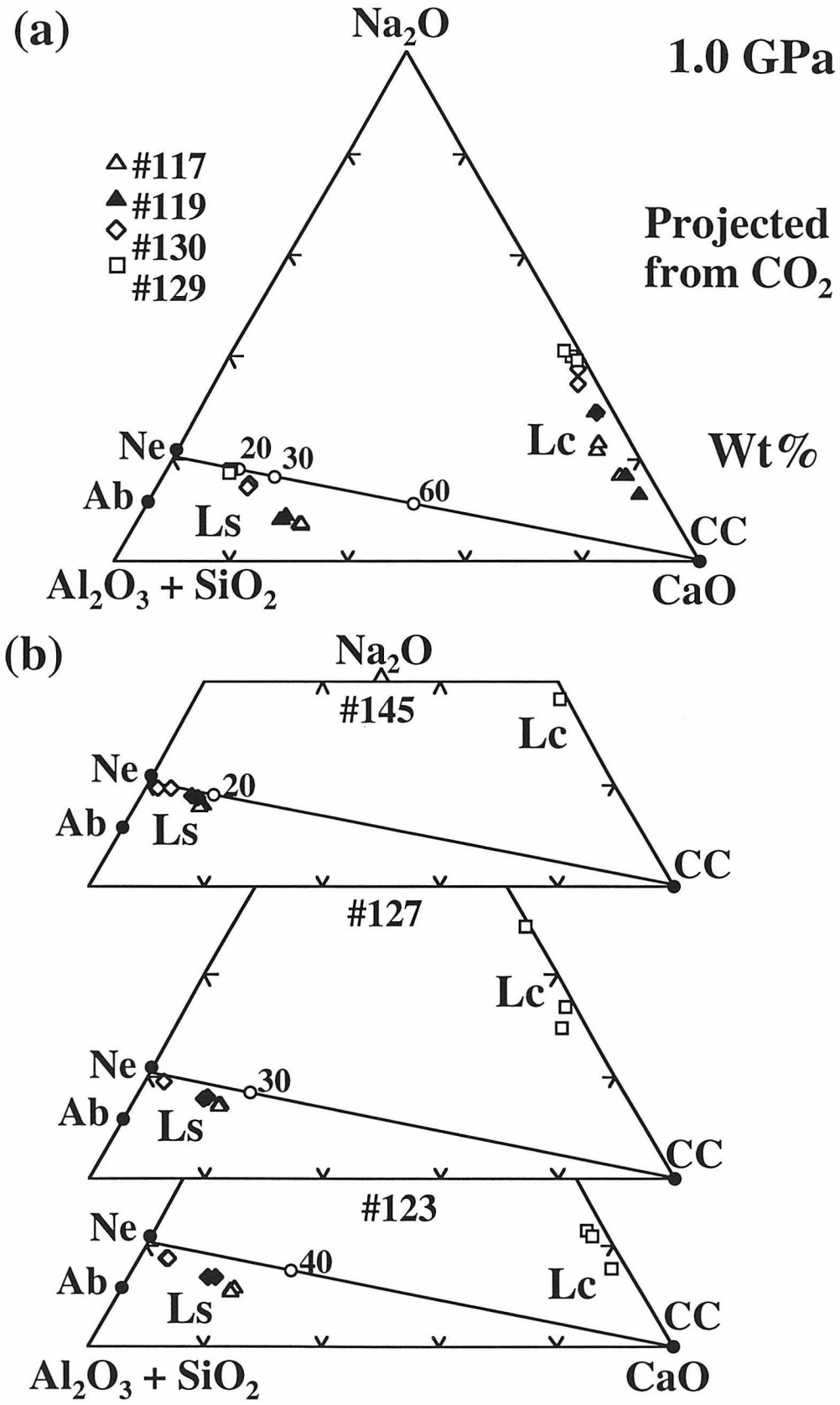
(a)
Na_2O
1.0 GPa
#117
#119
#130
#129
Projected from CO_2
Ne
20
30
60
Lc
Wt%
Ab
Ls
CC
$Al_2O_3 + SiO_2$
CaO
(b)
Na_2O
#145
Lc
Ne
20
Ab
Ls
CC
#127
Lc
Ne
30
Ab
Ls
CC
#123
Ne
40
Ab
Lc
Ls
CC
$Al_2O_3 + SiO_2$
CaO

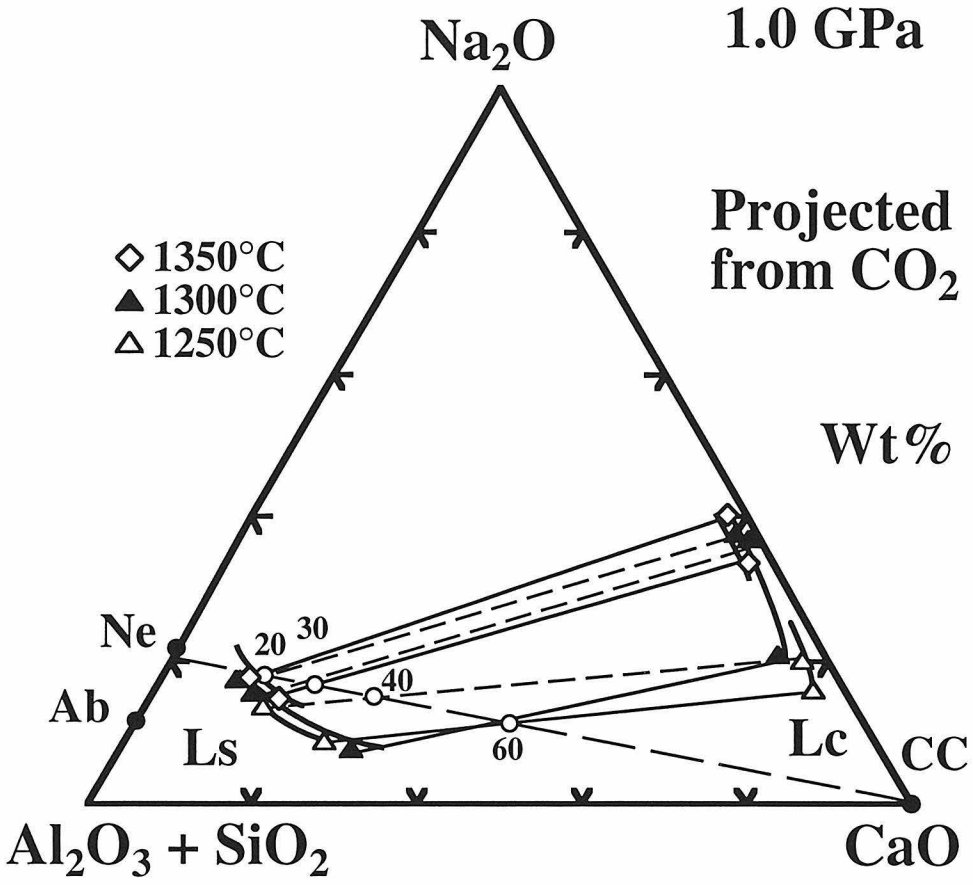

Figure 6. (a) Average two-liquid compositions shown in Fig. 5, including results at 1350°C (runs 130 and 129), 1300°C (117, 127 and 145), and 1250°C (119 and 123). The solid and dashed tie-lines represent the results from Figs. 5a and b, respectively. Three pairs of two-liquid isotherms are also drawn, with the lower temperature ones showing wider separation.

heterogeneity in calcite/nyerereite distribution. In order to obtain the most representative compositions for carbonate-rich liquids, areas up to 100 μm^2 were analyzed by the EDS method. However, the areas suitable for the rastering mode were still too small to compensate for the heterogeneity, and the compositional variations of carbonate-rich liquid analyses are illustrated in Fig. 5, with a trend generally subparallel to the CaO-Na_2O side of the projection.

The average liquid compositions from the seven experiments in Fig. 5 are projected in Fig. 6 with the tie-lines connecting the coexisting liquids (solid and dashed lines for the two-liquid pairs in Figs. 5a and b, respectively). The open diamonds, solid triangles and open triangles denote the liquids at 1350, 1300 and 1250°C, passed by the three pairs of two-liquid isotherms. Although all the tie-lines reasonably pass through the starting mixtures as we expect, we do not attempt to derive the orientation of the tie-lines as a function of silicate-rich liquid composition (e.g. Kjarsgaard and Peterson, 1991), due to large uncertainties on the analyses of liquid compositions (especially carbonate-rich liquids).

MISCIBILITY GAP AND LIQUIDUS FIELD BOUNDARIES IN THE SYSTEM Na_2O-CaO-Al_2O_3-SiO_2-CO_2

Using the data outlined above (Tables 1 and 2, Figs. 4 and 5), we are able to construct the miscibility gap field boundary, i.e., the intersection of the miscibility gap with the silicate and carbonate liquidus surfaces, in the projection of Fig. 7a. The figure reproduces the lower portion of the triangle (vertical exaggeration of 2) and the two-liquid data in Fig. 6, where the miscibility gap field boundary (the heavy curve) is constrained by the following key features. Points P and Q on the field boundary intersected by the join Ne-Ab-CC (the dashed line) correspond to the piercing points in Fig. 4 between the miscibility gap and the nepheline, and the melilite liquidi (the positions recalculated CO_2-

free). Three pairs of isotherms on the two-liquid surface are sketched: 1350, 1300 and 1250°C, with the lower-temperature isotherms wider than the higher ones. The two-liquid isotherm at 1350°C is above the temperatures of P and Q (Fig. 4), so it does not reach the field boundary between the two points, and intersects the join Ne-Ab-CC at the positions slightly inside the boundary in Fig. 7a. The 1300°C isotherm at silicate-rich side is terminated at one end by the nepheline liquidus surface (labeled *Ne*) before reaching the join, and at the other by the melilite liquidus field (*Mel*). Similarly at the carbonate-rich side, the isotherm is intersected by the two surfaces *Ne* and *Mel*. At 1250°C, the isotherm pair extends not far from either side of the silicate-rich and carbonate-rich liquids from run 123 (Tables 1 and 2, Fig. 4), and is bounded by nepheline and anorthite liquidus surfaces (*Ne* and *An*). The pseudo-invariants I_1 and I_1' on the miscibility gap field boundary for the 4-phase assemblage, Ls + Lc + Ne + An, occur slightly lower than 1250°C (corresponding to the bulk composition of point S, Fig. 4), and are thus located somewhat outside the 1250°C isotherms. Piercing point T in Fig. 4 for another 4-phase assemblage, Ls + Lc + An + Mel, is approximately bracketed by runs 117 and 119 (60 % CC at 1300 and 1250°C; Table 1), and its corresponding two-liquid compositions (pseudo-invariants I_2 and I_2' on the field boundary) are located between the two pairs of immiscible liquids from runs 117 and 119 (Fig. 7a). The positions of I_1-I_1' and I_2-I_2' are consistent with all the available data. Tie-lines L_1 and L_2 defined by these two-liquid pairs divide the field boundary into three parts: the two liquids with nepheline, anorthite, and melilite. Thus, the two-liquid surface is surrounded by the three silicate liquidus surfaces without contacting any carbonate-precipitating field. We have further estimated a temperature maximum K on the curve (near Q), and it also represents the critical point (consolute) where Ls = Lc. Figure 7b illustrates the complete miscibility gap field boundary along with the isotherms and the key features in Fig. 7a to correct scale.

Figure 7. (a) Lower portion of the compositional triangle (vertical exaggeration of 2; Fig. 6), showing the miscibility gap field boundary (heavy curve) through P, I_1, I_2, Q, K, I_2' and I_1', two-liquid isotherms at 1350, 1300 and 1250°C, and tie-lines L_1 and L_2 intersecting the join at S and T (see text). Italic letters *Ne*, *An* and *Mel* surrounding the field boundary indicate the liquidus fields for nepheline, anorthite and melilite. (b) Complete range of the field boundary to correct scale.

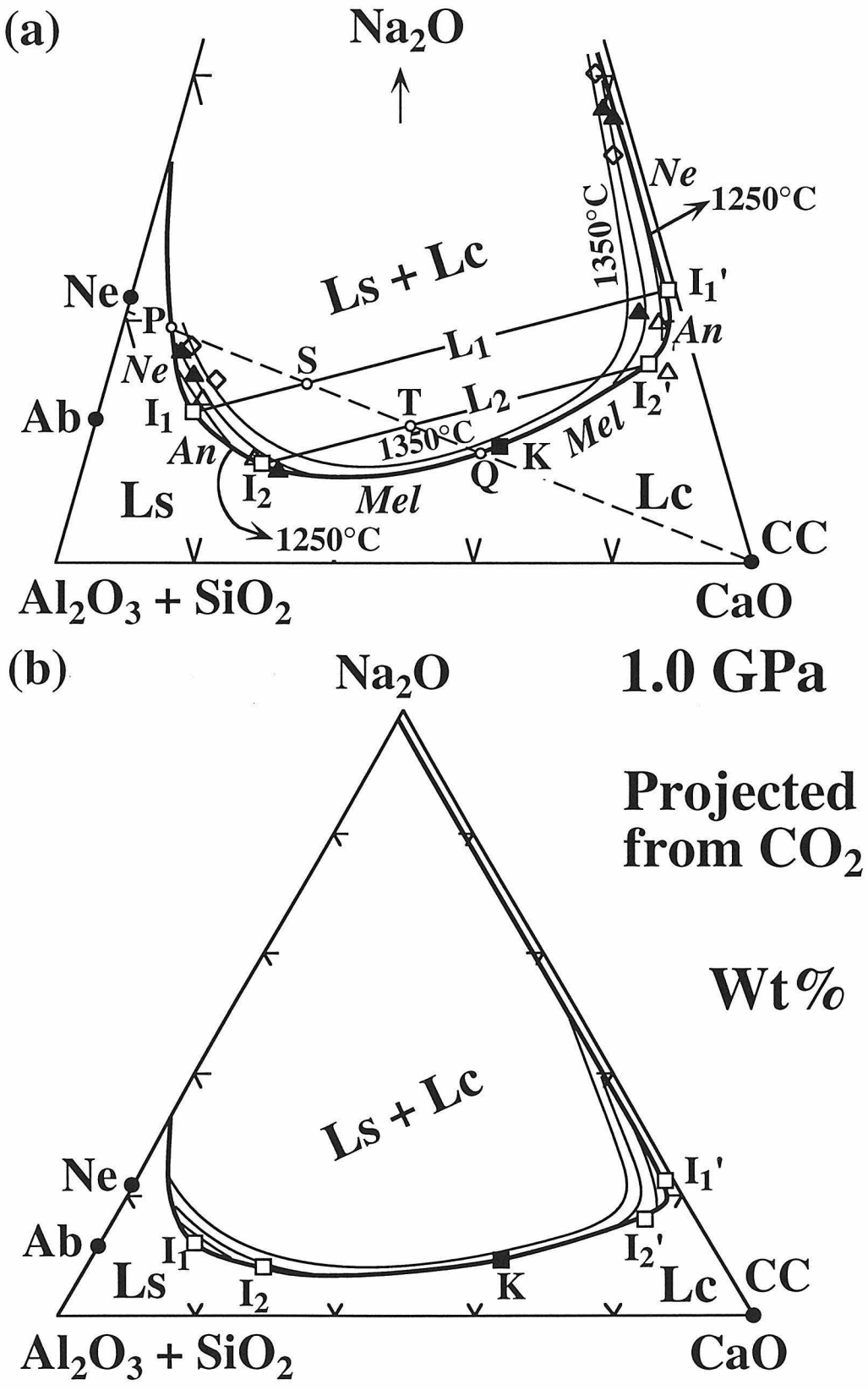
(a)
Na2O
Ne
P
Ne
Ab
I1
An
Ls
I2
Mel
1250°C
Ls + Lc
S
L1
T
L2
1350°C
Q
K
Mel
Lc
CC
Ne
1250°C
1350°C
I1'
An
I2'
Al2O3 + SiO2
CaO
(b)
Na2O
1.0 GPa
Projected
from CO2
Wt%
Ls + Lc
Ne
Ab
I1
Ls
I2
K
I1'
I2'
Lc
CC
Al2O3 + SiO2
CaO

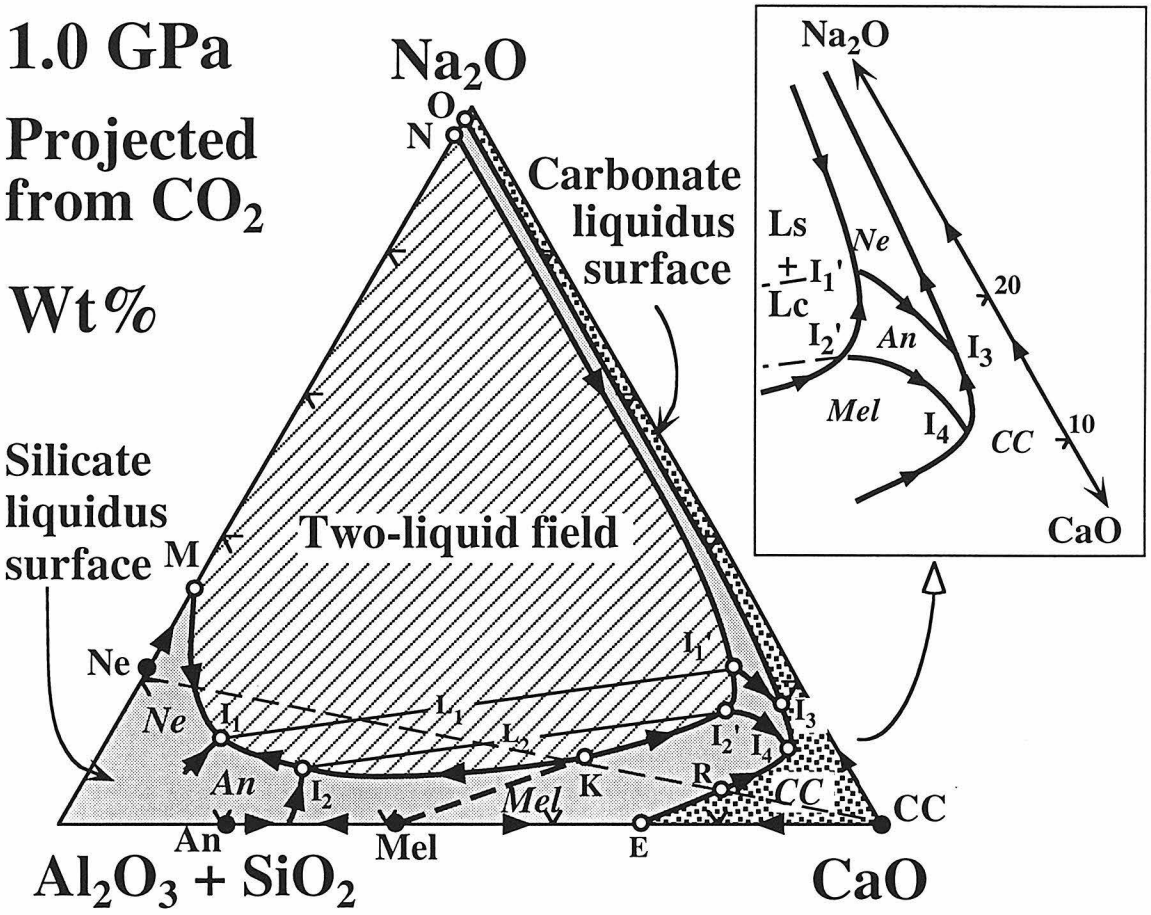

Figure 8. Completed liquidus field boundary diagram based on this study, showing the miscibility gap, the silicate and carbonate liquidus surfaces. The key boundaries, cooling directions and pseudo-invariants are also indicated. The details near the CaO corner of the projection are shown in the upper-right box.

Figure 8 illustrates the completed pseudo-ternary phase diagram, showing the three major features, the miscibility gap (straight-lined), the silicate liquidus surface (gray), and the carbonate liquidus surface (dotted); crystallization directions along the boundaries are also indicated by arrows. The miscibility gap field boundary is based on Fig. 7b, but the portion near the CaO-Na_2O side of the projection is slightly distorted to show some details in the region for carbonate-rich liquids Lc. Within the silicate liquidus surface, several curves are sketched for the field boundaries between *Ne* and *An*, and between *An* and *Mel*. Near the silicate-rich corner of the projection, the positions for the curves are largely schematic, starting at eutectics somewhere arbitrarily in the joins Ne-An and An-Mel, and terminating at the better-constrained compositions at I_1-I_1' and I_2-I_2'. In the carbonate-rich side of the projection, as shown in the enlarged diagram (upper-right), the two silicate-silicate field boundaries are defined between I_1' and I_3, and I_2' and I_4, where I_3 and I_4 are 4-phase pseudo-invariants (Lc + Ne + An + CC, and Lc + An + Mel + CC) close to the compositions of carbonate-rich liquids in runs 148 and 121 with similar phase assemblages (Table 1, Fig. 4). The critical point K is a temperature maximum between I_2 and I_2' of the miscibility gap field boundary, so the dashed-line K-Mel represents a thermal divide on the melilite liquidus surface.

The liquidus field boundary between silicates and carbonates starts from a postulated eutectic E between Mel and CC on the (Al_2O_3 + SiO_2)-CaO baseline, passes through the piercing point R along the join Ne-Ab-CC (Fig. 4), and reaches the 4-phase pseudo-invariant I_4; the boundary is then changed to between An and CC, and between Ne and CC after passing I_3. The field boundary is expected to extend into the narrow carbonate-rich liquid area outside the miscibility gap, and all the way to the (Al_2O_3 + SiO_2)-Na_2O side; the carbonate phases involved change from calcite to some alkali-rich carbonates (e.g. nyerereite, sodium carbonate).

The schematic liquidus diagram at 1 GPa based on the results of Ab-CC at 1-2.5 GPa is provided in Fig. 9, reproduced from Lee and Wyllie (1996a). The join Ab-CC does

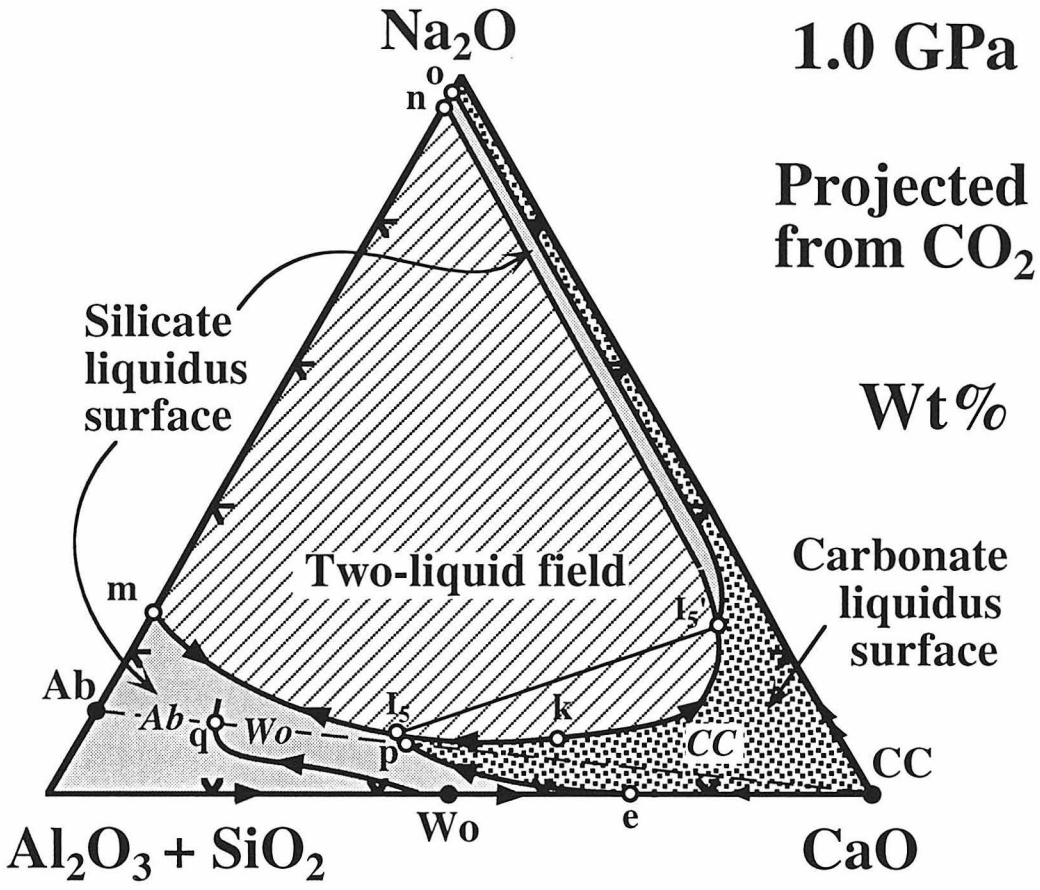

Figure 9. Liquidus field boundaries based on the results of Ab-CC, after Lee and Wyllie (1996a).

not intersect the two-liquid field at 1 GPa, but slices through the liquidus fields for calcite, wollastonite (Wo), and albite, with the liquidus piercing points along the join marked p and q. The miscibility gap field boundary is then estimated to between curves A-A and B-B in Fig. 1 without reaching the join. The silicate-carbonate field boundary is located between wollastonite and calcite, connecting the eutectic e of $CaSiO_3$-$CaCO_3$ (Huang and Wyllie, 1974), point p, and point I_5 (4-phase pseudo-invariant for Ls + Lc + Wo + CC) on the miscibility gap field boundary. Tie-line I_5-I_5' connects the immiscible liquid compositions coexisting with wollastonite and calcite. Starting from I_5' is another wollastonite-calcite field boundary, extending towards point o on the Ca-free side of the triangle while the boundary changes to involve other silicates and carbonates. There is also a temperature maximum/critical point k on the miscibility gap field boundary, between I_5 and I_5'.

Although the ranges and topology for the two miscibility gap field boundaries in Figs. 8 and 9 are similar, the minerals and the distribution of the silicate and carbonate liquidus surfaces vary significantly with Al/Si of the systems. The miscibility gap in Fig. 8 is completely surrounded by the silicate liquidus surfaces, whereas in Fig. 9 it intersects both silicate and carbonate liquidus fields. The effect of composition (Al/Si) can be depicted in Fig. 10, where Al_2O_3 is separated from SiO_2 to form a tetrahedron (Fig. 2a). Curves A and B in Fig. 10a are simply transferred from the miscibility gap field boundaries of Figs. 8 and 9 onto the $Ne_{90}Ab_{10}$-CC-NC and Ab-CC-NC planes in the tetrahedron. The ratios of Al to Si in the immiscible silicate-rich liquids for curve A (molecular Al/Si ~0.95; Table 2) indicate that this field boundary falls close to the plane $Ne_{90}Ab_{10}$-CC-NC (Al/Si = 0.9), so it is reasonable to assume curve B is also near plane Ab-CC-NC, although small deviations from the plane are expected. Thus, curves A and B in Fig. 10a represent the traces on the surface of the two-liquid volume sliced by the two silicate-carbonate planes. The possible range of this two-liquid volume can be extrapolated down to the Al-free basal triangle SiO_2-CaO-Na_2O (Qz-CC-NC), as denoted by curve C.

It is, however, difficult to extend further towards Al-rich region of the compositional space, so this part of the miscibility gap remains unknown.

The field boundary A in Fig. 10a terminates at M and N on the SiO_2-Al_2O_3-Na_2O triangle. The tie-line M-N defines the immiscible liquid pair on the Ca-free end-member system, whereas I_1-I_1' indicates a two-liquid tie-line more enriched in CaO. The tie-lines in between are expected to change directions corresponding to the change from M-N and I_1-I_1', consistent with the observations of Freestone and Hamilton (1980) and Kjarsgaard and Hamilton (1988, 1989). Kjarsgaard and Peterson (1991) compared the experimental two-liquid compositions from Shombole and Oldoinyo Lengai Lavas, suggesting that silicate-rich liquids of higher peralkalinity, (Na + K)/Al (molecular), exsolve carbonate-rich liquids higher in $Na_2CO_3/CaCO_3$. Triangle PA-Qz-CC in Fig. 10a with Na/Al = 1 separates the tetrahedron into two parts: below the plane for higher peralkaline compositions (e.g. section M-P on the miscibility gap field boundary A), and above for lower (section P-Q of curve A). The rotation of the tie-lines from M-N to I_1-I_1' indicates that silicate-rich liquids along M-P coexist with alkalic carbonate-rich liquids, whereas those on P-Q produce Ca-carbonate-rich liquids. This tendency agrees with the peralkalinity-carbonate composition relationship in Kjarsgaard and Peterson (1991). However, for curve C on the basal triangle where the silicate-rich liquids contain essentially no Al_2O_3 and the peralkalinity is definitely larger than that of the liquid M (with Ca-free, sodic carbonate-rich liquid N), the liquids are expected to exsolve a variety of Na/Ca carbonate-rich liquids. It appears that Na/Ca of silicate-rich liquids is another straight-forward indication for the compositions of the coexisting carbonate-rich liquids, when the comparison among silicate liquids of various Al/Si is necessary.

The changes in the phase relationships with changes in Al/Si are further shown in Fig. 10b. In the pseudo-quaternary system, each liquidus field is represented by a volume in space. The shaded area for the surface of the two-liquid volume is now drawn with the schematic 4-phase field boundaries for Ls and Lc + two minerals precipitated from them.

Figure 10. (a) CO_2-saturated, compositional tetrahedron (Fig. 2a), showing the miscibility gap field boundaries of Figs. 8 and 9 in space (curves A and B near the planes Ne-CC-NC and Ab-CC-NC). The miscibility gap field boundary C on the base of the tetrahedron is extrapolated from A and B. PA locates where peralkalinity equals 1 on the Al_2O_3-Na_2O axis. (b) Same projection as in (a), showing the surface of the miscibility gap volume (shaded area) with some 4-phase field boundaries for two liquids in equilibrium with two mineral phases. K- K' on the surface indicates the critical curve for Ls = Lc. Italic letters *Ne*, *Plag*, *Wo*, *Mel* and *CC* on the surface mark the fields for a mineral precipitated from immiscible liquids. Notice that minerals An and Mel are projected on the sodium-free endmember triangle.

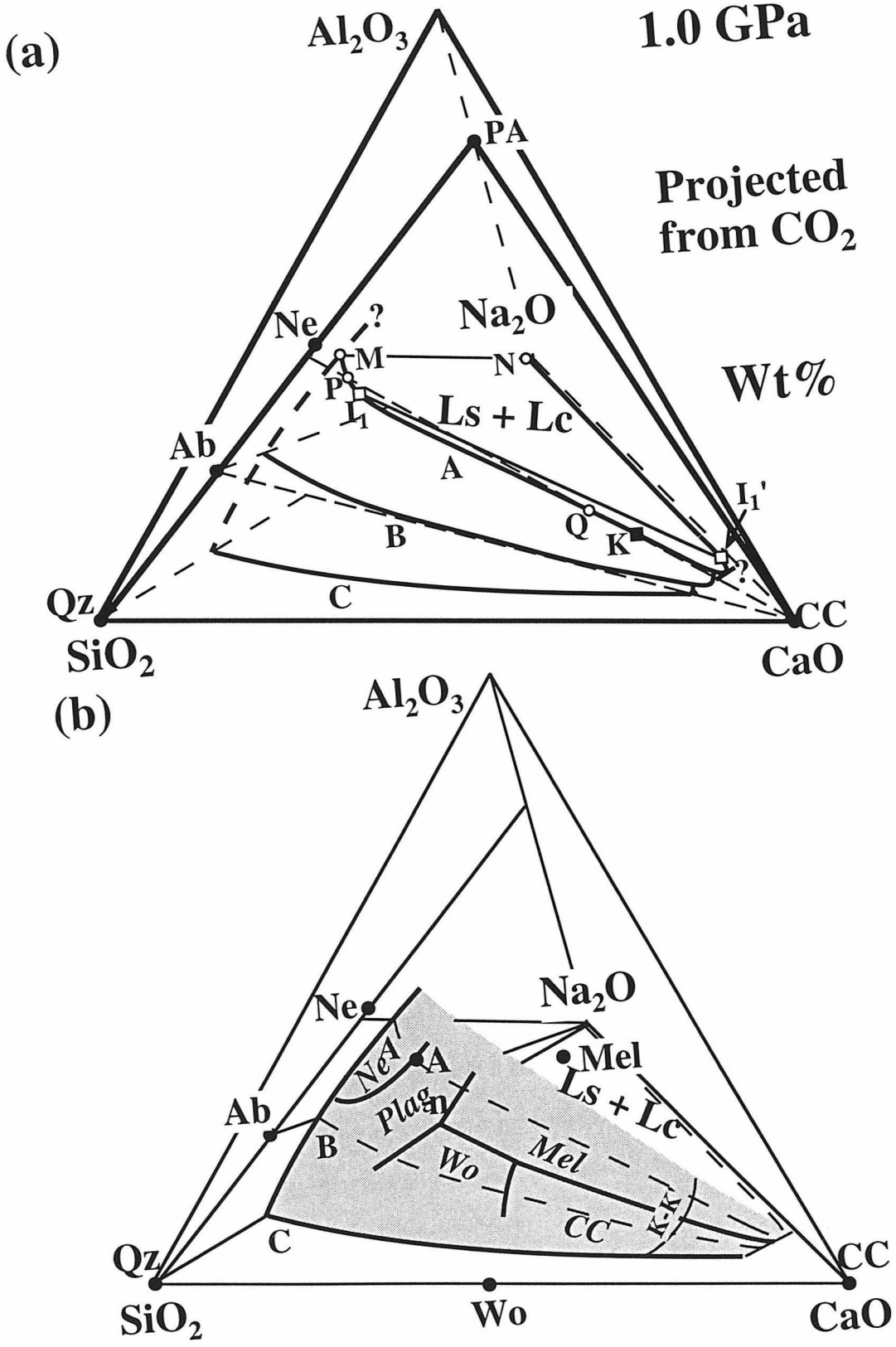
(a)
Al_2O_3
1.0 GPa
PA
Projected
from CO_2
Ne
?
Na_2O
M
N
P
I_1
Ls + Lc
Wt%
Ab
A
I_1'
B
Q
K
?
Qz
C
CC
SiO_2
CaO
(b)
Al_2O_3
Ne
Na_2O
Ne
A'
A
Mel
Ls + Lc
Ab
Plagn
B
Mel
Wo
CC
K-Fl
C
Qz
CC
SiO_2
Wo
CaO

These field boundaries outline the intersections of two liquidus volumes and the miscibility gap volume, and locate the fields for two liquids with nepheline, plagioclase, melilite, wollastonite and calcite. The area "Plag" indicates the field of two liquids with plagioclase whose composition changes continuously from anorthite to albite as the bulk composition progresses from Ne-CC-NC to Ab-CC-NC. The general ranges of the immiscible silicate-rich and carbonate-rich liquids in the tetrahedron are also defined—the carbonate-rich liquids are all concentrated near the axis CaO-Na_2O and near the CaO corner (i.e. the right-hand side of the critical curve K-K'), with no more than 70-80 % dissolved $CaCO_3$, and the immiscible silicate-rich liquids are located in a much larger area on the surface of the two-liquid volume.

CRYSTALLIZATION PATHS OF CARBONATED SILICATE LIQUIDS

The evolution of carbonated silicate liquids towards carbonatitic residua is constrained by the two major features in phase diagrams (e.g. Figs. 8 and 9): the silicate-carbonate liquid miscibility gap and liquidus field boundaries, which are both a function of temperature, pressure and composition. Lee and Wyllie (1996a) summarized the possible crystallization paths of carbonated silicate liquids by comparing the parental liquid compositions and the field boundaries from the results of Ab-CC at 2.5 and 1.0 GPa. The main emphasis was the effect of pressure on the liquidus features in controlling the cooling paths of various liquid types (nepheline- to quartz-normative), and the resultant carbonate-rich liquid compositions. Here we present a similar treatment for the paths of silicate-CO_2 liquids at 1.0 GPa, but the phase relationships to be compared now vary with composition (Figs. 11 and 12). Notice that the silicate-rich parental liquids for the following discussions are limited to those in the silicate liquidus field.

Figures 11a and b compare the key surfaces, boundaries and invariant points from the lower portions of Figs. 8 and 9, presenting the results near the compositional slices Ne-

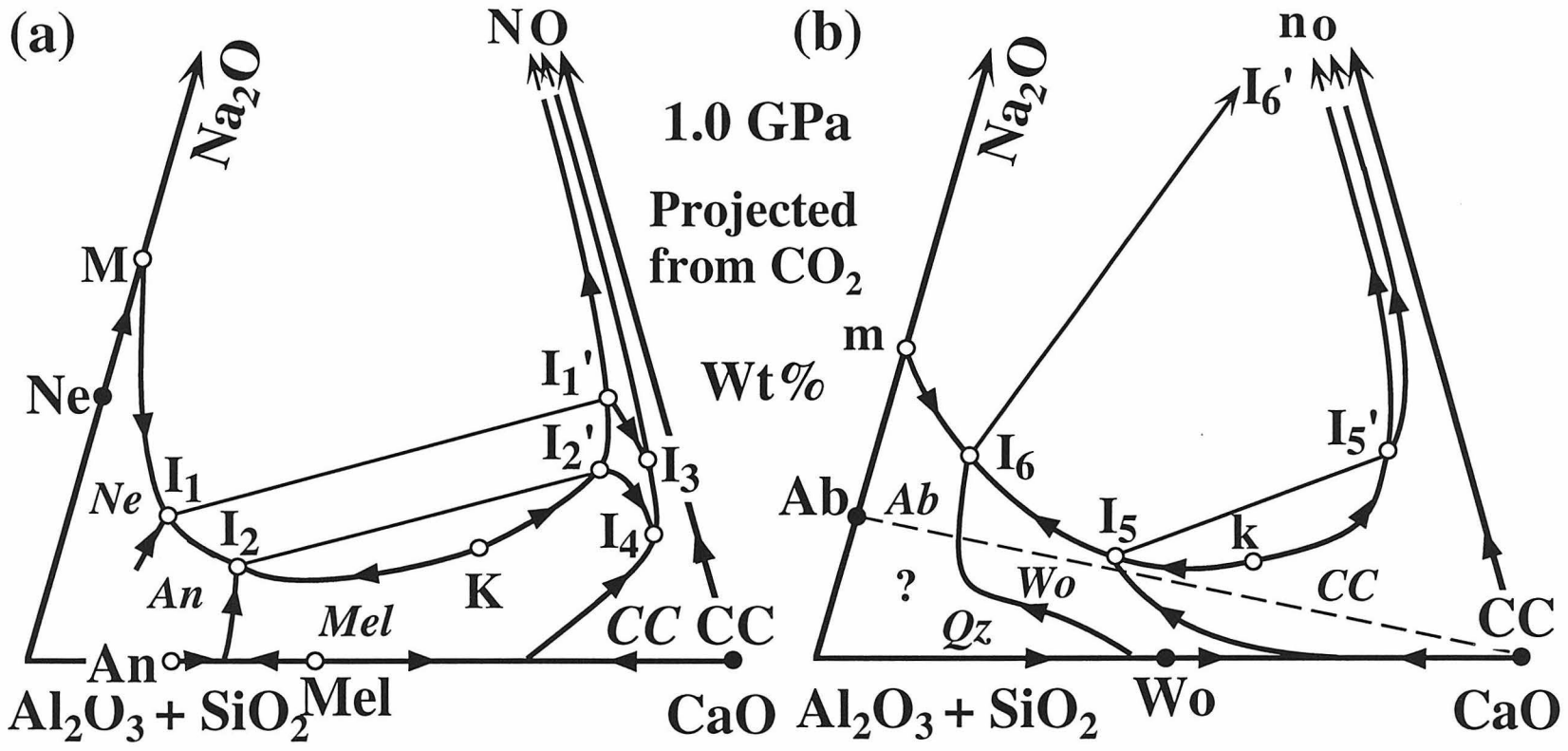

Figure 11(a) and (b). Comparison of the lower portions of the phase diagrams in Figs. 8 and 9. The Ab-Wo liquidus field boundary in (b) now extends to the miscibility gap at I_6, producing immiscible carbonate-rich liquid I_6' (exact position not shown) on the section I_5'-n.

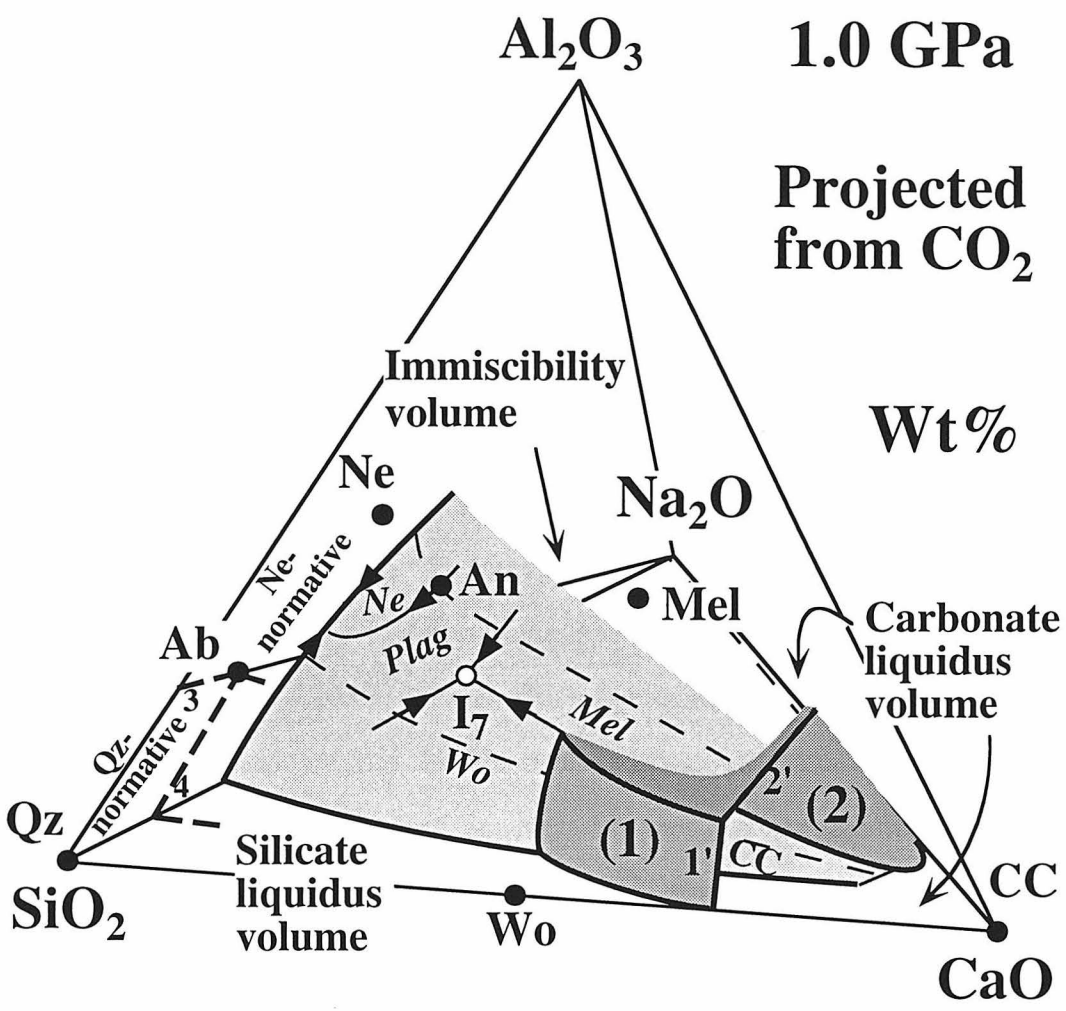

Figure 12. Compositional tetrahedron showing the three major liquidus features, the immiscibility volume (Fig. 10b), and the silicate and carbonate liquidus volumes. Possible cooling directions are now sketched for the 4-phase field boundaries on the surface of the immiscibility volume. The carbonate liquidus volume near the CaO-corner is for primary calcite, bounded by surface 1 (Wo-CC) and 2 (Mel-CC); the positions of the bounding field boundaries for the two surfaces are schematic (boundaries 1' and 2' on the sodium-free triangle). With higher sodium, this volume becomes limited to near the CaO-Na_2O axis. The general positions for qz- and ne-normative liquids are defined relative to Ab (e.g. lines 3 and 4), and extend towards the Ca-rich region, but the detailed ranges are not determined.

CC-NC and Ab-CC-NC (Al/Si = 1 and 1/3; Fig. 10). Ne-precipitating liquids in Fig. 11a may follow crystallization paths to the miscibility gap M-I_1, or to the Ne-An coprecipitation boundary, and with further cooling the evolving liquids in either case may ultimately reach the temperature minimum of the miscibility gap at I_1. The corresponding carbonate-rich liquids are exsolved between N and I_1' of the miscibility gap field boundary, rich in sodic contents. The silicate liquids below line Ne-An (the corner near SiO_2 + Al_2O_3) follow a direction away from the miscibility gap.

The liquids within the anorthite field may reach the miscibility gap between I_1 and I_2 directly, at I_1 following the Ne-An coprecipitation boundary, or at I_2 through the An-Mel boundary and continue towards I_1. The compositional range of the exsolved carbonate-rich liquids is thus between I_1' and I_2', less sodic than the liquids along N-I_1' in equilibrium with nepheline. The least sodic, carbonate-rich liquids (along K-I_2' of the miscibility gap field boundary) are produced from the Mel-bearing silicate-rich liquids, already enriched in $CaCO_3$, on the left side of the dashed-line Mel-K as they meet the miscibility gap on K-I_2. The immiscible carbonatite liquids contain substantial amounts of silicate components. No silicate-rich liquids could follow a path to the Mel-CC coprecipitation boundary because of the thermal barrier along Mel-K.

Immiscible carbonate-rich liquids in equilibrium with silicate-rich liquids remain on K-N while precipitating silicate minerals only. As the carbonate-rich liquids are separated from the silicate parents, they move across the silicate liquidus surface during cooling through a temperature interval, following a direction determined by the types of minerals precipitated. The liquids may finally reach the silicate-carbonate coprecipitation boundary along I_4-I_3-O, and become more enriched in sodium through additional crystallization of calcite. The phase relationships may be dominated by $CaCO_3$-Na_2CO_3, as the amounts of silicate are minor.

Possible liquid paths in Fig. 11b are derived following a similar argument. The Ab-Wo cotectic boundary is now simply connected to the miscibility gap field boundary at

I_6 where the tie-line points to a sodic carbonate-rich liquid I_6' (cf. Fig. 9). Ab-precipitating liquids may produce sodic carbonatitic liquids along n-I_6', whereas Wo-precipitating liquids generate carbonate-rich liquids between I_5' and I_6'. Some Wo-bearing liquids may reach the Wo-CC boundary to precipitate various proportions of wollastonite and calcite on the way to I_5. I_5' is the most $CaCO_3$-rich liquids which can be produced by carbonated silicate liquids near the compositional slice Ab-CC-NC. Silicate-CO_2 liquids close to the (Al_2O_3 + SiO_2) corner may be prevented from reaching the miscibility gap by a cotectic between two silicate phases, but there are no available experimental data for further discussion.

The paths of silicate-CO_2 liquids in Figs. 11a and b are assumed to satisfy ternary phase relationships. In reality, liquids can move out of the planes, and the liquid paths can be better described by the CO_2-saturated, pseudo-quaternary system SiO_2-Al_2O_3-CaO-Na_2O, as in Fig. 12. This figure reproduces the two-liquid miscibility volume and several 4-phase field boundaries in the compositional tetrahedron of Fig. 10b, with possible cooling directions for several boundaries indicated by arrows. Near the CaO corner, a large portion of the carbonate liquidus volume is also sketched, bounded by the Wo-CC (1) and Mel-CC (2) coprecipitation surfaces and the miscibility gap surface. The rest portion of the carbonate liquidus volume is restricted to near the Na_2O-CaO axis. The ranges of silica-undersaturated to oversaturated liquids can now be expressed clearly in the tetrahedron, with quartz-normative liquids limited by lines 3 and 4 on the triangle SiO_2-Al_2O_3-Na_2O and extending towards CaO-rich compositions, and with nepheline-normative liquids occupying a range closer to the miscibility volume.

Consider CO_2-bearing, ne-normative liquids in the nepheline liquidus volume somewhere below the Ne-CC-NC plane. Depending on their compositions and the detailed phase relationships, these liquids through cooling may (1) reach the miscibility gap, follow a path on the surface of the miscibility volume to intersect the Ne-Plag-Ls-Lc field boundary, and further move along the boundary by coprecipitation of nepheline and

plagioclase, (2) intersect the Ne-Plag coprecipitation surface first, and follow a path to, and along the 4-phase field boundary, or (3) reach the Ne-Plag coprecipitation surface, but follow a path on the surface away from the miscibility gap.

Silicate-CO_2 liquids in other liquidus domains (Plag, Mel, and Wo) follow a similar set of selections, leading to the miscibility gap directly, or to a coprecipitation surface, then towards or away from the miscibility field. Furthermore, some liquids may cross several liquidus fields finally reaching the two-liquid volume, or entirely within the silicate liquidus volume to precipitate silicates only while exsolving CO_2. For the silicate liquids with lower Al/Si, they may reach the calcite liquidus volume on the lower right corner of the tetrahedron, and move along the paths on surfaces 1 and 2 to produce silicates and calcite. Notice the pseudo-invariant I_7 (open circle in Fig. 12) on the intersection of three 4-phase field boundaries, indicating the coexistence of Ls, Lc, Mel, Wo and Plag. According to the arrangement of the arrows shown in Fig. 12, this is also a local temperature minimum on the surface of the two-liquid volume, and indicates the final composition of some crystallizing silicate-rich liquids. The corresponding carbonate-rich liquid is alkalic, bracketed by the compositions of the carbonate-rich liquids I_2' and I_6' in Figs. 11a and b, respectively.

PETROLOGICAL APPLICATIONS

The available field evidence for carbonatites and their associated silicate rocks, reviewed by Barker (1989), has revealed a possible genetic link between the two rock types in many intrusive complexes. The common occurrence of a compositional gap between the silicate and carbonatite rocks combined with experimentally determined wide miscibility gaps (e.g. Kjarsgaard and Hamilton, 1988, 1989) appears to point to an origin of crustal carbonatites by liquid immiscibility.

With the framework illustrated in Figs. 11 and 12, we now examine the validity and extent of liquid immiscibility in generation of calcio- to alkali carbonatites from carbonated silicate liquids at crustal levels in the model system. The actual evolution paths cannot be delineated in the Mg-free system, due to the mafic nature of parental silicate magmas and polybaric crystallization conditions, but the processes outlined below are generally applicable to natural magmatic systems.

Generation of calcio- to alkali carbonatites at crustal conditions

Lee and Wyllie (1996a) reviewed the experimental results for viable processes for formation of calciocarbonatites, suggesting that the occurrence of almost pure-$CaCO_3$ immiscible liquids is unlikely, and that intrusive calciocarbonatites (sovites) may be cumulates from immiscible carbonate-rich magmas, still containing some silicates and significant amounts of alkalis. Their experimental results are now extended in this study, confirming that the liquid miscibility gap in the model system is restricted to no more than 70-80 wt% dissolved $CaCO_3$ if all CaO and Na_2O are assigned to carbonate, and reinforcing that both the miscibility gap and liquidus field boundaries play an important role in controlling the evolution of carbonated silicate liquids towards carbonatitic compositions.

The previous discussions have indicated a variety of possible cooling paths for carbonated silicate liquids and carbonatitic liquids, and many of them involve processes of both liquid immiscibility and crystal fractionation. The choice of the paths in the model system includes that: (1) crystallizing liquids intersect the miscibility gay to produce a range of carbonatitic magmas which are capable of precipitating silicate minerals while in conjuction with the silicate parents, (2) the immiscible carbonate-rich liquids separated from their silicate parents follow a narrow silicate-precipitating path to a liquidus field boundary for the coprecipitation of silicates and carbonates (calcite, nyerereite or Na_2CO_3),

(3) silicate-CO_2 liquids follow a crystallization path to a silicate-silicate or silicate-calcite coprecipitation boundary, then move along the cotectic (a) to the miscibility gap, or (b) towards alkali-carbonate precipitating fields (along a silicate-calcite boundary) without intersecting the two-liquid field, and (4) the liquids evolve completely within the silicate liquidus volume and release CO_2 vapor without producing carbonate-rich residua. A variety of carbonatites can thus be produced, depending upon the compositions of parental liquids and the evolution paths defined by pressure and temperature conditions.

Calcite-rich carbonatite liquids can be generated from carbonated silicate liquids along the Ca-rich corner of the miscibility gap (Figs. 11 and 12), but the liquids are also alkali- and silicate-bearing, different in composition from most calciocarbonatite rocks. It appears that those rocks cannot be solidified directly from immiscible Ca-rich carbonatite liquids. Could carbonated silicate liquids or immiscible carbonate-rich liquids through crystal fractionation reach a liquid composition very similar to those of the reported, nearly pure-$CaCO_3$ calciocarbonatites (e.g. Keller, 1989)? The limit of carbonatite liquid compositions produced from silicate parental liquids through any reasonable magmatic processes is defined by the silicate-carbonate liquidus field boundary (e.g. surface 1 and 2, Fig. 12): the carbonate-rich liquids along the boundary are either more silicate-rich (near the alkali-poor side) or more alkalic (near silicate-poor compositions) than most calciocarbonatites. Any liquid following a path to intersect the field boundary at the $CaCO_3$-rich corner (Fig. 12) will precipitate calcite which consequently changes the liquid composition towards alkali-enrichment, rather than alkali depletion or calcite enrichment. Hence it is unlikely to produce a calciocarbonatite "liquid" matching the rock compositions by either liquid immiscibility or Crystal fractionation.

We feel that many calciocarbonatites may form by crystal accumulation processes from carbonatitic magmas along a silicate-calcite coprecipitation boundary. Such liquids can be produced by silicate-precipitating, immiscible carbonate-rich liquids (e.g. along K-I_2'-I_1', Fig. 11a; near I_5' towards I_6', Fig. 11b) reaching the silicate-calcite field boundary

(e.g. near I_4-I_3 towards O in Fig. 11a; near I_5' towards o in Fig. 11b), with relatively high sodium, and low silicate. The possible rock sequence produced from a silicate parental liquid may show a compositional gap reflecting the intermediate immiscibility process. Although silicate-CO_2 liquids near the plane Ne-CC-NC cannot reach the silicate-calcite liquidus field boundary due to the thermal barrier Mel-K (Fig. 11a), the cooling liquids with lower Al/Si on surface (2) (Fig. 12) may escape the barrier and lead to higher alkalic, lower silicic residual carbonatitic liquids. There may be a continuous spectrum of bulk rock compositions ranging from silicic to low-silicate carbonatitic resulting from such a process. For the carbonated silicate liquids with even lower Al/Si, they may reach a cotectic boundary such as surface (1) of Fig. 12, and precipitate silicate-rich carbonatite rocks.

Although the formation of natrocarbonatite liquids of Lengai type immiscible to highly peralkaline silicate liquids may be an extremely rare occurrence (Bell and Keller, 1995), other alkali carbonatitic liquids are probably commoner in nature through a variety of processes. They could be achieved by a direct immiscibility process +/- silicate crystallization (a range of compositions along the carbonate-rich liquid side of the miscibility gap, Figs. 11 and 12). Alternatively, alkali carbonatite magmas could be derived by crystal fractionation from Ca-rich carbonatitic liquids, as discussed previously (also see Cooper et al., 1975; Twyman and Gittins, 1987; Kogarko et al., 1991), or from nepheline-normative liquids under water-saturated conditions (Lee and Wyllie, 1994).

It appears that liquid paths leading to either calcio- or alkali carbonatites can be described by the processes outlined in this model system, and therefore in a more general sense, these two compositional extremes might share common parents through common magmatic processes. In fact, many calciocarbonatites should be linked with alkali-bearing carbonatite liquids during their formation, and the generation of alkali carbonatitic magmas is probably a part of normal history of carbonatite magmatism, although the magmas could not survive fenitization with wall rocks, or secondary calcitization process at surfacial

conditions. The unusual occurrence of natrocarbonatite in Oldoinyo Lengai is discussed below.

Formation of Natrocarbonatites at Oldoinyo Lengai

Peterson and Kjarsgaard (1995) observed two magmatic trends at the Oldoinyo Lengai volcanic center: the earlier series involving nephelinite to phonolite through crystal fractionation, and the later from melilite nephelinite to wollastonite nephelinite. Although silicate liquids similar in composition to the first series rocks have been demonstrated experimentally to be immiscible with a range of alkalic carbonatite liquids (Freestone and Hamilton, 1980), Peterson and Kjarsgaard (1995) indicated that the field evidence supports the generation of natrocarbonatite through immiscible separation from the second series wollastonite nephelinite. Kjarsgaard et al. (1995) further designed a set of two-liquid experiments between wollastonite nephelinite and natrocarbonatite compositions, and produced at 50-100 MPa and 700-750°C solids and liquids with compositions closely matching those occurred in the nephelinite-carbonatite complex. The 1993 eruptions yielded natrocarbonatite lavas with small silicate spheres (see Dawson et al., 1994, 1996; Church and Jones, 1995). Liquid immiscibility appears to be a convincing explanation, although the directions of the two-liquid tie-lines do not agree well with the general trends in experimental results (e.g. Freestone and Hamilton, 1980; Kjarsgaard and Hamilton, 1989). Following the differentiation trend from melilite nephelinite to wollastonite nephelinite, Peterson and Kjarsgaard (1995) indicated that the peralkalinity of the silicate magma was concomitantly built up until a stage when natrocarbonatite liquids could be exsolved from the silicate parent.

The previous section has outlined some possible liquid paths leading to the formation of alkali-rich carbonatite magmas. Natrocarbonatite probably corresponds to the immiscible carbonatitic liquid at a local temperature minimum on the surface of the

miscibility gap, such as that in equilibrium with silicate-rich liquid at I_7 in Fig. 12, and is thus restricted to within a limited compositional range. There also exist several ways for a variety of carbonated silicate liquids to reach the pseudo-invariant I_7, and the Lengai magmatic trend may be best modeled in the synthetic system by a path through which a parental liquid initiated in the melilite-precipitating field later follows a Mel-Plag-Wo coprecipitating boundary directly to point I_7. Notice again that the actual liquid path and involved mineral assemblages cannot be read in the phase diagram Fig. 12, due to differences in composition and pressure-temperature conditions between the natural example and our studied system.

The nephelinite lavas in the first series, although capable of exsolving immiscible carbonate liquids under some conditions (i.e. Freestone and Hamilton, 1980), followed a crystallization path to phonolitic derivatives (Peterson and Hamilton, 1995), similar to choice 4 in the previous section. The fact that the compositions of some alkalic silicate rocks in carbonatite complexes are projected near the silicate-rich limb of a miscibility gap does not necessarily indicate that the associated carbonatite rocks are produced from silicate magmas by liquid immiscibility. It should further rely on detailed studies (field, petrographic and geochemical) for each individual carbonatite complex to define the actual conditions for its magmatic evolution.

REFERENCES

Bailey D. K., 1993. Carbonate magmas. Jour. of Geol. Soc. London 150, 637-651.

Baker M. B. and Wyllie P. J., 1990. Liquid immiscibility in a nephelinite-carbonate system at 25 kbar and implications for carbonatite origin. Nature 346, 168-170.

Barker, D. S., 1989. Field relations of carbonatites. In: Bell, K. (ed) Carbonatites: Genesis and Evolution. Unwin Hyman, London, 38-69.

Brooker, R. A. and Hamilton, D. L., 1990. Three-liquid immiscibility and the origin of carbonatites. Nature 346, 459-462

Bell K. and Keller J., 1995. (Eds) Carbonatite volcanism: Oldoinyo Lengai and the petrogenesis of natrocarbonatites. IAVCEI Proceedings in Volcanology 4, Springer-Verlag, Berlin Heidelberg New York, pp 210.

Church A. A. and Jones A. P., 1995. Silicate-carbonate immiscibility at Oldoinyo Lengai. Jour. Petrol. 36, 869-889.

Cooper A. F., Gittins J. and Tuttle O. F., 1975. The system Na_2CO_3-K_2CO_3-$CaCO_3$ at 1 kilobar and its significance in carbonatite petrogenesis. Amer. Jour. Sci. 275, 534-560.

Dawson, J. B., 1989. Sodium carbonatite extrusions from Oldoinyo Lengai, Tanzania: implications for carbonatite complex genesis. In: Bell, K. (ed) Carbonatites: Genesis and Evolution. Unwin Hyman, London, 255-277.

Dawson J. B., Garson M. S. and Roberts B., 1987. Altered former alkalic carbonatite lava from Oldoinyo Lengai, Tanzania: inferences for calcite carbonatite lavas. Geology 15, 765-768.

Dawson J. B., Pinkerton H., Pyle D. M. and Nyamweru C., 1994. June 1993 eruption of Oldoinyo Lengai, Tanzania: exceptionally viscous and large carbonatite lava flows and evidence for coexisting silicate and carbonate magmas. Geology 22, 799-802.

Dawson J. B., Pyle D. M. and Pinkerton H., 1996. Evolution of natrocarbonatite from a wollastonite nephelinite parent: evidence from the June, 1993 eruption of Oldoinyo Lengai, Tanzania. Jour. Geology 104, 41-54.

Dean T. and Roberts B., 1984. Carbonatite tuffs and lava clasts of the Tinderet foothills, western Kenya: a study of calcified natrocarbonatites. Jour. Geol. Soc. London 141, 563-580.

Freestone I. C. and Hamilton D. L., 1980. The role of liquid immiscibility in the genesis of carbonatites - an experimental study. Contrib. Mineral. Petrol. 73, 105-117.

Goldsmith J. R. and Newton, R. C., 1977. Scapolite-plagioclase stability relations at high pressures and temperatures in the system $NaAlSi_3O_8$-$CaAl_2Si_2O_8$-$CaCO_3$-$CaSO_4$. Amer. Mineral. 62, 1063-1081.

Greig J. W. and Barth T. F. W., 1938. The system $Na_2O{\cdot}Al_2O_3{\cdot}2SiO_2$ (nepheline, carnegieite)-$Na_2O{\cdot}Al_2O_3{\cdot}6SiO_2$ (albite). Amer. Jour. Sci. 35A, 93-112.

Hamilton D. L. and Kjarsgaard B. A., 1993. The immiscibility of silicate and carbonate liquids. S. Afr. Jour. Geol. 96, 139-142.

Hamilton D. L., Bedson P. and Esson J., 1989. The behaviour of trace elements in the evolution of carbonatites. In: Bell, K. (ed) Carbonatites: Genesis and Evolution. Unwin Hyman, London, 405-427.

Huang W. L. and Wyllie P. J., 1974. Eutectic between wollastonite II and calcite contrasted with thermal barrier in MgO-SiO_2-CO_2 at 30 kilobars, with applications to kimberlite-carbonatite petrogenesis. Earth Planet. Sci. Lett. 24, 305-310.

Huang W.-L., Wyllie P. J. and Nehru C.E., 1980. Subsolidus and liquidus phase relationships in the system CaO-SiO_2-CO_2 to 30 kbar with geological applications. Amer. Mineral. 65, 285-301.

Irving A. J. and Wyllie P. J., 1975. Subsolidus and melting relationships for calcite, magnesite, and the join $CaCO_3$-$MgCO_3$ to 36 kilobars. Geochim. Cosmochim. Acta 39, 35-53.

Jones J. H., Walker D., Pickett D. A., Murrell M. T. and Beattie P., 1995. Experimental investigations of the partitioning of Nb, Mo, Ba, Ce, Pb, Ra, Th, Pa, and U between immiscible carbonate and silicate liquids. Geochim. et Cosmochim. Acta 59, 1307-1320.

Keller J., 1981. Carbonatite volcanism in the Kaiserstuhl alkaline complex: Evidence for highly fluid carbonatitic melts at the earth's surface. Jour. Volcano. Geotherm. Res. 9, 423-431.

Keller J., 1989. Extrusive carbonatites and their significance. In: Bell K. (ed) Carbonatites: Genesis and Evolution. Unwin Hyman, London, 70-88.

Keller J. and Spettel B., 1995. The trace element composition and petrogenesis of natrocarbonatites. In: Bell K, Keller J (eds) Carbonatite volcanism: Oldoinyo Lengai and the petrogenesis of natrocarbonatites. IAVCEI Proceedings in Volcanology 4, Springer-Verlag, Berlin Heidelberg New York, 70-86.

Kjarsgaard B. A. and Hamilton D. L. (1988) Liquid immiscibility and the origin of alkali-poor carbonatites. Mineral. Mag. 52, 43-55.

Kjarsgaard B. A. and Hamilton D. L., 1989. The genesis of carbonatites by immiscibility. In: Bell K (ed) Carbonatites: genesis and evolution. Unwin Hyman, London, 388-404.

Kjarsgaard B. A. and Peterson T., 1991. Nephelinite-carbonatite liquid immiscibility at Shombole volcano, East Africa: petrographic and experimental evidence. Mineral. Petrol. 43, 293-314.

Kjarsgaard B. A., Hamilton D. L. and Peterson T. D., 1995. Peralkaline nephelinite/carbonatite liquid immiscibility: comparison of phase compositions in experiments and natural lavas from Oldoinyo Lengai. In: Bell K, Keller J (eds) Carbonatite volcanism: Oldoinyo Lengai and the petrogenesis of natrocarbonatites. IAVCEI Proceedings in Volcanology 4, Springer-Verlag, Berlin Heidelberg New York, 163-190.

Kogarko L. N., Plant D. A., Henderson C. M. B. and Kjarsgaard B. A., 1991. Na-rich carbonate inclusions in perovskite and calzirtite from the Guli intrusive Ca-carbonatite, polar Siberia: Contrib. Mineral. Petrol. 109, 124-129.

Koster van Groos A. F., 1975. The effect of high CO_2 pressures on alkalic rocks and its bearing on the formation of alkalic ultrabasic rocks and the associated carbonatites. Amer. Jour. Sci. 275, 163-185.

Koster van Groos A. F. and Wyllie P. J., 1966. Liquid immiscibility in the system Na_2O-Al_2O_3-SiO_2-CO_2 at pressures to 1 kilobar. Amer. Jour. Sci. 264, 234-255.

Koster van Groos A. F. and Wyllie P. J., 1968. Liquid immiscibility in the join $NaAlSi_3O_8$-Na_2CO_3-H_2O and its bearing on the genesis of carbonatites. Amer. Jour. Sci. 266, 932-967.

Koster van Groos A. F. and Wyllie P. J., 1973. Liquid immiscibility in the join $NaAlSi_3O_8$-$CaAl_2Si_2O_8$-Na_2CO_3-H_2O. Amer. Jour. Sci. 273, 465-487.

Le Bas M. J., 1981. Carbonatite magmas. Mineral. Mag. 44, 133-140.

Lee W.-J. and Wyllie P. J., 1992a. New data on CO_2-rich immiscible liquids in Na_2O-CaO-Al_2O_3-SiO_2-CO_2 from 25 to 1 kb: carbonatite genesis (abstract). EOS 73, 349-350.

Lee W.-J. and Wyllie P. J., 1992b. Liquid immiscibility between silicates and carbonates must intersect suitable liquidus field boundaries to have petrogenetic significance. Abstracts, 29th International Geological Congress, Kyoto, 571.

Lee W.-J. and Wyllie P. J., 1994. Experimental data bearing on liquid immiscibility, crystal fractionation, and the origin of calciocarbonatites and natrocarbonatites. Int. Geol. Rev. 36, 797-819.

Lee W.-J. and Wyllie P. J., 1996a. Liquid immiscibility in the join $NaAlSi_3O_8$-$CaCO_3$ to 2.5 GPa and the origin of calciocarbonatite magmas. J Petrol (submitted).

Lee W.-J. and Wyllie P. J., 1996b. Liquid immiscibility between nephelinite and carbonatite from 2.5 to 1.0 GPa compared with mantle melt compositions. Contrib. Mineral. Petrol. (submitted).

Lee W.-J., Wyllie P. J. and Rossman G. R., 1994. CO_2-rich lass, round calcite crystals and no liquid immiscibility in the system CaO-SiO_2-CO_2 at 2.5 GPa. Amer. Mineral. 79, 1135-1144.

Twyman J. D. and Gittins J., 1987. Alkalic carbonatite magmas: Parental or derivative? In: Fitton J. G. and Upton B. G. J. (eds) Alkaline Igneous Rocks: Geological Society Special Publication No. 30, 85-94.

Verwoerd W. J., 1978. Liquid immiscibility and the carbonatite-ijolite relationship: Preliminary data on the join $NaFe^{3+}Si_2O_6$-$CaCO_3$ and related compositions: Carnegie Inst. Washington Year Book, 77, 767-774.

Wendlandt R. F. and Harrison W. J., 1979. Rare earth partitioning between immiscible carbonate and silicate liquids and CO_2 vapor: Results and implications for the formation of light rare earth-enriched rocks. Contrib. Mineral. Petrol. 69, 409-419.

Woolley A. R. and Kempe D. R. C., 1989. Carbonatites: nomenclature, average chemical compositions, and element distribution. In: Bell K. (ed) Carbonatites: genesis and evolution. Unwin Hyman, London, 1-14.

CHAPTER 5

LIQUID IMMISCIBILITY BETWEEN NEPHELINITE AND CARBONATITE FROM 2.5 TO 1.0 GPa COMPARED WITH MANTLE MELT COMPOSITIONS

(Lee W.-J. & Wyllie P. J., 1996. Contributions to Mineralogy and Petrology, submitted)

ABSTRACT

In order to define the conditions for the formation of immiscible carbonatite magmas in the lithosphere and in the crust, we have conducted phase equilibrium experiments to determine the effect of pressure and temperature on the silicate-carbonate liquid miscibility gap in bulk compositions appropriate for magmas in the upper mantle. A primitive (magnesian) nephelinite (NEPH) was used as a starting material, mixed with carbonates. Experiments were made with mixtures in the joins NEPH-dolomite-Na_2CO_3 (NEPH-Dol-NC) at 1.0 to 2.5 GPa, and NEPH-calcite (NEPH-CC) at 1.0 GPa. The miscibility gap was intersected by the join NEPH-Dol-NC (liquids with olivine and spinel), but not by NEPH-CC, and coexisting liquid compositions were analyzed. Together with previous results for the Mg-free system (Na_2O-CaO-Al_2O_3-SiO_2-CO_2), it was established that the size of the miscibility gap for magnesian compositions increases with decreasing pressures from depths of ~100 km to ~35 km; it increases further as compositions are changed by decreasing Mg/Ca. The maximum $CaCO_3$ in liquids associated with the miscibility gap is 50 wt% for Mg-bearing liquids, and 80 wt% for Mg-free liquids; 86 wt% $CaCO_3$ is the maximum reported in carbonate-rich liquid generated by progressive reaction of lherzolite to wehrlite. There is no experimental evidence for nearly pure-$CaCO_3$ immiscible liquids, but abundant evidence for the precipitation of rounded calcite crystals from carbonate-rich liquids. The join NEPH-CC locates a piercing point on the liquidus field boundary for coprecipitation of olivine and calcite at $NEPH_{50}CC_{50}$ (wt%), part of the silicate-carbonate liquidus field boundary which defines the locus of liquids formed from carbonate-peridotites. The miscibility gap results are compared with magmas formed during partial fusion of CO_2-bearing mantle peridotites, and during fractional crystallization of mantle-derived magmas. None of the probable magma paths in mantle processes intersects the miscibility gap. CO_2-bearing mantle-derived alkalic magmas such as nephelinites and melilitites may fractionate during uprise through the

mantle and crystallization within the crust. The compositions of these evolved nephelinites and phonolites approach the silicate side of the miscibility gap, confirming the probable generation of immiscible, alkalic carbonate-rich liquids at crustal pressures.

INTRODUCTION

Integrated evidence from field, experimental and geochemical studies all point to a magmatic origin for carbonatites (e.g. Bell 1989, and references therein). The three favored mechanisms for their genesis are (1) unmixing of a CO_2-rich silicate magma upon intersecting a silicate-carbonate liquid immiscibility field, (2) partial melting of carbonated mantle peridotite at pressures $\geq$ 2.0 GPa, and (3) extreme fractional crystallization of a CO_2-bearing silicate liquid. Mantle-derived carbonatitic magmas have been called upon to explain aspects of the major- and trace-element signatures of selected mantle nodules (e.g. Green and Wallace 1988; Yaxley et al. 1991; Baker and Wyllie 1992; Ionov et al. 1993; Hauri et al. 1993). Evidence for the existence of carbonate-rich liquids in the mantle include silicate and carbonate immiscible liquid textures in mantle xenoliths (Amundsen 1987; Ionov et al. 1993; Pyle and Haggerty 1994; Kogarko et al. 1995). Pyle and Haggerty (1994) and Kogarko et al. (1995) interpreted rounded calcite crystals in mantle xenoliths as products of liquid immiscibility. What is poorly known is how such carbonatitic to carbonate-rich silicate melts evolve during transit within the mantle. Bailey (1993) has argued the case for primary mantle-derived calcicocarbonatite magmas including Keller's (1989) evidence for effusive $CaCO_3$-rich magmas.

Figure 1 outlines the problem to be addressed. Baker and Wyllie (1990) compared their experimentally determined silicate-carbonate liquid miscibility gap at 2.5 GPa and 1250° C (curve A-A, Fig. 1), using a primitive mantle-derived nephelinite (magnesian), with the compositions of mantle magmas trending from near-solidus carbonatite (WG, Wallace and Green 1988) to alkali basalts (e.g. Frey et al. 1978). They concluded that

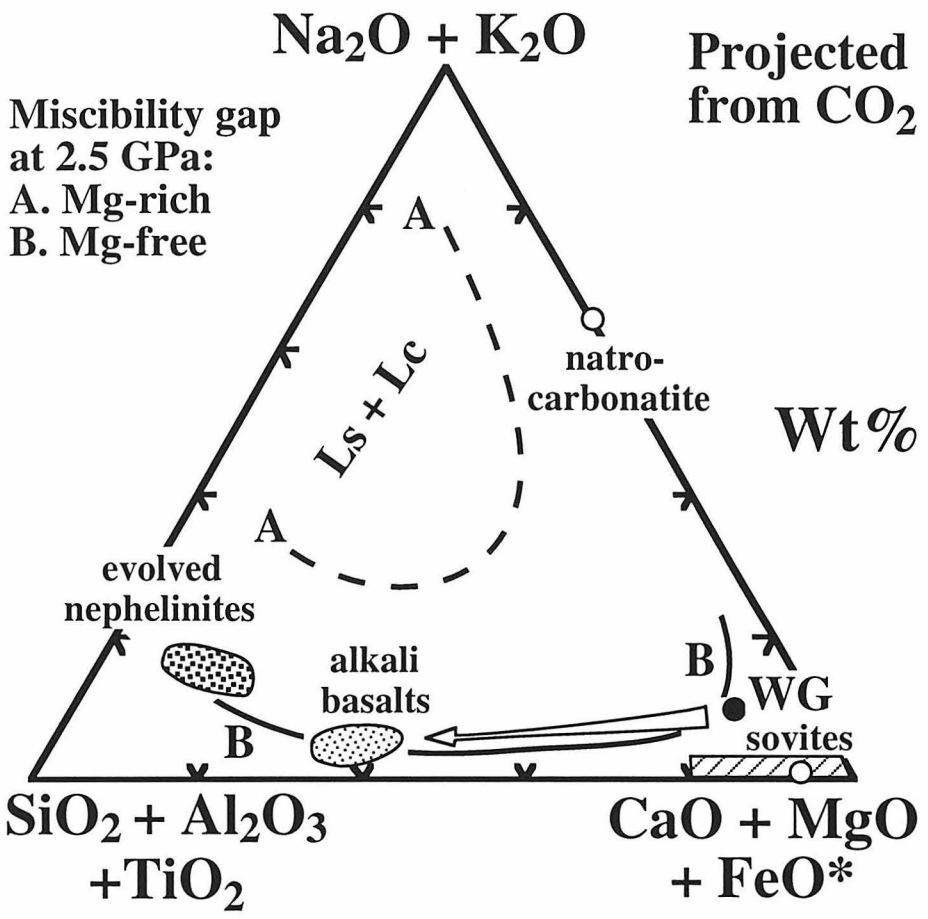

Figure 1. Comparison of silicate-carbonate liquid miscibility gaps (curves A-A and B-B) and a possible melting path of carbonated peridotite (the arrow from WG to the area of alkali basalts), illustrated in the compositional triangle ($SiO_2 + Al_2O_3 + TiO_2$)-(CaO + Mg + FeO*)-($Na_2O + K_2O$), projected from CO_2. Ls: silicate-rich liquid, Lc: carbonate-rich liquid. The open circles denote the compositions of natrocarbonatite (Dawson et al. 1987) and average sovite (within the shaded area showing the range of calciocarbonatites, magnesiocarbonatites and ferrocarbonatites; Woolley and Kempe 1989). The area of evolved nephelinites includes nephelinite to phonolite compositions reported in Freestone and Hamilton (1980) and Kjarsgaard and Peterson (1991). FeO*: all iron expressed as oxide.

mantle-derived magmas in the lower lithosphere were unlikely to intersect a liquid miscibility gap. Experimental results by Freestone and Hamilton (1980) and Kjarsgaard and Peterson (1991) have confirmed that evolved nephelinites at crustal pressures can exsolve carbonate-rich melts. Recent petrographic and experimental investigations of liquid immiscibility involving the natrocarbonatites of Oldoinyo Lengai have been summarized by Dawson et al. (1994), Church and Jones (1995), and Kjarsgaard et al. (1995). In order to determine whether carbonate-bearing magmas rising through the mantle would exsolve a second liquid before they reach crustal levels, it is necessary to know the effect of decreasing pressure and increasing Ca/Mg on the liquid miscibility gap.

Liquid immiscibility in the Mg-free system Na_2O-CaO-Al_2O_3-SiO_2-CO_2 was subject to a systematic study from 1.0-2.5 GPa by Lee and Wyllie (1992a, 1992b, 1996) and Lee et al. (1994), with results demonstrating that the miscibility gap does not extend to nearly pure $CaCO_3$ liquids, as reported by Kjarsgaard and Hamilton (1988, 1989) and Brooker and Hamilton (1990). Kjarsgaard and Hamilton (in preparation, in Macdonald et al. 1993) revised the earlier interpretation, and their miscibility gap at 0.5 GPa is now similar in position to that reported by Lee et al. (1994). Figure 1 compares the miscibility gap B-B at 2.5 GPa (Lee and Wyllie 1996) with the gap A-A for the Mg-bearing system. Note that the maximum $CaCO_3$ content of an immiscible liquid is 80 wt%, and this decreases with decreasing pressure (Lee and Wyllie 1996). At constant pressure, the extent of the miscibility gap increases with decreasing MgO content, and the projected mantle-magma path in Fig. 1 overlaps the Mg-free miscibility gap.

We have conducted experiments to define the topology of the two-liquid field for carbonate-rich primitive mantle melts over a pressure range of 2.5 GPa to 1.0 GPa, to determine whether the mantle-magma path intersects the miscibility gap. We compare the results with published data on the variation of near-solidus carbonated mantle magmas through a range of pressures.

EXPERIMENTAL METHODS

Starting materials

Table 1 gives the compositions of the starting materials and the mixtures made from them. The silicate material is a primitive magnesian nephelinite (NEPH) from Hawaii (68KEE-1, Clague and Frey 1982), selected to provide a silicate component related to mantle magmas. On an anhydrous basis (with all Fe as FeO), the rock contains 39.9 wt% SiO_2; FeO* and MgO contents are 14.0 and 15.7 wt%, respectively. The rock powder (from F. Frey) was de-watered at 1000° C for ~1 hour under a CO_2-H_2 gas stream that approximated the quartz-fayalite-magnetite buffer. The eight starting mixtures consisted of varying proportions of the NEPH ± natural dolomite (Dol) ± reagent grade Na_2CO_3 (NC) ± reagent grade $CaCO_3$ (CC) (Table 1). All of the constituent powders were dried for ~1 hour at 110° C in a vacuum oven prior to being weighed; all mixtures (200-500 mg in weight) were grounded by hand under ethanol for 30 to 60 minutes.

Figure 2a shows the compositions of starting materials and mixtures projected into Fig. 1, along with relevant minerals. Figure 2b shows the spatial relationships in three dimensions in the tetrahedron (SiO_2 + Al_2O_3 + TiO_2)-(MgO + FeO*)-CaO-(Na_2O + K_2O) (+ excess CO_2), where the variables CaO and (MgO + FeO*) have been separated. All but one mixture lie along one of two joins in the tetrahedron. Mixes #1-5 lie on the triangle NEPH-Dol-NC. Mixes #1, 2, 3 and 5 along AB contain 50 % NEPH and 50 % carbonate (by weight) — the carbonate component varies from pure NC to a mixture of 25 % NC and 75 % Dol. Mix #4 contains 30 % NEPH, 35 % NC and 35 % Dol. Mixes #6, 7 and 8 lie along the join NEPH-CC; the wt% of CC varies from 70 (mix #6) to 40 (mix #8). Silica contents in the mixtures vary from 12 wt% (mix #4) to 24 wt% (mix #8; Table 1), while CaO/(MgO + FeO*) weight ratios range from 4.8 (mix #6) to 0.4 (mix #1). Sodium contents vary widely, from 0.81 wt% (mix #6) to 30.6 wt% (mix #1).

Table 1. Compositions in wt% of starting materials and base mixes

	NEPH	Dol	NC	CC	Mix #1	Mix #2	Mix #3	Mix #4	Mix #5	Mix #6	Mix #7	Mix #8
SiO_2	39.9	—	—	—	20.0	20.0	20.0	12.0	20.0	12.0	20.0	24.0
TiO_2	2.71	—	—	—	1.36	1.36	1.36	0.82	1.36	0.82	1.36	1.63
Al_2O_3	11.4	—	—	—	5.70	5.70	5.70	3.42	5.70	3.42	5.70	6.84
FeO*	14.0	0.02	—	—	7.02	7.02	7.02	4.22	7.02	4.22	7.02	8.42
MgO	15.7	21.6	—	—	7.86	10.6	13.3	12.3	16.1	4.72	7.86	9.44
CaO	11.5	30.9	—	56.0	5.76	9.56	13.4	14.3	17.2	42.7	33.8	29.3
Na_2O	2.69	—	58.5	—	30.6	23.3	16.0	21.3	8.66	0.81	1.35	1.62
K_2O	0.97	—	—	—	0.49	0.49	0.49	0.29	0.49	0.29	0.49	0.58
P_2O_5	0.91	—	—	—	0.46	0.46	0.46	0.27	0.46	0.27	0.46	0.55
CO_2	—	47.4	41.5	44.0	20.8	21.5	22.3	31.1	23.1	30.8	22.0	17.6

NEPH = 68KEE-1 on an anhydrous basis with all Fe as FeO (Clague and Frey 1982); Dol = natural dolomite, analysis by electron microprobe, CO_2 by difference; NC and CC = reagent-grade sodium and calcium carbonate, respectively, listed compositions are based on ideal stoichiometry. Mix #1 = 50 % NEPH + 50 % NC; mix #2 = 50 % NEPH + 37.5 % NC + 12.5 Dol; mix #3 = 50 % NEPH + 25 % NC + 25 % Dol; mix #4 = 30 % NEPH + 35 % NC + 35 % Dol; mix #5 = 50 % NEPH + 12.5 % NC + 37.5 % Dol; mix #6 = 30 % NEPH + 70 % CC; mix #7 = 50 % NEPH + 50 % CC; mix #8 = 60 % NEPH + 40 % CC.

Fig. 2. Studied joins and starting mixtures in compositional projections. Some relevant minerals are also plotted (open and solid squares): forsterite (Fo), spinel (Sp, $MgAl_2O_4$), enstatite (En), diopside (Di), larnite (La), calcite (CC), dolomite (Dol) and natrocarbonate (NC). (a) Projections on the triangle (Fig. 1). The shaded area represents the join nephelinite-dolomite-Na_2CO_3 (NEPH-Dol-NC), including mixes #1-5 (solid circles; Table 1). AB is the mixture line of 50 % nephelinite with carbonate (various NC/Dol). Mixes #6-8 (open circles; Table 1) are in the join NEPH-CC. (b) Projections into the tetrahedron (SiO_2 + Al_2O_3 + TiO_2)-CaO-(MgO + FeO*)-(Na_2O + K_2O), projected from CO_2. The two joins NEPH-Dol-NC and NEPH-CC are now well separated in space. NEPH is located in space by the dashed line projected through (MgO + FeO*) to N' on the base of the tetrahedron.

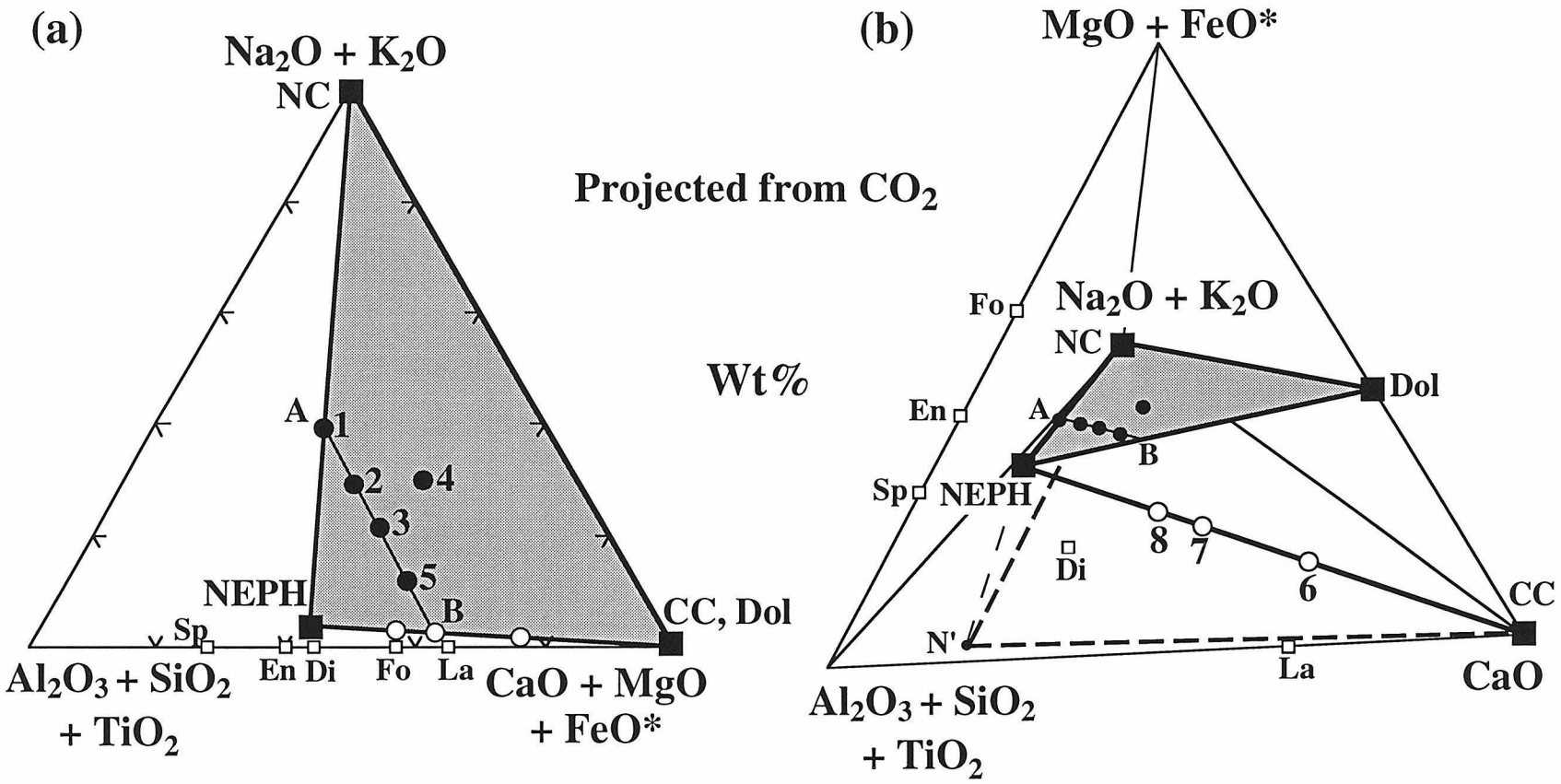
(a)
$Na_2O + K_2O$
NC
Projected from CO_2
Wt%
A
1
2
4
3
5
B
NEPH
CC, Dol
Sp
En
Di
Fo
La
$Al_2O_3 + SiO_2 + TiO_2$
$CaO + MgO + FeO^*$
(b)
$MgO + FeO^*$
Fo
$Na_2O + K_2O$
NC
Dol
En
A
B
Sp
NEPH
8
7
Di
6
CC
N'
La
CaO
$Al_2O_3 + SiO_2 + TiO_2$

Experiments

Experiments were run in a 1.27 cm piston cylinder apparatus using outer sleeves of CaF_2, straight-walled graphite furnaces, and inner pieces of crushable MgO dried at 1000° C. Each starting mixture was dried for 30-60 minutes at 110° C in a vacuum oven prior to being loaded into a graphite crucible which in turn was sealed inside a 3.81 mm diameter Pt capsule. All experiments were hot-piston in, i.e., pressure was applied cold and as power was supplied to the furnace, the apparatus was pumped to maintain the desired run pressure. Reported pressures have not been corrected for possible friction effects, although these effects are probably small for our assemblies. Temperature was controlled and monitored to within 1-2° C by $W_{95}Rh_5$-$W_{74}Rh_{26}$ thermocouple, and no correction was made for the effect of pressure on thermocouple EMF. On the basis of previous determinations of the thermal profile of our run assemblies, we estimate that temperatures are accurate to ± 10° C, and that the thermal gradient over the region of the capsule containing the sample is < 5° C.

At 2.5 GPa and 1300° C, time series experiments using mix #1 show that the compositions of the silicate- and carbonate-rich liquids become time invariant after ~4 hours. Run times at 2.5 GPa ranged from 6 to 11 hours. At lower pressures, all experiments were run for at least 12 hours. Experiments were terminated by shutting off the power and initial quench rates were on the order of 100° C/second. For most experiments the pressure was held nearly constant during the quench — the experiments where this was not done are noted in Table 2.

Analytical methods and identification of phases

After removing the Pt capsule from the piston cylinder assembly at the end of the run, each charge was mounted inside a brass holder with epoxy, and dry-polished (NC-rich

glasses are extremely water-soluble) using alumina grit. The final polishing was done with 0.3 μ powder and the surface was then thoroughly cleaned with compressed air. We analyzed quenched liquids (both silicate-rich and carbonate-rich) and crystalline phases using a Camscan scanning electron microscope (SEM) fitted with an energy dispersive system. The beam current was 0.1 nA on brass and spectra were collected for 30 seconds. The raw counts were reduced using a modified ZAF procedure (CITZAF; Armstrong 1988). Analyses of the quenched silicate- and carbonate-rich liquids were done using a rastered beam that covered an area of ~100 μm^2; crystalline phases were analyzed using a < 1 μm^2 spot.

A sketch of run L75 (Table 2; 1.0 GPa, 1200° C) illustrates a typical two-liquid texture (Fig. 3); the large silicate bead (Ls) is surrounded by quenched carbonate-rich liquid (Lc), which is characteristic for our bulk compositions. The presence of large (>> 100 μm in longest dimension) circular to ellipsoidal areas of quenched liquid that are distinctly more silica-rich than the surrounding quenched liquid is the major criterion used for identifying stable liquid immiscibility. In time series experiments, an experiment on mix #2 for 0.5 hour displayed silicate- and carbonate-rich spheres with wide ranges of sizes and of compositions. We interpret these short-lived immiscible liquids to the heterogeneous distribution (on a length scale of tens of μm) of the silicate and carbonate components of our starting mixes; longer runs (6-9 hours) with the same bulk composition produced more texturally and compositionally uniform melts.

Although the silicate-rich liquids generally quench to glasses (e.g. Fig. 3b), the carbonate-rich liquids display a variety of quench textures that depend on bulk composition and run conditions. Figure 3c, a back-scattered electron image, shows a magnified region of the quenched carbonate-rich liquid from run L75. The dark and light dendrites are Na-rich and (Na,Ca,Mg)-rich carbonates, respectively. The much lighter equant regions (~1 μm in size) are more silicate-rich areas that probably exsolved during the quench.

Table 2. Run conditions and experimental results

Run #	Starting mix	P (GPa)	T (°C)	time (hr)	Equilibrium phase assemblage
NEPH-Dol-NC Compositions					
TL63	Mix #1	2.5	1300	0.5	Ls + Lc
TL100	Mix #1	2.5	1300	4.0	Ls + Lc + Sp
TL105	Mix #1	2.5	1300	8.0	Ls + Lc + Sp
TL116	Mix #1	2.5	1250	10.0	Ls + Lc + Ol + Sp
TL32	Mix #1	2.5	1200	6.0	Ls + Lc + Ol + Sp
TL99	Mix #2	2.5	1350	2.0	L + Ol + Sp
TL103	Mix #2	2.5	1350	9.0	L + Ol + Sp
TL106	Mix #2	2.5	1300	6.0	L + Ol + Sp
TL57	Mix #2	2.5	1300	7.5	L + Ol + Sp
TL118	Mix #2	2.5	1250	11.0	Ls + Lc + Ol + Sp
TL98	Mix #3	2.5	1400	2.0	L + Ol + Sp
TL102	Mix #3	2.5	1400	8.0	L + Ol + Sp
TL54	Mix #3	2.5	1300	4.0	L + Ol + Cpx + Sp
TL117	Mix #3	2.5	1250	10.0	L + Ol + Cpx + Sp
TL120	Mix #4	2.5	1250	9.5	L + Ol + Cpx + Sp
L71*	Mix #3	2.0	1225	12.0	Lc + Ls + Ol + Sp
L76*	Mix #5	2.0	1300	24.0	L + Ol + Sp
L69*	Mix #3	1.5	1250	12.0	Lc + Ls + Ol + Sp
L70*	Mix #3	1.5	1225	12.0	Lc + Ls + Ol + Sp
L72*	Mix #5	1.5	1300	24.0	L + Ol + Sp
L75*	Mix #1	1.0	1200	24.0	Lc + Ls
L77*	Mix #3	1.0	1225	12.0	Lc + Ls + Ol + Sp
L65*	Mix #3	1.0	1200	12.0	Lc + Ls + Ol + Sp
L68*	Mix #5	1.0	1275	24.0	L + Ol + Sp
L168	Mix #5	1.0	1200	24.0	L + Ol + Sp
L169	Mix #5	1.0	1150	27.0	L + Ol + Sp + Cpx

NEPH-CC Compositions					
L159	Mix #6	1.0	1300	12.0	L + Sp
L155	Mix #6	1.0	1250	18.0	L + CC + Sp
L158	Mix #6	1.0	1200	24.0	L + CC + Sp + Ol (tr)
L152	Mix #7	1.0	1300	12.0	L + Sp
L157	Mix #7	1.0	1250	18.0	L + Sp
L161	Mix #7	1.0	1225	26.0	L + CC + Ol + Cpx + Sp
L153	Mix #7	1.0	1200	24.0	L + CC + Cpx + Sp
L165	Mix #8	1.0	1300	15.0	L + Sp
L166	Mix #8	1.0	1250	18.0	L + Ol + Sp

---

* indicates that pressure was not held constant during quenching. Compositions of the mixes are reported in Table 1. Abbreviations: L - quenched liquid; Ls - quenche silicate-rich liquid; Lc - quenched carbonate-rich liquid; Ol - olivine; Cpx - clinopyroxene; Sp - spinel.

Fig. 3. (a) Sketch of the cross section for run L75 (Table 2), showing the distribution of immiscible silicate- and carbonate-rich liquids (Ls and Lc). Some silicate globules (to 30 μm) also occur inside Lc near the bottom of the charge. The black outline represents the graphite crucible, and the lined areas mark cracks and lost material. (b) Low magnification of back-scattered electron photomicrograph, showing the features of Ls and Lc at the lower-right corner of the sketch (square b). (c) High magnification photomicrograph for Lc (square c in the sketch), showing carbonate dendrites with light silicate-rich spots.

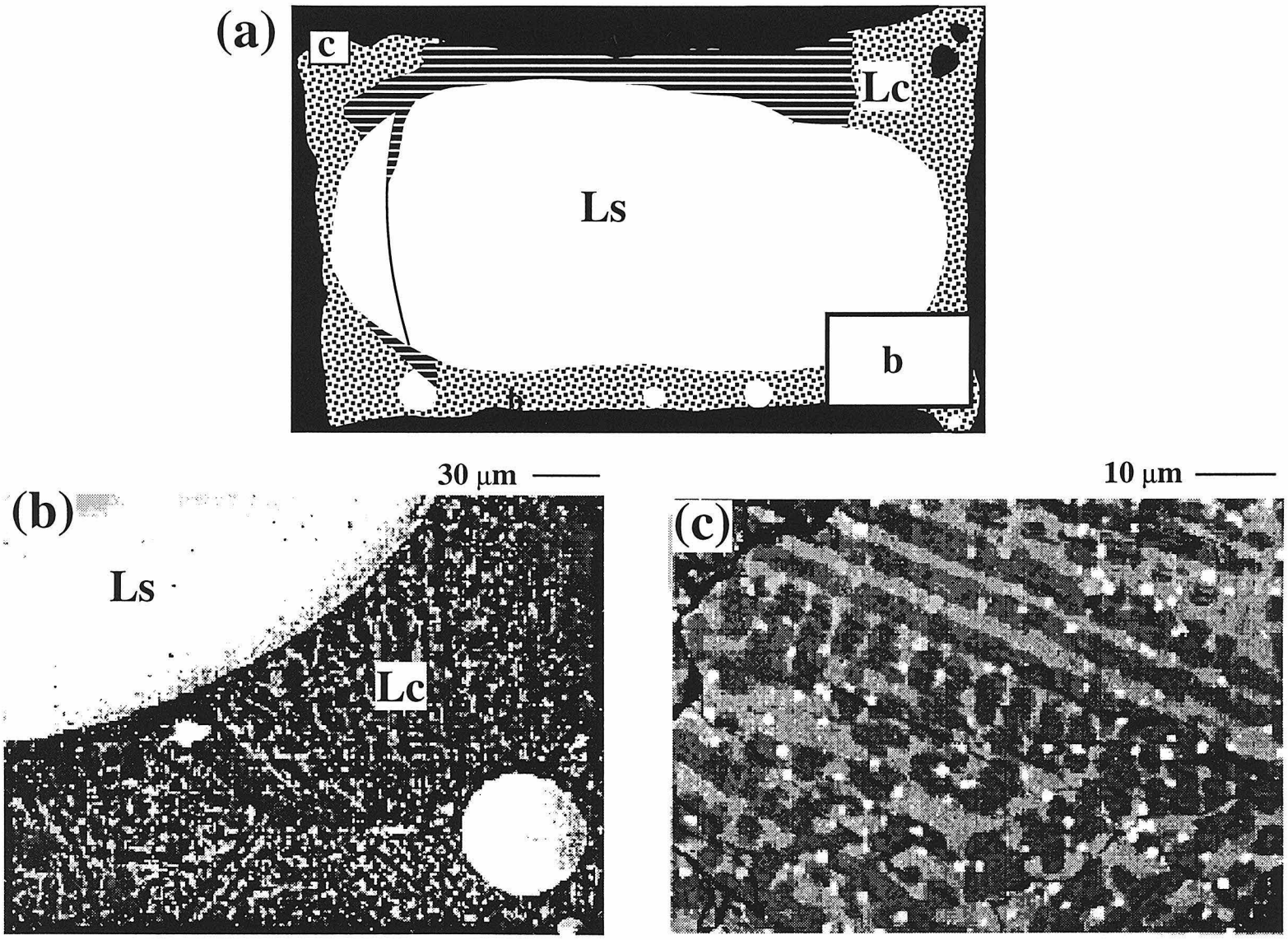
(a)
c
Lc
Ls
b
30 μm
(b)
Ls
Lc
10 μm
(c)

Fig. 4. Back-scattered electron photomicrographs, showing phases in some experimental products (Table 2). (a) Run L71. The image shows that the distribution of the quenched immiscible liquids is similar to that in Fig. 3, but the texture of the carbonate dendrites is somewhat different. The large euhedral crystals (to 50 μm) are olivine. (b) Run L169. It contains a layer of quenched carbonate-rich liquid above large light-colored clinopyroxene (~100 μm) and smaller dark olivine crystals (~30 μm). (c) Run L153. Rounded calcite crystals (light colored, to 100 μm) occur in quenched carbonate-rich liquid.

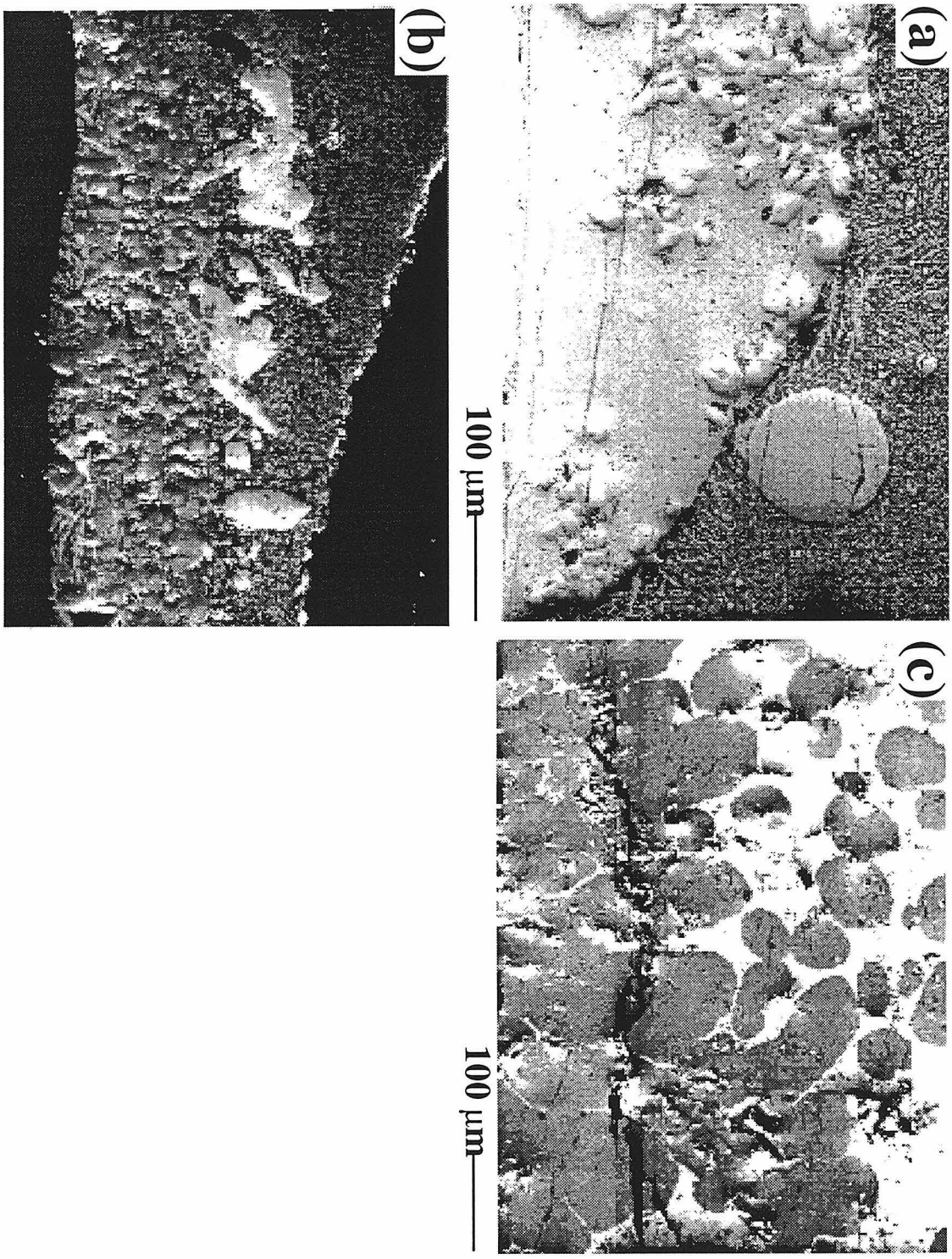
(a)
100 μm
(b)
100 μm
(c)
100 μm

The presence of olivine (Ol), clinopyroxene (Cpx), spinel (Sp), and calcite was confirmed using the SEM. Olivine appears as euhedral crystals up to 50 μm (Figs. 4a and b), generally distributed in the silicate-rich bead, but also along the boundary between two liquid phases, as shown in Fig. 4a. Figure 4b illustrates olivine crystals (dark) accumulated at the lower portion of the sample charge. Clinopyroxene in Fig. 4b occurs as large euhedral crystals (light colored, ~100 μm) above the olivine layer. Round calcite crystals are shown in Fig. 4c (light colored, up to > 100 μm). They sometimes formed a layer at the bottom of a capsule, but the individual grains can still be distinguished under the microscope (cf. Fig. 4c). Criteria for identification of similar stoichiometric $CaCO_3$ phases as crystalline calcite rather than quenched immiscible carbonate liquid (Kjarsgaard and Hamilton 1989) have been presented by Lee et al. (1994) and Lee and Wyllie (1996). Spinel crystals occur in most experiments (Table 2), suspended in liquid or as inclusions in other minerals, but they are too small (~several μm) to be clearly seen in Fig. 4. It was difficult to find unambiguous evidence for the expected vapor phase (from known phase relationships in many silicate-carbonate composition joins, e.g. Lee et al. 1994), and it appears that the vapor migrates into the graphite liner.

EXPERIMENTAL RESULTS

Experimental results listed in Table 2 and plotted in Fig. 5 show the phase fields intersected by the composition join AB (Fig. 2) as a function of pressure and temperature. Selected immiscible liquid compositions normalized to a CO_2-free basis are listed in Table 3, and plotted in Figs. 6-8 to define the two-liquid field projected from CO_2 onto the plane $(SiO_2 + Al_2O_3 + TiO_2)$-$(CaO + MgO + FeO^*)$-$(Na_2O + K_2O)$. Three-dimensional relationships are shown as in Fig. 2b, with CaO and (MgO + FeO*) separated as apices of a tetrahedron. Figure 6 shows the quality of the analytical data used to define the miscibility gap, Fig. 7 shows the effect of pressure on its extent, and Fig. 8 shows the

effect of temperature. The experimental points plotted in Fig. 9 (Table 2) define the 1.0 GPa liquidus piercing point P between calcite and olivine on the join NEPH-CC (Fig. 2).

Nephelinite-Dolomite-Na_2CO_3

The phase fields intersected by the composition join A-B (Fig. 2b) for four pressures are given in Fig. 5a (1.0, 1.5, 2.0, and 2.5 GPa). These results, and the analyzed compositions of immiscible liquid pairs, are used to constrain the three intersecting surfaces in Fig. 5b. The surfaces define the positions of the phase boundaries in Fig. 5a, separating six phase fields. Minor amounts of spinel are present in all experiments except in run L75 (mix #1, 1.0 GPa, 1200° C; Table 2), which suffered some iron loss (see below).

The boundary of the miscibility gap is shown by the heavy line in Fig. 5a, and the heavy-shaded surface in Fig. 5b. The size of the miscibility gap at each pressure decreases with increasing temperature, and it also decreases between 2.0 and 2.5 GPa with no obvious changes between 1.0, 1.5 and 2.0 GPa. With decreasing temperature, the minerals olivine and then clinopyroxene are precipitated, the phase boundaries decreasing in temperature with decreasing pressure. If we assume that spinel is a quench mineral, then Fig. 5 shows the changing positions of a piercing point on the field boundary between the olivine liquidus and the miscibility gap.

Figure 6 shows results for 1.0 GPa at 1200° C, with one result at 1225° C. Figure 6a shows individual analyses from experiments with mixes #1 and #3, and Fig. 6b shows the tie-lines connecting average values. The analyses for each silicate liquid are more tightly clustered than those for the coexisting carbonate-rich liquid. The silicate glasses are more homogeneous than quenched carbonate-rich liquids, and larger areas of Ls (twice as much as for Lc) were available for analysis. Run L75 contains only immiscible liquids, but the tie-line does not pass through the starting mix #1; the liquid analyses are deficient in

Fig. 5. Phase fields intersected by the join NEPH-Dol-CC, along line AB in Fig. 2. Positions of mixes #1, #2, #3 and #5 are also denoted. (a) Isobaric phase fields at 2.5, 2.0, 1.5 and 1.0 GPa. Ol: olivine, Sp: spinel, Cpx: clinopyroxene, Ls: silicate-rich liquid, Lc: carbonate-rich liquid. (b) Phase volumes in P-T-X space based on the results shown in (a). The experiments on the 2.5- and 1.0-GPa planes are indicated by the open and solid squares, and the 2.5 GPa boundaries are shown by heavy dashed curves. The three intersecting surfaces define the miscibility gap (darkest shading), the Ol-in (lightest), and the Cpx-in (intermediate) field boundaries.

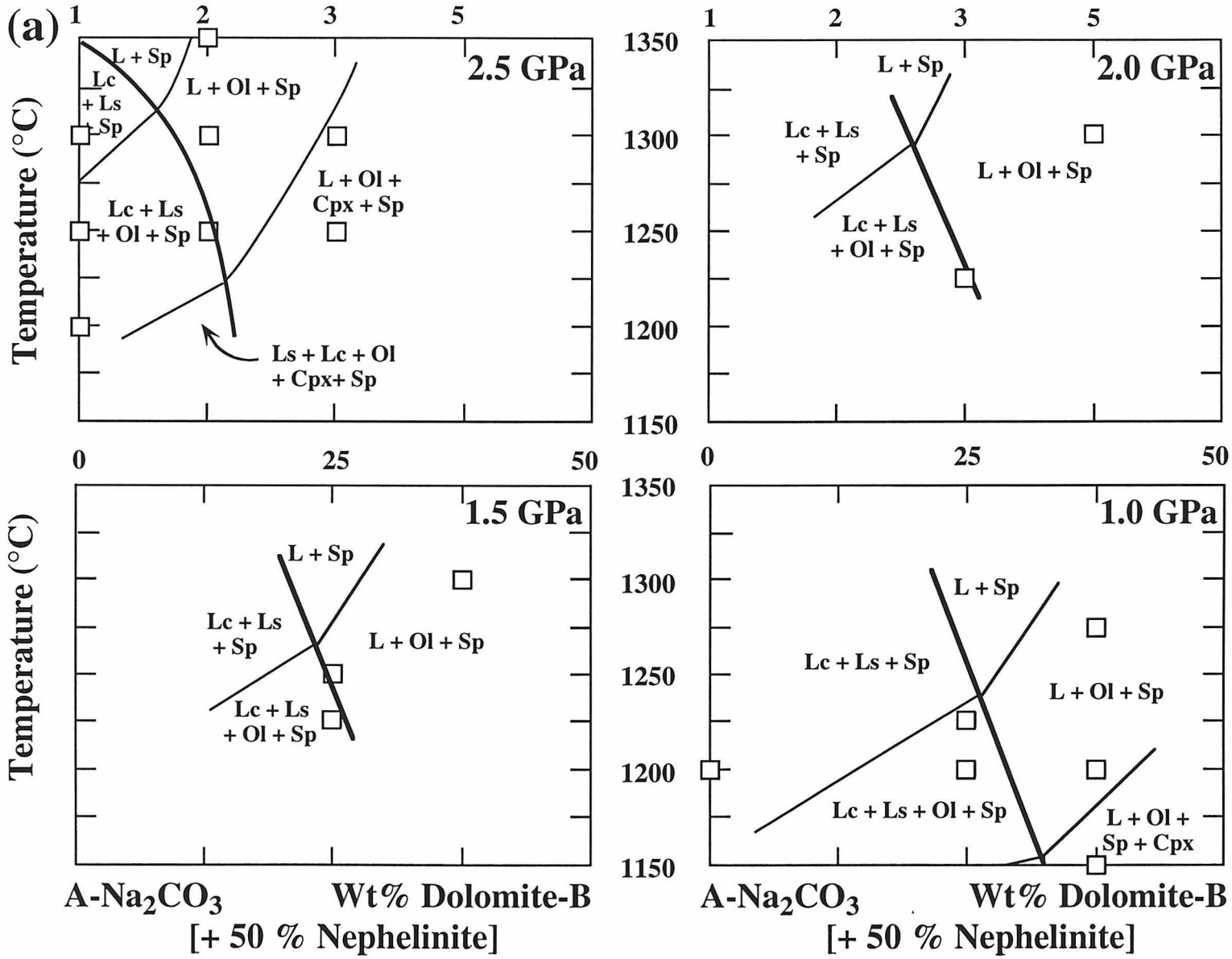
(a)
2.5 GPa
L + Sp
Lc + Ls + Sp
L + Ol + Sp
L + Ol + Cpx + Sp
Lc + Ls + Ol + Sp
Ls + Lc + Ol + Cpx+ Sp
2.0 GPa
L + Sp
Lc + Ls + Sp
L + Ol + Sp
Lc + Ls + Ol + Sp
1.5 GPa
L + Sp
Lc + Ls + Sp
L + Ol + Sp
Lc + Ls + Ol + Sp
1.0 GPa
L + Sp
Lc + Ls + Sp
L + Ol + Sp
Lc + Ls + Ol + Sp
L + Ol + Sp + Cpx
Temperature (°C)
1350
1300
1250
1200
1150
0
25
50
A-Na2CO3
Wt% Dolomite-B
[+ 50 % Nephelinite]

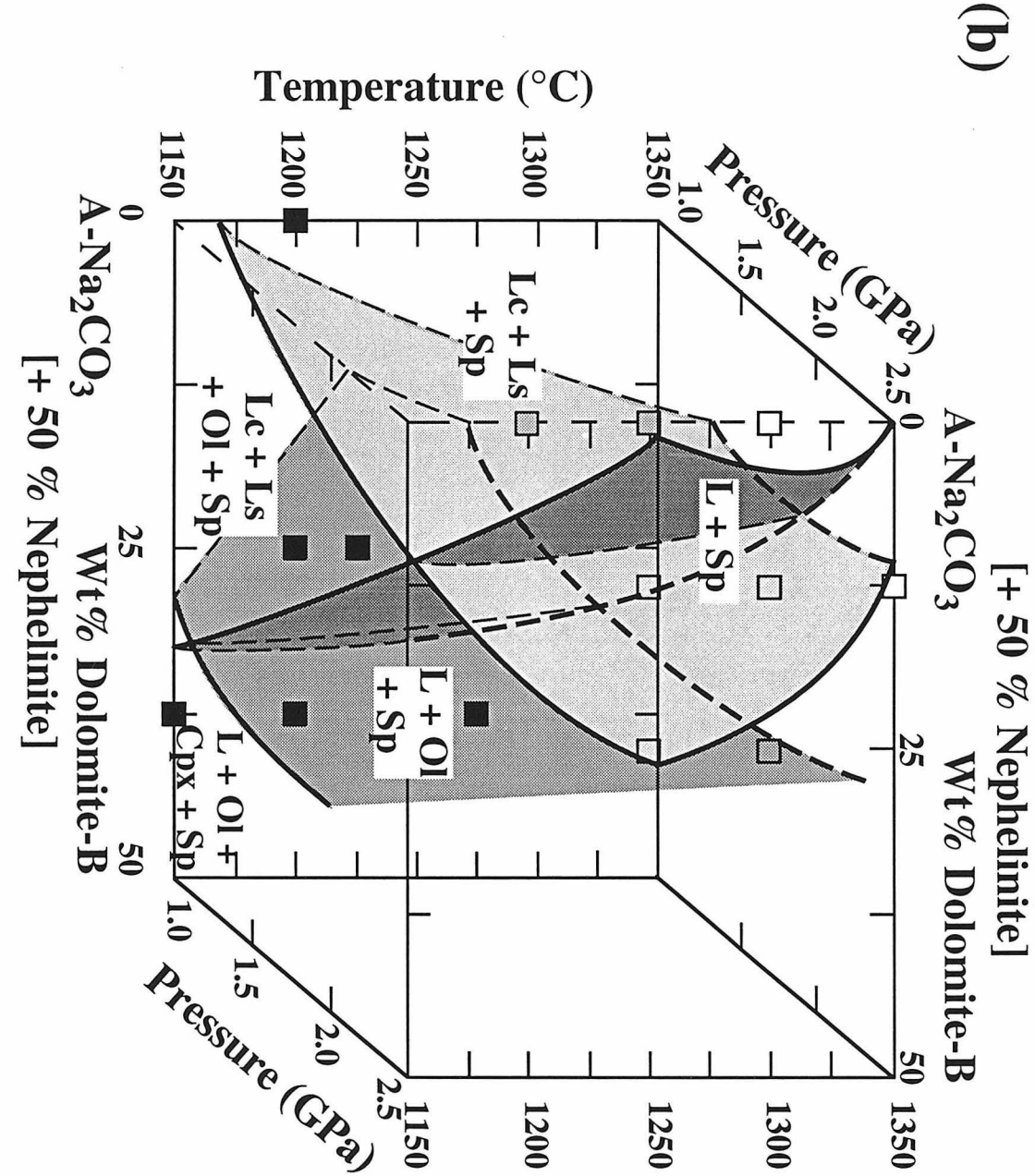
(b)
[+ 50 % Nephelinite]
A-Na2CO3
Wt% Dolomite-B
Pressure (GPa)
Temperature (°C)
L + Sp
Lc + Ls + Sp
Lc + Ls + Ol + Sp
L + Ol + Sp
L + Ol + Cpx + Sp
1.0
1.5
2.0
2.5
1150
1200
1250
1300
1350
0
25
50

Table 3. Compositions of quenched melts from selected experiments

Run #	TL105		TL116		TL118		L65		L75		L75†	
Phase	Ls(13)	Lc(15)	Ls(11)	Lc(13)	Ls(11)	Lc(10)	Ls(5)	Lc(5)	Ls(5)	Lc(5)	Ls	Lc
SiO_2	31.8	13.4	33.7	9.5	33.4	12.7	38.3	7.6	44.3	3.9	40.4	3.7
TiO_2	2.1	1.1	2.4	1.0	2.5	1.3	3.2	1.2	2.9	0.7	2.6	0.6
Al_2O_3	8.4	3.3	9.7	1.9	11.6	3.1	15.0	1.9	13.3	0.9	12.1	0.8
FeO*	10.2	6.9	10.3	6.0	8.6	6.8	4.8	2.8	1.2	0.8	9.8	7.0
MgO	9.0	8.6	7.6	6.6	8.3	9.8	8.1	11.6	8.3	7.9	7.6	7.5
CaO	6.3	11.3	5.8	11.7	9.4	19.4	12.0	35.5	4.5	14.2	4.0	13.2
Na_2O	31.6	54.3	29.8	61.5	26.6	46.0	18.1	38.3	25.0	69.0	22.8	64.8
K_2O	0.5	1.0	0.5	1.0	0.5	0.9	0.5	1.1	0.4	1.1	0.4	1.1
P_2O_5	—	—	0.3	1.1	—	—	—	—	0.1	1.4	0.1	1.2

All reported compositions are in wt%, normalized on a CO_2-free basis. Abbreviations as in Table 2; number of analyses used to calculate the mean composition are in parentheses.

†Analyses of the silicate- and carbonate-rich liquids after correcting for iron loss; see discussion in text.

Fig. 6. Chemical analyses of coexisting silicate- and carbonate-rich liquids at 1.0 GPa. (a) Individual measurements for runs L75 (mix #1) and L65 (#3), showing the range for each quenched liquid. The representative analyses for olivine (Ol) and spinel (Sp) of run L65 are also indicated. (b) Average liquid compositions for runs L75 and L65 (Table 3), with tie-lines connecting the immiscible liquid pairs. Note that some iron was lost to the Pt capsule in run L75 (compare the tie-line and mix #1), and the solid squares (L75†) represent the corrected values for L75. The phase assemblage in run L65 is illustrated by the tie-figure Ls-Lc-Ol-Sp. The heavy curve passing through the average compositions defines the miscibility gap at 1200° C and 1.0 GPa. Also shown in the figure are the immiscible liquids of run L77 (+ Ol + Sp) at 1225° C from mix #3. (c) Liquid compositions, tie-lines and tie-figure from (b) expressed in the tetrahedron (Fig. 2b).

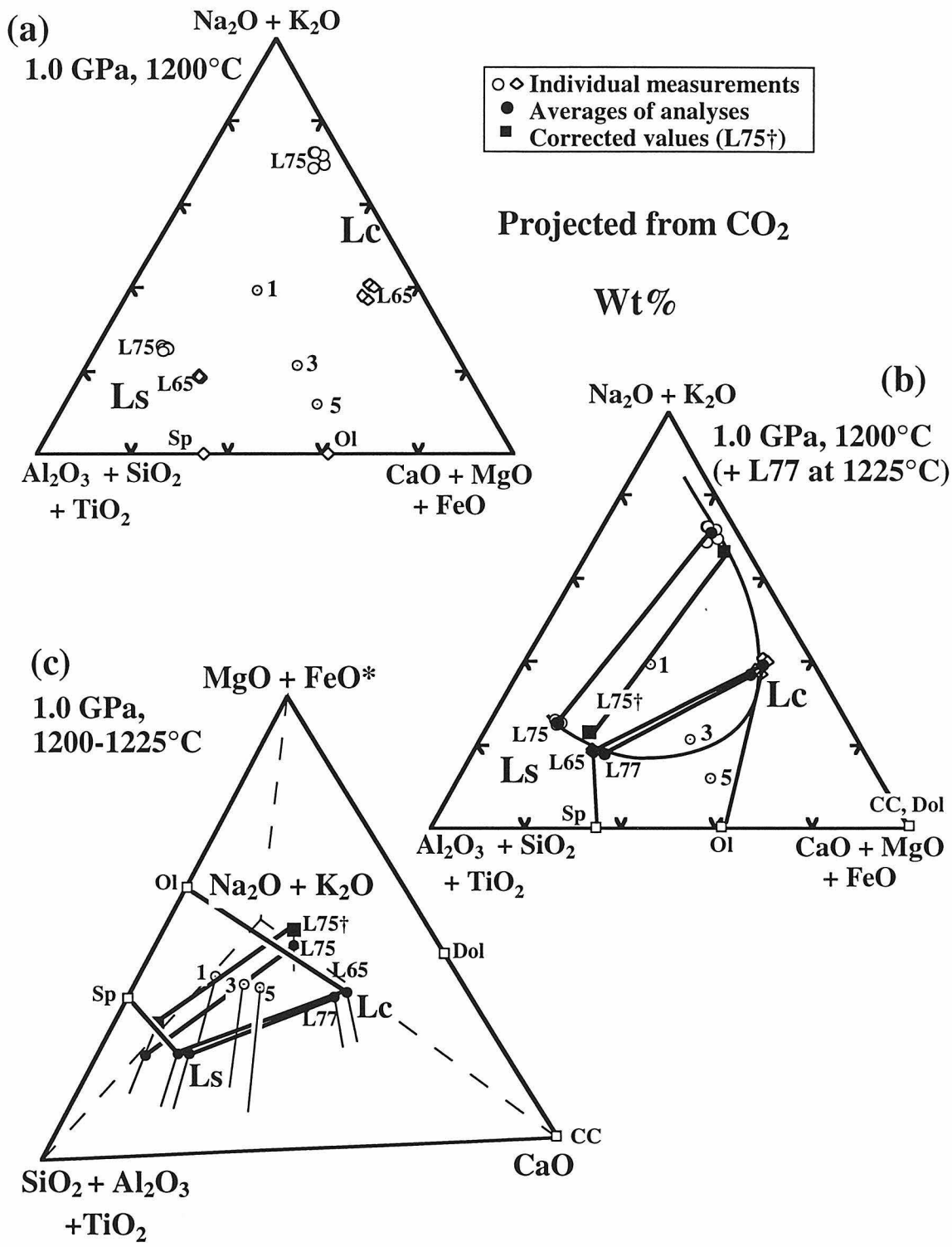
(a)
1.0 GPa, 1200°C
Na2O + K2O
Al2O3 + SiO2 + TiO2
CaO + MgO + FeO
Individual measurements
Averages of analyses
Corrected values (L75†)
Projected from CO2
Wt%
L75
Lc
L65
Ls
Sp
Ol
1
3
5
(b)
1.0 GPa, 1200°C
(+ L77 at 1225°C)
L75†
L77
CC, Dol
(c)
1.0 GPa,
1200-1225°C
MgO + FeO*
SiO2 + Al2O3 +TiO2
CaO
Dol
CC

iron, indicating that the liquid reached the Pt capsule through a crack in the graphite crucible. In a correction procedure, the estimated lost FeO (~6 wt%) was re-allocated into the liquids, using the partition coefficient of iron between Ls and Lc from the original analyses (L75, Table 3). The corrected results (L75† - solid squares in Figs. 6b and c, Table 3) provide a tie-line which does pass through mix #1 (the amount of spinel, whether primary or quench, is volumetrically insignificant for the calculation).

For run L65, mix #3, the immiscible liquids were joined by spinel and olivine, so the tie-line does not pass through mix #3; the phase assemblage is indicated by the tie-figure Ls-Lc-Ol-Sp in Fig. 6b, with the distribution of the phases in the sample charge similar to that shown in Fig. 4a (L71 - mix #3, 2.0 GPa, 1225° C; Table 2). The results at 1225° C for the same mix (tie-line L77) are almost indistinguishable from those of run L65.

Experiments with mix #5 at 1.0 GPa were interpreted as one liquid with minerals, olivine and spinel at higher temperatures, joined by aluminous clinopyroxene at 1150° C. Figure 4b shows the minerals in the 1150° C experiment, with the liquid quenched to intergrowths of calcite, nyerereite laths, and irregular silicate-rich patches but with no evidence for immiscible liquids. The liquids from the 1275 and 1200° C experiments were quenched to a glassy silicate host with carbonate-rich globules (up to 30 μm) throughout the charge. There was no segregation or agglomeration of the carbonate droplets as in unambiguous two-liquid experiments. This texture is what would be expected during quenching, and we conclude that the experiments did not produce immiscible liquids. The similar texture was observed in the experiments with the same mixture at 1.5 and 2.0 GPa.

Figure 6b shows the 1200° C isotherm at 1.0 GPa on the miscibility gap liquidus dome separating the fields for silicate-rich (Ls) and carbonate-rich (Lc) liquids, drawn through the average liquid analyses. It closes between mixes #3 and #5 because no liquid immiscibility was found in experiments with mix #5. The isotherm is divided into two segments, a segment without minerals (except for probable quench spinel), and a segment

where the liquids coexist with olivine and spinel. The compositions of immiscible liquids in the latter segment are therefore not coplanar with the mixture line 1-3-5 (AB in Fig. 2b), but are situated lower within the tetrahedron, as illustrated in Fig. 6c (cf. Fig. 2b). Mixes #1, #3 and #5 are located in space by the thin lines projected through (MgO + FeO*) to the base of the tetrahedron. The liquid compositions are similarly located. The correction of original analyses L75 by addition of FeO is shown by the position of L75†.

The results in Fig. 7 show that the size of the miscibility gap decreases with increasing pressure at constant temperature, 1200-1225° C, nearly isothermal. Figure 7a compares the 1200° C isotherm for the miscibility gap from Fig. 6b with 1225° C tie-lines L70 and L71 from 1.5 GPa and 2.0 GPa, respectively. The sub-parallel tie-lines are located inside the miscibility gap, but the difference is close to the analytical errors. The tie-line for run TL32 at 2.5 GPa and 1200° C (Fig. 7) is located well inside the 1.0 GPa miscibility gap.

The pressure effect is clearly displayed in the tetrahedron by immiscible liquid compositions obtained from mix #3 at three pressures. At 1200-1225° C, all of the liquids coexist with olivine and spinel. The 1.0 GPa tie-line L65 from Fig. 6c, and the 1.5 and 2.0 GPa tie-lines (L70 and L71, respectively) from Fig. 7a are approximately coplanar, lying close to the triangular slice X-(SiO_2 + Al_2O_3 + TiO_2)-(MgO + FeO*), which contains mix #3 and the minerals, Ol and Sp. At 2.5 GPa mix #3 is situated outside of the miscibility gap (Figs. 5a, 8), indicating that the gap closes below mix #3 in Fig. 7b. The line through the liquid compositions in Fig.7b shows the isothermal polybaric two-liquid surface decreasing in width with increasing pressure.

The effect of temperature at 2.5 GPa (Fig. 5a; Table 3) is shown in Fig. 8 by three isotherms, consolidating and amplifying the partial phase diagram published by Baker and Wyllie (1990). The isotherms define the classic dome shape of a liquid miscibility gap. All of the liquids coexist with spinel ± olivine (Fig. 5a). At 1300° C using mix #1, immiscible silicate- and carbonate-rich melts coexist with spinel. Experiments with mix

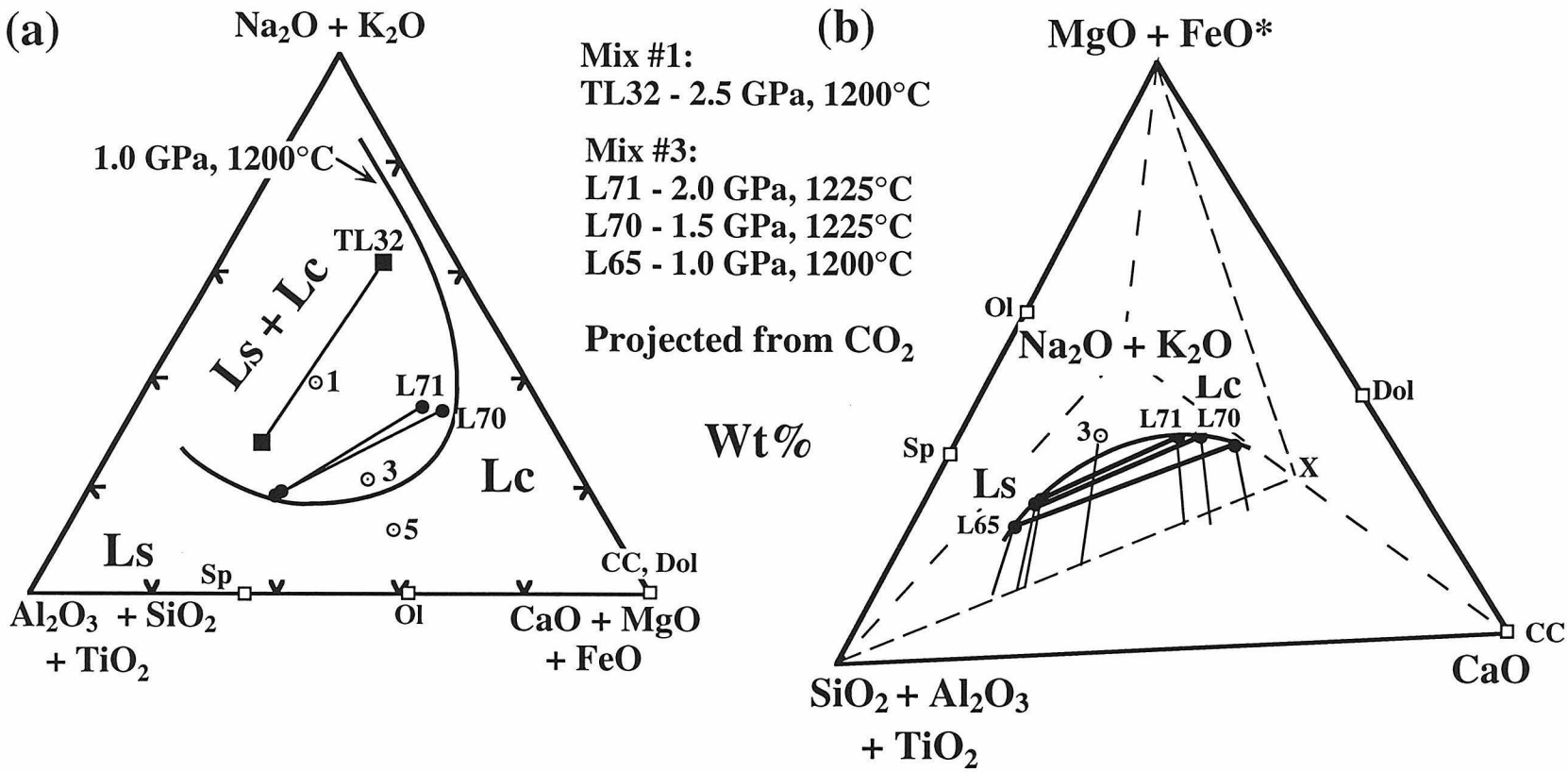

Figure 7. Comparison of two-liquid compositions at various pressures. (a) The two liquids of TL32 are placed well inside the two-liquid isotherm at 1.0 GPa and 1200° C (Fig. 6b), whereas those of L70 and L71 are slightly inside the isotherm. (b) The two liquids of L65 are compared with those of L70 and L71 in the tetrahedron. All the two-liquid pairs lie close to the triangular slice X-(MgO + FeO)-(SiO_2 + Al_2O_3 + TiO_2) including mix #3, olivine and spinel. The heavy curve illustrates the polybaric miscibility gap at constant temperature (1200-1225° C).

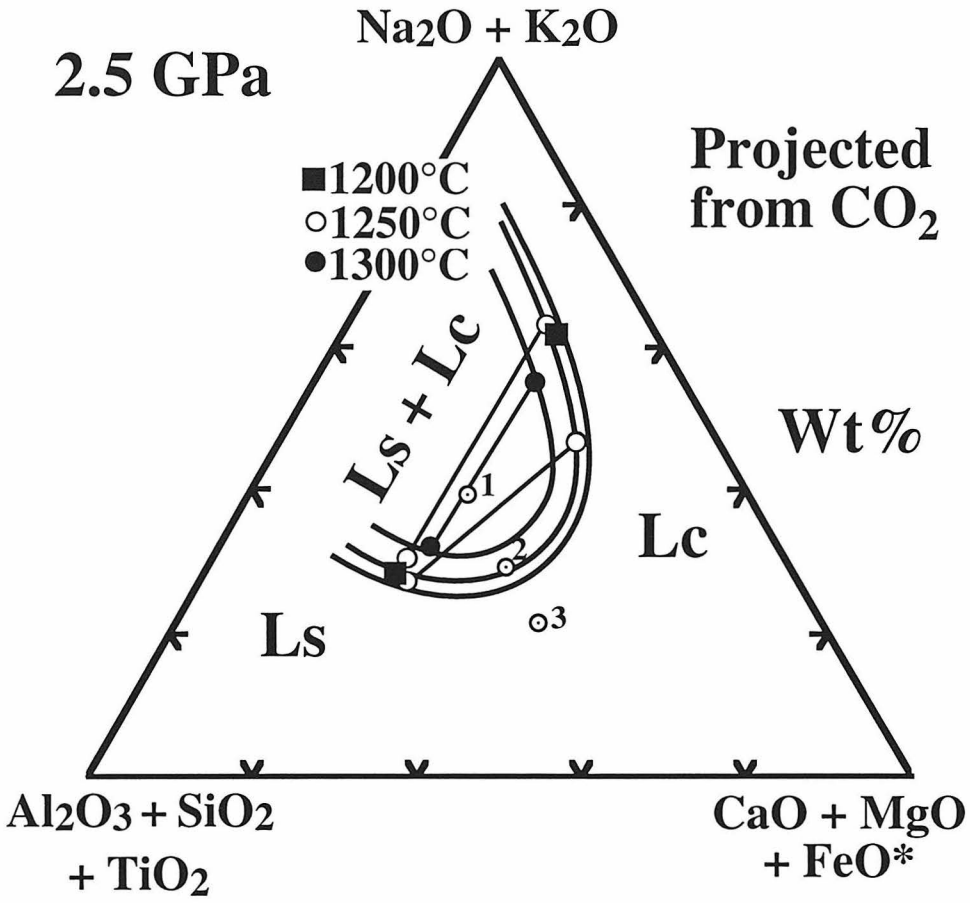

Figure 8. Two-liquid compositions at 2.5 GPa, based on runs TL105, TL116, TL118 and TL32 (see Table 2; compositions listed in Table 3, except for TL32). These results define the two-liquid isotherms (heavy curves) at 1300, 1250 and 1200° C. Notice that all experiments contained spinel ± olivine. Mixes #1-3 are also plotted.

#2 contain a single liquid and olivine + spinel at 1350° C and 1300° C, respectively; a second liquid is added at 1250° C. None of the experiments using mix #3 exhibit evidence of immiscible liquids. A single liquid coexists with minerals, olivine + spinel at 1400° C, with clinopyroxene in addition at 1300 and 1250° C.

The orientation of the tie-lines shows that alkalis (Na_2O) are strongly partitioned into the carbonate-rich liquid, while TiO_2 and Al_2O_3 are partitioned into the silicate-rich liquid (Table 3). For the most Na_2O-rich bulk composition (mix #1), MgO is distributed nearly evenly between the two liquids, while CaO is partitioned into the carbonate-rich melt and FeO* is enriched in the silica-rich liquid. At 1200° C, all of the coexisting liquids are sodic, with Na_2O contents ranging from ~19 wt% to ~63 wt% (all on a CO_2-free basis).

Nephelinite-$CaCO_3$ at 1.0 GPa

Figure 2b shows that the join NEPH-CC is geometrically far removed from the triangle NEPH-Dol-NC. The experiments at 1.0 GPa listed in Table 2 and plotted in Fig. 9 show no immiscible liquids. No spinel is shown in Fig. 9 because we conclude that the trace of spinel present in all experiments was formed during the quench. The results define liquidi for olivine and calcite, separated by a piercing point P with composition near $NEPH_{50}CC5_{50}$ at 1235° C.

The experiment with mix #6 at 1250° C has a layer of calcite at the bottom, with a curved contact against the liquid. The 1200° C experiment is illustrated in Fig. 4c. In addition to the layer of calcite and the rounded calcite crystals in the overlying liquid, there are just a few olivine crystals, indicating that it is near a field boundary. The experiment with mix #8 at 1250° C consists mostly of quenched liquid, with a small amount of olivine at the bottom. The 1225° C experiment with mix #7 contains calcite, olivine and clinopyroxene accumulated at the bottom of the capsule. Most of the calcite coalesced to form a single layer, intergrown with some olivine grains, and with a few clinopyroxene

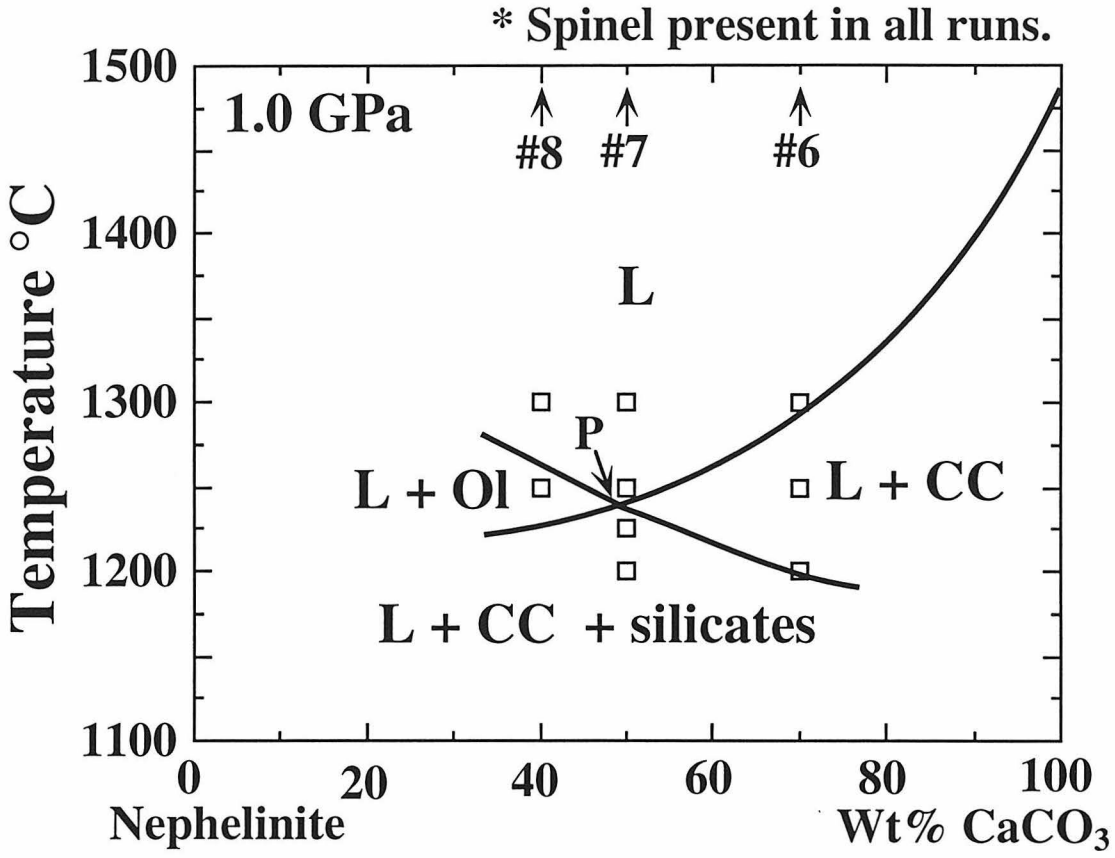

Figure 9. Phase fields intersected by the join NEPH-CC (Fig. 2) at 1.0 GPa, showing no liquid immiscibility. Spinel is present in all experiments, but is interpreted as a quenched product. The calcite liquidus intersects the olivine liquidus at point P (1235° C, 50 % NEPH) which defines a liquid composition for the coprecipitation of olivine and calcite. The melting temperature of calcite is based on Irving and Wyllie (1975). The phase relationships underneath P involve crystallization of calcite, olivine and clinopyroxene, and are indicated by the field L + CC + silicates.

crystals above it. In the 1200° C experiment, a layer of interlocked calcite, olivine and clinopyroxene occupies about half the capsule beneath a layer of quenched liquid.

Phase geometry at 1.0 GPa

Experimental results from the two composition joins NEPH-CC and A-B (across NEPH-Dol-NC) in Fig. 2b intersect only limited parts of the overall phase relationships in the system, but they begin to show the topology of two key petrological features in the system. These are the miscibility gap between silicate and carbonate liquids, and the liquidus field boundary separating primary silicates from carbonates.

Figure 10 shows the compositions of coexisting liquids at 1.0 GPa and 1200° C, transferred from Figs. 6 and 7. Figure 10a reproduces the projected isotherm from Fig. 7b, and Fig. 10b shows that the liquid compositions are not coplanar. Liquids without coexisting minerals remain near the triangle NEPH-Dol-NC (light shaded area), but with precipitation of minerals the liquids are driven to compositions below this triangle (dark shaded area) as indicated in Figs. 6c and 7b. The change occurs at tie-line T_2 between mix #1 and mix #3 in Fig. 6c. The geometry can be related to Figs. 6b and c by means of the four pairs of dashed lines 1 to 4 in Fig. 10b. Pairs 2 and 4 correspond to the immiscible liquids L75† and L65 in Fig. 6b. Pair 3 shows the projection of the tie-line T_2 to the triangular base (Fig. 10a). The dashed-line pair 1 for the hypothetical tie-line T_1 is produced by extrapolating the measured immiscible liquid boundaries in Figs. 6b and c and 10b to meet the CaO-free side of the tetrahedron. The line T_1 projects within the triangle in Fig. 10a because although it is CaO-free, it contains (MgO + FeO*).

The point P on the join NEPH-CC in Fig. 10 is the piercing point at about 1235° C (Fig. 9) on the polythermal liquidus field boundary for the coprecipitation of olivine and calcite. P has been connected by a line to the corresponding point on the tetrahedron's edge (SiO_2 + Al_2O_3 + TiO_2)-CaO in Fig. 10b (point Q), based on the piercing point determined

Fig. 10. The miscibility gap at 1.0 GPa and 1200° C in NEPH-Dol-NC (Fig. 6b), and a liquidus field boundary between silicates and calcite passing through the join NEPH-CC. (a) The miscibility gap is divided into two parts: the fields for the coexistence of two liquids with minerals (dark area), and without minerals (light). The miscibility gap terminates at the hypothetical, CaO-free tie-line T_1. The tie-line T_2 locates the boundary where minerals start to precipitate. The short heavy curve from Q passing through P indicates a liquidus field boundary for the coprecipitation of silicates and calcite. (b) The same features as in (a) projected into the tetrahedron. The miscibility gap is projected through (MgO + FeO*) to the dashed curve on the basal triangle, with four pairs of dashed lines (numbered 1 to 4) showing the position of the isotherm in space. The heavy curve for the liquidus field boundary situates close to the alkali-free triangle of the tetrahedron.

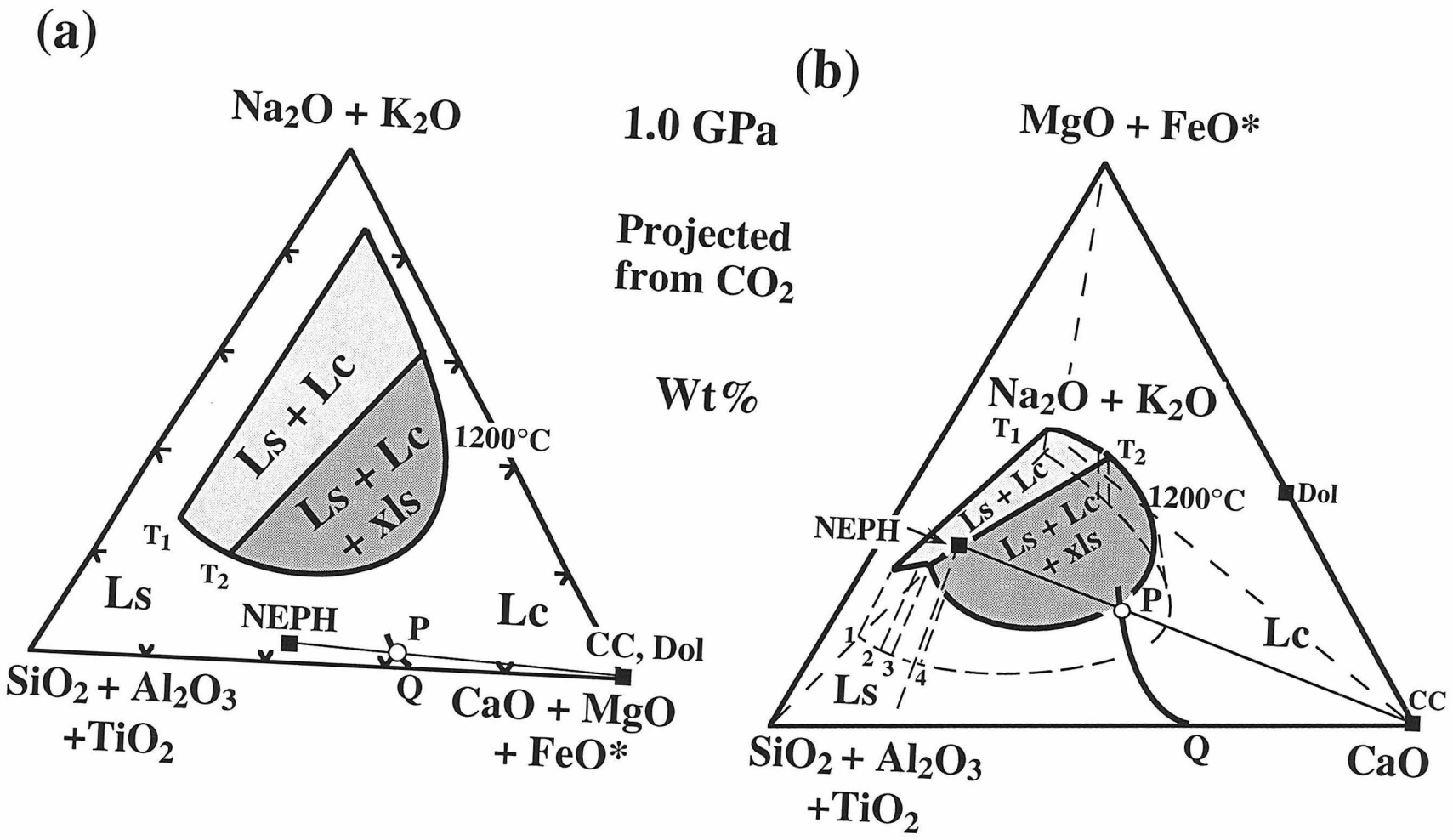
(a)
$Na_2O + K_2O$
1.0 GPa
Projected from CO_2
Wt%
Ls + Lc
Ls + Lc + xls
1200°C
T_1
T_2
Ls
NEPH
P
Lc
CC, Dol
$SiO_2 + Al_2O_3 + TiO_2$
Q
$CaO + MgO + FeO^*$
(b)
$MgO + FeO^*$
$Na_2O + K_2O$
T_1
T_2
Ls + Lc
Ls + Lc + xls
1200°C
Dol
NEPH
P
Lc
1
2
3
4
Ls
CC
$SiO_2 + Al_2O_3 + TiO_2$
Q
CaO

between calcite and quartz or wollastonite (depending on the pressure) in the join $CaSiO_3$-$CaCO_3$ (Huang et al. 1980). This line is situated on a liquidus surface between the volumes for primary silicate and carbonate within the tetrahedron, a surface which meets the miscibility gap surface in a field boundary.

Variations in size of liquid miscibility gap

The size of a liquid miscibility gap varies as a function of temperature, pressure and bulk composition. It normally decreases with increasing temperature (e.g. Freestone and Hamilton 1980; Baker and Wyllie 1990), as indicated in Fig. 8. Figure 7 shows that it decreases with increasing pressure in this system, whereas Lee and Wyllie (1992a, 1996) showed that it increases with increasing pressure in the MgO-free system Na_2O-CaO-Al_2O_3-SiO_2-CO_2, on the base of the tetrahedron (Figs. 2b and 7b). At a given pressure and temperature, Fig. 1 shows that the miscibility gap is considerably larger in the MgO-free system (B) than in the MgO-bearing system (A). Kjarsgaard and Peterson (1991) showed that the peralkalinity, (Na + K)/(Al + Fe^{3+}), of a system can also affect the compositions of immiscible liquids, changing the size of the miscibility gap.

CARBONATITE LIQUIDS FROM PERIDOTITES

In order to evaluate the possible involvement of silicate-carbonate liquid immiscibility in mantle magmatic processes, we present here a compilation of the phase relationships of carbonated mantle peridotites, and the compositions of liquids derived from them.

Phase relationships of carbonated peridotites

A selection of reactions for CO_2-bearing lherzolite, harzburgite, wehrlite and websterite is shown in Fig. 11, and five melting curves are among the array of reactions around invariant point Q. The curves are based on studies in the model system CaO-MgO-SiO_2-CO_2(-H_2O) (e.g. Eggler 1974, 1976, 1978; Newton and Sharp 1975; Wyllie and Huang 1975, 1976; Wyllie 1978; Brey et al. 1983; Wyllie et al. 1983; Woermann and Rosenhauer 1985; White and Wyllie 1992), and on natural peridotite compositions or assemblages of minerals separated from peridotites (e.g. Olafsson and Eggler 1983; Wyllie and Rutter 1986; Wyllie 1987; Wallace and Green 1988; Falloon and Green 1989; Dalton and Wood 1993a). The positions of the solidus curves and the melting reactions depend on the relative compositions of subsolidus clinopyroxene, dolomitic carbonate and the liquid at the solidus.

The point Q is located between 2.0 and 2.2 GPa, 1050-1090° C in natural peridotite compositions (Wyllie and Rutter 1986; Wyllie 1987; Wallace and Green 1988; Falloon and Green 1989). The precise locations of the phase boundaries vary with bulk composition, and the subsolidus reactions [A] and [G] are not univariant for rocks. Peridotite names are given in Fig. 11, and the rock reactions are represented by the following univariant reactions in the model system (where "enstatite" and "diopside" refer to solid solutions).

The carbonation reaction:

forsterite + diopside + CO_2 = dolomite + enstatite ..... [A]

defines the boundary where CO_2 reacts with lherzolite to form dolomite. Subsolidus carbonate in reaction [A] varies from calcic dolomite to magnesian calcite composition (Wyllie et al. 1983; Dalton and Wood 1993b).

The reaction [A] terminates at Q where the assemblage begins to melt. At lower pressures, lherzolite with CO_2 melts by reaction:

forsterite + enstatite + diopside + CO_2 = liquid ..... [B]

which passes through a singular point at higher pressure, becoming incongruent as it drops toward Q:

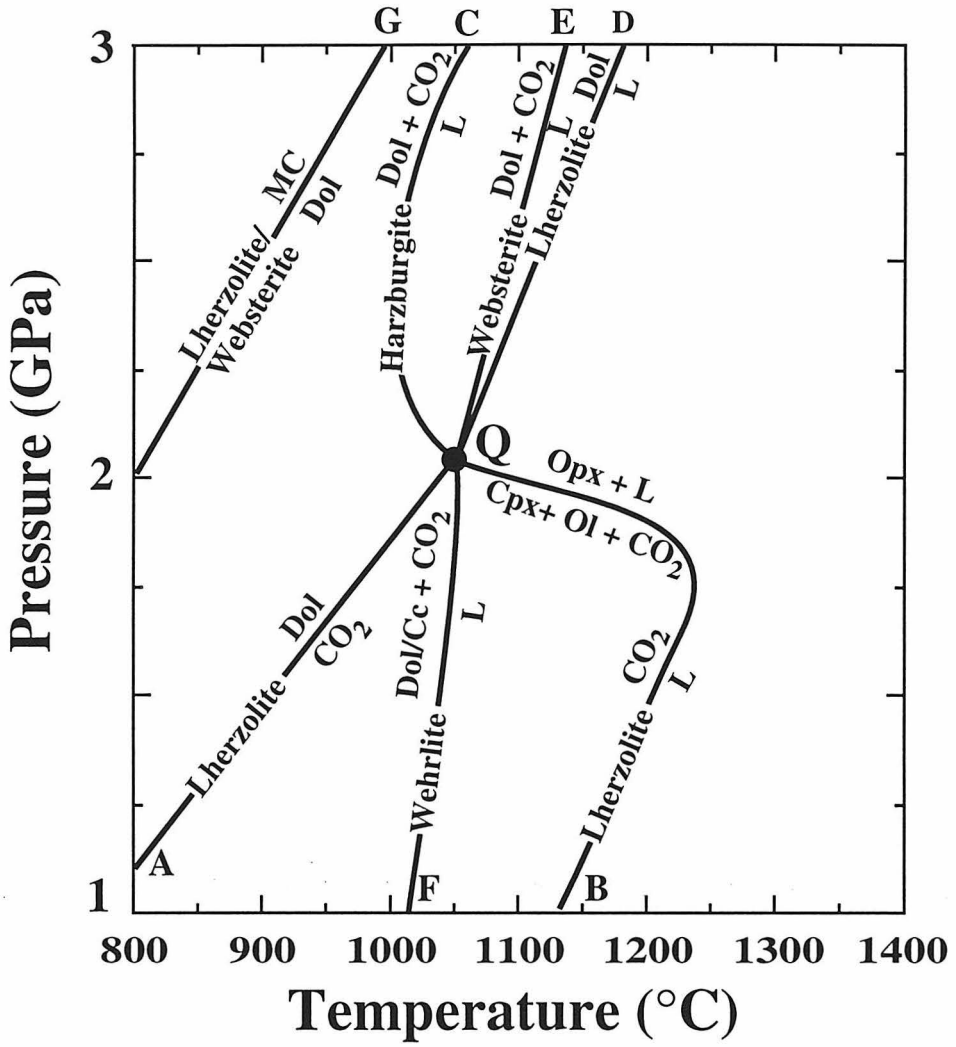

Figure 11. Reaction boundaries for carbonated peridotite. Q is the invariant point involving olivine (Ol), orthopyroxene (Opx), clinopyroxene (Cpx), dolomite/magnesian calcie (Dol/Cc), liquid (L) and vapor, and is located between 2 and 2.2 GPa at 1050-1090° C in natural peridotite compositions. Emanating from Q are the carbonation reaction for CO_2-lherzolite (curve A), the four vapor-saturated solidi for CO2-lherzolite (B), dolomite-harzburgite (C), dolomite-websterite (E) and dolomite/magnesian calcite-wehrlite (F), and the vapor-absent solidus for dolomite-lherzolite (D). Curve G is the subsolidus reaction for converting dolomite-lherzolite/websterite to magnesite (MC)-lherzolite/websterite.

forsterite + diopside + CO_2 = enstatite + liquid .....[B']

With conditions of excess CO_2, all clinopyroxene would react in [A] leaving dolomite-harzburgite, and this would begin to melt by the reaction above Q:

dolomite + olivine + CO_2 = enstatite + liquid ..... [C]

Under normal mantle conditions, however, reaction [A] would use all available CO_2 and at higher pressures dolomite-lherzolite would begin to melt by the vapor-absent reaction rising from Q:

dolomite + enstatite = forsterite + diopside + liquid .....[D]

In the absence of olivine, there is another melting reaction above Q for dolomite-websterite, represented by the model reaction:

dolomite + enstatite + CO_2 = diopside + liquid ..... [E]

The fifth solidus curve is the incongruent melting reaction for wehrlite extending to pressures below Q (reaction 6y in Fig. 10, Wyllie and Huang 1976), investigated by Dalton and Wood (1993a):

forsterite + dolomite/magnesian calcite + CO_2 = diopside + liquid .....[F]

There is another subsolidus reaction at higher pressures converting dolomite-websterite to magnesite-websterite

dolomite + enstatite = magnesite + diopside .....[G]

which is coincident with the conversion of dolomite-lherzolite to magnesite-lherzolite.

There are many other relevant reactions at pressures above Q (Wyllie and Huang 1976, Figs. 5 and 10; Wyllie et al. 1983; Huang and Wyllie 1984, Fig. 7). For example, at pressures somewhat higher than reaction [A] there are subsolidus reactions for the carbonation of harzburgite to form magnesite-harzburgite, and for the conversion of dolomite-harzburgite to magnesite-harzburgite; each subsolidus reaction terminates at a point analogous to Q, with the generation of another array of melting reactions which are related to each other on the silicate-carbonate liquidus field boundary (Wyllie and Huang 1976, Figs. 9-11).

Near-solidus melt compositions

The near-solidus melt compositions for carbonated lherzolite, harzburgite, wehrlite and websterite with CO_2 are coincident at Q, diverging from this common value as the reaction curves for each rock type extend to higher and lower pressures from Q. The compositions of liquids formed at the solidus from carbonated peridotites are located at isobaric near-invariant points on the silicate-carbonate liquidus field boundary, and dominated by the phase relationships in the carbonate system (Wyllie and Huang 1976; Eggler 1978). At pressures above Q, the liquid compositions are carbonatitic, with 1.32-8.16 wt% SiO_2, CaO/MgO $\geq$ 1, alkali carbonates to the extent that alkalis are available in the source rocks, and low water, TiO_2 and FeO/MgO relative to primary basanitic liquids (Wyllie and Huang 1975, 1976; Wyllie 1977; Eggler 1978; Wallace and Green 1988; Baker and Wyllie 1988, unpublished; Thibault et al. 1992; Dalton and Wood 1993a; Sweeney 1994).

Figure 12 compares results from synthetic systems with the compositions of experimentally determined liquids from carbonated peridotites, in terms of the molar percentages of their carbonate components. The temperature minimum on the liquidus and solidus for $CaCO_3$-$MgCO_3$ is IW at 3.0 GPa (Irving and Wyllie 1975), and BW at 1.0 GPa (Byrnes and Wyllie 1981), a shift from 60 % to 70 % $CaCO_3$ with pressure decrease of 2.0 GPa. In the model system CaO-MgO-SiO_2-CO_2 the near-solidus liquid composition for dolomite-lherzolite at 2.7 GPa is W (Wyllie et al. 1983). Liquid compositions for natural dolomite-lherzolite (curve D, Fig. 11) are near D_2-D_3 according to Dalton and Wood (1993a). They are somewhat richer in $MgCO_3$ for harzburgites (curve C, Fig. 11), as shown by D_1 (Dalton and Wood, 1993a) and B (Baker and Wyllie 1988). For carbonate-wehrlites at 1.5 GPa (curve F, Fig. 11), Dalton and Wood (1993a) reported liquids D_5-D_6 greatly enriched in $CaCO_3$.

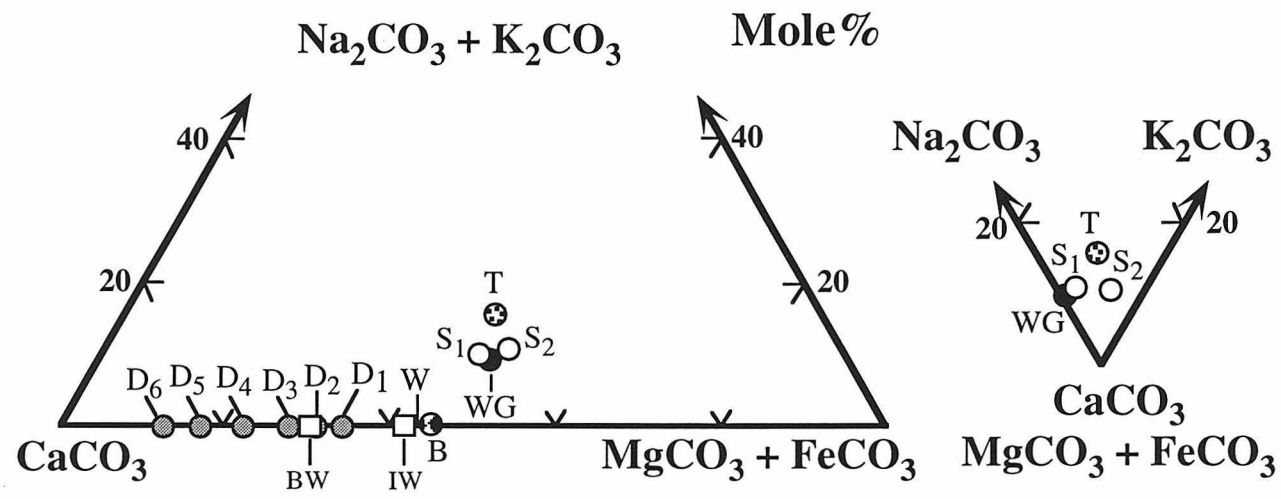

Figure 12. Experimental carbonatitic liquid compositions from synthetic systems and carbonated peridotite assemblages, expressed as carbonate components, mole%. The projection on the left illustrates the liquids discussed in the text ("near-solidus melt compositions"). The projection on the right shows the four alkali-bearing liquids with various Na/K.

Only four lherzolites produced liquids with more than trivial alkali contents, and these contained amphibole or phlogopite. The liquids reported between 2.2 and 3.2 GPa (WG - Wallace and Green 1988; T - Thibault et al. 1992; S_1 and S_2 - Sweeney 1994) have about 40 wt% $CaCO_3$ if all CaO is assigned to $CaCO_3$, and the total alkalis and ratio Na/K are direct reflections of the alkalis in the source peridotite. The trend from the low-alkali experiments (D_3, D_2, D_1, B) to the alkali-bearing experiments (WG, S_1, S_2, T) suggests that with alkali present, CaO/(CaO + MgO + FeO*) decreases in the liquid. Ryabchikov et al. (1989) concluded that the sodium concentration of mantle carbonatitic liquids decreases with increasing pressure, due to the preferential partitioning of Na into jadeite.

The range of liquid compositions measured from carbonated natural lherzolites is shown by the cross-hatched area in Fig. 13. The liquid WG locates the cluster of liquids from alkali-bearing lherzolites, and this is extended to the more calcic low-alkali liquids, D_{23}, reported by Dalton and Wood (1993a). Figures 12 and 13a illustrate their low content of (SiO_2 + Al_2O_3 + TiO_2), and the relatively high alkali content of melts from phlogopite-lherzolite (T). Figures 12 and 13b confirm the dominance of the dolomite component in these liquids, but show in addition the possible range of CaO/(MgO + FeO*).

We are uncertain of the significance of the calcic liquids reported by Dalton and Wood (1993a) as the products of repeated reaction of orthopyroxene with dolomitic carbonatite liquid, derived from lherzolite. The liquids so produced, $D_{3\text{-}6}$ in Figs. 12 and 13b, coexist with olivine, clinopyroxene and magnesian calcite. They correspond to liquids associated with an isobaric invariant point in the model system (6y in Fig. 11D, Wyllie and Huang, 1976). Although we expect the Ca/Mg in the liquids to increase with decreasing pressure as the olivine field expands (Wyllie and Huang 1976, Fig. 11), we see no reason why the liquid composition should continue to be enriched in $CaCO_3$ with continued reaction at a fixed pressure, as long as all phases remain present. Carbonatite path (4), D_{23}-D_6 in Fig. 13b, cannot continue into the $CaCO_3$ corner, because the silicate-carbonate liquidus field boundary has to swing around toward the SiO_2 corner as shown by

Fig. 13a,b. Comparison of miscibility gaps (curves A, B and C), near-solidus liquid compositions from carbonated lherzolite (cross-hatched area including WG and D_{23}), natural rock compositions (AB, EN, NA, SV and BF), and possible magmatic processes (paths 1 to 4) in silicate-carbonate systems at mantle to crustal conditions. The miscibility gaps are all at 1200°C, showing the effect of pressure (cf. A and C) and composition (B and C). The compositions for natrocarbonatite (NA), average sovite (SV) and WG, and the ranges of alkali basalts (AB), evolved nephelinites (EN), and alklai-poor carbonatites are reproduced from Fig. 1. D_{23} is the inferred carbonatite liquid from lherzolite (Dalton and Wood 1993), located between D_2 and D_3 (Fig. 12). Also plotted are D_6 (Fig. 12) and the average beforsite composition (BF). Arrow (1) - progressive melting path for carbonated peridotite (Fig. 1); arrow (2) - cooling path of a carbonated, undersaturated mantle silicate melt through the crystallization of pargasitic amphibole (Amph); arrow (3) - fractional crystallization path of the mantle carbonatite liquid WG to natrocarbonatite; arrow (4) - metasomatic trend for the formation of wehrlite and the liquid D_6 by successive reation of lherzolite with the liquid D_{23} below invariant point Q (Fig. 11).

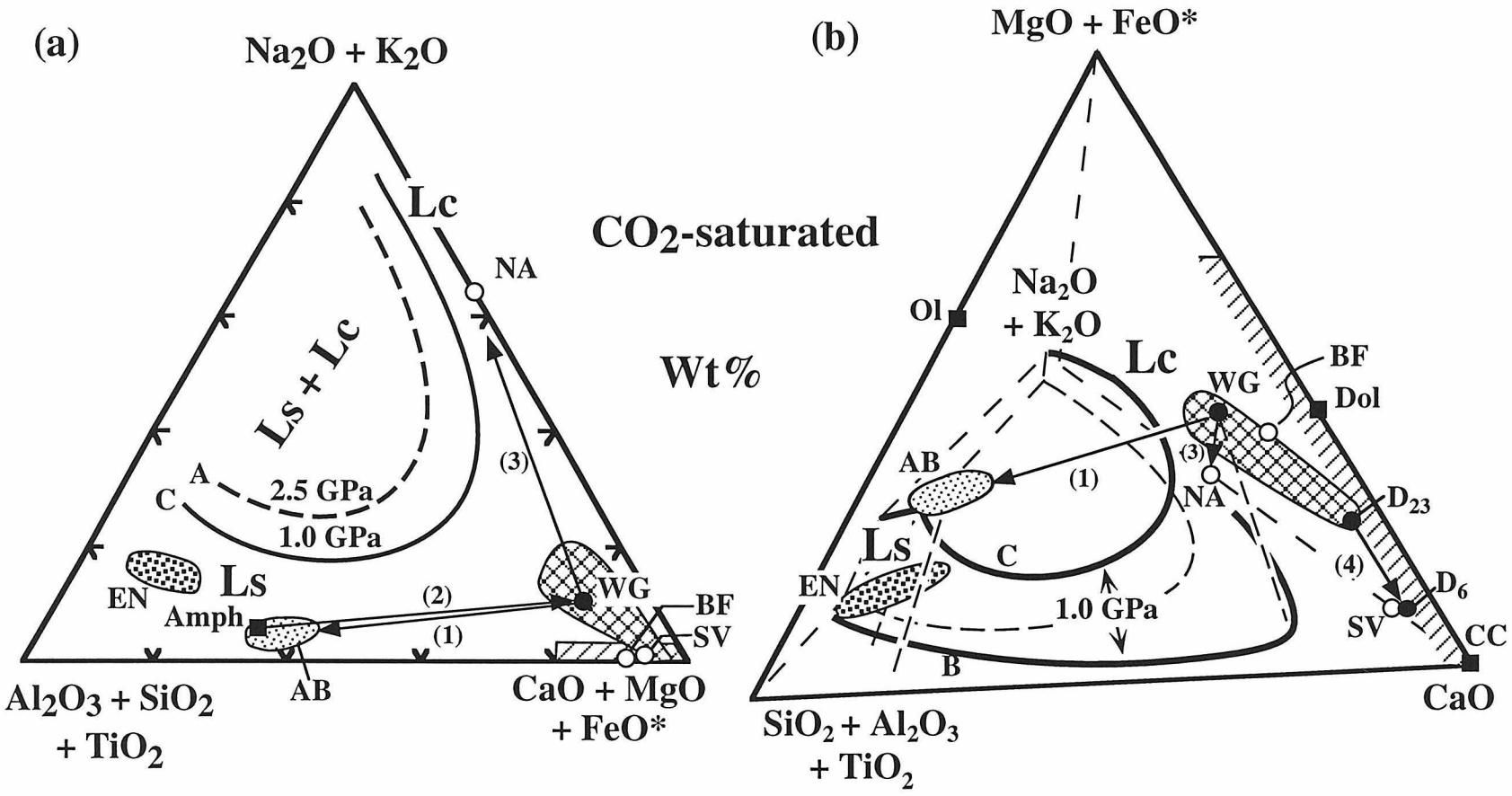
(a)
Na2O + K2O
Lc
NA
Ls + Lc
A
C
2.5 GPa
1.0 GPa
(3)
EN
Ls
Amph
(2)
(1)
WG
BF
SV
AB
Al2O3 + SiO2
+ TiO2
CaO + MgO
+ FeO*
CO2-saturated
Wt%
(b)
MgO + FeO*
Ol
Na2O
+ K2O
Lc
BF
WG
Dol
AB
(3)
(1)
NA
D23
Ls
C
(4)
EN
D6
1.0 GPa
SV
CC
B
CaO
SiO2 + Al2O3
+ TiO2

the field boundary (6y-58) in Fig. 11D of Wyllie and Huang (1976). All of the carbonatitic liquids in the cross hatched area in Fig. 13 are associated with the silicate-carbonate liquidus field boundary, and this area should therefore connect smoothly with the field boundary QP between olivine and calcite located as shown in Fig. 10.

PETROLOGICAL APPLICATIONS

The petrological problems addressed in this paper were outlined in Fig. 1. Baker and Wyllie (1990), on the basis of results summarized in Fig. 1, concluded that the paths of carbonated liquids from lherzolite at pressures above ~2.0 GPa (from WG to alkali basalts) were unlikely to intersect a miscibility gap between carbonate and silicate liquids (isobaric isotherm A-A in Fig. 1). Since then, Pyle and Haggerty (1994) and Kogarko et al. (1995) have reported rounded calcite crystals in mantle xenoliths and interpreted them as products of liquid immiscibility, and Bailey (1993) has argued a compelling case for primary mantle-derived calcicocarbonatite magmas. We presented a review of carbonatite petrogenesis based on detailed phase relationships in the Mg-free system (Lee and Wyllie 1996), with particular attention to the interpretation of rounded calcite crystals in experimental systems, and the non-existence of immiscible liquids with compositions near pure $CaCO_3$. We now compare a more detailed evaluation of carbonatite liquid compositions from a variety of peridotites with our new experimental data on the size variations of the liquid miscibility gap in terms of pressure and CaO/(MgO + FeO*), covering mantle conditions up to the depth of the continental Moho. Figures 11-13 compare these liquid compositions from peridotites with the liquid miscibility gap and the compositions of igneous rocks.

Silicate-carbonate liquid miscibility gap and mantle magma paths

The curves A, B, and C for isobaric intersections of the miscibility gap at 1200° C presented in Fig. 8 (A) and Figs. 6b, 7a, and 10 (C), and estimated based on Lee and Wyllie (1996; B) are reproduced in Fig. 13 to show the variation in the size of the miscibility gap as a function of pressure and composition, CaO/(MgO + FeO*). Figure 13a (cf. Fig. 8) shows the limits of the miscibility gap for the magnesian compositions at mantle pressures, with area expanding from A to C with decreasing pressure from 2.5 GPa to 1.0 GPa. Figure 13b shows the additional increase in size at 1.0 GPa from C to B as the composition changes from magnesian to Mg-free. Curves C and B in Fig. 13b sketch the shape of the two-liquid volume at 1.0 GPa between the more magnesian mantle magma compositions and the more evolved crustal magma compositions with very low Mg.

The compositions of selected natural magmatic rocks are compared with the miscibility gap in Fig. 13. Alkali basalts (AB) and our starting material, primitive olivine nephelinite, are well separated from the gap, but evolved nephelinites (EN, with less MgO and higher alkalis) are situated close to the low-MgO flank of the miscibility gap, as discussed by Le Bas (1987), Kjarsgaard and Hamilton (1989) and Macdonald et al. (1993). The shaded area in the (CaO + MgO + FeO*) corner of Fig. 13a shows the range of compositions of calciocarbonatites, magnesiocarbonatites and ferrocarbonatites, and the compositions of average sovite and beforsite (Woolley and Kempe 1989). The range of CaO/(MgO + FeO*) in carbonatites is shown by the same shading in Fig. 13b, but the extension of this area toward SiO_2 - compare Fig. 13a - has been omitted so as not to obscure the other relationships. The normal carbonatite compositions do not reach the miscibility gap, but the alkali-rich side of the miscibility gap approaches quite close to the natrocarbonatite of Oldoinyo Lengai (NA).

The sodic, dolomitic carbonatite melt determined by Wallace and Green (1988) has been widely cited in discussions of primary melt compositions, mantle metasomatism, and the relationships with natrocarbonatites (e.g. Yaxley et al. 1991; Lee and Wyllie 1994; Sweeney et al. 1995). For this reason, we take the melt composition WG as the

representative primary carbonate melt produced by partial melting of carbonated lherzolite or harzburgite at depths greater than ~70 km (pressures above Q, Fig. 11). With progressive melting of carbonated lherzolite in the mantle, the liquid composition is expected to follow fairly close to path (1) in Fig. 13 (see Fig. 1).

Yaxley et al. (1991) proposed that the cooling path of a carbonated, undersaturated mantle silicate melt (~3 GPa) would yield a carbonatitic liquid of the WG composition in the amphibole stability field, through the crystallization of pargasitic amphibole. The composition of the parental silicate melt was not given, but it is presumably between the WG and pargasite (Amph, solid square, Fig. 13a) compositions. The proposed path (2) would be fairly close to the reverse of path (1) in Fig. 13a.

As noted by Baker and Wyllie (1990), path (1) remains well clear of the miscibility gap at 2.5 GPa. Figure 1 shows that the projected liquid path does overlap with the 2.5 GPa miscibility gap in the Mg-free system, but Fig. 13b confirms the wide separation between this path and the miscibility gap when viewed in three dimensions. The same conclusion holds for initial liquid T (Fig. 12), the most alkalic of the primitive carbonatitic melts.

The results of Cooper et al. (1975) in the system Na_2CO_3-K_2CO_3-$CaCO_3$ demonstrate that fractional crystallization of a calcic carbonatite liquid will produce an alkalic carbonatite. The possible relationship between mantle carbonatite WG and the Oldoinyo Lengai natrocarbonatite (NA, Fig. 13; Dawson et al. 1987) was explored by Wallace and Green (1988). They calculated that extensive fractional crystallization (61 % dolomite, 7 % olivine, 3 % spinel, 1 % ilmenite) of the WG melt at either mantle or crustal pressures could generate a liquid similar to NA, along a path such as (3) in Fig. 13. Sweeney et al. (1995) tested this proposal experimentally, and found that if liquid NA were derived by fractionation of a dolomitic parent, the parent would have to be more silicic and potassic, with less iron than liquid WG. Path (3) does not intersect the miscibility gap, and

it can be shown in other systems that similar paths would be separated from the miscibility gap by a silicate-carbonate liquidus field boundary (Lee and Wyllie 1996).

At conditions below Q (Fig. 11), carbonatitic melts cannot coexist with lherzolite, harzburgite or websterite, but only with the more calcic wehrlite. Carbonatite liquids rising from depths greater than Q would react with lherzolite causing replacement of orthopyroxene by clinopyroxene and olivine (i.e. conversion toward wehrlite), as shown by reaction [B'] in Fig. 11 (e.g. Green and Wallace 1988; Rudnick et al. 1993). This process was investigated experimentally by Dalton and Wood (1993a) in the context of the metasomatic conversion of lherzolite to wehrlite by reaction with rising carbonatite melt at reaction [B']. Through successive reaction of lherzolite or orthopyroxene with carbonatite liquids, they produced a wehrlite assemblage coexisting with magnesian calcite and liquids becoming progressively enriched in $CaCO_3$ as shown by D_3-D_6 in Fig. 12. This is represented by path (4) from D_{23} to D_6 in Fig.13, reaching ~81-86 wt% $CaCO_3$ at 1150° C, 1.5 GPa. In Fig. 13a, the projected path (4) is almost coincident with the point SV. The path does not reach the miscibility gap.

Finally, considering the paths followed by silicate melts during uprise from mantle into crust, there are several trends possible from deep-seated alkalic magmas, depending on the conditions. One trend from primitive magnesian nephelinites and melilitites involves fractionation to evolved nephelinites and phonolites (e.g. Le Bas 1987; Church and Jones 1995; Peterson and Kjarsgaard 1995). This is represented by a path in Fig. 13 from AB to EN, which approaches the silicate side of the immiscibility volume with decreasing pressure and MgO content.

Conclusions

(1) The geometry of the miscibility gap between silicate-rich and carbonate-rich liquids for bulk compositions appropriate for upper mantle magmatic processes is outlined

in Fig. 13 by the three isobaric isotherms A, B, and C. The size of the miscibility gap for magnesian compositions increases with decreasing pressures from depths of ~100 km to ~35 km. It increases further as compositions are changed by decreasing MgO content, a change expected during fractionation of silicate magmas.

(2) Carbonatite liquid compositions derived by partial melting of peridotite at depths greater than ~70 km are generated along a silicate-carbonate liquidus field boundary, dominated by the dolomite component, and none of the reported liquids approaches the liquid miscibility gap.

(3) None of the proposed paths of progressive partial fusion of carbonated peridotite, or of fractional crystallization of the carbonate-rich liquids, intersects the miscibility gap. It is unlikely that silicate-carbonate liquid immiscibility occurs during magmatic processes in the mantle.

(4) Rounded calcite crystals in mantle xenoliths have been interpreted as immiscible liquids. For Mg-bearing liquids at mantle pressures > 1.0 GPa, 50 wt% $CaCO_3$ is the maximum in liquids associated with the miscibility gap, assuming that all CaO is assigned to $CaCO_3$; in fact, some of the CaO must be associated with silicates. For Mg-free liquids at up to 2.5 GPa, 80 wt% $CaCO_3$ is the maximum in liquids associated with the miscibility gap. 86 wt% $CaCO_3$ is the maximum reported in carbonate-rich liquid generated by progressive reaction with peridotite (lherzolite to wehrlite). It has been established that calcite crystals are precipitated in remarkably rounded forms in experimental systems (Fig. 4c). The experimental evidence therefore indicates that the rounded calcite in mantle xenoliths were precipitated as solids, and not formed from an immiscibile, nearly pure $CaCO_3$ liquid.

(5) Although extreme fractionation of the dolomitic mantle-derived carbonatite liquids could yield liquids corresponding to natrocarbonatites, it is unlikely that suitable conditions for such fractionation are achieved at mantle depths.

(6) Carbonatite liquids rising through mantle peridotite crystallize and evolve CO_2 at a depth of about ~70 km. We would therefore expect primary dolomitic carbonatite magmas, if they reach the surface, to pierce the crust in style similar to that of kimberlites.

(7) The metasomatic process associated with reaction [B'] at ~70 km tends to generate wehrlite from lherzolite. Carbonatite liquid enriched in the $CaCO_3$ component can exist in equilibrium with wehrlite to shallower levels through the mantle and into the crust. Very large volumes of dolomitic carbonatite melt would be required to metasomatize a column of mantle to wehrlite between ~70 km depth and the Moho at ~35 km, in order to permit egress of calciocarbonatite magma through the mantle and into the crust.

(8) As the MgO content decreases in evolving nephelinites and phonolites derived by fractionation of CO_2-bearing mantle-derived alkalic magmas (e.g. nephelinites, melilitites), their compositions are brought close to the silicate side of the miscibility gap, and immiscible carbonate-rich liquids may thus be generated at crustal pressures.

ACKNOWLEDGEMENTS

We thank Dr. M. B. Baker for making available his 2.5 GPa results given in Table 2, Table 3 and Fig. 8, and incorporated into Fig. 5, and for critical review of an early manuscript draft. This research was supported by the Earth Science section of the U.S. National Science Foundation, grant EAR-921886.

REFERENCES

Amundsen HEF (1987) Evidence for liquid immiscibility in the upper mantle. Nature 327: 692-695.

Armstrong JT (1988) Quantitative analysis of silicate and oxide minerals: comparison of Monte Carlo, ZAF and $\phi(\rho z)$ procedures. In: Newbury DE (ed) Microbeam Analysis. San Francisco Press, San Francisco, pp 239-246.

Bailey DK (1993) Carbonate magmas. J Geol Soc London 150: 637-651.

Baker MB, Wyllie PJ (1990) Liquid immiscibility in a nephelinite-carbonate system at 25 kbar and implications for carbonatite origin. Nature 346: 168-170.

Baker MB, Wyllie PJ (1992) High-pressure apatite solubility in carbonate-rich liquids: implications for mantle metasomatism. Geochim Cosmochim Acta 56: 3409-3422.

Bell K (1989) Editor. Carbonatites: genesis and evolution. Unwin Hyman, London, 618 pp.

Brey G, Brice WR, Ellis DJ, Green DH, Harris KL, Ryabchikov ID (1983) Pyroxene-carbonate reactions in the upper mantle. Earth Planet Sci Lett 62: 63-74.

Brooker RA, Hamilton DL (1990) Three-liquid immiscibility and the origin of carbonatites. Nature 346: 459-462.

Byrnes AP, Wyllie PJ (1981) Subsolidus and melting relations for the join $CaCO_3$-$MgCO_3$ at 10 kb. Geochim Cosmochim Acta 45: 321-328.

Church AA, Jones AP (1995) Silicate-carbonate immiscibility at Oldoinyo Lengai. J Petrol 36: 869-889.

Clague DA, Frey FA (1982) Petrology and trace-element geochemistry of the Honolulu volcanics, Oahu - implications for the oceanic mantle below Hawaii. J Petrol 23: 447-504.

Cooper AF, Gittins J, Tuttle OF (1975) The system Na_2CO_3-K_2CO_3-$CaCO_3$ at 1 kilobar and its significance in carbonatite petrogenesis. Am J Sci 275: 534-560.

Dalton JA, Wood BJ (1993a) The compositions of primary carbonate melts and their evolution through wallrock reaction in the mantle. Earth Planet Sci Lett 119: 511-525.

Dalton JA, Wood BJ (1993b) The partitioning of Fe and Mg between olivine and carbonate and the

stability of carbonate under mantle conditions. Contrib Mineral Petrol 114: 501-509.

Dawson JB, Garson MS, Roberts B (1987) Altered former alkalic carbonatite lava from Oldoinyo Lengai, Tanzania: inferences for calcite carbonatite lavas. Geology 15: 765-768.

Dawson JB, Pinkerton H, Pyle DM, Nyamweru C (1994) June 1993 eruption of Oldoinyo Lengai, Tanzania: exceptionally viscous and large carbonatite lava flows and evidence for coexisting silicate and carbonate magmas. Geology 22: 799-802.

Eggler DH (1974) Effect of CO_2 on the melting of peridotite. Carnegie Inst Washington Yearb 73: 215-224.

Eggler DH (1976) Composition of the partial melt of carbonated peridotite in the system CaO-MgO-SiO_2-CO_2. Carnegie Inst Washington Yearb 75: 623-626.

Eggler DH (1978) The effect of CO_2 upon partial melting of peridotite in the system Na_2O-CaO-Al_2O_3-MgO-SiO_2-CO_2 to 35 kb, with an analysis of melting in a peridotite-H_2O-CO_2 system. Am J Sci 278: 305-343.

Falloon TJ, Green DH (1989) The solidus of carbonated, fertile peridotite. Earth Planet Sci Lett 94: 364-370.

Freestone IC, Hamilton, DL (1980) The role of liquid immiscibility in the genesis of carbonatites - an experimental study. Contrib Mineral Petrol 73: 105-117.

Frey FA, Green DH, Roy SD (1978) Integrated models of basalt petrogenesis: a study of quartz tholeiites to olivine melilitites from south eastern Australia utilizing geochemical and experimental petrological data. J Petrol 19: 463-513.

Green DH, Wallace ME (1988) Mantle metasomatism by ephemeral carbonatite melts. Nature 336: 459-462.

Hauri EH, Shimizu N, Dieu JJ, Hart SR (1993) Evidence for hotspot-related carbonatite metasomatism in the oceanic upper mantle. Nature 365: 221-227.

Huang WL, Wyllie PJ (1984) Carbonation reactions for mantle lherzolite and harzburgite. In: Porceedings of the 27th International Geological Congress, Moscow, vol 9. pp 455-473.

Huang WL, Wyllie PJ, Nehru, CE (1980) Subsolidus and liquidus phase relationships in the system CaO-SiO_2-CO_2 to 30 kbar with geological applications. Am Mineral 65: 285-301.

Ionov DA, Dupuy C, O'Reilly SY, Kopylova MG, Genshaft, YS (1993) Carbonated peridotite xenoliths from Spitsbergen: implications for trace element signature of mantle carbonate metasomatism. Earth Planet Sci Lett 119: 283-297.

Irving AJ, Wyllie PJ (1975) Subsolidus and melting relationships for calcite, magnesite, and the join $CaCO_3$-$MgCO_3$ to 36 kilobars. Geochim Cosmochim Acta 39: 35-53.

Keller J (1989) Extrusive carbonatites and their significance. In: Bell K (ed) Carbonatites: genesis and evolution. Unwin Hyman, London, pp 70-88.

Kjarsgaard BA, Hamilton DL (1988) Liquid immiscibility and the origin of alkali-poor carbonatites. Mineral Mag 52: 43-55.

Kjarsgaard BA, Hamilton DL (1989) The genesis of carbonatites by immiscibility. In: Bell K (ed) Carbonatites: genesis and evolution. Unwin Hyman, London, pp 388-404.

Kjarsgaard BA, Peterson T (1991) Nephelinite-carbonatite liquid immiscibility at Shombole volcano, East Africa: petrographic and experimental evidence. Mineral Petrol 43: 293-314.

Kjarsgaard BA, Hamilton DL, Peterson TD (1995) Peralkaline nephelinite/carbonatite liquid immiscibility: comparison of phase compositions in experiments and natural lavas from Oldoinyo Lengai. In: Bell K, Keller J (eds) Carbonatite volcanism: Oldoinyo Lengai and the petrogenesis of natrocarbonatites. IAVCEI Proceedings in Volcanology 4, Springer-Verlag, Berlin Heidelberg New York, pp 163-190.

Kogarko LN, Henderson CMB, Pacheco H (1995) Primary Ca-rich carbonatite magma and carbonate-silicate-sulfide liquid immiscibility in the upper mantle. Contrib Mineral Petrol 121: 267-274.

Le Bas MJ (1987) Nephelinites and carbonatites. In: Fitton JG, Upton BGJ (eds) Alkaline igneous rocks. Geol Soc Spec Publ 30, pp 53-83.

Lee WJ, Wyllie PJ (1992a) New data on CO_2-rich immiscible liquids in Na_2O-CaO-Al_2O_3-SiO_2-CO_2 from 25 to 1 kb: carbonatite genesis (abstract). EOS 73: 349-350.

Lee WJ, Wyllie PJ (1992b) Liquid immiscibility between silicates and carbonates must intersect suitable liquidus field boundaries to have petrogenetic significance. Abstracts, 29th International Geological Congress, Kyoto, pp 571.

Lee WJ, Wyllie PJ (1994) Experimental data bearing on liquid immiscibility, crystal fractionation, and the origin of calciocarbonatites and natrocarbonatites. Int Geol Rev 36: 797-819.

Lee WJ, Wyllie PJ (1996) Liquid immiscibility in the join $NaAlSi_3O_8$-$CaCO_3$ to 2.5 GPa and the origin of calciocarbonatite magmas. J Petrol (submitted).

Lee W-J, Wyllie PJ, Rossman GR (1994) CO_2-rich lass, round calcite crystals and no liquid immiscibility in the system CaO-SiO_2-CO_2 at 2.5 GPa. Am Mineral 79: 1135-1144.

Macdonald R, Kjarsgaard BA, Skilling IP, Davies GR, Hamilton DL, Black S (1993) Liquid immiscibility between trachyte and carbonate in ash flow tuffs from Kenya. Contrib Mineral Petrol 114: 276-287.

Newton RC, Sharp WE (1975) Stability of forsterite+CO_2 and its bearing on CO_2 in the mantle. Earth Planet Sci Lett 26: 239-244.

Olafsson M, Eggler DH (1983) Phase relations of amphibole-carbonate, and phlogopite-carbonate peridotite: petrologic constraints on the asthenopsphere. Earth Planet Sci Lett 64: 305-315.

Peterson TD, Kjarsgaard BA (1995) What are the parental magmas at Oldoinyo Lengai? In: Bell K, Keller J (eds) Carbonatite volcanism: Oldoinyo Lengai and the petrogenesis of natrocarbonatites. IAVCEI Proceedings in Volcanology 4, Springer-Verlag, Berlin Heidelberg New York, pp 148-162.

Pyle JM, Haggerty SE (1994) Silicate-carbonate liquid immiscibility in upper-mantle eclogites: implications for natrosilicic and carbonatitic conjugate melts. Geochim Cosmochim Acta 58: 2997-3011.

Rudnick RL, Mcdonough WF, Chappell BW (1993) Carbonatite metasomatism in the northern Tanzanian mantle - petrographic and geochemical characteristics. Earth Planet Sci Lett 114: 463-475.

Ryabchikov ID, Brey G, Kogarko LN, Bulatov VK (1989) Partial melting of carbonated peridotite at 50 kbar. Geokhimiya 1: 3-9.

Sweeney RJ (1994) Carbonatite melt compositions in the Earth's mantle. Earth Planet Sci Lett 128: 259-270.

Sweeney RJ, Falloon TJ, Green DH (1995) Experimental constraints on the possible mantle origin of natrocarbonatite. In: Bell K, Keller J (eds) Carbonatite volcanism: Oldoinyo Lengai and the petrogenesis of natrocarbonatites. IAVCEI Proceedings in Vocanology 4, Springer-Verlag, Berlin Heidelberg New York, pp 191-207.

Thibault Y, Edgar AD, Lloyd FE (1992) Experimental investigation of melts from a carbonated phlogopite lherzolite: implications for metasomatism in the continental lithosperic mantle. Am Mineral 77: 784-794.

Wallace ME, Green DH (1988) An experimental determination of primaty carbonatite magma composition. Nature 335: 343-346.

White BS, Wyllie PJ (1992) Solidus reactions in synthetic lherzolite-H_2O-CO_2 from 20-30 kbar, with applications to melting and metasomatism. J Volcanol Geotherm Res 50: 117-130.

Woermann E, Rosenhauer M (1985) Fluid phases and the redox state of the Earth's mantle: extrapolations based on experimental, phase-theoretical and petrological data. Fortschr Mineral 63: 263-349.

Woolley AR, Kempe DRC (1989) Carbonatites: nomenclature, average chemical compositions, and element distribution. In: Bell K (ed) Carbonatites: genesis and evolution. Unwin Hyman, London, pp 1-14.

Wyllie PJ (1977) Mantle fluid compositions buffered by carbonates in peridotite-CO_2-H_2O. J Geol 85: 187-207.

Wyllie PJ (1978) Mantle fluid compositions buffered in peridotite-CO_2-H_2O by carbonates, amphibole, and phlogopite. J Geol 86: 687-713.

Wyllie PJ (1987) Discussion of recent papers on carbonated peridotite, bearing on mantle metasomatism and magmatism. Earth Planet Sci Lett 82: 391-397, 401-402.

Wyllie PJ, Huang WL (1975) Peridotite, kimberlite, and carbonatite explained in the system CaO-MgO-SiO_2-CO_2. Geology 3: 621-624.

Wyllie PJ, Huang WL (1976) Carbonation and melting reactions in the system CaO-MgO-SiO_2-CO_2 at mantle pressures with geophysical and petrological applications. Contrib Mineral Petrol 54: 79-107.

Wyllie PJ, Rutter M (1986) Experimental data on the solidus of peridotite-CO_2, with applications to alkaline magmatism and mantle metasomatism (abstract). EOS 67: 390.

Wyllie PJ, Huang WL, Otto J, Byrnes AP (1983) Carbonation of peridotites and decarbonation of siliceous dolomites represented in the system CaO-MgO-SiO_2-CO_2 to 30 kbar. Tectonophysics 100: 359-388.

Yaxley GM, Crawford AJ, Green DH (1991) Evidence for carbonatite metasomatism in spinel peridotite xenoliths from western Victoria, Australia. Earth Planet Sci Lett 107: 305-317.

CHAPTER 6

SUMMARY OF EXPERIMENTAL RESULTS AND MODEL FRAMEWORK FOR THE FORMATION OF CARBONATITES

INTRODUCTION

Debates about the origin of carbonatites are summarized in Chapter 1. In short, the major questions to be answered are the detailed evolution paths—the processes involving the generation of carbonatitic or carbonated silicate liquids within the mantle, and the differentiation of the magmas by crystal fractionation or silicate-carbonate liquid immiscibility before the final emplacement at the shallower crustal levels, along with the compositional variation, alkalic, dolomitic or calcitic, associated with these processes. While field observations and geochemical data have provided critical information for understanding the overall history of carbonatite magmatism, these studies also pose new enigmas and challenges to the carbonatite petrology (see a review by Bailey, 1993). Thus, it is essential to examine phase equilibrium data for silicate-carbonate systems—these results can be useful for constraining the possible liquid paths linking the deep mantle sources to the surface carbonatite activities, the interaction of carbonate-rich liquids with wall rocks within the mantle and the crust, and the compositional ranges of the resulting magmas.

Previous experimental studies relevant to the formation of carbonatitic liquids are outlined in Chapters 1 and 3 for silicate-carbonate liquid immiscibility, and in Chapter 5 for the melting and metasomatism of carbonated mantle peridotite. Our new data have also been discussed in detail in Chapters 2-5, including the results from quartz-calcite, albite-calcite (Ab-CC), nepheline (Ne)-albite-calcite, nephelinite-dolomite-Na_2CO_3 (NEPH-Dol-NC) and nephelinite-calcite, up to 2.5 GPa. In this chapter, we summarize the effect of composition, pressure and temperature on the silicate-carbonate melting relationships, with emphasis on the variation of the liquid miscibility gap and the silicate-carbonate liquidus field boundary, and utilize these data to construct a generalized phase diagram. CO_2-rich primary liquid compositions from carbonated peridotite, crustal silicate and carbonatite

liquid compositions, and possible liquid paths are then compared with the generalized field boundaries to discuss the origin of carbonatites.

VARIATIONS ON MISCIBILITY GAP AND LIQUIDUS FIELD BOUNDARIES

The topology and positions of the miscibility gap and the silicate-carbonate liquidus field boundary are strongly a function of pressure, temperature and composition of the system, as discussed in detail in the previous chapters. In this section, we first summarize these results in the synthetic system Na_2O-CaO-Al_2O_3-SiO_2-CO_2. This information is then extended to a more complex compositional set involving additional mafic components. The relevant figures have been discussed previously, and are reproduced and combined in Figs. 1 (Mg-free) and 2 (Mg-rich).

The system Na_2O-CaO-Al_2O_3-SiO_2-CO_2

Figure 1a illustrates the lower portion of the pseudo-ternary phase diagram at 2.5 GPa constructed in the compositional triangle, (Al_2O_3 + SiO_2)-CaO-Na_2O (+ CO_2), showing the general arrangement of the miscibility gap, and the silicate and carbonate liquidus fields (based on the results for Ab-CC; Fig. 13, Chapter 3). The construction procedure has been presented in the same chapter. The Na_2O-CaO(+ CO_2) side represents the carbonate end-member of the system, and silicate minerals generally plot near the (Al_2O_3 + SiO_2) corner. The field Ls + Lc is the miscibility gap, which is intersected by the silicate and carbonate liquidus surfaces along curve MFQKR. The curve E-P-F within the one-liquid region indicates the liquidus field boundary between calcite and a silicate mineral. The complete ranges of the three major fields, the miscibility gap, the silicate and carbonate liquidus surfaces, are illustrated in Fig.

Figure 1. Phase relationships in the synthetic system Na_2O-CaO-Al_2O_3-SiO_2-CO_2. (a) Lower portion of the compositional triangle (Al_2O_3 + SiO_2)-CaO-Na_2O, CO_2-saturated, showing the pseudo-ternary phase diagram at 2.5 GPa, derived from the Ab-CC results (Fig. 13, Chapter 3). Vertical exaggeration of two. (b) Complete ranges for the three major phase fields at 2.5 GPa: the two-liquid field, the silicate and carbonate liquidus fields, based on the results of Ab-CC (Fig. 15a, Chapter 3). (c)-(e) Lower portion of the pseudo-ternary phase diagram without the temperature contours at 2.5 GPa and 1 GPa from the results of Ab-CC (Fig. 17a and b, Chapter 3), and at 1 GPa from the results of Ne-Ab-CC (Fig. 8a, Chapter 4). (f) Pseudo-quaternary phase diagram at 1 GPa based on the results of Ab-CC and Ne-Ab-CC, expressed in the CO_2-saturated tetrahedron Al_2O_3-SiO_2-CaO-Na_2O (Fig. 8c, Chapter 4).

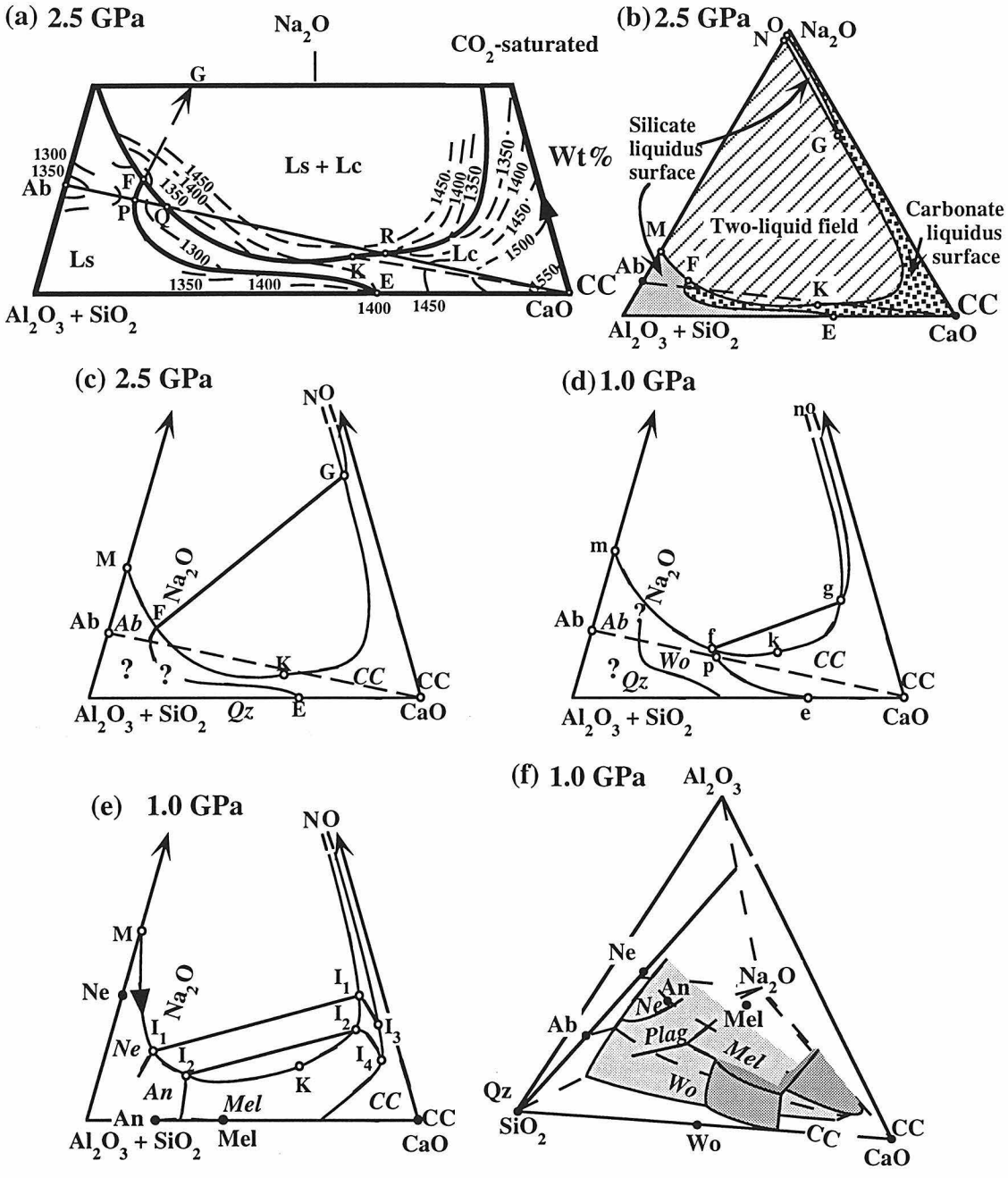
(a) 2.5 GPa
Na2O
CO2-saturated
G
Ls + Lc
Wt%
Ab
F
P
Q
R
Ls
Lc
K
E
CC
Al2O3 + SiO2
CaO
(b) 2.5 GPa
N
Na2O
Silicate liquidus surface
G
M
Two-liquid field
Carbonate liquidus surface
Ab
F
K
E
CC
Al2O3 + SiO2
CaO
(c) 2.5 GPa
NO
G
M
Na2O
Ab
Ab
F
?
?
K
CC
CC
Al2O3 + SiO2
Qz
E
CaO
(d) 1.0 GPa
no
m
Na2O
g
Ab
Ab
?
f
k
Wo
p
CC
?Qz
CC
Al2O3 + SiO2
e
CaO
(e) 1.0 GPa
NO
M
Ne
Na2O
I1
I2
I3
Ne
I1
I2
I4
An
K
Mel
CC
An
CC
Al2O3 + SiO2
Mel
CaO
(f) 1.0 GPa
Al2O3
Ne
An
Na2O
Ne
Ab
Mel
Plag
Mel
Wo
Qz
SiO2
Wo
CC
CC
CaO

1b by the lined, gray and dotted areas, respectively. K on the miscibility gap field boundary is the critical point where compositions of the two liquids become identical; silicate-rich and carbonate-rich liquids (Ls and Lc) are defined relative to the point.

The extent of the miscibility gap decreases with increasing temperature, as indicated by the isotherms at 1350, 1400 and 1450°C on the two-liquid surface in Fig. 1a. The effect of pressure and composition on the variations of the three major fields are illustrated in Figs. 1c-e. The silicate liquidus surface is divided into several silicate-precipitating fields (e.g. albite, wollastonite, nepheline), depending on the composition and pressure conditions; the species of the carbonate minerals within the carbonate liquidus surface are less complicated, always involving calcite near the CaO apex, natrocarbonate at the Na_2O corner, and Ca-Na-carbonate compound(s) in between (e.g. nyerereite). Figures 1c and d compare the phase diagrams at 2.5 and 1 GPa from the join Ab-CC (Chapter 3), indicating that with decreasing pressure, the size of the miscibility gap decreases, and the silicate-carbonate liquidus field boundary moves towards more carbonate-rich compositions; there is also a wollastonite field between albite and calcite at 1 GPa. Figures 1d and e compare the results with different Al/Si of the system at 1 GPa (Ab-CC and Ne-Ab-CC, Chapter 4). While the extent of the miscibility gap does not vary significantly in the projection, the position of the silicate-carbonate liquidus field boundary changes with the change in the mineral phases involved. The variation of the phase fields and boundaries in response to the change in Al/Si is depicted in Fig. 1f, where the phase relationships are expressed in the compositional tetrahedron with Al_2O_3 separated from SiO_2 to form an additional apex.

Magnesian silicate-carbonate system

The miscibility gap involving more mafic compositions, a primitive (magnesian) nephelinite with (Ca, Mg, Na)-carbonate, has been determined between 2.5 and 1 GPa in Chapter 5 (join NEPH-Dol-NC). Figure 2a summarizes the major experimental results in

the compositional triangle modified from Fig. 1, showing that the size of the miscibility gap increases (1) with decreasing temperature (compare curves A, B and C), (2) with decreasing pressure (compare C and D), and (3) with decreasing Mg/Ca (compare D and E). Curve E is the estimated two-liquid isobaric isotherm at 1 GPa and 1200°C in the Mg-free synthetic system (see above), and is outside the two-liquid field at 0.5 GPa and 1250°C (Fig. 16, Chapter 3) without intersecting the join Ab-CC. Note that the plot is now designed to accommodate the major chemistry of natural mineral and rock compositions, containing up to eight components (+ CO_2).

Figure 2b reproduces curve D in 2a with two areas marked, separated by tie-line T_2: light- and dark-shaded fields for the two liquids without and with additional crystals. Tie-line T_1 is located by extrapolation of the light area to the Ca-free end-member compositions. Also added in the diagram is the liquidus piercing point P between olivine and calcite in the join NEPH-CC, and a field boundary F passing through it. Figure 2c is the compositional tetrahedron which separates MgO and FeO* from CaO for the cafemic corner of the compositional triangle (Fig. 2a), showing the spatial positions of curves D and E in Fig. 2a and F in 2b. Points 1, 3 and 5 are three of the starting mixtures in the join NEPH-Dol-NC. The two-liquid compositions remain nearly coplanar with line 1-3-5 between T_1 and T_2, but become deviated from the line beyond T_2 due to the crystallization of olivine.

CONSTRUCTION OF THE GENERALIZED PHASE DIAGRAM

Here we construct the phase diagram integrating the experimental data summarized in Figs. 1 and 2. The framework for illustrating the results is the compositional tetrahedron shown in Fig. 2b, but the phase relationships described in this tetrahedron are pseudo-quaternary, where the field boundaries and the phase assemblages vary as a function of Al/Si, Fe/Mg and Na/K of the system. The effect of Al/Si was explored (Figs. 1d-f;

Figure 2. Experimental results in the magnesian system of Chapter 5. (a) Isobaric two-liquid isotherms for the Mg-rich compositions (curves A to D: 2.5 GPa at 1300, 1250 and 1200°C, and 1 GPa at 1200°C), and for a Mg-free system (curve E at 1 GPa and 1200°C). Data are taken from Chapter 5. (b) Phase fields and boundaries derived from the join NEPH-Dol-NC and NEPH-CC at 1 GPa, projected onto the triangle. (Fig. 10a, Chapter 5). (c) The same phase fields and boundaries of (b) expressed in the compositional tetrahedron separating the effect of (MgO + FeO*) and CaO (Fig. 10b, Chapter 5). Mg-free curve E of (a) is also reproduced on the base of the tetrahedron.

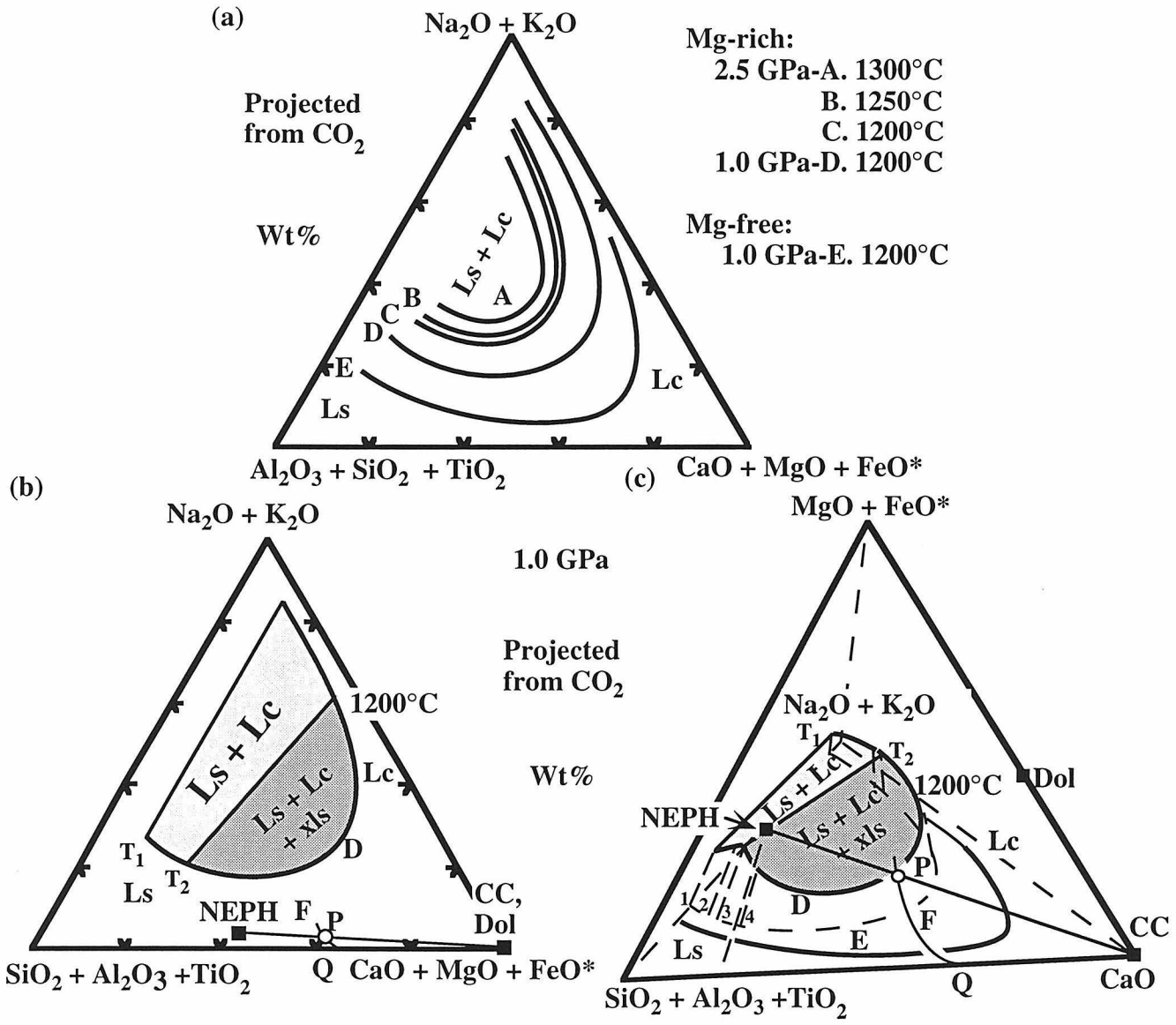
(a)
$Na_2O + K_2O$
Projected from CO_2
Wt%
Ls + Lc
A
B
C
D
E
Ls
Lc
$Al_2O_3 + SiO_2 + TiO_2$
$CaO + MgO + FeO^*$
Mg-rich:
2.5 GPa-A. 1300°C
B. 1250°C
C. 1200°C
1.0 GPa-D. 1200°C
Mg-free:
1.0 GPa-E. 1200°C
(b)
$Na_2O + K_2O$
1.0 GPa
Projected from CO_2
Wt%
1200°C
Ls + Lc
Ls + Lc + xls
Lc
D
T_1
T_2
Ls
NEPH
F
P
CC, Dol
$SiO_2 + Al_2O_3 + TiO_2$
Q
$CaO + MgO + FeO^*$
(c)
$MgO + FeO^*$
$Na_2O + K_2O$
T_1
T_2
Ls + Lc
Ls + Lc + xls
1200°C
Dol
NEPH
Lc
P
D
F
CC
E
Ls
Q
CaO
$SiO_2 + Al_2O_3 + TiO_2$

Chapter 4), but there is lack of information for the effect of latter two ratios on the silicate-carbonate phase relationships. Thus, the phase diagram presented in this section can only be considered as a generalized interpretation.

The field boundaries at 1 GPa in Fig. 3 are based on our new results (Figs. 1 and 2), and supplemental information from the literature as outlined below. The tetrahedron (Fig. 2b) is opened up to show the four end-member triangles in Fig. 3a. The phase relationships near the compositional slice Ab-CC-NC in Fig. 1f are chosen to be representative for the central triangle (base of the tetrahedron) due to the comparable Al_2O_3/SiO_2 to that of the primitive nephelinite (NEPH, Fig. 2), and the results in Fig. 1d are thus reproduced in the triangle. The two-liquid curve is the polythermal miscibility gap field boundary associated with minerals, not the isobaric isotherm E in Fig. 2a , but their positions are not very different.

The triangle CaO-(MgO + FeO*)-(Na_2O + K_2O) (upper-right, Fig. 3a) represents the carbonate end-member of the system. Melting relationships in part of the triangle have been determined, such as in NC-KC-CC at 0.1 GPa by Cooper et al. (1975) and CC-MC up to 3.6 GPa by Irving and Wyllie (1973, 1975) and Huang and Wyllie (1976), but no further data exist for NC-KC-CC-MC-FC. As we focus only on the relationships between silicates and carbonates, the generalized phase diagram in the carbonate triangle is not sketched (Fig. 3a). Note that magnesite melts incongruently at low pressures (< ~2.8 GPa; Irving and Wyllie, 1975), so periclase is present at those conditions near the (MgO + FeO*) corner (not shown in the diagram).

The experimental data with alkali-free compositions (lower triangle, Fig. 3a) include the system CaO-MgO-SiO_2-CO_2 and its sub-systems by Wyllie and associates (e.g. Huang and Wyllie, 1974; Wyllie and Huang, 1975, 1976), and calcite-grassularite by Maaloe and Wyllie (1975). There is no silicate-carbonate liquid immiscibility in this pseudo-ternary system, and the liquidus field boundary between silicates and carbonates is sketched in the triangle (SiO_2 + Al_2O_3 + TiO_2)-CaO-(MgO + FeO*) of Fig. 3a, based on

Figure 3. (a) silicate-carbonate phase field boundaries at 1 GPa illustrated in the end-member triangles of the tetrahedron (Fig. 2). (b) Construction basis for the two-liquid volume in the tetrahedron. See text for the discussion of each curve. (c) Construction basis for the liquidus field boundary surface in the tetrahedron. (d) Generalized phase diagram at 1 GPa combining the data from (b) and (c), showing the three phase volumes for the miscibility gap, and the primary silicate and carbonate fields.

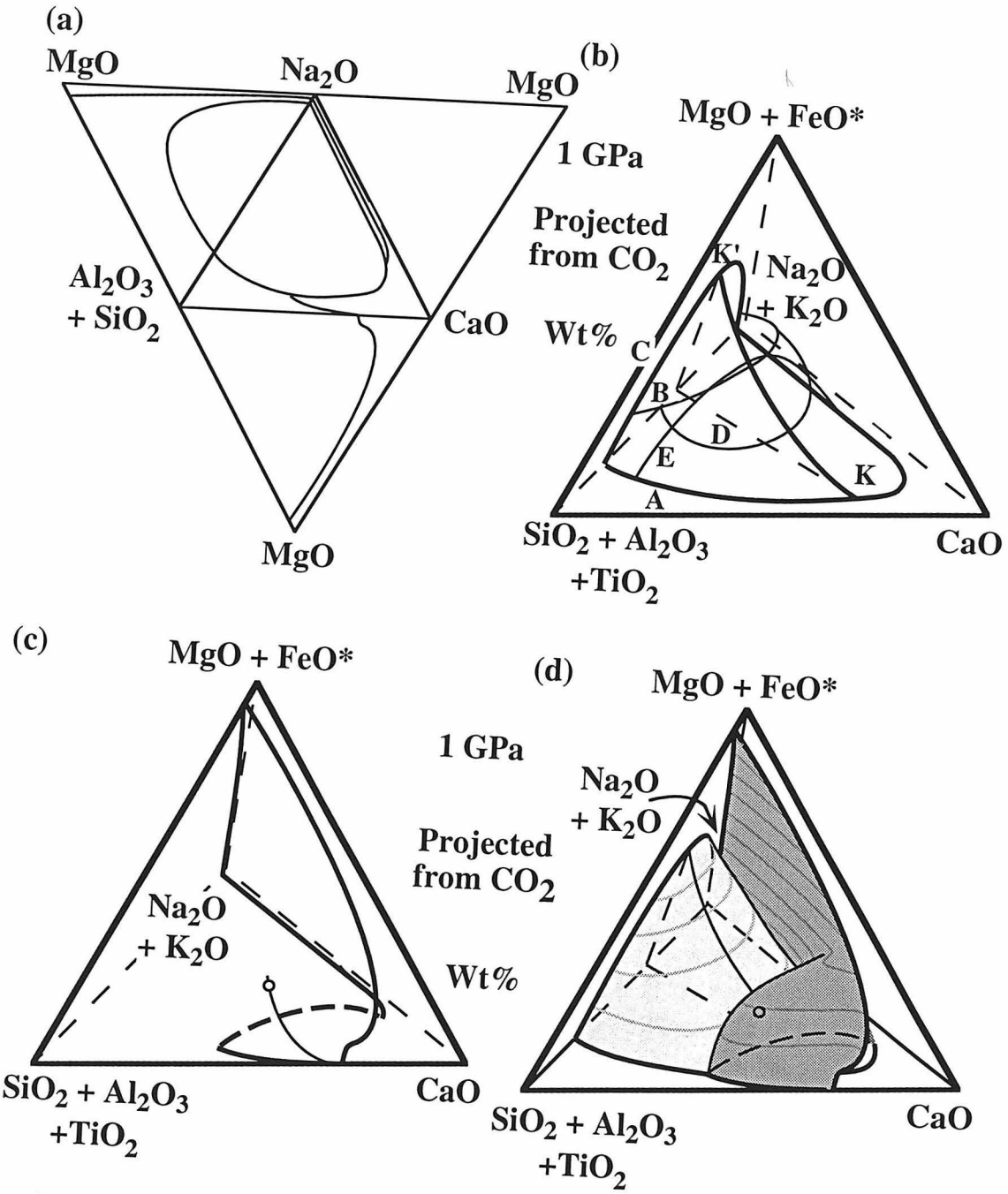
(a)
MgO
Na2O
MgO
1 GPa
Al2O3
+ SiO2
CaO
MgO
(b)
MgO + FeO*
Projected
from CO2
K'
Na2O
+ K2O
Wt%
C
B
D
E
K
A
SiO2 + Al2O3
+TiO2
CaO
(c)
MgO + FeO*
Na2O
+ K2O
Wt%
SiO2 + Al2O3
+TiO2
CaO
(d)
MgO + FeO*
1 GPa
Na2O
+ K2O
Projected
from CO2
SiO2 + Al2O3
+TiO2
CaO

Wyllie and Huang (1976). For the end-member system (SiO_2 + Al_2O_3 + TiO_2)-(MgO + FeO*)-(Na_2O + K_2O) (upper-left, Fig. 3a), there are no available data for the melting relationships within the triangle; the extent of the two-liquid field is estimated using the data from the magnesian compositions (Fig. 2), as described below (curve C, Fig. 3b).

Figure 3b illustrates the construction basis for the two-liquid volume in the tetrahedron at 1 GPa. The surface of the volume is polythermal, analogous to the miscibility gap field boundary in Fig. 1 (curve A in Fig. 3a and b) where the two liquids are joined by an additional mineral. Curve B is the polythermal trace on the surface of the miscibility volume by intersecting plane T_1-T_2 and the two-liquid volume. It is slightly outside the light area [Ls + Lc] of Fig. 2c to meet the olivine liquidus field at temperatures below 1200°C, passing through the two-liquid compositions defining T_2 (1200°C) and the liquidus piercing point along the join 1-3-5 between the miscibility gap and the olivine field (between points 3 and 5 at ~1235°C; see Fig. 5, Chapter 5). Curve C defines the miscibility gap field boundary on the Ca-free triangle, and it is expected to close off above tie-line T_1. Isotherm D (1200°C) outlining the dark area [Ls + Lc + minerals] in Fig. 2c is on the surface of the two-liquid volume, and curve E is coincident with the cooling direction of the bulk liquid 3 on the same surface; the two curves intersect at the two-liquid compositions from mix 3 at 1 GPa and 1200°C (run L65, Chapter 5). Curve K-K' is the estimated critical curve where Ls = Lc.

Construction for the surface between the primary silicate and carbonate volumes is less well-constrained, due to lack of information within the tetrahedron. The location of the surface in the projection is not unique, changing with composition of the system. A representative construction basis is illustrated in Fig. 3c, which includes the field boundaries in the end-member triangles (Fig. 3a), and the piercing point P between the olivine and calcite liquidi in the join NEPH-CC (Fig. 2c; Chapter 5). The surface connects through these field boundaries and P, and intersects the two-liquid volume at the dashed curve.

The completed two-liquid volume at 1 GPa is illustrated in Fig. 3d, with its spatial position delineated by the contours of wt% (MgO + FeO*) on its surface. The liquidus field boundary surface for coprecipitation of silicate and carbonate minerals is also combined to show the generalized phase diagram which defines the three major volumes for the miscibility gap, the silicate and carbonate liquidus fields.

PETROLOGICAL APPLICATIONS

Figures 4-6 compare rock compositions related to carbonatite magmatism with the tetrahedron framework shown in Fig. 3d. The phase relationships are now sketched for both 2.5 GPa (Fig. 4) and 1 GPa (Figs. 5 and 6). The geometry of each field boundary changes with pressure: with decreasing pressure, the size of the Mg-free miscibility gap decreases, the size of the Ca-free miscibility gap increases, and the coprecipitation surface moves towards more carbonate-rich compositions (closer to the carbonate triangle). However, we do not expect the Ca-free miscibility gap to be much wider below 1 GPa, since the enlargement of periclase field at low pressures (Irving and Wyllie, 1975) would limit the extent of the miscibility gap.

Generation of carbonatite liquids in the mantle

It has been established experimentally that small-degree partial melting of carbonated peridotite can produce carbonatitic liquids with various Ca/Mg and alkalis, depending on the peridotite assemblages and melting conditions (see Chapter 5 for a review). The range of liquid compositions from lherzolite is reproduced in Fig. 4 (Fig. 13, Chapter 5), with point WG showing the dolomitic nature of the near-solidus liquids. This range falls close to the silicate-carbonate coprecipitation surface, but is far removed from the two-liquid volume.

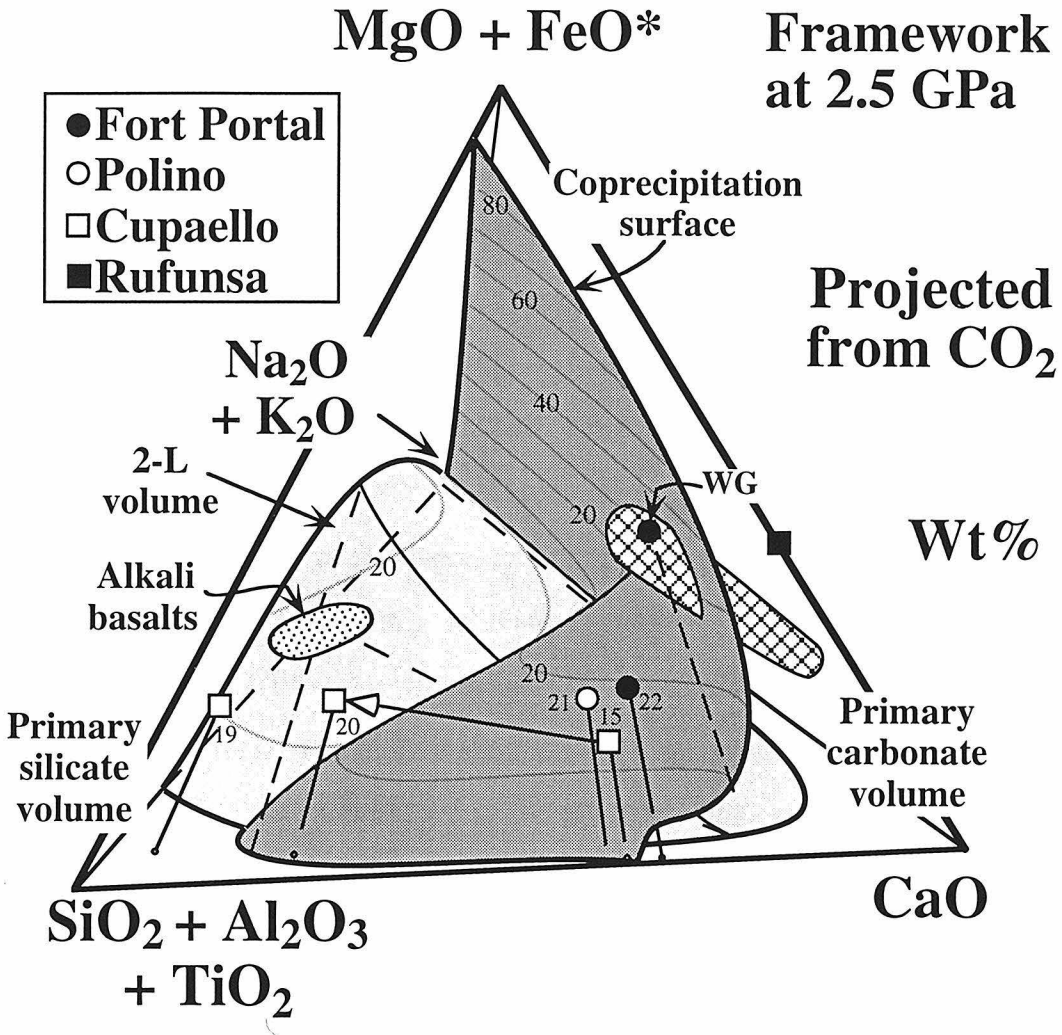

Figure 4. Generalized phase diagram at 2.5 GPa, showing compositions of carbonatites carrying mantle debris at Fort Portal, Polino and Cupaello. The silicate rocks associated with the Cupaello carbonatite are also plotted. The shaded area including WG shows the range for experimental carbonatitic liquids from lherzolite (Chapter 5), and is sketched to penetrate the coprecipitation surface.

Bailey (1993) summarized the occurrence of effusive carbonatites, indicating that for carbonatites which have minor or no association of silicate magmatism, they commonly carry mantle debris. He suggested that those carbonatites were directly from the mantle without much modification. We choose four such examples for the following discussion. Three average calciocarbonatite compositions from Fort Portal (Barker and Nixon, 1989), Polino (Stoppa and Lupini, 1993), and Cupaello (Stoppa and Cundari, 1995), plus a dolomite droplet analysis from magnesiocarbonatite of Rufunsa (Bailey, 1989), are shown in the tetrahedron of Fig. 4. Each composition is labeled by a number indicating its wt% (MgO + FeO*) on a volatile-free basis. The dolomite (solid square, Fig. 4) projects onto the (MgO + FeO*)-CaO axis, close to the liquid compositions from carbonated lherzolite, and probably represents a mineral precipitated from such a dolomitic mantle melt. The calciocarbonatites (solid and open circles, open square "15", Fig. 4) all contain high silica (~15-19 wt%), with (MgO + FeO*) ranging from 10 to 16 wt% (before normalized volatile-free). The rocks project into the primary silicate volume, but near the silicate-carbonate coprecipitation surface (compare the numbers for the rocks and the contours on the surface). Given the variations of the field boundaries as a function of pressure and composition, these calciocarbonatites may lie on a silicate-carbonate coprecipitation surface slightly different from that in Fig. 4.

On the basis of their field study on the Cupaello carbonatite tuff and associated melilitite pyroclastic breccia, Stoppa and Cundari (1995) concluded that the suite provides a direct evidence of immiscibility of carbonatite from "kamafugite" (melilitite) magma. The analyses of a silicate fragment and its matrix (Stoppa and Lavecchia, 1992) are shown in Fig. 4 (open squares "20" and "19"). Both analyses and the associated carbonatite composition project away from the miscibility gap, so liquid immiscibility could not produce the silicate and carbonatitic magmas.

The explanation for the coexistence of silicate and carbonatite rocks in Cupaello may lie on the melting relationships in carbonated peridotite: the rocks might both represent

partial melts of carbonated mantle assemblages, but with different degrees of melting. Depending on carbonate activity in the source region, near-solidus dolomitic liquids through progressive melting of peridotite may either follow a straight path to undersaturated silicate compositions (e.g. from WG to the alkali basalt field; Chapter 5), or follow a melting trend on the silicate-carbonate coprecipitation surface towards higher silica and lower mafic compositions until all carbonates are consumed, then the liquids evolve to primitive nephelinite or melilitite along a path subparallel to that described previously. The similar partial-melting scenario may also be applicable to the generation of Fort Portal and Polino carbonatites.

Carbonate ocelli in mantle xenoliths

The occurrence of carbonate ocelli has been discovered in several upper mantle peridotite and eclogite xenoliths (e.g. Amundsen, 1987; Ionov et al., 1993; Pyle and Haggerty, 1994; Kogarko et al., 1995). The ocelli are generally associated with metasomatic events, and are adjacent to silicate glasses of various compositions, with texture being interpreted as product of silicate-carbonate liquid immiscibility. The selected compositions of conjugate glasses and carbonates are shown in Fig. 5, compared with the 1-GPa framework representing the conditions for the upper-most mantle where these xenoliths were possibly from.

The carbonate globules in harzburgite nodules from Canary Islands (Kogarko et al., 1995) show compositions (solid diamonds near the carbonate triangle) very similar to magnesian calcite, with nearly no alkalis. The representative silicate glass projects well within the primary silicate volume (solid diamond, near the silicate corner), about 10 wt% alkalis outside the corresponding miscibility gap (contour 10%). It appears that liquid immiscibility can not generate conjugate silicate and carbonate liquids with compositions similar to the data presented above. Instead, the calcite globules may represent a solid

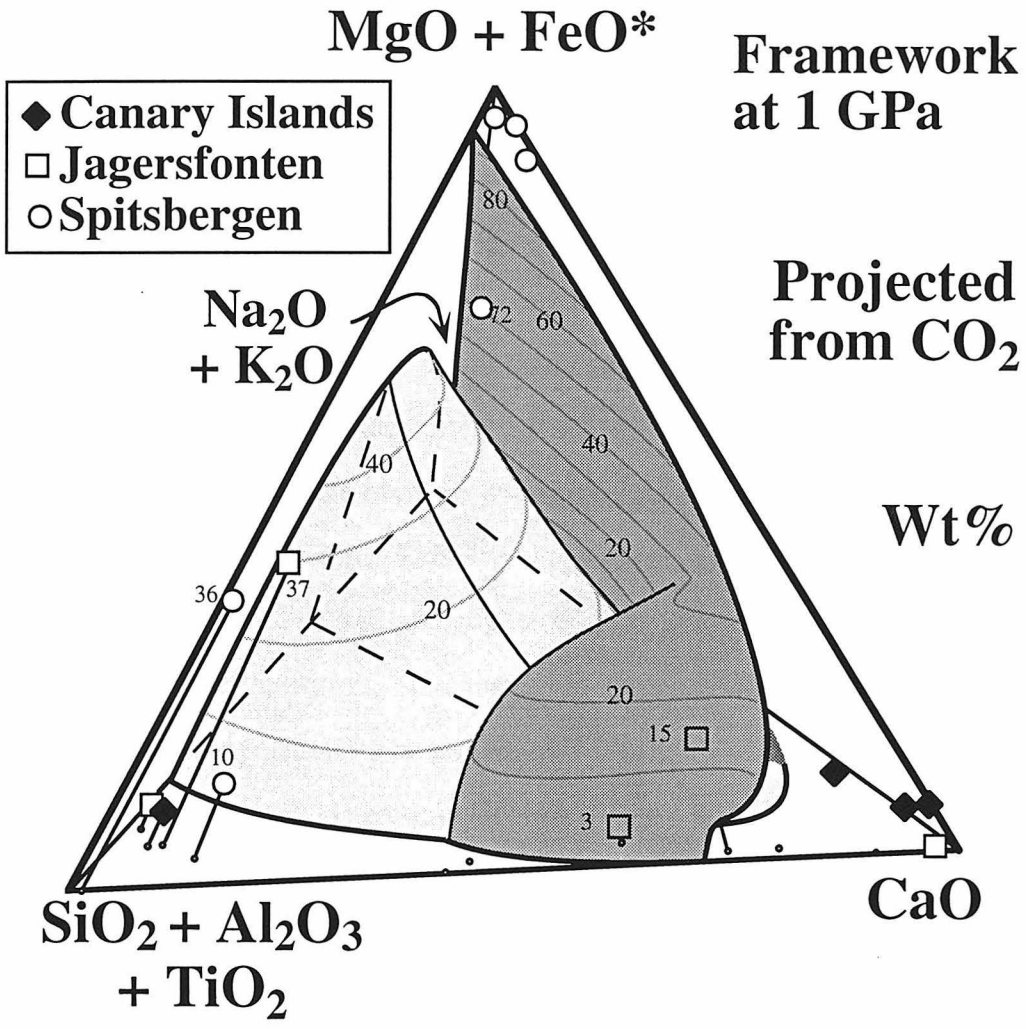

Figure 5. Compositions of silicate glasses and carbonate globules in mantle xenoliths including Canary Islands harzburgite, Jagersfontein eclogite and Spitsbergen lherzolite. The framework is at 1 GPa.

phase, and their geometry is consistent with the rounded calcite crystals in many experimental studies (see Chapters 2, 3 and 5). The silica contents of the globules might result from silicate inclusions in the carbonates, and one analysis does show no sign of silicate. The silicate glass composition is also far removed from the silicate-carbonate coprecipitation surface, leaving a question whether or not the corresponding liquid would be capable of precipitating calcite.

Two sets of compositions for glasses associated with carbonate globules were reported in the Jagersfontein eclogite samples (open squares near the silicate corner, Fig. 5; Pyle and Haggerty, 1994) . The Na-Al-rich silicate glass (referred to as sodic glass), similar in composition to those of the Canary Islands harzburgite nodules, contains low Ca, Mg and Fe. The Mg-rich silicate glass (as potassic glass) is also Ca-poor, with the major alkali component being potassium. Pyle and Haggerty (1994) noticed that the sodic and potassic varieties are of jadeite and phlogopite affinities, and that the sodic glass is very similar to natrolite in composition. An example of carbonate ocelli is also shown in the figure, very near the composition for pure calcite.

Pyle and Haggerty (1994) proposed a model involving liquid immiscibility for the coexistence of silicate glasses and calcite ocelli, where decompressive melting of alkali-bearing phases in the eclogite is combined with injection and through-flushing of a CO_2-H_2O rich fluid/melt to form two immiscible liquids; a Ca-rich carbonatite liquid, and a conjugate alkali-rich silicate liquid. It is clear in Fig. 5 that the alkali contents of the glasses and ocelli are too low to approach the immiscibility volume. In addition, none of the glasses is capable of precipitating calcite—the glass compositions are also removed from the silicate-carbonate coprecipitation surface. However, the estimated parental liquid composition for each affinity (A and B, Fig. 5; Pyle and Haggerty, 1994) projects very close to the coprecipitation surface. We here provide an alternative interpretation for the occurrence of silicate glasses and calcite ocelli in the eclogite samples: the metasomatic melts A and B precipitated both calcite and silicate minerals (mainly natrolite and

phlogopite, respectively) after infiltration to the eclogites. Upon arising, some portions of the alkali-bearing silicate minerals were subject to decompressive melting, producing sodic and potassic glasses at locally volatile-rich region.

It appears to be difficult to interpret the texture of coexisting ultramafic glass, basaltic (Na-Al-rich silicate) glass, and carbonate ocelli (open circles, Fig. 5) observed in Spitsbergen lherzolite xenoliths (compare Amundsen, 1987; Ionov et al., 1993). The ultramafic glass contains nearly no alkalis, with the mafic content similar to that of the potassic glass, whereas the basaltic glass is near the sodic glass, but contains higher (CaO + MgO + FeO*). The various carbonate phases (near the mafic corner) also have very low alkali contents. All of the compositions locate outside the immiscibility volume, so neither the three-liquid immiscibility (Amundsen, 1987), nor the coexistence of Na-Al-rich silicate liquid and carbonate-rich silicate-bearing liquid (subsequently separated into Mg-rich silicate glass and carbonate; Ionov et al., 1993) could satisfy the phase relationships.

Liquid paths of carbonated silicate magmas and the generation of crustal carbonatites

Liquid immiscibility is frequently invoked to explain the formation of crustal carbonatites. The criterion for the magmatic process to occur is that the liquid path of a CO_2-bearing, silicate parent must intersect the miscibility gap in order to exsolve a carbonatite liquid. Chapters 3 and 4 have presented various crystallization paths for silicate-CO_2 liquids in the synthetic system Na_2O-CaO-Al_2O_3-SiO_2-CO_2, with the confining field boundaries outlined in Fig. 1. Depending on the initial composition and P-T condition, these cooling liquids may either reach the miscibility gap, or follow a path to the silicate-carbonate coprecipitation boundary. Both liquid immiscibility and fractional crystallization may be important in the genesis of subvolcanic and volcanic carbonatites,

and the question is to define the most probable path for a particular occurrence based on integrated evidence from field, geochemical and experimental studies.

The convincing evidence for possible immiscibility origin of Oldoinyo Lengai natrocarbonatite has been presented elsewhere (e.g. Dawson et al., 1994, 1996; Church and Jones, 1995; Peterson and Kjarsgaard, 1995; Kjarsgaard et al., 1995). For the calcite-rich globules representing immiscible "calciocarbonatite" liquids in Shombole lavas, Kjarsgaard and Peterson (1991) suggested that they require a nephelinite parent less peralkaline than that of the natrocarbonatite. Notice that the calciocarbonatite liquid still contains significant amounts of alkalis and silicate compared to that in most calciocarbonatite rocks (sovites). Hamilton and Kjarsgaard (1993) indicated that the sovites may be precipitated from such an immiscible carbonatite liquid.

The popular view for the petrogenesis of Oldoinyo Lengai natrocarbonatite involves a parental olivine melilitite originated from the mantle, which evolves within the crust to wollastonite nephelinites capable of exsolving alkali-rich carbonatite liquids (e.g. Church and Jones, 1995; Peterson and Kjarsgaard, 1995; Dawson et al., 1996). Chapter 5 confirms that primitive nephelinite and the alkali basalt field are far removed from the magnesian miscibility gap, but through a crystallization trend, those liquids could lead to evolved nephelinites approaching the miscibility gap. Figure 6 illustrates such a path, using an example from the alkaline-carbonatite complex of Juquiá, São Paulo (Beccaluva et al., 1992). The bulk compositions of silicate rocks representing both cumulates and magmas are shown in the figure (open squares and circles, respectively, in area A). The most primitive liquid is basanitic, marked by B. The data in Fig. 6 define a linear array from the mafic rocks to the more evolved, nepheline syenites. Although all the silicate rocks project within the silicate volume, they do follow a crystallization path towards the immiscibility volume at the more differentiated compositions, and possibly intersect the miscibility gap at a condition somewhat different from that defining the gap in Fig. 6. Immiscible carbonatite liquids could then be generated from the evolved silicate liquids, but such

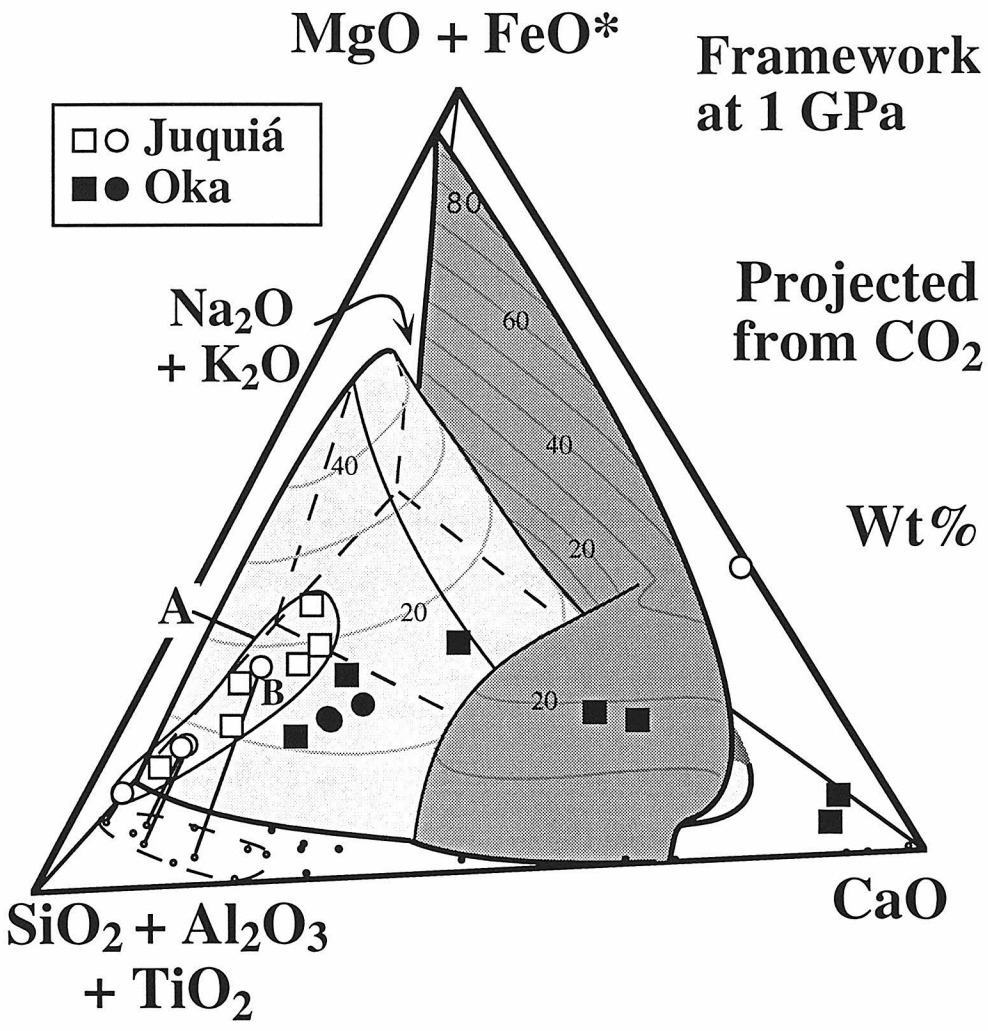

Figure 6. Bulk compositions of cumulates and fine-garined rocks from Juquiá (in envelope A) and Oka carbonatite complexes. The framework is at 1 GPa.

carbonatite liquids should be calcite-rich, and if they separated from the silicate parent, they would precipitate silicate minerals first until reaching the silicate-carbonate coprecipitation surface where calcite could be joined. The carbonatite core in Juquiá complex is Mg-rich (open circle, carbonate side, Fig. 6). This rock, if related to the associated alkalic rocks by liquid immiscibility, must have been derived from a more calcite-rich immiscible liquid by crystallization of both silicates and calcite along the coprecipitation surface. The involvement of calcite fractionation for the formation of the Mg-carbonatite is consistent with the observations of Beccaluva et al. (1992).

The compositions of silicate and carbonatite rocks from Oka complex, tabulated in Treiman and Essene (1985), appear to follow a different path, also shown in Fig. 6. All of the listed compositions, either for cumulates or for fine-grained rocks (solid squares and circles), project well outside the 1-GPa miscibility gap, and form a trend from the primary silicate volume to the carbonate-rich corner. This trending is consistent with a crystallization path of a CO_2-bearing, silicate parental liquid towards the silicate-carbonate coprecipitation surface, which produces silicate-calcite rocks when the evolving liquid follows a path on the cotectic surface. Through further fractionation of calcite and silicates, the liquid becomes more alkalic, and less siliceous, and thus is capable of precipitating carbonatitic rocks with higher carbonate to silicate ratios (e.g. the most calcite-rich rocks in the figure).

CONCLUSIONS

We illustrate in Figs. 4-6 the major field boundaries, the silicate-carbonate liquid miscibility gap and coprecipitation surface, in controlling the generation of various carbonatites from mantle to crustal conditions. The main conclusions are drawn from the comparisons between the natural rock compositions and the field boundaries:

(1) Liquid immiscibility is not involved in the formation of carbonate-rich melts in the mantle. Effusive carbonatites which carry mantle debris locate near the coprecipitation surface, probably representing primary carbonatite liquids from carbonated mantle assemblages. Primary silicate magmas, if associated with carbonatites of this kind, can not be related to the carbonatitic magmas by liquid immiscibility.

(2) Calcite globules in mantle nodules may represent a solid phase precipitated from metasomatic fluids/melts, not an immiscible liquid exsolved from the associated silicate melts (subsequently quenched to glass), since neither the globule nor glass compositions are close to the miscibility gap. The silicate glasses are also far from the coprecipitation surface, so their corresponding melts can not precipitate calcite. The glasses may represent quenched liquids produced by decompressive melting of volatile-rich silicate phases during uprise of the xenoliths.

(3) Both liquid immiscibility and fractional crystallization may play an important role in the generation of crustal carbonatites. Primitive alkaline silicate liquids may follow a crystallization trend to more evolved alkalic liquids which can produce immiscible carbonatite liquids with various Na/Ca. Natrocarbonatite lavas could be a direct immiscible product, whereas many calciocarbonatites associated with alkaline rocks might be precipitated from immiscible calcite-rich liquids along the coprecipitation surface. The sequence of rocks from the Oka carbonatite complex follows a direction to the coprecipitation surface, and these silicate-carbonate rocks could be produced by crystal fractionation without the involvement of liquid immiscibility.

REFERENCES

Amundsen H. E. F. (1987) Evidence for liquid immiscibility in the upper mantle. Nature 327, 692-695.

Bailey D. K. (1989) Carbonate melt from the mantle in the volcanoes of south-east Zambia. Nature 338, 415-418.

Bailey D. K. (1993) Carbonate magmas. Jour. Geol. Soc. London 150, 637-651.

Barker D. S. and Nixon P. H. (1989) High-Ca, low-alkali carbonatite volcanism at Fort Portal, Uganda. Contrib. Mineral. Petrol. 103, 166-177.

Beccaluva L., Barbieri M., Born H., Brotzu P., Coltorti M., Conte. A., Garbarino C., Gomes C. B., Macciotta G., Morbidelli L., Ruberti E., Siena F. and Traversa G. (1992) Fractional crystallization and liquid immiscibility processes in the alkaline-carbonatite complex of Juquiá (São Paulo, Brazil). Jour. Petrol. 33, 1371-1404.

Church A. A. and Jones A. P. (1995) Silicate-carbonate immiscibility at Oldoinyo Lengai. J Petrol 36, 869-889.

Cooper A. F., Gittins J. and Tuttle O. F. (1975) The system Na_2CO_3-K_2CO_3-$CaCO_3$ at 1 kilobar and its significance in carbonatite petrogenesis. Amer. Jour. Sci. 275, 534-560.

Cundari A. and Ferguson A. K. (1991) Petrogenetic relationships between melilitite and lamproite - in the Roman Comagmatic region - the lavas of S. Venanzo and Cupaello. Contrib. Mineral. Petrol. 107, 343-357.

Dawson J. B., Pinkerton H., Pyle D. M. and Nyamweru C. (1994) June 1993 eruption of Oldoinyo Lengai, Tanzania: exceptionally viscous and large carbonatite lava flows and evidence for coexisting silicate and carbonate magmas. Geology 22, 799-802.

Dawson J. B., Pyle D. M. and Pinkerton H. (1996) Evolution of natrocarbonatite from a wollastonite nephelinite parent: evidence from the June, 1993 eruption of Oldoinyo Lengai, Tanzania. Jour. Geology 104, 41-54.

Hamilton D. L. and Kjarsgaard B. A. (1993) The immiscibility of silicate and carbonate liquids. S. Afr. Jour. Geology 96, 139-142.

Huang W.-L. and Wyllie P. J. (1974) Eutectic between wollastonite II and calcite contrasted with thermal barrier in MgO-SiO_2-CO_2 at 30 kilobars, with applications to kimberlite-carbonatite petrogenesis. Earth Planet. Sci. Lett. 24, 305-310.

Huang W.-L. and Wyllie P. J. (1976) Melting relationships in the systems CaO-CO_2 and MgO-CO_2 to 36 kilobars. Geochim. et Cosmochim. Acta 40, 129-132.

Ionov D. A., Dupuy C., O'Reilly S. Y., Kopylova M. G. and Genshaft Y. S. (1993) Carbonated peridotite xenoliths from Spitsbergen: implications for trace element signature of mantle carbonate metasomatism. Earth Planet Sci Lett 119: 283-297.

Irving A. J. and Wyllie P. J. (1973) Melting relationships in systems CaO-CO_2 and MgO-CO_2 to 36 kilobars, with comments on CO_2 in the mantle. Earth Planet. Sci. Lett. 20, 220-225.

Irving A. J. and Wyllie P. J. (1975) Subsolidus and melting relationships for calcite, magnesite, and the join $CaCO_3$-$MgCO_3$ to 36 kilobars. Geochim Cosmochim Acta 39, 35-53.

Kjarsgaard B. and Peterson T. (1991) Nephelinite-carbonatite liquid immiscibility at Shombole Volcano, East Africa: petrographic and experimental evidence. Mineral. Petrol. 43, 293-314.

Kjarsgaard B. A., Hamilton D. L. and Peterson T. D. (1995) Peralkaline nephelinite/carbonatite liquid immiscibility: comparison of phase compositions in experiments and natural lavas from Oldoinyo Lengai. In: Bell K, Keller J (eds) Carbonatite volcanism: Oldoinyo Lengai and the petrogenesis of natrocarbonatites. IAVCEI Proceedings in Volcanology 4, Springer-Verlag, Berlin Heidelberg New York, pp 163-190.

Kogarko L. N., Henderson C. M. B. and Pacheco H. (1995) Primary Ca-rich carbonatite magma and carbonate-silicate-sulfide liquid immiscibility in the upper mantle. Contrib. Mineral. Petrol. 121, 267-274.

Maaloe S. and Wyllie P. J. (1975) The join grossularite-calcite through the system CaO-Al_2O_3-SiO_2-CO_2 at 30 kilobars: Crystallization range of silicates and carbonates on the liquidus. Earth Planet. Sci. Lett. 28, 205-208.

Macdonald R., Kjarsgaard B. A., Skilling I. P., Davies G. R., Hamilton D. L. and Black S. (1993) Liquid immiscibility between trachyte and carbonate in ash flow tuffs from Kenya. Contrib. Mineral. Petrol. 114, 276-287.

Peterson T. D. and Kjarsgaard B. A. (1995) What are the parental magmas at Oldoinyo Lengai? In: Bell K, Keller J (eds) Carbonatite volcanism: Oldoinyo Lengai and the petrogenesis of natrocarbonatites. IAVCEI Proceedings in Volcanology 4, Springer-Verlag, Berlin Heidelberg New York, pp 148-162.

Pyle J. M. and Haggerty S. E. (1994) Silicate-carbonate liquid immiscibility in upper-mantle eclogites: Implications for natrosilicic and carbonatitic conjugate melts. Geochim. et Cosmochim. Acta 58, 2997-3011.

Stoppa F. and Cundari A. (1995) A new Italian carbonatite occurrence at Cupaello (Rieti) and its genetic significance. Contrib. Mineral. Petrol. 122, 275-288.

Stoppa F. and Lupini L. (1993) Mineralogy and petrology of the Polino monticellite calciocarbonatite (central Italy). Mineral. Petrol. 49, 213-231.

Stoppa F. and Lavecchia G. (1992) Late Pleistocene ultra-alkaline magmatic activity in the Umbria-Latium region (Italy) - an overview. Jour. Volcano. Geotherm. Res. 52, 277-293.

Treiman A. H. and Essene E. J. (1985) The Oka carbonatite complex, Quebec: geology and evidence for silicate-carbonate liquid immiscibility. Amer. Mineral. 70, 1101-1113.

Wyllie P. J. and Huang W.-L (1975) Peridotite, kimberlite, and carbonatite explained in the system CaO-MgO-SiO_2-CO_2. Geology 3, 621-624.

Wyllie P. J. and Huang W.-L. (1976) Carbonation and melting reactions in the system CaO-MgO-SiO_2-CO_2 at mantle pressures with geophysical and petrological applications: Contrib. Mineral. Petrol. 54, 79-107.

Chapter 1: Lee W.-J. and Wyllie P. J. (1994) Experimental data bearing on liquid immiscibility, crystal fractionation, and the origin of calciocarbonatites and natrocarbonatites. Int. Geol. Rev. 36: 797-819.

Chapter 2: Lee W.-J., Wyllie P. J. and Rossman G. R. (1994) CO_2-rich glass, round calcite crystals and no liquid immiscibility in the system CaO-SiO_2-CO_2 at 2.5 GPa: Amer. Mineral., v. 79, p. 1135-1144.

Chapter 3: Lee W.-J. and Wyllie P. J. (1996) Liquid immiscibility in the join $NaAlSi_3O_8$-$CaCO_3$ to 2.5 GPa and the origin of calciocarbonatite magmas. Jour. Petrol. (in revision).

Chapter 4: Lee W.-J. and Wyllie P. J. (1996) Liquid immiscibility in the join $NaAlSiO_4$-$NaAlSi_3O_8$-$CaCO_3$ at 1.0 GPa with applications to the formation of crustal carbonatites. In preparation.

Chapter 5: Lee W.-J. and Wyllie P. J. (1996) Liquid immiscibility between nephelinite and carbonatite from 2.5 to 1.0 GPa compared with mantle melt compositions. Contrib. Mineral. Petrol. (submitted).

SUMMARY OF PETROLOGICAL CONCLUSIONS

Petrological applications are discussed at the end of each chapter in the thesis, and because each chapter was prepared for independent publication there is inevitably some repetition. In this summary, the main conclusions are gathered together from the previous chapters, and presented succinctly in an orderly, numbered list.

1. There is no experimental evidence for immiscible calciocarbonatite liquids containing more than 70-80% $CaCO_3$, and from many silicate parents the immiscible liquids may be richer in alkali carbonates and lower in $CaCO_3$. Appeals should no longer be made to experimental evidence for immiscible liquids with 99% $CaCO_3$ to explain calciocarbonatite magmas or calcite ocelli in mantle xenoliths.

2. The miscibility gap and silicate-carbonate liquidus field boundaries are two major features controlling liquid paths of carbonated silicate liquids to carbonatite residua. Carbonated silicate liquids through cooling may follow one of the three paths: (1) reach the miscibility gap directly to exsolve carbonate-rich liquids; (2) reach the silicate-carbonate liquidus field boundary, and either (a) follow the boundary to the miscibility gap, or (b) crystallize fully to produce silicate-carbonate rocks; and (3) evolve completely within the silicate liquidus field without (1) or (2) while exsolving CO_2. Immiscible carbonate-rich liquids separating from their silicate parent cool through a steep silicate liquidus surface before reaching the silicate-carbonate coprecipitation boundary.

3. Most calciocarbonatites are cumulates, probably precipitated from the carbonatitic liquids along the coprecipitation boundary at crustal pressures, reached either across the silicate liquidus surface, or more probably via the miscibility gap.

4. A range of alkali carbonatite liquids can be produced directly by liquid immiscibility. Carbonatitic liquids may reach the coprecipitation boundary through separation from the parent and crystallization of silicate minerals, and the residual liquids can then evolve toward alkali (and/or dolomite) enrichment and silica depletion, while precipitating additional silicates and calcite. Residual alkali melts/fluids through such prolonged differentiation processes may escape from the system, or interact with wall

rocks to form metasomatic zones (fenitization). The Oldoinyo Lengai natrocarbonatite may be an example that such liquids erupt to the surface of the earth. More likely extrusive alkali-bearing carbonatitic rocks may not survive surface processes (i.e. calcitization), and lose their alkali contents later. It appears that alkali-bearing carbonatite liquids are a common product associated with carbonatite magmatism by various processes.

5. Alkali-rich carbonatitic magmas may also be produced by crystal fractionation of hydrous CO_2-bearing nepheline-normative liquids through the precipitation of both silicates and calcite on the liquidus field boundary, completely underneath the high-temperature miscibility gap. Some carbonated silicate liquids, in contrast, may not be able to reach the liquidus field boundary due to the existence of thermal barriers on the silicate liquidus surface.

6. Small-degree partial melting of carbonated peridotite above ~2 GPa produces carbonatitic liquids, rich in dolomite with the alkali contents reflecting the compositions of the source rocks. These magmas could reach the surface of the earth without much modification, with eruptive style corresponding to that of kimberlites. These extrusions may carry mantle debris and show little or no association of silicate magmatism. The compositions of the reported examples (e.g. Fort Portal, Polino) project near the experimentally determined silicate-carbonate coprecipitation boundary in compositional space (ranging from silica-poor, dolomitic to more siliceous, magnesian calciocarbonatitic). This is consistent with their proposed origin by direct partial melting of peridotite.

7. Carbonate-rich liquids may be responsible for metasomatic events observed in some mantle xenoliths (e.g. harzburgite, lherzolite, eclogite). The generation of carbonate globules with a variety of silicate glasses in some samples cannot be explained by liquid immiscibility, since none of the phase compositions projects near the miscibility gap. Instead, the carbonate ocelli may represent solid phases crystallized from carbonate-rich liquids while the liquids are infiltrating the mantle rocks. The morphology of the ocelli is consistent with that of rounded crystalline calcite produced in many silicate-carbonate

experiments. The compositions of the silicate glasses are also far removed from the silicate-carbonate coprecipitation boundary, indicating that they are not the liquids in equilibrium with the carbonates. These glasses may be a product of decompressive melting of volatile-rich minerals (probably of metasomatic origin) during the rapid ascent of the mantle rocks.

8. The magnesian miscibility gap is restricted to alkali-rich compositions, much smaller in size than the Mg-free ones at mantle conditions. With increasing pressure, the size of the miscibility gap increases for the Mg-free system, but decreases for the magnesian system.

9. All possible mantle melt compositions (silica-undersaturated or dolomitic carbonatitic) and the associated melt paths (e.g. progressive melting of carbonated peridotite and crystallization trends) are far removed from the magnesian miscibility gap. Liquid immiscibility is not involved in the formation of carbonatitic melts in the mantle.

10. Most volcanic and subvolcanic carbonatites are associated with silicate rocks, and the available field evidence indicates that such alkaline complexes may be generated by differentiation of CO_2-bearing undersaturated silicate magmas within the crust. The paths of such parental liquids to carbonatitic residua must be constrained by the miscibility gap and silicate-carbonate liquidus field boundaries in phase diagrams, and the evolution of the liquids may vary significantly, due to the variations on the pressure and temperature conditions of the cooling paths, and on the parental compositions (e.g. magnesium, alkali and volatile contents).

11. Two crystallization trends from alkaline complexes are compared. The characteristics of the complexes formed with liquid immiscibility are (1) a series of rock compositions leading toward the miscibility gap, and (2) a compositional gap between silicate and carbonatite rocks. Many carbonatite complexes in east Africa have these characteristics. Carbonatite complexes may be also produced by crystal fractionation without involvement of immiscibility. The complexes so generated may contain a

relatively continuous spectrum of rocks ranging from silicate-rich to carbonatitic compositions. One example may be the Oka carbonatites.

12. Carbonate phases may be involved in the melting of warm subducted oceanic crust. The products would be carbonated, undersaturated silicate liquids, not carbonatitic liquids similar to those from mantle peridotite. These liquids may further contribute to the melting of mantle wedges above the slabs.

13. Carbonatites are of multiple origin. They may be a direct partial melting product in the mantle, or may be formed by liquid immiscibility or crystal fractionation from CO_2-enriched magmas capable of producing a variety of carbonatites in the crust. The field, geochemical and petrographic information must be evaluated with the phase equilibrium constraints to unravel the history of carbonatite magmatism.